SYNTHETIC, STRUCTURAL AND SPECTROSCOPIC STUDIES OF PERI-SUBSTITUTED SYSTEMS AND THEIR COMPLEXES

Louise M. Diamond

A Thesis Submitted for the Degree of PhD
at the
University of St Andrews

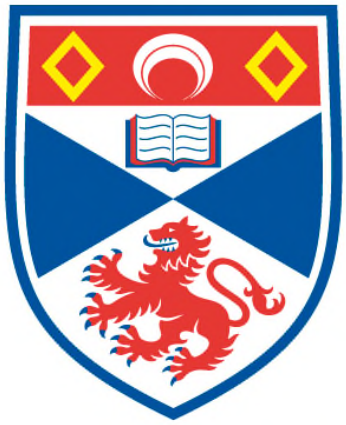

2014

Synthetic, Structural and Spectroscopic Studies of *Peri*-Substituted Systems and their Complexes

by

Louise M Diamond

Thesis submitted in partial fulfilment for the degree of

Doctor of Philosophy

The University of St Andrews

March 2014

Under the supervision of Prof. J. D. Woollins and Prof. A. M. Z. Slawin

Declaration

I, Louise M Diamond, hereby certify that this thesis, which is approximately 56,500 words in length, has been written by me, and that it is the record of work carried out by me or principally by myself in collaboration with others as acknowledged, and that it has not been submitted in any previous application for a higher degree.

I was admitted as a research student in September 2010 and as a candidate for the degree of Ph.D. in August 2011; the higher study for which this is a record was carried out in the University of St Andrews between 2010 and 2014.

Date …….. Signature of Candidate ……..

I hereby certify that the candidate has fulfilled the conditions of the Resolution and Regulations appropriate for the degree of Ph.D. in the University of St Andrews and that the candidate is qualified to submit this thesis in application for that degree.

Date …….. Signature of Supervisor ……..

In submitting this thesis to the University of St Andrews I understand that I am giving permission for it to be made available for use in accordance with the regulations of the University Library for the time being in force, subject to any copyright vested in the work not being affected thereby. I also understand that the title and the abstract will be published, and that a copy of the work may be made and supplied to any bona fide library or research worker, that my thesis will be electronically accessible for personal or research use unless exempt by award of an embargo as requested below, and that the library has the right to migrate my thesis into new electronic forms as required to ensure continued access to the thesis. I have obtained any third-party

copyright permissions that may be required in order to allow such access and migration, or have requested the appropriate embargo below.

The following is an agreed request by candidate and supervisor regarding the electronic publication of this thesis:

Embargo on both all of printed copy and electronic copy for a period of two years on the following grounds:

Publication would preclude future publication

Date ….. Signature of Candidate ……

Signature of Supervisor ……

Collaboration Statement

I am grateful to Kasun S. Athukorala Arachchige and Rebecca A. M. Randall for X-ray crystal structure determinations, Michael Buhl for DFT calculations and Dr Fergus R. Knight for his day to day support in the laboratory. Elemental analyses were performed by Stephen Boyer at the London Metropolitan University. Mass spectrometry was performed by Caroline Horsburgh at the University of St. Andrews Mass Spectrometry Service and by the EPSRC National Mass Spectrometry Service in Swansea.

Acknowledgements

What a journey the past 3.5 years have been... there has been the roller coaster ride of the ups and downs that go with research, loss of friendships, making of friendships, multiple tattoos, loss of a gall bladder and I found my husband.

I would like to extend my sincere gratitude to everyone at the Univeristy of St Andrews that has helped me along the way. My utmost thanks go to my supervisors Prof. J. D. Woollins and Prof. A. M. Z. Slawin. Their guidance, support and understanding have been invaluable and I am extremely grateful to them for giving me the opportunity to work with them. They are always there no matter how trivial the question and I simply couldn't ask for better supervisors. I wish them health, happiness and an early retirement!

I would also like to extend my thanks to all members of the lab, past and present. Special thanks must go to Fergus, my lab/office buddy. There are no words to describe how thankful I am for all your support. You have been my research rock and have kept me going when the downs of research got too much. Don't ever change, nice people like you are too few. Also Kasun, you have shown me what dedication, courage and hope are and I am thankful to have met you and worked alongside you.

My friends have been there every step of the way with words of encouragment and a drink when needed. Thank you guys! Especially Dean for being my most frequent visitor and Sara for proof reading this thesis.

Dad, Mum, Gran and Fiona thank you for supporting me through this, without you all I wouldn't be where I am today. My parents have worked incredibly hard to finance me through univeristy and I am extremely grateful for that. I hope I can repay you one day.

Finally, I want to thank the univeristy for employing Chris and allowing us the chance to meet. One way or another I will be leaving the university with the love of my life and that's priceless.

Abstract

The family of polycyclic aromatic hydrocarbons naphthalene, acenaphthene and acenaphthylene, containing rigid organic backbones, allow the study of non-bonded intramolecular interactions. Due to the rigid framework, heteroatoms that are substituted at the *peri*-positions (positions 1- and 8- of the naphthalene ring and positions 5- and 6- of the acenaphthene and acenaphthylene rings) are forced to occupy space that is closer than the sum of their van der Waals radii, resulting in severe steric strain and unique interactions. In spite of this, a vast amount of *peri*-substituted naphthalenes have been prepared, however acenaphthene and acenaphthylene compounds have received much less attention.

Preparation of these sterically crowded systems is possible because of the backbones ability to relieve strain as a result of both attractive and repulsive interactions. Attractive interactions relax the backbone *via* formation of weak or strong bonds between the substituents. Alternatively, repulsive interactions can result in the deformation of the backbone away from its natural geometry by buckling the ring system and causing the *peri*-bonds to distort in-plane and out-of-plane. *Peri*-substituted systems can also ease strain by forming compounds with bridging atoms or through bidentate coordination to form metal complexes with, for example, metal *bis*(phosphine) or *bis*(thiolate) moieties.

The competition between attractive and repulsive forces, the method by which *peri*-substituted compounds relieve steric strain, is investigated in this thesis using a variety of different *peri*-moieties and the aforementioned organic backbones.

Chapter 2 initially focuses on the formation of a series of platinum *bis*(phosphine) complexes, constructed from corresponding *peri*-substituted naphthalenes, 1,8-naphthosultone and 1,8-naphthosultam, the chemistry of which is outlined in Chapter 1. A corresponding study of platinum *bis*(phosphine) complexes, constructed from analogous 5,6-dihydroacenaphtho[5,6-*cd*]-1,2-dithiole and 5,6-dihydroacenaphtho[5,6-*cd*]-1,2-diselenole bidentate ligands is provided in Chapter 6.

The chemistry of *peri*-substituted naphthalenes is well documented and a number of reviews have been written on this subject. Chapter 3, meanwhile, reviews the chemistry of related

acenaphthene and acenaphthylenes which have seen increasing use in the literature over the last few years.

Chapter 4 investigates the relationship between repulsive and attractive interactions that occur between the *peri*-substituents in a series of *bis*-chalcogen, mixed chalcogen-chalcogen and mixed halogen-chalcogen acenaphthylenes. By comparison with their known naphthalene and acenaphthene counterparts, the effect the rigid aromatic ring system has on the molecular geometry is examined. Finally, Chapter 5 looks at a series of acenaphthene and acenaphthylene compounds containing ArTe *peri*-substituents and explores how repulsive and attractive interactions affect molecular conformation and Te···Te spin-spin coupling constants.

Contents

Abbreviations

5-HT/HT_2	5 - hydroxytryptamine
5-HT_7R	5 - hydroxytryptamine 7 receptor
λ	wavelength
Å	Ångström, 1 x 10^{-10} m
Acenap	acenaphthene
Acenapyl	acenaphthylene
An-*o*	2-methoxyphenyl
An-*p*	4-methoxyphenyl
br s	broad singlet
°C	degrees Celsius
ca.	*circa*
CCDC	Cambridge Crystallographic Data Centre
Cg	centroid
cm^{-1}	wavenumber
COD	1,5-cyclooctadiene
COSY	correlation spectroscopy
d	doublet
DBU	1,8-diazabicyclo[5.4.0.]undec-7-ene
decomp	decomposition
DDQ	2,3-dichloro-5,6-dicyano-1,4-benzoquinone
DFT	density functional theory
DMF	dimethylformamide
DMSO	dimethylsulfoxide
E	chalcogen i.e. sulfur, selenium, tellurium
EPSRC	Engineering and Physical Sciences Research Council
eq.	equivalent
et al.	*et alii*
Fc	ferrocene
FP	4-fluorophenyl
g	grams

h	hour
Hz	Hertz
HSQC	heteronuclear single quantum coherence
*i*Pr	isopropyl
IR	infra red
IUPAC	International Union of Pure and Applied Chemistry
J	coupling constant
m	multiplet
Me	methyl, CH_3
Mes	2,4,6-trimethylphenyl
min	minutes
mp	melting point
MS	mass spectrometry
m/z	mass to charge ratio
*n*BuLi	*n*-butyllithiuym
nap	naphthalene
NBS	N-bromosuccinimide
nm	nanometer, 1 $x10^{-9}$ m
NMR	nuclear magnetic resonance
Ph	phenyl, C_6H_5
pK_a	acid dissociation constant
ppm	parts per million
R_f	retardation factor
r_{vdW}	van der Waals radius
s	singlet
Σr_{vdw}	sum of the van der Waals radii
tert	tertiary
THF	tetrahydrofuran
Tip	2,4,6-triisopropanylphenyl
TMEDA	N,N,N',N'-tetramethyl-1,2-ethanediamine
TMS	tetramethylsilane
Tol	4-methylphenyl

TP	4-*tert*butylphenyl
WBIs	Wiberg bond indices
X	halogen i.e. bromine, chlorine, iodine, fluorine

Chapter 1

A literature review of 1,8-naphthosultone and 1,8-naphthosultam

Introduction

1,8-Naphthosultone and 1,8-naphthosultam are both commercially available, but surprisingly no coordination chemistry has been reported. Previously the Woollins' group studied the coordination chemistry of 1,8-dichalcogen naphthalenes and the oxidised derivatives of naphtho[1,8-*cd*]1,2-dithiole, to platinum *bis*phosphines.[1] Due to the structural similarity of these compounds to the oxidised derivatives of naphtho[1,8-*cd*]1,2-dithiole and their ease of availability it was decided to study their coordination chemistry to platinum *bis*phosphines. The following provides a brief introduction to the chemistry and uses of 1,8-naphthosultone and 1,8-naphthosultam.

1,8-Naphthosultone was first discovered by Mensching, and then synthesised by Schultz in 1887.[2] It was the first known compound of this type, and was termed a sultone by Erdmann, who confirmed its structure in 1888.[3] A sultone is defined by IUPAC as an, "intramolecular cyclic ester of hydroxy sulfonic acids, which are analogous to lactones."[4] Due to the similarity to lactones, the comparison was made between 1,8-naphthosultone and the lactone of hydroxybenzoic acid. In turn, it was thought a similar naphthalene analogue must exist for the lactam of amino-benzoic acid. Dressel and Kothe prepared this analogue in 1894, and called it 1,8-naphthosultam.[5]

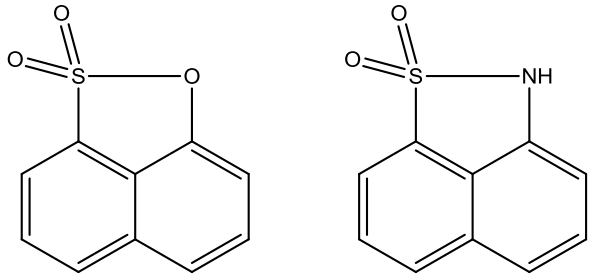

Figure 1 1,8-naphthosultone and 1,8-naphthosultam.

There are various methods for the preparation of 1,8-naphthosultone (Scheme 1), the most efficient method, with a 92% yield, was that developed by Parker and Iqbal,[6] who modified the original preparation used by Erdmann[3] in 1888. 8-amino-1-naphthalenesulfonic acid was suspended in 13% aqueous hydrochloric acid and sodium nitrite in water was added drop wise. The resulting mixture was then heated and once cooled the precipitate was collected and washed with water. The solid collected was dissolved in chloroform and the resulting solution was

decolourised with activated charcoal and concentrated. Needles of 1,8-naphthosultone grew upon cooling.

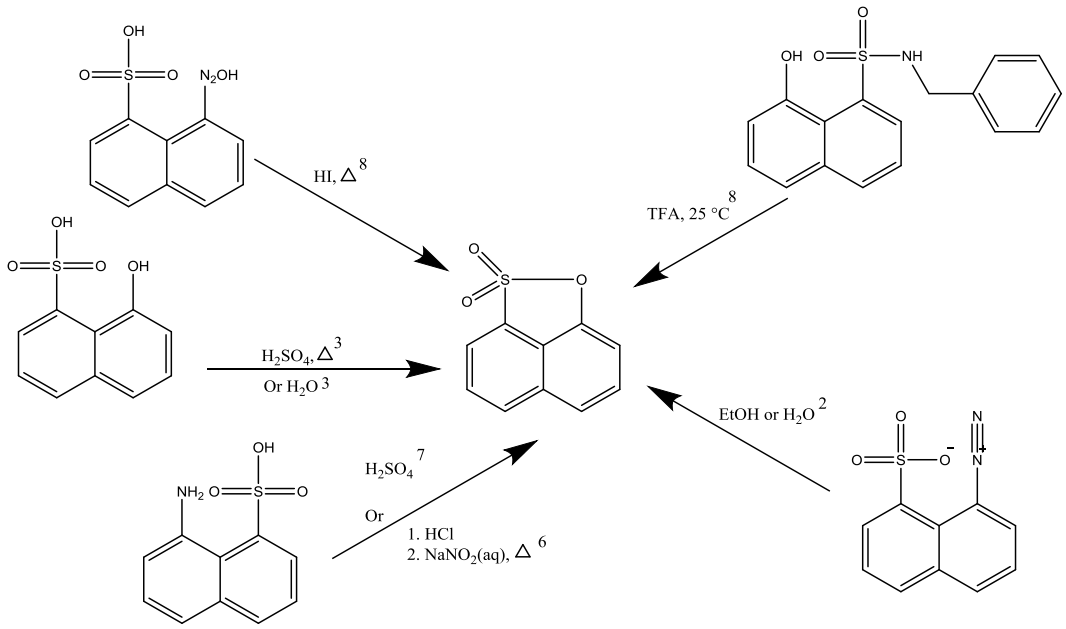

Scheme 1 Preparative methods of 1,8-naphthosultone.[2,3,6,7,8]

Similar to 1,8-naphthosultone, 1,8-naphthosultam, has different methods of preparation (Scheme 2).

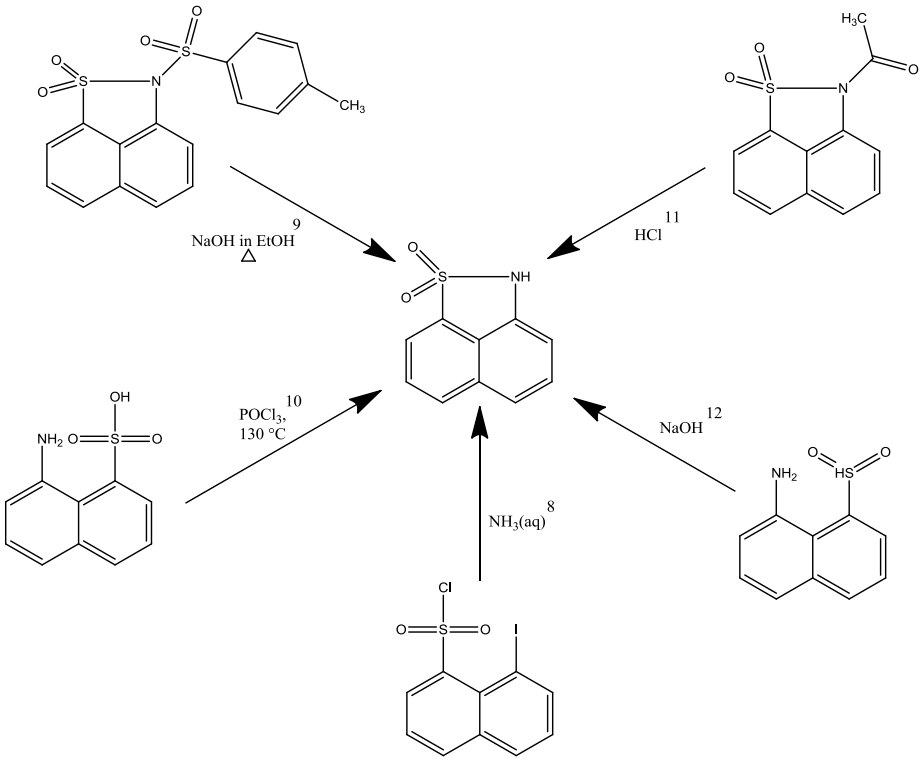

Scheme 2 Preparative methods of 1,8-naphthosultam.[8,9,10,11,12]

The most popular method, and one which has been used for over a century, is the reaction of 8-aminonaphthalene-1-sulfonic acid with phosphorus oxychloride. The potassium salt of 8-aminonaphthalene-1-sulfonic acid and three weight equivalents of phosphorus oxychloride are refluxed at 130 °C for three hours. The crude product is collected by filtration and is then recrystallized from benzene.[10]

Reactions of 1,8-naphthosultone

1,8-naphthosultone undergoes two main 'types' of reaction. The first involves the opening of the sultone ring and the second involves substitution of the naphthalene backbone. Electrophilic substitution is known to happen readily at the 4-position of the naphthalene backbone. Nucleophilic attack occurs at the sulfur atom causing opening of the sultone ring.[13]

The ring opening reaction that results in 1,8-naphthalenediol is the most utilised reaction of 1,8-naphthosultone. The ring is opened by the action of potassium hydroxide and heat[6,14,15] (Scheme 3) or a mixture of potassium hydroxide and sodium hydroxide.[16,17] Once synthesised 1,8-

naphthalenediol is used as a precursor for the formation of a variety of compounds. Some uses are discussed later in this section in more detail.

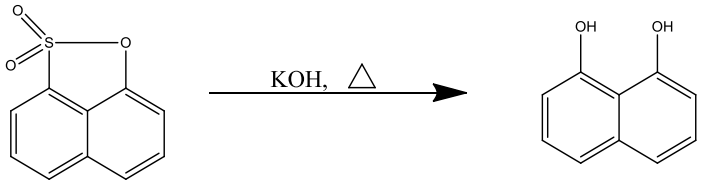

Scheme 3 Conversion of 1,8-naphthosultone to 1,8-naphthalenediol.[6,14,15]

Interestingly, using sodium hydroxide only results in a SO_3H at the 1- position and an OH at the 8-position.[18]

Once produced 1,8-naphthalenediol can be further reacted to form a series of spiro-*bis*naphthalenes (Scheme 4) which are fungal metabolites. They contain two units bridged by a spiro-acetal linkage; further manipulation is possible, such as, substitution on the naphthalene rings and/or the spiro rings. This group of compounds have many biological properties, for example; antimicrobial, antifungal, herbicidal and antitumour.[14,15,19]

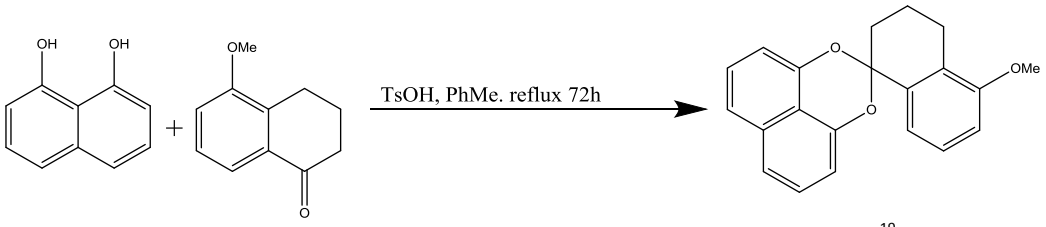

Scheme 4 Reaction of 1,8-naphthalenediol to form a Spiro-*bis*naphthalene.[19]

The red dye, 10-hydroxy-2H-naphtho[1,2-*b*]pyran also forms from 1,8-naphthalenediol when it is reacted with 1,1-diphenylprop-2-yn-1-ol under acid catalysis.[20]

1,8-Naphthalenediol is used as a precursor in the synthesis of a neutral dinickel 2,7-imino-1,8-dioxynaphthalene catalyst. This catalyst is used for ethylene polymerisation and ethylene-co-norbornene copolymerisation.[21]

The S-O linkage can be opened by the action of Grignard reagents (Scheme 5).[22]

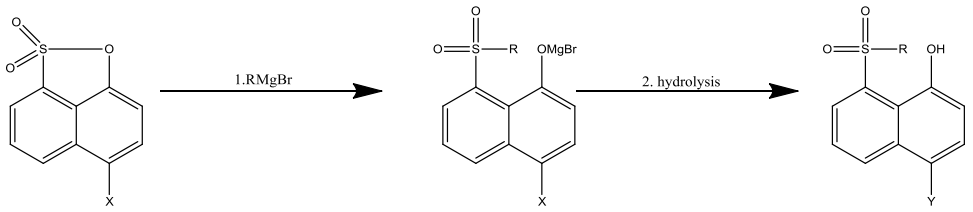

X = H	Y = H	R = C_6H_5
X = H	Y = H	R = C_6H_5
X = Br	Y = Br	R = C_6H_5
X = CH_2Br	Y = Br	R = α - $C_{10}H_7$
X = CH_2Cl	Y = $CH_2C_6H_5$	R = C_6H_5
X = CH_3	Y = $CH_2C_{10}H_7$ - α	R = α - $C_{10}H_7$

Scheme 5 Reaction of Grignard reagents with 1,8-naphthosultone and its derivatives.[22]

Organolithium compounds also react at the S-O bond in a reaction analogous to that of the Grignard reagents (Scheme 6).

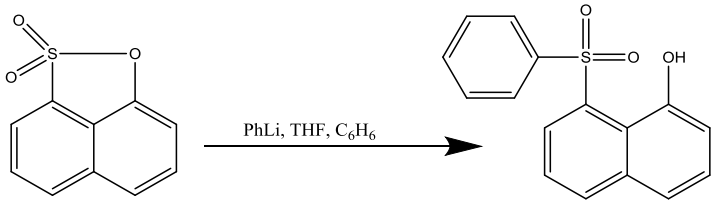

Scheme 6 Action of phenyl lithium on 1,8-naphthosultone.[23]

Whilst lithium aluminium hydride reduces the SO_2 to an SH group; the resulting 1-hydroxy-8-naphthalenethiol is oxidised in air to the disulfide (Scheme 7).[23]

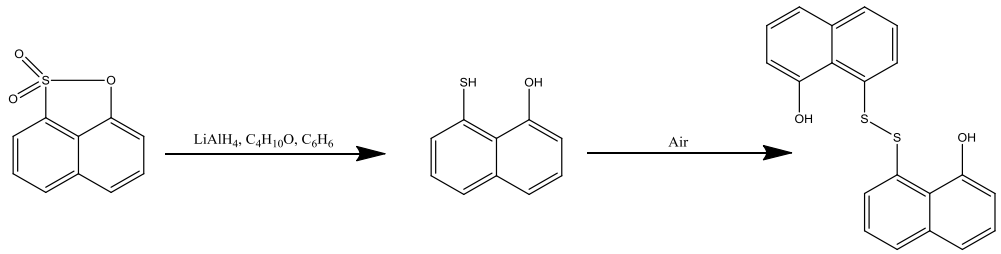

Scheme 7 Synthesis of 1-hydroxy-8-naphthalenethiol.[23]

The naphthalene backbone in 1,8-naphthosultone can be substituted by exploiting the Friedel-Crafts reaction. Schetty[23] synthesised many substituted 1,8-naphthosultones using aluminium trichloride and the corresponding halide. A few examples are shown below.

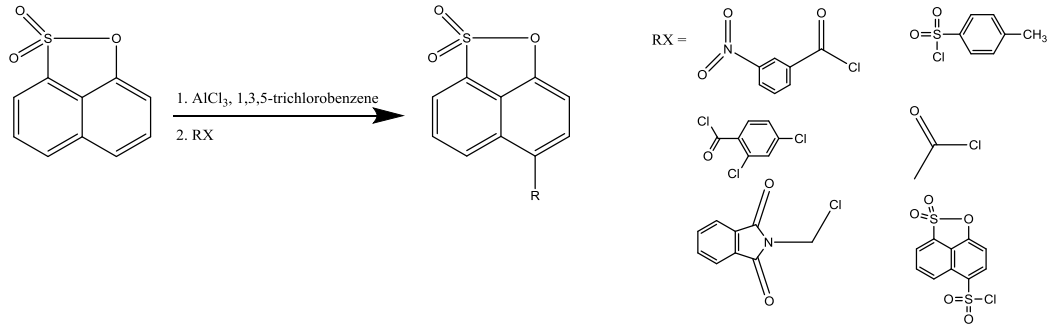

Scheme 8 Friedel-Crafts substitution of 1,8-naphthosultone.[23]

Schetty then proceeded to use zinc chloride with acetic acid and hydrogen chloride, which behaved analogously to that of aluminium trichloride.[24]

Halogenation of 1,8-naphthosultone has been achieved with bromine, chlorine and iodine.

Chlorination resulting in 4-chloro-1,8-naphthosultone can be achieved following three routes: 1) 1,8-naphthosultone and chlorine with iron powder at 160-200 °C, 2) 1,8-naphthosultone and hydrogen chloride in the presence of manganese (IV) oxide at 80-90 °C, 3) 4-SO_3H-1,8-naphthosultone and hot hydrochloric acid.[25]

Bromination resulting in 4-bromo-1,8-naphthosultone can occur through two routes: 1) cold solution of 1,8-naphthosultone in acetic acid and bromine in acetic acid or 2) aqueous solution of the sodium salt of 4-SO_3H-1,8-naphthosultone and bromine in acetic acid.[18]

Iodination resulting in 4-iodo-1,8-naphthosultone is attained by reacting 1,8-naphthosultone with, iodine and nitric acid.[26]

A mixture of mono- and dinitro- 1,8-naphthosultone can be obtained by reacting the sultone with one or two equivalents of nitric acid in sulfuric acid. In order to synthesise the pure mononitro-product, 4-nitro-1,8-naphthosultone, a solution of 1,8-naphthosultone in acetic anhydride is heated to 55 °C and nitric acid is added. The pure dinitro-product, 2,4-dinitro-1,8-

naphthosultone, is prepared by reacting nitric acid with a solution of the mono-nitro product in concentrated sulfuric acid at 50 °C.[27]

4-nitro-1,8-naphthosultone is used as a coupling reagent for peptide synthesis (Scheme 9). First, a mixture of acid and triethylamine are added to a solution of 4-nitro-1,8-naphthosultone. A solution of amine is then added and after work-up the pure amide is obtained. The acid and amine used depend on the amide desired.[27]

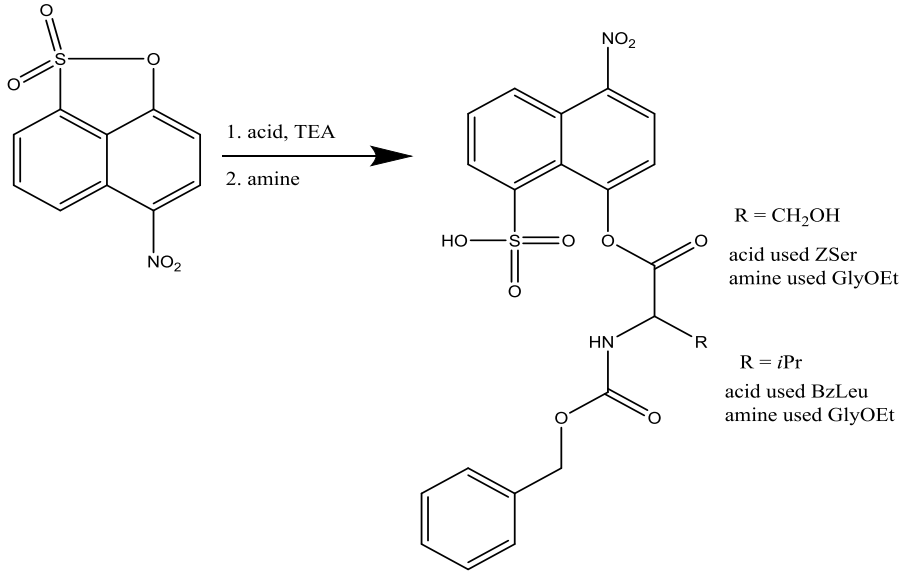

Scheme 9 Peptide synthesis using 1,8-naphthosultone as a coupling reagent.[27]

Some reactions utilise, both the opening of the sultone ring and substitution of the naphthalene backbone.

In 1928 Heller carried out the reactions, shown in Scheme 10, to form 8-hydroxy-7-*p*-tolylazo-naphthalene-1-sulfonic acid and 5,7-dibromo-8-hydroxy-naphthalene-1-sulfonic acid.[18]

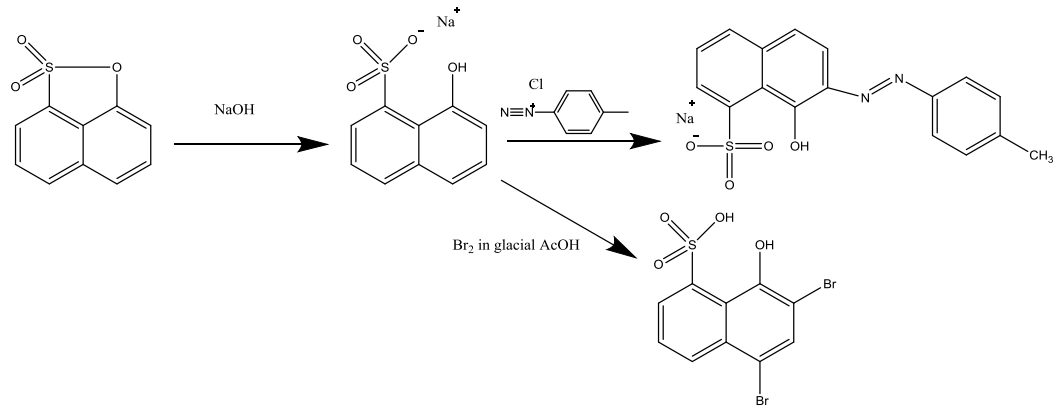

Scheme 10 Reaction carried out by Heller in 1928.[18]

Recently Georghiou *et al.*[13] have used 1,8-naphthosultone as a precursor for cyclooligomerisation, forming *peri*-tetrasulfonatocalix[4]naphthalene (Figure 2). 1,8-naphthosultone is first refluxed with caesium carbonate and formaldehyde in DMF, and it is then acidified.

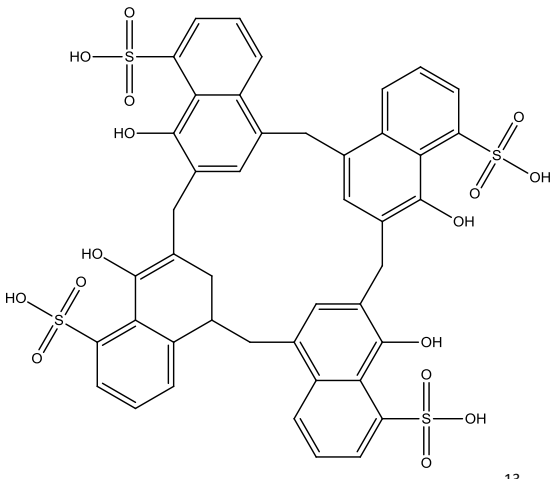

Figure 2 *Peri*-tetrasulfonatocalix[4]naphthalene.[13]

Reactions of 1,8-naphthosultam

1,8-naphthosultam undergoes three reaction-'types'. Like 1,8-naphthosultone the sultam ring can be opened and the naphthalene backbone can be substituted. However, unlike the analogous

sultone, the sultam can be substituted at the nitrogen on the sultam ring by replacement of the hydrogen atom.

Intriguingly, due to this ability to be deprotonated at the nitrogen atom, 1,8-naphthosultam displays multiple fluorescence. The emission is composed of two bands; the first is for the acidic naphthosultam, with a λ_{MAX} of 480 nm and the second is for the respective anion, with a λ_{MAX} of 600 nm.[28]

The sultam ring of 1,8-naphthosultam is opened on reaction with potassium hydroxide and heat. At higher temperatures 1,8-naphthalenediol is synthesised (Scheme 11).[10]

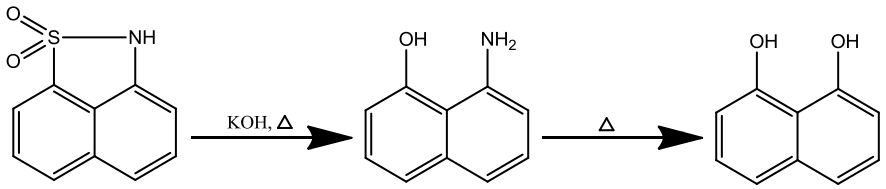

Scheme 11 Action of KOH on 1,8-naphthosultam and the corresponding formation of 1,8-naphthalenediol.[10]

Lithium aluminium hydride also acts upon 1,8-naphthosultam to open the sultam ring.[29] The resulting 1-amino-8-naphthalenethiol can be diazotized to produce naphtho[1,8-*de*]-1,2,3-thiadiazine (Scheme 12). A study was carried out on the thermal decomposition, photolysis and oxidation of this compound, and it was found that it is a useful precursor for the formation of *peri*-bridged naphthalenes, where the bridging group is S, SO and SO_2.[30]

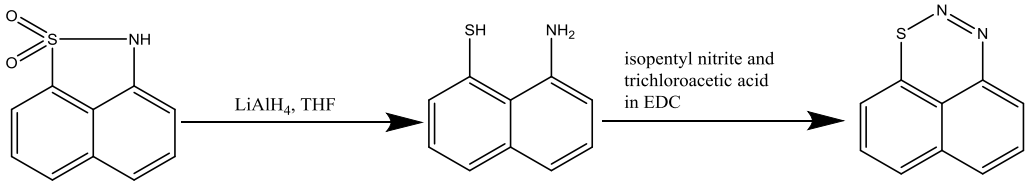

Scheme 12 Action of lithium aluminium hydride on 1,8-naphthosultam and the corresponding formation of thiadiazine.[29]

Unlike 1,8-naphthosultone, 1,8-naphthosultam is stable in the presence of Grignard reagent phenylmagnesium bromide. However, the N-benzenesulfonyl-1,8-naphthosultam is reactive and the sultam ring can be opened (Scheme 13).[31]

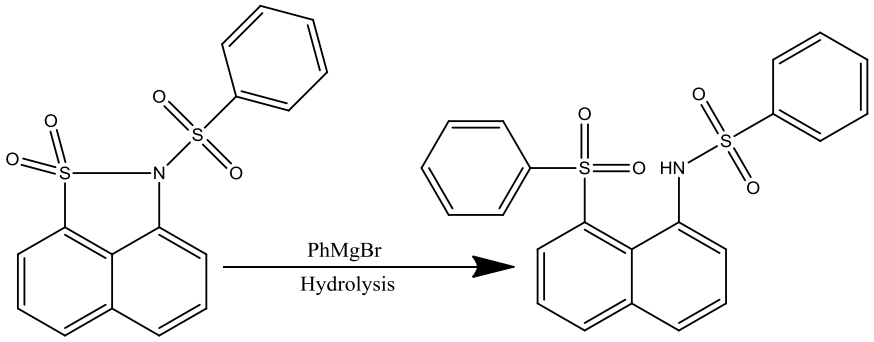

Scheme 13 Action of Grignard reagent on N-benzenesulfonyl-1,8-naphthosultam.[31]

1,8-naphthosultam undergoes halogenation reactions to form a variety of products. Mono-substitutions occur at the four position on the naphthalene ring with bromine and iodine (Scheme 14).[32]

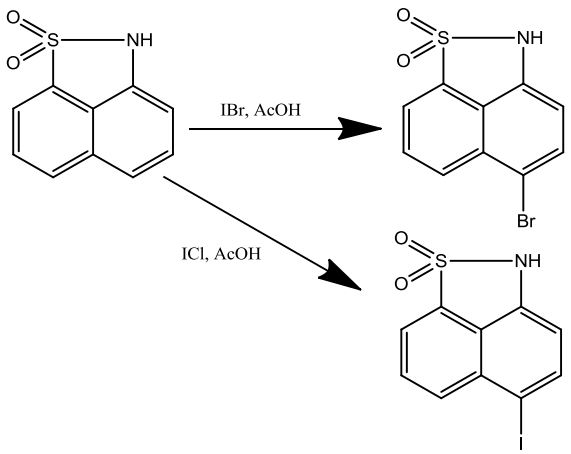

Scheme 14 Mono-halogenation reactions of 1,8-naphthosultam.[32]

A dibromo- product, 2,4-dibromo-1,8-naphthosultam, is also known. This is synthesised from the reaction of the sultam with bromine in acetic acid.[10]

Di-, tri- and penta-halogenated products (Figure 3) have been prepared with chlorine. The method and length of chlorination determines the extent of substitution.[25]

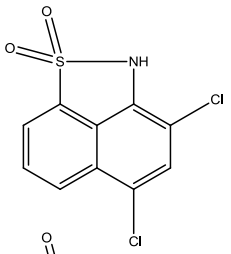

3,5-dichloro-2*H*-naphtho[1,8-*cd*]isothiazole 1,1-dioxide

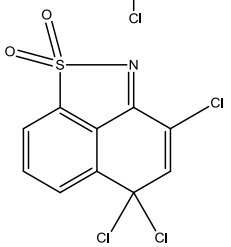

3,5,5-trichloro-5*H*-naphtho[1,8-*cd*]isothiazole 1,1-dioxide

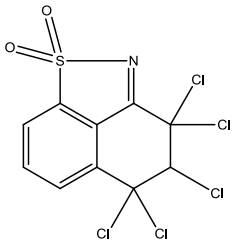

3,3,4,5,5-pentachloro-4,5-dihydro-3*H*-naphtho[1,8-*cd*]isothiazole 1,1-dioxide

Figure 3 Di-, tri- and penta-chloro derivatives of 1,8-naphthosultam.[25]

Dannerth nitrated the naphthalene backbone of 1,8-naphthosultam by using varying strengths of nitric acid. Dilute nitric acid resulted in the mono- substituted product, 4-nitro-1,8-naphthosultam. Concentrated nitric acid resulted in the di-substituted product, 2,4-dinitro-1,8-naphthosultam.[10] The 2,4-dinitro product can be easily reduced to the 2,4-diamino product by the action of tin and hydrochloric acid.[25]

Sulfonation of the naphthalene ring can also occur at the 4 position (Scheme 15), resulting in 1,8-naphthosultam-4-sulfonic acid.[33]

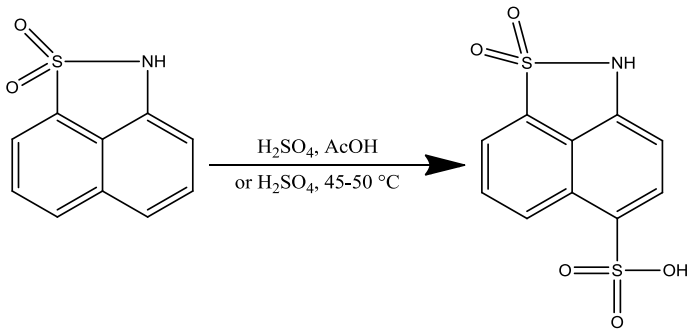

Scheme 15 Sulfonation reaction of 1,8-naphthosultam.[33]

Once prepared, this can be reacted further with arenediazonium salts to yield azo dyes.[34] It was later confirmed that if the 4-position is occupied, that reactions with arenediazonium salts will result in substitution at the 2-position.[35]

1,8-naphthosultam can be mono-substituted at the 4-position using a Friedel-Crafts reaction with aluminium trichloride (Scheme 16).[36]

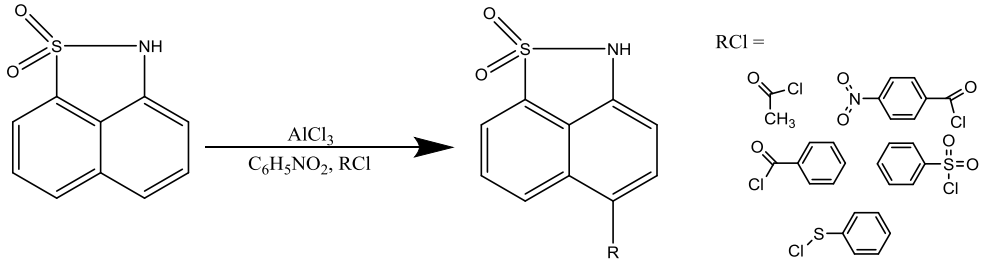

Scheme 16 Friedel-Crafts substitution of 1,8-naphthosultam.[36]

The NH group in 1,8-naphthosultam is acidic in nature due to the influence of the SO_2 group. The group can therefore be easily deprotonated by the action of a base, such as potassium hydroxide, sodium hydride, triethylamine or *n*-butyllithium. This opens the nitrogen atom up to substitution from a variety of groups.

1,8-Naphthosultam reacts with chlorinated phosphorus reagents to give the respective phosphorylated product (Scheme 17).[37]

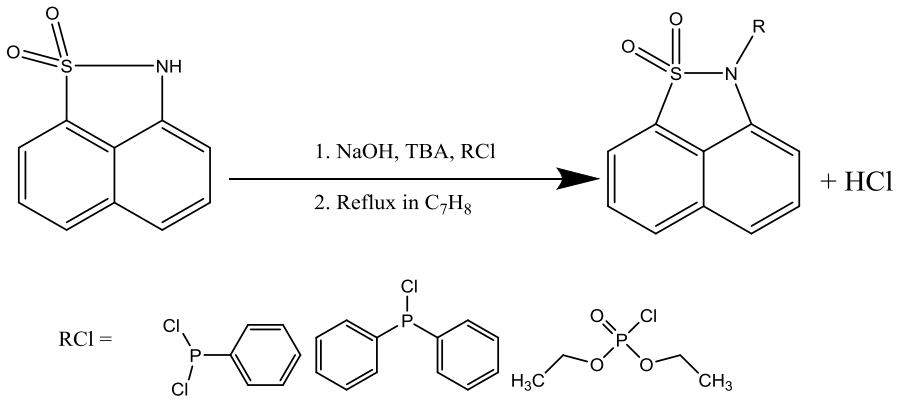

Scheme 17 Action of chlorinated phosphorus reagents on 1,8-naphthosultam.[37]

Trialkylphosphites and 1,8-naphthosultam react under heating to give the corresponding N-alkylated product (Scheme 18). It should be noted that unlike the other products, the N-methylated product can be obtained in two ways. The first using trimethylphosphite and the second using dimethyl phosphorochloridate.[37]

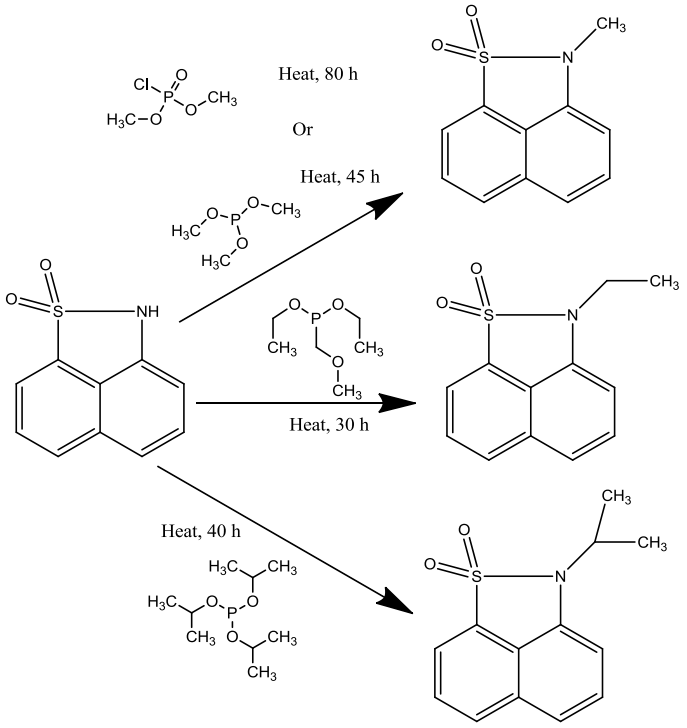

Scheme 18 Action of trialkylphosphites on 1,8-naphthosultam.[37]

Alkali metal salts of 1,8-naphthosultam can be prepared and then used as precursors in N-substitution reactions (Scheme 19). The formation of alkali metal chlorides drives the reaction.[38]

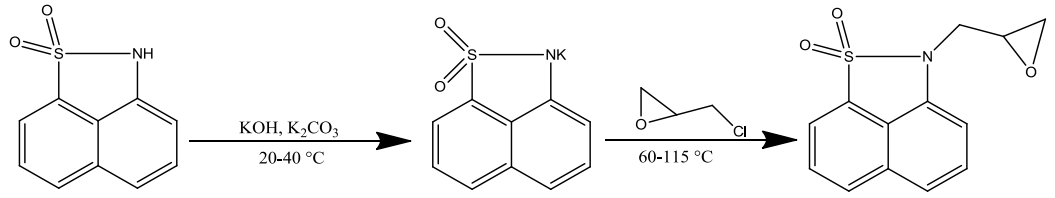

Scheme 19 Formation of 2-(oxiran-2-ylmethyl)-2H-naphtho[1,8-*cd*]isothiazole-1,1-dioxide.[38]

A series of sultam derivatives have been synthesised for use as 5-HT receptors (Scheme 20). 5-HT is 5-hydroxytryptamine, otherwise known as serotonin, and it functions in the body as a neurotransmitter.

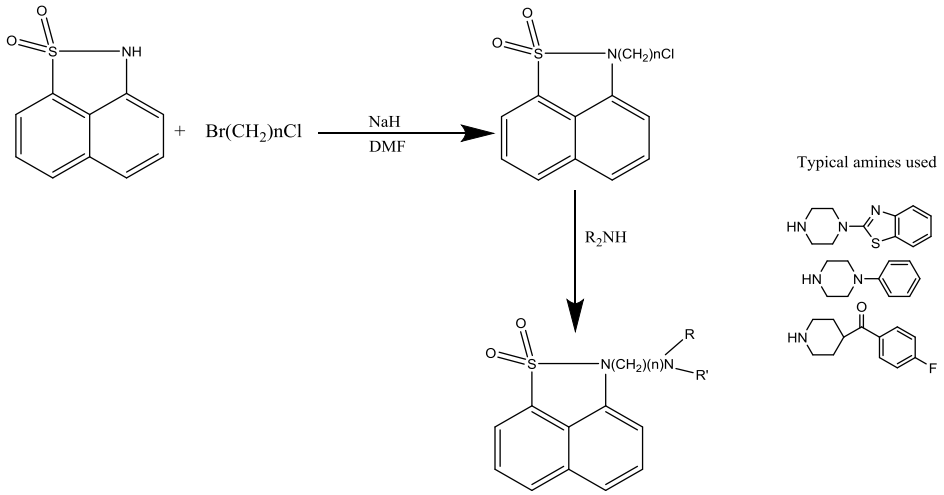

Scheme 20 Synthesis of 1,8-naphthosultam derivatives for use as 5-HT receptors.[39]

These derivatives were first used as 5-HT receptors in a study by Malleron and co-workers[39] in the early 1990s. They discovered the derivative, named RP62203 (Figure 4), to have the highest receptor affinity and it was chosen for clinical evaluation. Lever and Johnson[40] then developed RP62203 with a 4-I and 4-^{125}I group on the naphthalene ring. This allowed it to be used as serotonergic radio ligand for in vivo and in vitro studies.

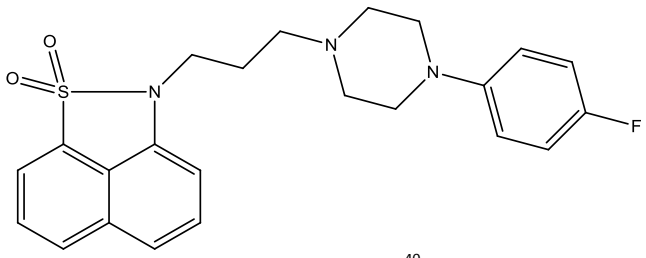

Figure 4 RP62203.[40]

During their study Malleron *et al.*[39] also synthesised a series of N-chloroalklyated naphthosultams (Scheme 21). A similar series of N-bromoalkylated naphthosultams have also been developed.[41]

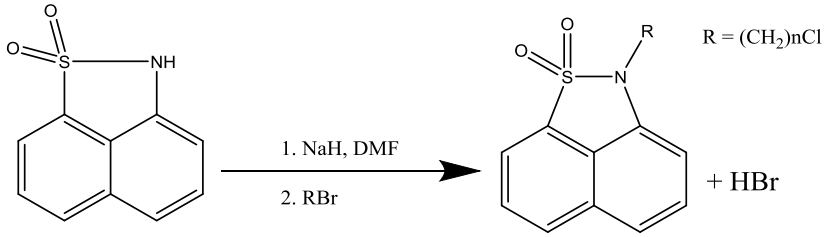

Scheme 21 Synthesis of N-chloroalkylated naphthosultams.[39]

Another serotonin receptor, 5-HT_7R, is thought to be involved in the disturbance of circadian rhythms in the body and therefore, a 5-HT_7R antagonist may be a useful drug for the treatment of sleep disorders. Lopez-Rodriguez *et al*.[41] studied a series of sultam derivatives for their antagonistic properties through a pharmacophore modelling program. The derivatives were prepared (Scheme 22) and studied in order to support the model.

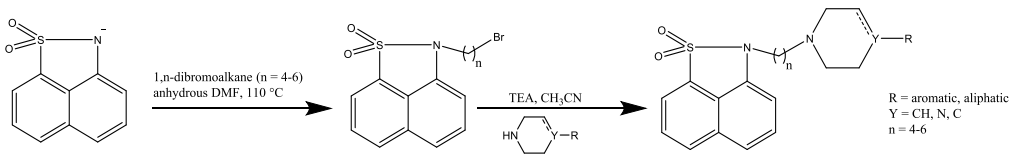

Scheme 22 Preparation of a 5-HT_7R antagonist using 1,8-naphthosultam.[41]

1,8-naphthosultam attached to an α-methacryloyl group has been used as an achiral template in the development of an enantioselective H-atom transfer reaction. It was found to be rather

effective, resulting in high enantioselectivity. The template is formed, by reacting a suspension of 1,8-naphthosultam in THF with sodium hydride, in a nitrogen atmosphere, at 20 °C. Methacryloyl chloride is then added, and after stirring overnight the reaction is quenched with ammonium chloride. This template is then used in various enantioselective H-atom transfer reactions catalysed by aryl oxazoline ligands.[42]

In a recent study, naphthosultam has been used to synthesise (z)-butenylthymines (e.g. Figure 5). These have been shown to be strong inhibitors of the enzyme, thymidine monophosphate kinase, of mycobacterium tuberculosis which is involved in pathogen replication. The development of a new drug is essential as mycobacterium tuberculosis causes two million deaths worldwide each year. The use of naphthosultam may prove to be the key in preventing these deaths.[43]

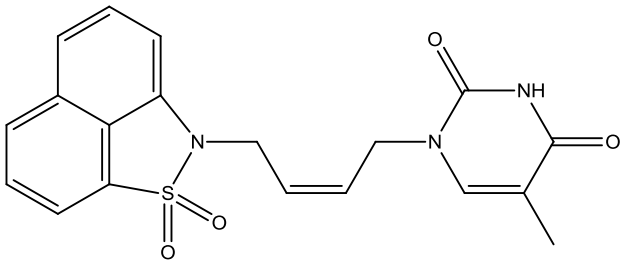

Figure 5 (Z)-2-(4-Thymin-1-yl) but-2-enyl-2H-naphtho[1,8 *cd*]isothiazole-1,1-dioxide.[43]

A 2-substituted- methyl carbapenem, bearing naphthosultam as a releasable acidic group (Figure 6), has been tested for use as an anti-methicillin resistant staphylococci (MRS) antibiotic. MRS is multidrug resistant and the current drugs that have an effect on this bacteria have a slow clinical response and adverse side effects. Preparation of a new drug is essential and the carbapenem bearing naphthosultam was shown to have a good in vitro activity profile. Further studies are underway.[44]

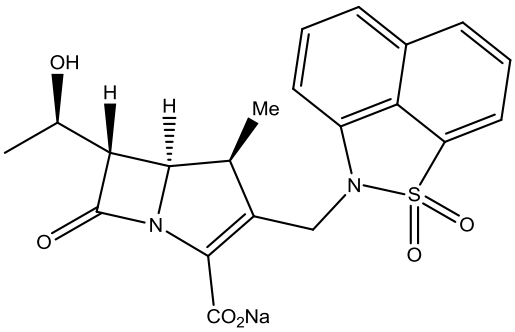

Figure 6 Carbapenem bearing 1,8-naphthosultam.[44]

As previously discussed, 1,8-naphthosultam when occupied at the 4-position can be substituted at the 2-position. This substitution behaviour was employed in order to yield the novel ring system of [1,2]-benzisothiazolo[2,3,4-*cde*]benzotriazole (Scheme 23), which combines N-substitution and naphthalene ring substitution in a unique way.[35]

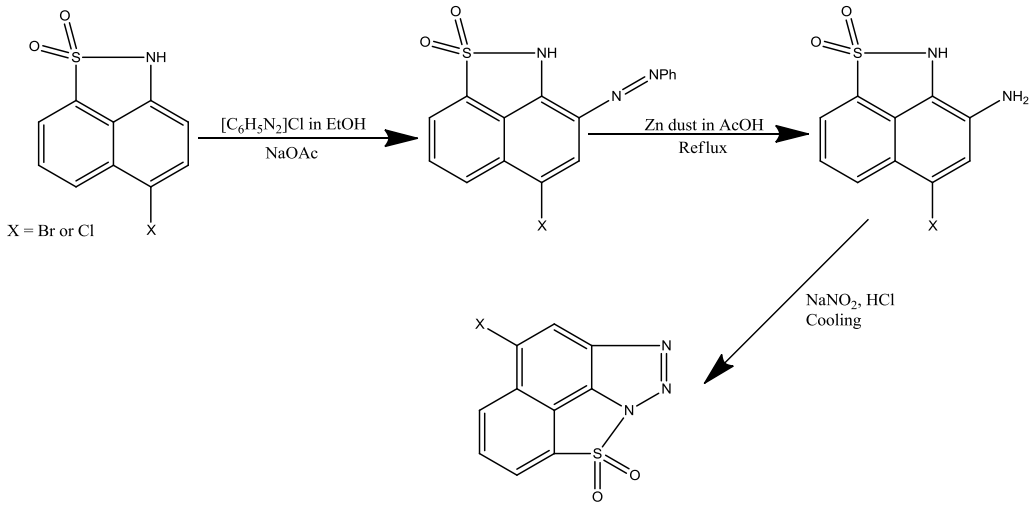

Scheme 23 Synthesis of [1,2]-benzisothiazolo[2,3,4-*cde*]benzotriazole.[35]

A series of reactions (Scheme 24) have been derived that involve halogenation at the 4-position on the naphthalene backbone, followed by N-substitution with varying groups.[32,40]

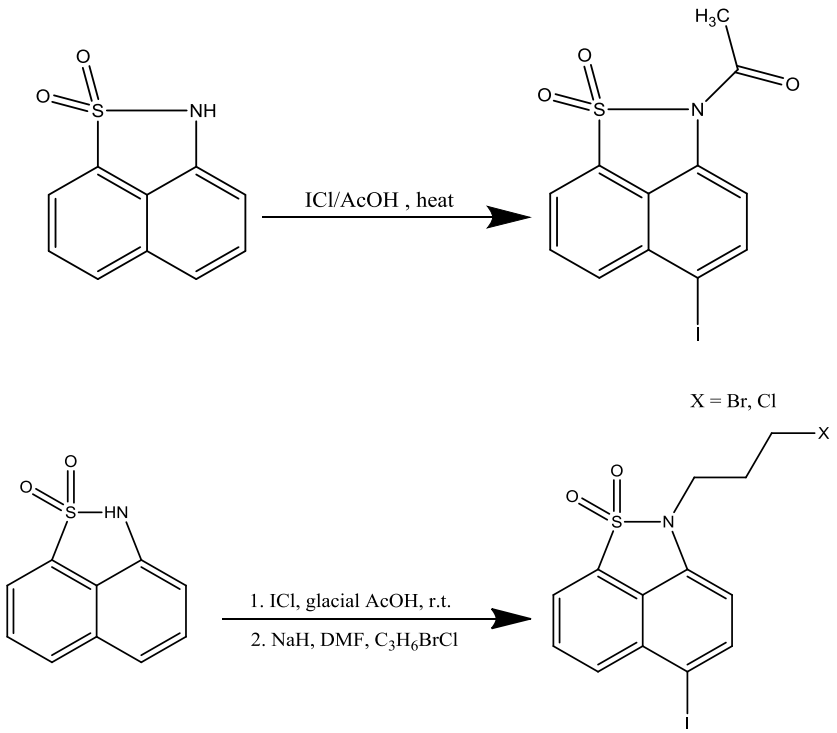

Scheme 24 Reactions involving 4-halogenation followed by N-substitution.[32,40]

Complexes of 1,8-naphthosultone and 1,8-naphthosultam with Transition Metals

There are no known metal complexes of 1,8-naphthosultone with the ring S-O bond intact. There are however, known complexes with Co^{2+},[45] Co^{3+},[46] Cr^{+},[47] Cr^{2+},[48] Cr^{3+},[49] Cu^{2+},[50] Cd^{2+},[51] Zn^{2+},[51] V^{2+} [52] and Ni^{2+},[45] derived from 8-oxidonaphthalene-1-sulfonate. Complexes that contain the azo-linkage are known for all metals listed, with the exception of Cd^{2+}, and these have applications as dyes (e.g. Figure 7).

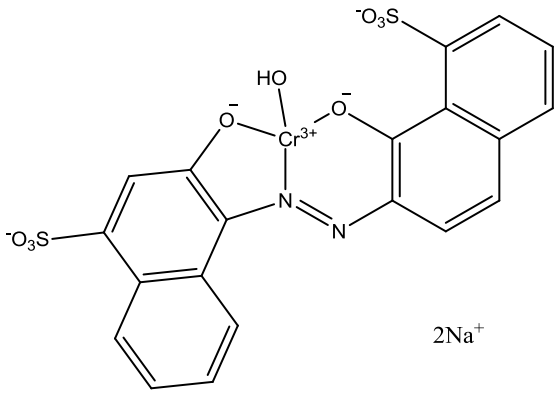

Figure 7 The azo dye - C.I. acid blue 158.[49]

The only known complex where 1,8-naphthosultam, with the S-N linkage intact, is bonded to a metal is shown in Figure 8. Here the nitrogen atom has been deprotonated and substituted with a methoxyethyl mercury group. This compound was used for mercury stimulated germination of Tilletia controversa spores.[53]

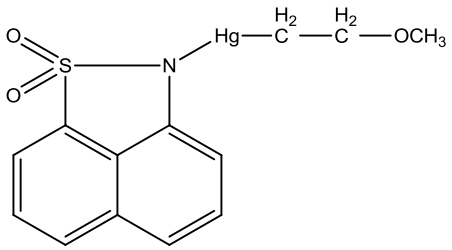

Figure 8 (1,1-dioxido-2H-naphtho[1,8-*cd*]isothiazol-2-yl)(2-methoxyethyl)mercury.[53]

Complexes of 1,8-naphthosultam are known for Co^{2+},[48] Co^{3+},[54] Zn^{2+},[55] Mo^{2+},[56] Mo^{3+},[56] Mo^{4+},[56] Fe^{3+},[45] W^{2+},[57] Cu^{2+},[45] Cr^{3+} [54] and Ni^{2+}.[45] However, they are derived from species such as, 8-aminonaphthalene-1-sulfonate. All of the above metals form complexes with an azo group present and they are used as dyes (e.g. Figure 9).

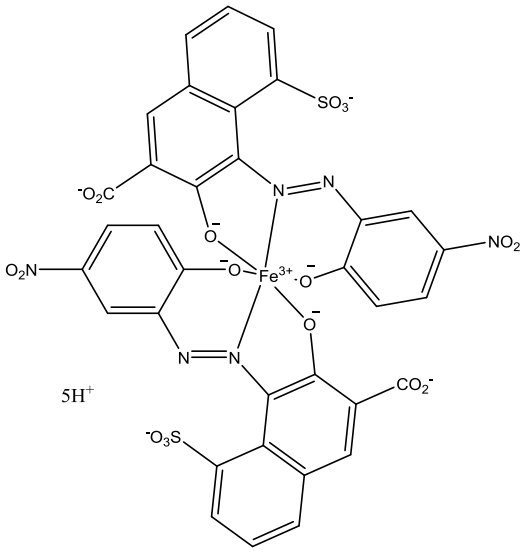

Figure 9 Ferrate(5-), *bis*[3-(hydroxy-*κ*O)-4-[[2-(hydroxy-*κ*O)-5-nitrophenyl]azo-*κ*N1]-5-sulfo-2-naphthalenecarboxylato(4-)]-pentahydrogen.[45]

Conclusion

From this study, it can be concluded that, 1,8-naphthosultone and 1,8-naphthosultam have similar chemical behaviour. Both compounds will undergo substitution on the naphthalene backbone and opening of the sultone and sultam ring systems, through a variety of methods. Differences arise in their behaviour due to the ability of the NH group in 1,8-naphthosultam to deprotonate, allowing for an additional reaction site.

1,8-naphthosultone is widely used as a precursor for 1,8-naphthalenediol, which in turn is used in a wide array of reactions. 1,8-naphthosultam is mainly used to synthesise compounds for use in biological applications. Both compounds have also been vastly employed to make dyes.
The chemistry of these compounds, although over a century old, is still evolving and it has only been in the past forty years that they have found their place as useful synthetic precursors. However, their full potential has still to be reached and future work is essential.

References

[1] S. M. Aucott, H. L. Milton, S. D. Robertson, A. M. Z. Slawin, G. D. Walker and J. D. Woollins, *Chem. Eur. J.,* 2004, **10**, 1666; S. D. Robertson, PhD Thesis, University of St Andrews (UK), 2005. and the references therein.

[2] G. Schultz, *Chem. Ber.,* 1887, **20**, 3162.

[3] H. Erdmann, *Justus Liebigs Ann. Chem.,* 1888, **247**, 345.

[4] A. D. McNaught and A. Wilkinson, *IUPAC Compendium of Chemical Terminology,* 2nd ed., Blackwell Scientific Publications, Oxford, 1997.

[5] O. Dressel and R. Kothe, *Chem. Ber.,* 1894, **27**, 2139.

[6] K. A. Parker and T. Iqbal, *J. Org. Chem.,* 1980, **45**, 1149.

[7] L. Blangey, *Helv. Chim. Acta.,* 1938, **21**, 1579.

[8] J.-P. Mozakyrat and M. Wakselman, *Tetrahedron. Lett.,* 1985, **26**, 6071.

[9] K. K. Andersen, D. D. Bray, S. Chumpradit, M. E. Clark and G. J. Habgood, *J. Org. Chem.,* 1991, **56**, 5508.

[10] F. Dannerth, *J. Am. Chem. Soc.,* 1907, **29**, 1320.

[11] T. Zincke, *Justus Liebigs Ann. Chem.,* 1916, **411**, 205.

[12] A. Reissert, *Chem. Ber.,* 1922, **55**, 873.

[13] P. E. Georghiou, Z. Li and M. Ashram, *J. Org. Chem.,* 1998, **63**, 3748.

[14] J. P. Ragot, C. Steeneck, M. Alcaraz and R. J. K. Taylor, *J. Chem. Soc., Perkin Trans. I,* 1999, **8**, 1013.

[15] A. C. Murphy, S. R. A. Devenish, A. C. Muscroft-Taylor, J. W. Blunt and M. H. G. Munro, *Org. Biomol. Chem.,* 2008, **6**, 3854.

[16] S. A. Snyder, T. C. Sherwood and A. G. Ross, *Angew. Chem. Int. Ed.,* 2010, **49**, 5146.

[17] M. C. Foti, E. R. Johnson, M. R. Vinquist, J. S. Wright, L. Barclay, C. Ross and K. U. Ingold, *J. Org. Chem.,* 2002, **67**, 5190.

[18] G. Heller, *Angew. Chem.,* 1928, **41**, 174.

[19] A. G. M. Barrett, F. Blaney, A. D. Campbell, D. Hamprecht, T. Meyer, A. J. P. White, D. Witty and D. J. Williams, *J. Org. Chem.,* 2002, **67**, 2735.

[20] C. I. Martins, P. J. Coelho, L. M. Carvalho and A. M. F. Oliveira-Campos, *Tetrahedron lett.,* 2002, **43**, 2203.

[21] B. A. Rodriguez, M. Delferro and T. J. Marks, *Organometallics,* 2008, **27**, 2166.

[22] A. Mustafa, W. Asker, O. H. Hishmat, A. F. A. Shalaby and M. Kamel, *J. Am. Chem. Soc.,* 1954, **76**, 5447.

[23] G. Schetty, *Helv. Chim. Acta.,* 1947, **30**, 1650.

[24] G. Schetty, *Helv. Chim. Acta.,* 1948, **31**, 1229.

[25] A. Mustafa, *Chem. Rev.,* 1954, **54**, 195.

[26] D. C. Allport and J. D. Bu'Lock, *J. Chem. Soc.,* 1958, 4090.

[27] F. Acher and M. Wakselman, *J. Org. Chem.,* 1984, **49**, 4133.

[28] H. Kanety and E. M. Kosower, *J. Phys. Chem.,* 1982, **86**, 3776.

[29] J. D. Wallis, R. J. C. Easton and J. D. Dunitz, *Helv. Chim. Acta.,* 1993, **76**, 1411.

[30] J. Nakayama, T. Fukushima, E. Seki and M. Hoshino, *J. Am. Chem. Soc.,* 1979, 7684.

[31] A. Mustafa and O. H. Hishmat, *J. Am. Chem. Soc.,* 1953, **75**, 4647.

[32] A. Mustafa, M. Ali and M. F. El-Miniawy, *Arch. Pharm. Ber. Dtsch. Pharm. Ges.,* 1965, **298**, 741.

[33] K. Koenig, *Chem. Ber.*, 1922, **55**, 2151.

[34] W. König and K. Kohler, *Chem. Ber.,* 1922, **55**, 2139.

[35] H. A. Hammouda, A. M. El-Reedy, M. A. F. Sharaf and A. M. Abdel-Fattah, *J. Heterocycl. Chem.,* 1984, **2**, 337.

[36] A. Mustafa, *J. Am. Chem. Soc.,* 1955, **77**, 4593.

[37] W. M. Abdou, H. A. Abd El. Monem, and M. R. Mahran, *Z. Naturfo. B.,* 1990, **45**, 1027.

[38] A. A. Stanishauskaite and V. A. Paulauskas, *Chem. Heterocycl. Compd.,* 2000, **30**, 195.

[39] J. L. Malleron, M. T. Comte, C. Gueremy, J. F. Peyronel, A. Truchon, J. C. Blanchard, A. Doble, O. Piot, J. L. Zundel, C. Huon, B. Martin, P. Mouton, A. Viroulaud, D. Allam and J. Betschart, *J. Med. Chem.,* 1991, **34**, 2477.

[40] J. R. Lever and S. M. Johnson, *J. Labelled Compd. Radiopharm.,* 1998, **41**, 143.

[41] M. L. Lopez-Rodriguez, E. Porras, J. M. Morcillo, B. Benhamu, L. J. Sorto, J. L. Lavandera, J. A. Ramos, M. Olivella, M. Campillo and L. Pardo, *J. Med. Chem.,* 2003, **46**, 5638.

[42] M. P. Sibi and J. B. Sausker, *J. Am. Chem. Soc.,* 2002, **124**, 984.

[43] O. Familiar, H. Munier-Lehmann, A. Negri, F. Gago, D. Douguet, L. Rigouts, A-I. Hernández, M-J. Camarasa and M-J. Pérez-Pérez, *Chem. Med. Chem.,* 2008, **3**, 1083.

[44] R. R. Wilkening, R. W. Ratcliffe, K. J. Wildonger, L. D. Cama, K. D. Dykstra, F. P. DiNinno, T. A. Blizzard, M. L. Hammond, J. V. Heck, K. L. Dorso, E. St. Rose, J. Kohler and G. G. Hammond, *Bioorg. Med. Chem. Lett.,* 1999, **9**, 673.

[45] JP Pat. 2000-204061-20000705, 2002.

[46] NL Pat. 1966-1317, 1966.

[47] J. C. Greene and G. L. Baughman, *Text. Chem. Color.,* 1996, **28**, 23.

[48] FR Pat. 1486661 19670630, 1967.

[49] G. McKay, S. H. Blair and J. R. Gardener, *J. Appl. Polym. Sci.,* 1982, **27**, 3043.

[50] P. Bineesh, P. Siva Rama Kumar, G. G. Pawar and V. R. Kanetkar, *Adv. in Colour Science and Technology,* 2004, **7**, 43.

[51] O. Makitie and H. Saarinen, *Suomen Kemistilehti,* 1969, **42**, 394.

[52] L. I. Aranova, E. S. Orlova, I. A. Tserkovnitskaya, *Zavodskaya Laboratoriya,* 1978, **44**, 142.

[53] E. Niemann, *Angew. Bot.,* 1957, **31**, 191.

[54] JP Pat. 1983-67852 19830419, 1984.

[55] A. Kawase, *Natl. Res. Inst. Metals,* 1965, **12**, 195.

[56] J. Rouchad and A. Mumbieni, *Bull. Soc. Chim. Fr.,* 1970, **8**, 2907.

[57] DE Pat. 1969-1945470 19690909, 1970.

Chapter 2

Platinum complexes of 1,8-naphthosultone and 1,8-naphthosultam

Introduction

Naphthalene consists of two fused benzene rings and has a unique geometry when compared to the benzene ring. In benzene the C-C bond lengths are all equal with a value of 1.39 Å and the bond angles are also all equal at 120°.[1] In comparison the bond lengths and bond angles in naphthalene are slightly unequal (Figure 1).[2]

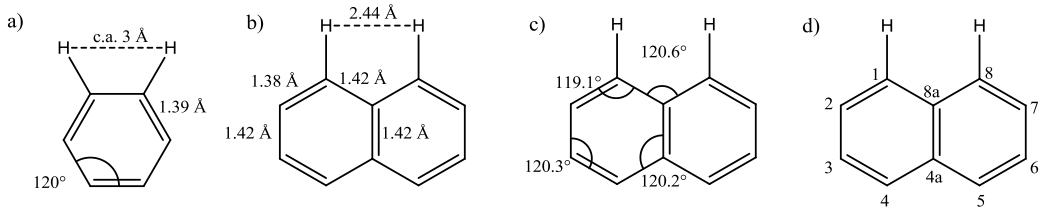

Figure 1 a) geometry in *ortho*-benzene, b) bond lengths in naphthalene, c) bond angles in naphthalene, d) numbering system in naphthalene.

Naphthalene has a rigid, planar structure with a C_2 symmetry. The 1- and 8- positions on the naphthalene ring are known as the *peri*-positions. In naphthalene, the hydrogen atoms attached to C1 and C8 have a non-bonded distance of 2.44 Å. In contrast the non-bonded hydrogen distance in *ortho*-substituted benzene is *ca*. 3 Å. This difference is due to the substituent bonds in naphthalene being parallel whereas in benzene they are tilted away from each other.[3] Therefore, in naphthalene the *peri*-substituents sit significantly closer together than is typical for ortho-substitution. If the substituents on the carbon atoms are hydrogen atoms they can be accommodated with ease. This is due to the non-bonded hydrogen distance (2.44 Å) being greater than the sum of their van der Waals radii (Σr_{vdw} = 2.18 Å).[4] If these *peri*-hydrogens were to be replaced with larger substituents one would expect a considerable amount of steric hindrance as there is not enough space for the larger groups to be accommodated.[3]

Although steric strain is present when the hydrogen atoms are replaced by larger heteroatoms, a great array of *peri*-substituted naphthalenes have been prepared. This is possible because the rigid backbone in naphthalene forces the *peri*-substituents to occupy the limited space. In turn they experience steric strain as a consequence of sub van der Waals contacts.[5] This strain, however, can be alleviated in two ways allowing the larger *peri*-substituents to remain. Firstly, attractive interactions can occur which relieve the strain by causing formation of weak or strong

bonds between the substituents.[3,5] Secondly, repulsive interactions cause the *peri*-bonds to distort in-plane or out-of-plane or they distort the naphthalene backbone away from its normal geometry.[3,5]

X-ray crystallography has played a key part in understanding these repulsive and attractive interactions. Three specific parameters are measured and compared to those in unsubstituted naphthalene. Collectively these three parameters are conveyed by the *peri*-distance (Figure 2).[5]

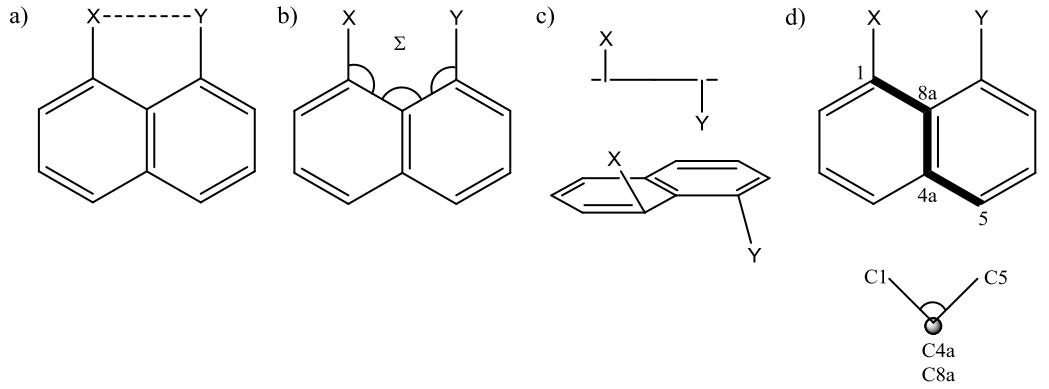

Figure 2 Measuring steric interactions and naphthalene distortions: a) *peri*-distance, b) total of splay angles, c) distance *peri*-atoms sit above and below plane, d) torsion angles.

Furthermore the splay angles in the bay region (Figure 2 part b) may be calculated and totalled. They can then be compared to the total in unsubstituted naphthalene, which is 357.2°.[5] This information is used to give an insight into in-plane distortion. If the total is lower this implies that the bonds have moved closer together due to an attractive interaction. Whereas a higher total implies that the bonds have moved further apart due to repulsive interactions.[5]

Out-of-plane distortion is assessed by measuring the distance the *peri*-atoms are sitting above and/or below the mean plane of the naphthalene ring (Figure 2 part c). The *peri*-hydrogens in 'ideal' naphthalene lie in the same plane as the naphthalene ring.[5]

The planarity of the 1,8-disubstituted naphthalene is determined by measuring the torsion angles of the carbon backbone, for example C1-C8a-C4a-C5 (Figure 2 part d). The torsion angles in

'ideal' naphthalene are 0 or 180° which indicates total planarity. The degree of variation from these values provides an idea of how distorted the naphthalene backbone is.[5]

The unique ability of the naphthalene backbone to force *peri*-substituents to accommodate limited space has allowed the distortions described above to be investigated and thus has helped develop an understanding of the interactions that occur. Since the first review of *peri*-substituted naphthalenes in 1966,[3] research in this area has grown. Reviews published in recent years include discussions of proton sponges[6]; *peri*-substituted naphthalenes with group 13[7] (B, In, Ga) substituents; those with heavier group 15 (P, As, Sb, Bi) and group 16 (S, Se, Te) substituents[8] and also the coordination chemistry of the aforementioned group 15 and group 16 *peri*-substituted naphthalenes as ligands in metal complexes.[9]

The chemistry of *peri*-substituted naphthalenes is large and diverse. Unfortunately a full discussion of this is not possible within the scope of this work. Instead this chapter will focus on two *peri*-substituted naphthalenes, 1,8-naphthosultone and 1,8-naphthosultam. The initial aims of the research were to investigate the coordination chemistry of 1,8-naphthosultone and 1,8-naphthosultam. A brief review of some related coordination chemistry, which inspired this work is given below.

In the late 1970's and early 1980's Teo and co-workers[10] coordinated tetrathionaphthalene (TTN), tetrachlorotetrathionaphthalene (TCTTN) and tetrathiotetracene (TTT) (Figure 3) to a $Pt(PPh_3)_2$ centre through oxidative addition reactions with $[Pt(PPh_3)_4]$. Due to the structural similarity of these compounds to naphthalene, the Woollins' group used this oxidative reaction to study the coordination chemistry of 1,8-dichalcogen naphthalenes and the oxidised derivatives of naphtho [1,8-*cd*]1,2-dithiole, to platinum *bis*phosphines.[11]

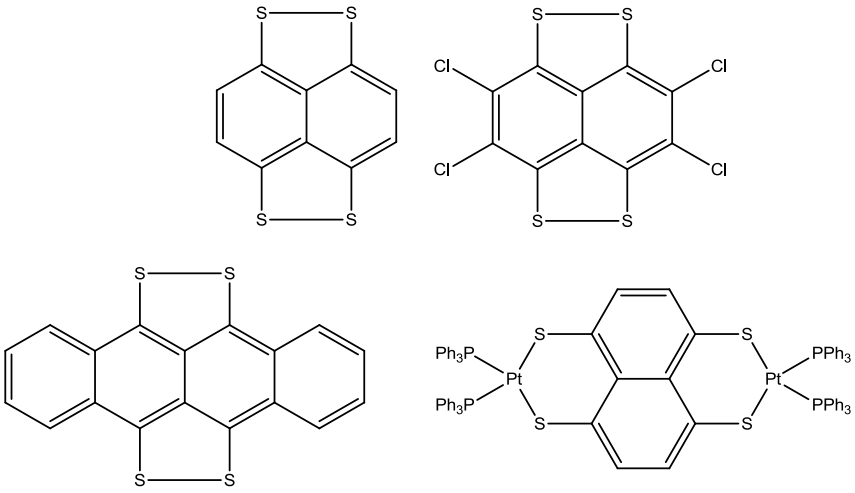

Figure 3 Structures of TTN, TCTTN, TTT and the platinum *bis*phosphine complex of TTN.[9]

Platinum complexes of naphtho[1,8-*cd*][1,2]dithiole, naphtho[1,8-*cd*][1,2]diselenole and naphtho[1,8-*cd*][1,2]selanthiole were obtained by an oxidative addition reaction of the corresponding naphthalene derivative with $[Pt(PPh_3)_4]$ in toluene at room temperature (Scheme 1). The trimethylphosphine derivatives were synthesised by an oxidative addition reaction of the dichalcogen naphthalene with $[Pt(C_2H_4)(PMe_3)_2]$, which was generated *in situ*, under an ethene atmosphere, by reduction of $[Pt(PMe_3)_2Cl_2]$ with two equivalents of lithium triethylborohydride or sodium naphthalide in THF.[11]

The acenaphthene-, phenanthrene-, 2-*tert*-butyl-substituted naphthalene dithiolate and the oxides of naphtho[1,8-*cd*]-1,2-dithiole (with the exception of the tetra oxide) were also successfully complexed to platinum *bis*phosphines through the oxidative addition route with $[Pt(PPh_3)_4]$ (Scheme 1).[11]

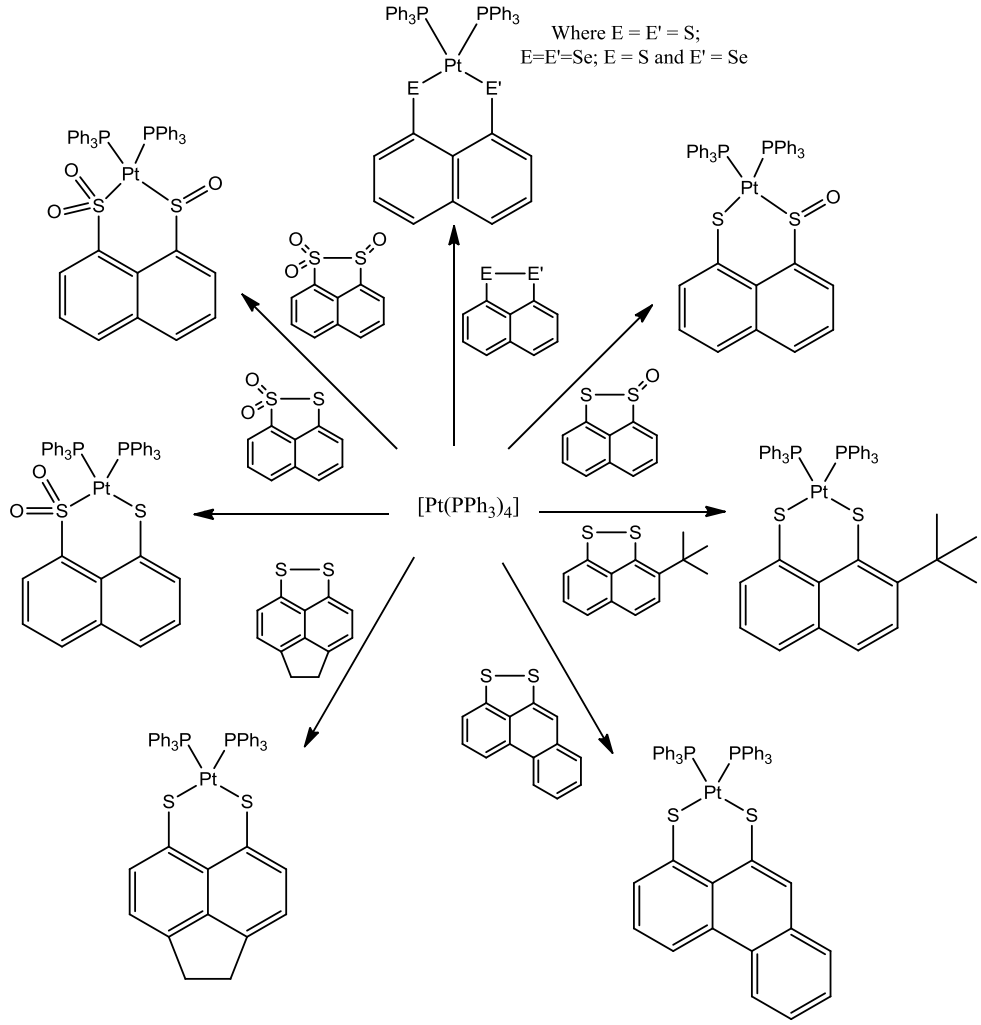

Scheme 1 Oxidative addition reactions of dichalcogen ligands to platinum *bis*phosphines.[11]

The naphtho[1,8-*cd*][1,2]dithiole, naphtho[1,8-*cd*][1,2]diselenole and naphtho[1,8-*cd*][1,2]selanthiole platinum complexes were also prepared through a metathetical reaction of the dilithio-1,8-dichalcogenato naphthalene, which was reacted with *cis*-$[Pt(PR_3)_2Cl_2]$ (where R = Ph or Me) in THF at room temperature (Scheme 2).[11]

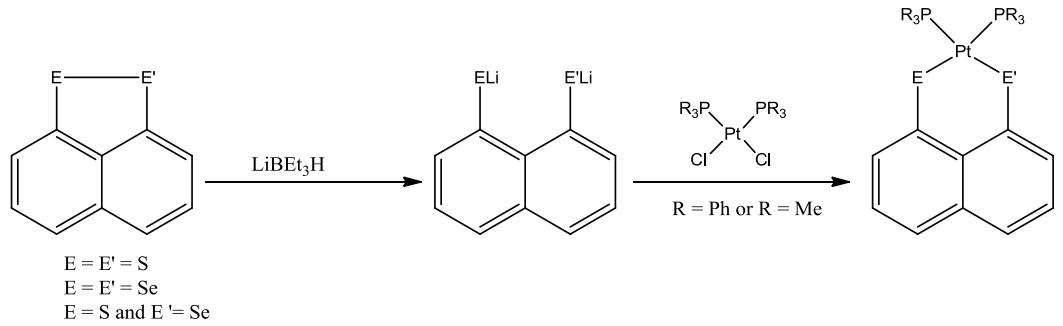

Scheme 2 Metathetical reactions of dichalcogen ligands to platinum *bis*phosphines.[11]

As previously mentioned, the oxidative addition reaction of the tetra oxide derivative of naphtho[1,8-*cd*][1,2]dithiole with $[Pt(PPh_3)_4]$ was unsuccessful. However, the desired complex was obtained by reacting the disodium salt of naphthalene-1,8-disulfinic acid with *cis*-$[Pt(PPh_3)_2Cl_2]$. The reaction was also repeated using *cis*-$[Pt(PMe_2Ph)_2Cl_2]$ (Scheme 3).[11]

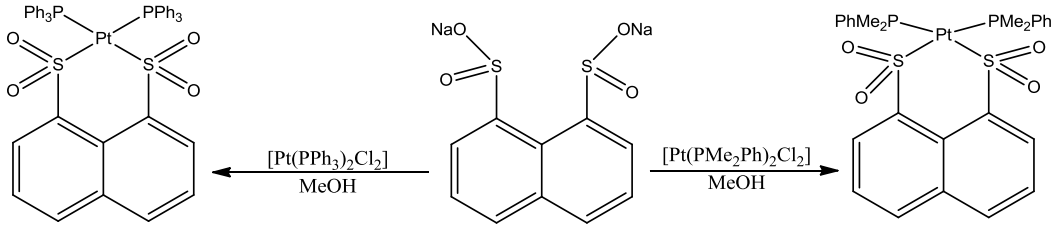

Scheme 3 Reaction of disodium salt of naphthalene-1,8-disulfinic acid with platinum *bis*phosphines.[11]

The initial aims of the research were to investigate the coordination chemistry of 1,8-naphthosultone and 1,8-naphthosultam. In the following we describe the reactions of the two ligands with a series of *cis*-dichloro*bis*(phosphine)platinum species. The resulting platinum-complexes are compared through structural analysis and ^{31}P NMR.

Results and Discussion

In order to analyse the impact on the *peri*-naphthalene system caused by forming platinum complexes, the crystal structures of 1,8-naphthosultone (**1**) and 1,8-naphthosultam (**2**) were first studied.

The crystal structure of 1,8-naphthosultone shows a *peri* sulfur-oxygen bond distance of 1.6407(14) Å. This is shorter than the 2.44 Å[4] *peri*-distance in unsubstituted naphthalene; which is expected as there is a bond between the *peri*-substituents. However, it is longer than the typical sulfur-oxygen bond in a (C-O-SO_2-C) system (1.577 Å)[12] due to the rigid naphthalene backbone causing the sulfur-oxygen bond to be stretched. The *peri*-angles in naphthalene are 118.3(1)°, 120.6(1)° and 118.3(1)° with the sum being 357.2°.[5] In 1,8-naphthosultone the sum of the bay angles is 333.31(12)°, less than those of ideal naphthalene confirming a favourable interaction is occurring between the *peri*-atoms resulting in a *peri*-bond. There is little distortion to the geometry of the naphthalene carbon skeleton with torsion angles deviating by 0.62° and 0.86° from the 'ideal' 180°. Minor out-of-plane distortion is also observed with the oxygen atom sitting 0.018(1) Å above the naphthyl plane. The sulfur atom, however, lies in the naphthyl plane.

The crystal structure of 1,8-naphthosultam shows a sulfur-nitrogen bond distance of 1.676(9) Å. Similar to 1,8-naphthosultone this bond distance is longer than the 1.633 Å sulfur-nitrogen bond length for a typical (C-SO_2-NH-C) system.[12] The *peri*-bond in 1,8-naphthosultone is shorter than that in 1,8-naphthosultam and this can be explained by the decrease in the covalent radii from nitrogen (0.75 Å)[4] to oxygen (0.73 Å)[4] and also the difference in electronegativity between sulfur-oxygen (2.5-3.5)[13] and sulfur-nitrogen (2.5-3.0).[13]

The sum of the bay angles in 1,8-naphthosultam is 334.4(12)°, which indicates that the atoms have moved closer together due to a favourable interaction, again confirming the presence of the *peri*-bond. In comparison to 1,8-naphthosultone there is greater, though still minor, distortion of the naphthalene geometry with torsion angles of 179.2(6)° and 177.8(7)°. The sulfur atom lies in the naphthyl plane; however, the nitrogen atom lies below the plane by a distance of 0.110(1) Å.

In a typical trigonal pyramidal nitrogen species, such as NH_3, the angle observed between the substituents is 107°.[14] In 1,8-naphthosultam the S(1)-N(9)-C(9) angle is 113.0(7)° this is due to the nitrogen being held in a rigid five-membered ring system [C(10)-C(9)-N(9)-S(1)-C(1)].

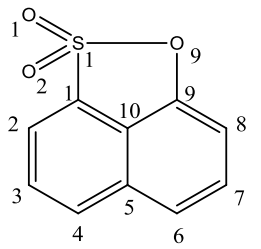

(1)

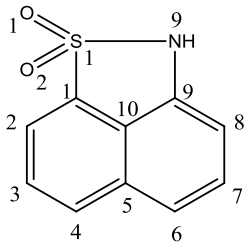

(2)

Figure 4 X-ray crystallography numbering scheme for **1** and **2**.

Table 1 Selected Bond Lengths [Å] and Angles [°] for compounds **1** and **2**.

Compound	**1**	**2**
X-ray code	afdw28	afdw23
E, E'	SO_2, O	SO_2, NH
E(1), E(9)	S, O	S, N
Peri-region distance		
E(1)-E(9)	**1.6407(14)**	**1.676(9)**
Bond lengths		
C(1)-S(1)	1.760(3)	1.756(9)
C(9)-E(9)	1.402(4)	1.374(11)
S(1)-O(1)	1.424(3)	1.440(6)
S(1)-O(2)	1.4243(18)	1.431(6)
C(1)-C(2)	1.372(2)	1.319(13)
C(2)-C(3)	1.422(4)	1.420(15)
C(3)-C(4)	1.379(3)	1.387(16)
C(4)-C(5)	1.423(3)	1.484(14)
C(5)-C(10)	1.405(4)	1.392(11)
C(5)-C(6)	1.421(3)	1.398(17)
C(6)-C(7)	1.373(3)	1.34(3)
C(7)-C(8)	1.425(4)	1.402(15)
C(8)-C(9)	1.358(3)	1.388(12)
C(9)-C(10)	1.406(3)	1.443(11)
C(1)-C(10)	1.390(3)	1.348(12)
Peri-region bond angles		
E(1)-C(1)-C(10)	106.63(15)	110.2(7)

C(1)-C(10)-C(9)	114.9(3)	113.4(7)
E(9)-C(9)-C(10)	111.78(17)	110.8(7)
∑ of bay angles	**333.31(22)**	**334.4(12)**
Splay angle[a]	-26.69	-25.6
Bond angles		
C(4)-C(5)-C(6)	128.3(3)	129.0(10)
E(9)-E(1)-C(1)	95.15(10)	92.1(4)
E(1)-E(9)-C(9)	111.54(13)	113.0(7)
O(1)-S(1)-O(2)	118.53(13)	116.3(3)
O(1)-S(1)-E(9)	107.01(9)	109.41(1)
O(2)-S(1)-E(9)	107.31(9)	108.06(1)
C(1)-S(1)-O(1)	113.03(11)	113.9(4)
C(1)-S(1)-O(2)	112.77(12)	114.1(4)
Out of plane displacement		
E(1)	+0.001(1)	+0.003(1)
E(9)	+0.018(1)	-0.110(1)
Central naphthalene ring torsion angles		
C(6)-C(5)-C(10)-C(1)	179.14(16)	177.8(7)
C(4)-C(5)-C(10)-C(9)	-179.38(16)	179.2(6)

[a]Splay angle: ∑ of the three bay region angles - 360.

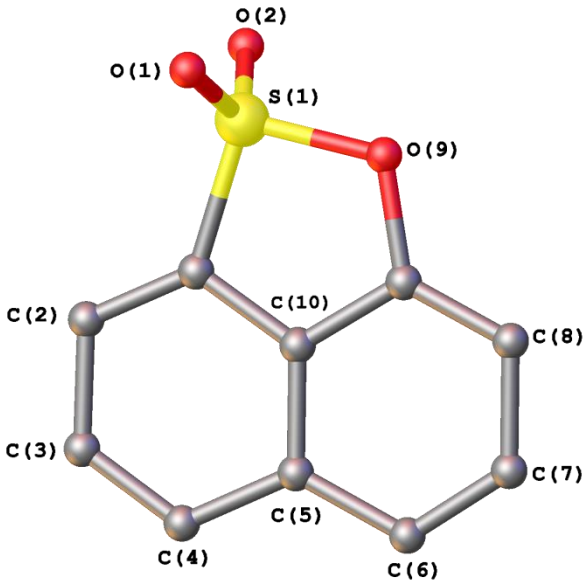

Figure 5 The molecular structure of 1,8-naphthosultone (**1**) with H atoms omitted for clarity.[15]

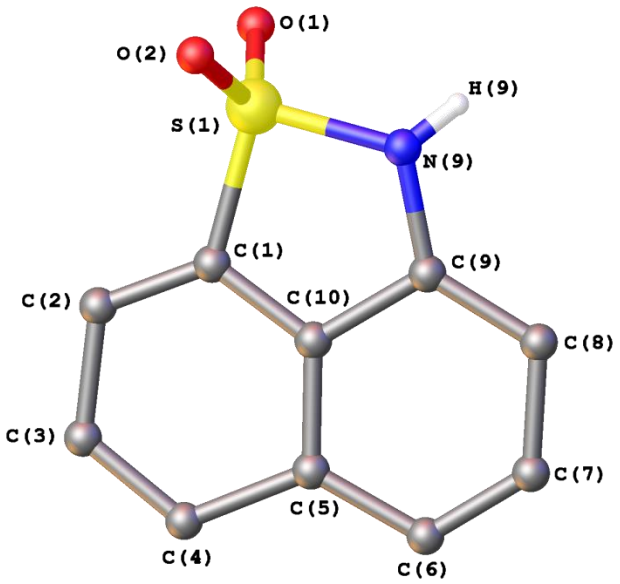

Figure 6 The molecular structure of 1,8-naphthosultam (**2**) with C-H atoms omitted for clarity.

Platinum Complexes of 1,8-Naphthosultone

The sulfur-oxygen bond in 1,8-naphthosultone was reduced with two equivalents of lithium triethylborohydride to form the dilithio-species, which was then added to a suspension of the appropriate *cis*-dichloro*bis*(phosphine)platinum in THF resulting in the formation of [Pt(1-(SO_2),8-(O)-nap)(PPh_3)$_2$] (**1a**), [Pt(1-(SO_2),8-(O)-nap)(PPh_2Me)$_2$] (**1b**) and [Pt(1-(SO_2),8-(O)-nap)(PMe_2Ph)$_2$] (**1c**).

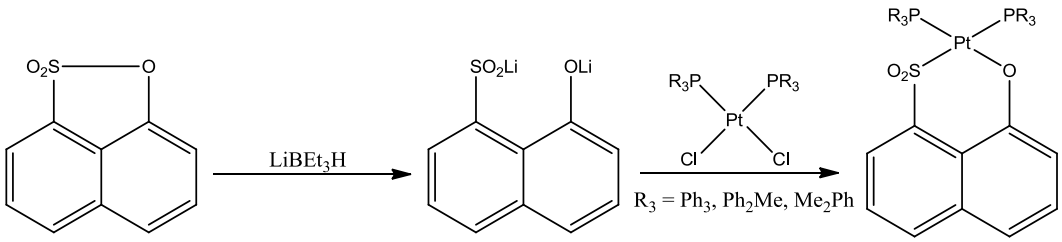

Scheme 4 Reaction route for synthesis of [Pt(1-(SO_2),8-(O)-nap)(PPh_3)$_2$] (**1a**), [Pt(1-(SO_2),8-(O)-nap)(PPh_2Me)$_2$] (**1b**) and [Pt(1-(SO_2),8-(O)-nap)(PMe_2Ph)$_2$] (**1c**).

The $^{31}P\{^1H\}$ NMR ($CDCl_3$) spectra of the three complexes (Table 2) all display similar AX patterns with appropriate platinum satellites. The phosphorus resonances and $^1J(^{31}P\text{-}^{195}Pt)$ coupling

constants of e.g. complex **1a** (Figure 7) are $\delta(P_A)$ = 19.1 ppm (2504 Hz) and $\delta(P_X)$ = 10.6 ppm (3876 Hz) are assigned to the phosphine groups *trans* to the SO_2 group and the oxygen atom, respectively. In previously characterised $[(PPh_3)_2Pt]$ complexes containing (-S(O)R) and -(SR) ligands, the phosphine groups *trans* to the (-S(O)R) group have smaller $^{1}J(^{31}P\text{-}^{195}Pt)$ coupling constants because of the larger *trans* influence of the (-S(O)R) moiety.[11]

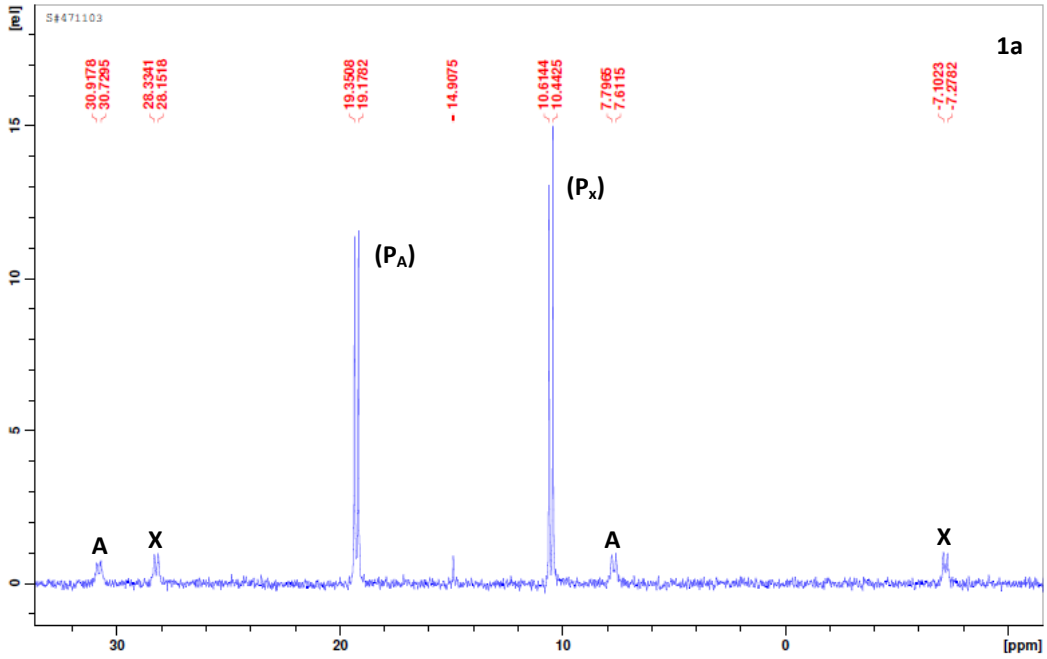

Figure 7 The $^{31}P\{^{1}H\}$ NMR ($CDCl_3$) spectrum for **1a** showing a typical AX pattern with appropriate platinum satellites.

The *trans* influence, also known as the structural *trans* effect, is defined as the ability of a ligand to weaken the bond *trans* to itself.[16] The *trans* influence is a thermodynamic concept and must not be mistaken for the *trans* effect which is a kinetic concept. The *trans* effect, otherwise known as the kinetic *trans* effect, describes the ability of a ligand to alter the lability of a ligand *trans* to itself.[16] If the ligand is a strong σ-donor ligand or π-acceptor ligand then it increases the rate of substitution of a ligand that lies *trans* to itself.[17]

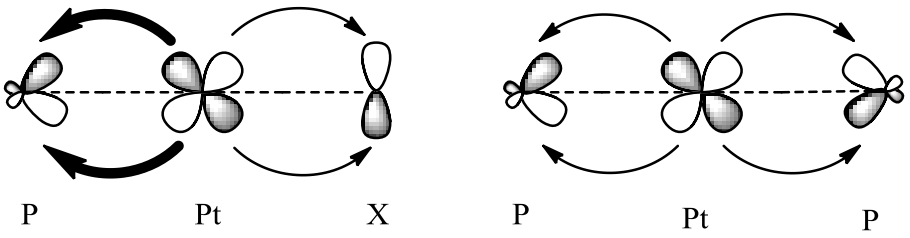

(a) Strong π-back bonding to P when *trans* to X

(b) Competition for π-back bonding when *trans* to P

Figure 8 π-back bonding in Pt-P bonds in (a) *cis*-$[PtCl_2(PR_3)_2]$ and (b) *trans*-$[PtCl_2(PR_3)_2]$.[18]

With regard to *trans* influence, ligands that are poor π-acceptors, e.g. halides, are less competitive than phosphorus ligands for electron back-donation and therefore have lower *trans* influence, (Figure 8 part a) this results in larger coupling constants. In contrast, ligands that are strong π-acceptors, e.g. phosphorus ligands, are more competitive with other phosphorus ligands for electron back-donation and hence have higher *trans* influence. (Figure 8 part b). This results in smaller $^{1}J(^{31}P\text{-}^{195}Pt)$ coupling constants. In the case of the 'sultone' complexes **1a** to **1c** the (-S(O)R) group is a stronger π-acceptor than the oxygen atom resulting in the SO_2 group having a larger *trans* influence than the oxygen atom and hence the smaller $^{1}J(^{31}P\text{-}^{195}Pt)$ coupling constant value has been assigned to the phosphine group *trans* to the SO_2 group. Following this, the remaining resonances and coupling constants have been assigned.

Table 2 $^{31}P\{^{1}H\}$ NMR data for complexes **1a** to **1c**.

Product	**Chemical Shifts [ppm]**		**Coupling Constants [Hz]**		
	$\delta(^{31}P_A)$	$\delta(^{31}P_x)$	$^{1}J(P_A\text{-Pt})$	$^{1}J(P_X\text{-Pt})$	$^{2}J(P_A\text{-}P_X)$
1a	19.1	10.6	2504	3876	19
1b	3.0	-2.4	2537	3700	19
1c	-9.6	-17.6	2504	3603	21

It has been shown that higher $^{1}J(^{31}P\text{-}^{195}Pt)$ coupling constants are observed for more electron withdrawing R groups, with $^{1}J(^{31}P\text{-}^{195}Pt)$ decreasing as phenyl groups are replaced with electron donating methyl groups.[18] It can be seen from Table 2 that there is a steady decrease in value for

$^{1}J(^{31}P_X\text{-}^{195}Pt)$ coupling constant as the phenyl groups are replaced by methyl groups as expected. This effect is less apparent for the signals for the phosphorus *trans* to the SO_2 group. The $^{2}J(^{31}P_A\text{-}^{31}P_X)$ values of 19-21 Hz are indicative of unsymmetrically substituted *cis*-platinum diphosphine complexes.[11]

It was also noted, when the products were left overnight in chlorinated solvent, the solution changed colour from yellow to green. ^{31}P NMR of the green solution showed degradation of product, with the only peaks being those from the corresponding platinum chloro phosphine complex. Similar behaviour was also observed with the platinum complexes of naphthalene-1,8-dichalcogens and the oxidised derivatives of naphtho[1,8-*cd*]-1,2-dithiole.[11] The authors found that addition of small quantities of triethylamine to work-up and NMR solvents prevented decomposition; leading them to conclude that free hydrogen chloride in the solvent was causing decomposition. The same can be concluded in this instance.

X-ray Investigations

Single crystals were obtained for **1a**, **1b** and **1c** by diffusion of hexane into saturated dichloromethane solutions. Both **1a** and **1b** crystallise with two dichloromethane molecules per platinum molecule. The molecular structures of **1a**, **1b** and **1c** are shown in Figures 14, 15 and 16 respectively. In all three structures, as expected from the NMR studies, the 1,8-naphthosultone acts as a bidentate ligand, coordinating to the platinum via the sulfur and the oxygen atom to form a six-membered chelate ring. The central platinum metal adopts a distorted square planar geometry in each case, with angles deviating significantly from the ideal (90°).

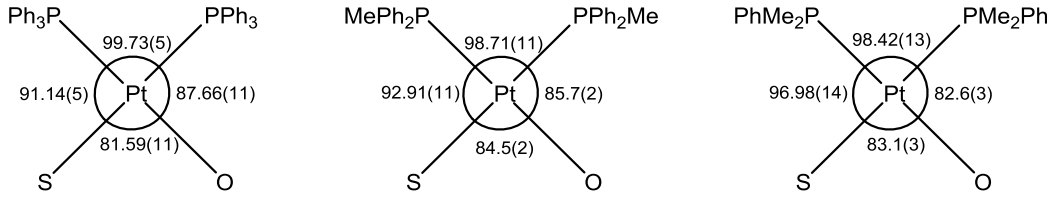

Figure 9 The angles (°) associated with the square planar geometry of the platinum metal in complexes **1a** (left), **1b** (middle) and **1c** (right).

The Tolman cone angles for PPh_3, PPh_2Me and $PPhMe_2$ are 145°, 136° and 122°, respectively.[19] Therefore, one would anticipate a steady contraction in the P-Pt-P angle on going from **1a** to **1c** and this is observed.

In **1a** the P(1)-Pt(1)-P(2) angle of 99.73(5)° is enlarged to greater than the ideal 90° in order to accommodate the bulky *cis*-triphenylphosphine groups. The same applies to the P(1)-Pt(1)-P(2) angle of 98.71(11)° in **1b**. However, it is less enlarged than that of **1a** due to the replacement of a phenyl group with a less sterically demanding methyl group. The S(1)-Pt(1)-O(9) angles, 81.59(11)° and 84.5(2)°, are smaller than 90° due to the restriction imposed by the *peri*-naphthalene geometry which fixes the sulfur and oxygen atoms. The S(1)-Pt(1)-P(1) angles, [91.14(5)° for **1a** and 92.91(11)° for **1b**], are larger than the O(9)-Pt(1)-P(2) angles, [87.66(11)° for **1a** and 85.7(2)° for **1b**].

There are no significant differences in the bond lengths around the platinum centre between **1a** and **1b**. Whilst the effect of *trans* influence on bond weakening does not always cause bond lengthening,[16] in this case, the Pt(1)-P(1) and Pt(1)-P(2) bond lengths are significantly different as a consequence of the differing *trans* influence of the oxygen and the SO_2 group. The Pt(1)-P(1) bond (2.3319(15) Å for **1a** and 2.338(3) Å for **1b**) which is *trans* to SO_2 is longer than the Pt(1)-P(2) bond (2.2480(16) Å for **1a** and 2.252(3) Å for **1b**) which is *trans* to the oxygen.

As expected the *peri*-distance has been elongated due to the breaking of the sulfur-oxygen bond and insertion of the platinum. The non-bonded sulfur-oxygen distance being 2.842(3) Å for **1a** and 2.928(7) Å for **1b** compared to the bonded distance of 1.6407(14) Å in the free ligand **1**. However, the *peri*-distance in the two complexes is still shorter than the sum of the van der Waals radii for sulfur and oxygen by 12-14%. The increase in *peri*-distance causes an increase in the angles of the bay region, with positive splay angles of 9° and 13° being seen for **1a** and **1b** respectively. This is significantly greater than in 1,8-naphthosultone where there is a negative splay angle of 27° due to the presence of the sulfur-oxygen bond.

Complex **1a** displays greater distortion of the naphthalene backbone than complex **1b**. The non-bonded *peri*-distance and the splay angle in **1b** are larger than those in **1a** resulting in a more relaxed geometry which can accommodate the diphenylmethylphosphine group without causing great distortion to the naphthalene-carbon framework. In 1,8-naphthosultone the sulfur atom

lies on the naphthyl plane and the oxygen atom sits 0.018 Å above the plane. In **1a** the sulfur atom now lies 0.426(1) Å below the naphthyl plane and the oxygen atom 0.271(1) Å above the plane. This distortion is due to a combination of the rigid naphthalene backbone, the maintenance of a square planar environment around the platinum centre and the bulky triphenylphosphine groups. The C(6)-C(5)-C(10)-C(1) and C(4)-C(5)-C(10)-C(9) torsion angles also deviate from the free ligand by *ca.* 5.5-7.0°. In comparison, complex **1b** shows little difference in distortion when compared to the free ligand. The oxygen atom has not moved from its original position and the sulfur atom now sits 0.057(1) Å above the plane. The torsion angles show slight differences which can be deemed negligible.

In the ligand 1,8-naphthosultone (**1**) O(1)-S(1)-O(9) is 107.01(9)° and O(2)-S(1)-O(9) angle is 107.31(9)°. In compounds **1a** and **1b** there is a noticeable difference in these angles. The O(1)-S(1)···O(9) angles are 78.20(1)° and 90.96(1)°, and the O(2)-S(1)···O(9) angles are 164.68(1)° and 154.31(1)° for **1a** and **1b**, respectively. O(1)-S(1)···O(9) has been reduced whereas O(2)-S(1)···O(9) has been enlarged, this is a consequence of the S(1)-O(9) *peri*-bond being broken and the ligand forming a complex with a Pt-PR_3 species.

The differences observed between **1a** and **1b** are due to a combination of steric effects and weak intramolecular interactions. In **1a** two phenyl rings, one from each of the two PPh_3 groups, adopt face-to-face alignment leading to a weak π···π interaction (Figure 10) with a Cg(C23-C28)····Cg(C29-C34) distance of 3.605(1) Å (where Cg = centroid). In going from **1a** to **1b** not only is the strain on the naphthalene system reduced by replacing a bulky phenyl group with a methyl group, there is also a change and further weakening of the intramolecular interaction from a π-π interaction to a C-H····π interaction. In **1b** it is now a phenyl ring, from one PPh_2Me group, that is interacting with a methyl group, from the other PPh_2Me group (Figure 10) giving a C11-H11····Cg(C25-C30) distance of 3.696(1) Å.

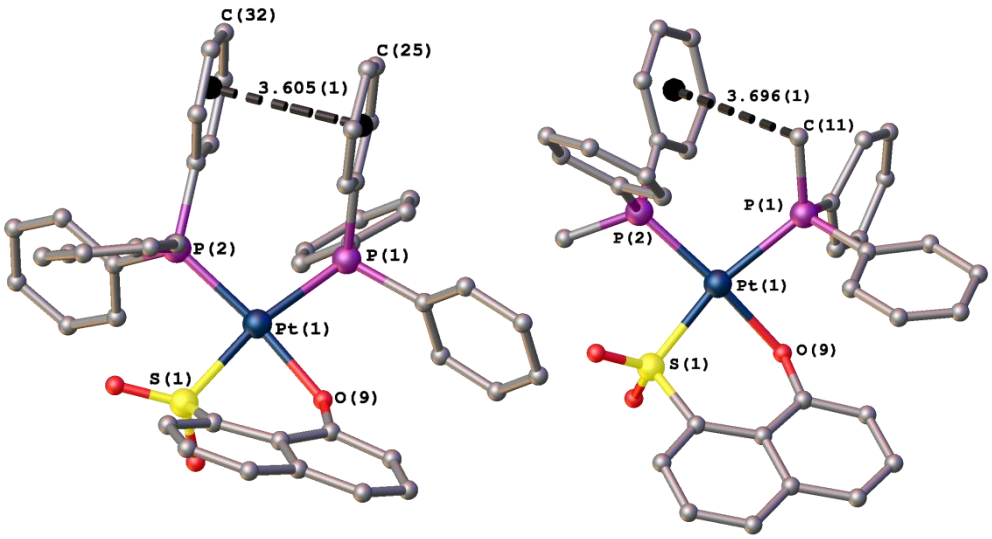

Figure 10 The crystal structures of **1a** and **1b** showing weak π···π and C-H···π interactions.

One would expect that replacing another phenyl with a methyl would result in less steric strain and in turn even less distortion of the naphthalene system. However, for complex **1c** this proved not to be the case. In **1c** it would appear that the intramolecular interaction may dominate over steric effects, which in turn causes the complex to become more distorted than that of **1b**, but less than that of **1a**. Like **1b**, **1c** also has a weak C-H····π interaction (Figure 11) with a C18-H18····Cg(C19-C24) distance of 3.602(1) Å. This distance is shorter than that in **1b**, resulting in a stronger interaction which in turn will have more effect on the overall molecular structure of the complex.

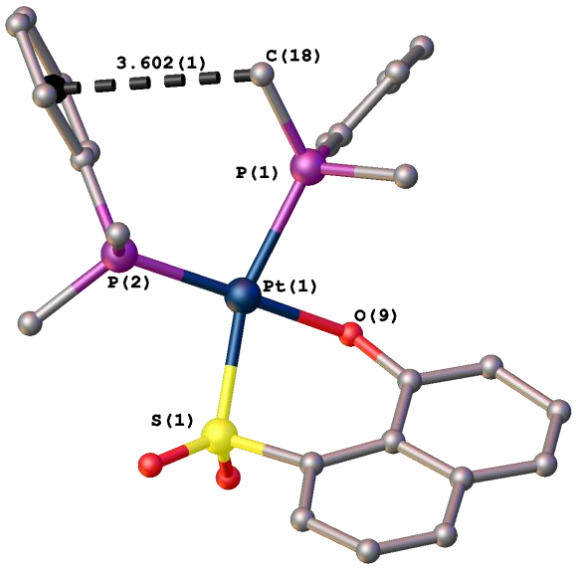

Figure 11 The crystal structures of **1c** showing the weak C-H···π interaction.

1c has a P(1)-Pt(1)-P(2) angle of 98.42(13)° (Figure 9), although this is greater than the ideal 90° square planar geometry, it is still similar to those observed in **1a** and **1b**, which are 99.73(5)° and 98.71(11)°, respectively. The S(1)-Pt(1)-O(9) angle of 83.1(3)° is intermediate to those of **1a**, 81.59(11)°, and **1b**, 84.5(2)°, this is due to the dominating intramolecular interactions that occur in **1c**. The S(1)-Pt(1)-P(1) angles, [91.14(5)° for **1a** and 92.91(11)° for **1b**], are larger than the O(9)-Pt(1)-P(2) angles, [87.66(11)° for **1a** and 85.7(2)° for **1b**]. The same is true for **1c** with an S(1)-Pt(1)-P(1) angle of 96.98(14)° and an O(9)-Pt(1)-P(2) angle of 82.6(3)°.

1c has similar bond lengths around the platinum centre to **1a** and **1b**. The Pt(1)-P(1) bond length of 2.325(4) Å and Pt(1)-P(2) bond length of 2.234(4) Å are significantly different as a consequence of the differing *trans* influence of the oxygen and the SO_2 group. This is also seen for **1a** and **1b**.

As expected the *peri*-distance in **1c** is elongated due to the breaking of the sulfur-oxygen bond and insertion of the platinum, the non-bonded sulfur-oxygen distance being 2.889(6) Å compared to the bonded distance of 1.6407(14) Å in the free ligand **1**. The *peri*-distance is 2.842(3) Å for **1a** and 2.928(7) Å for **1b**. The *peri*-distance of **1c** is intermediate between **1a** and **1b**, again this is due to the competition between steric effects and intramolecular interactions. The *peri*-distance in the three complexes is shorter than the sum of the van der Waals radii for sulfur and oxygen

by 12-14%. The increase in *peri*-distance causes an increase in the angles of the bay region, with positive splay angles of 9°, 13° and 11° being seen for **1a**, **1b** and **1c** respectively.

Complex **1c** displays distortion of the naphthalene backbone that is intermediate between complex **1a** and **1b**. The non-bonded *peri*-distance and the splay angle in **1c** are also intermediate resulting in a more relaxed geometry than **1a**, but a more strained geometry than **1b**. In 1,8-naphthosultone the sulfur atom lies in the naphthyl plane and the oxygen atom sits 0.018(1) Å above the plane. By comparison, in **1c** the sulfur atom now lies 0.379(1) Å above the naphthyl plane and the oxygen atom 0.231(1) Å below the plane. Again this distortion is intermediate to that of **1a** and **1b** and is due to a combination of the rigid naphthalene backbone, the maintenance of a square planar environment around the platinum centre and the intramolecular interaction that is occurring within the complex. The torsion angles, C(6)-C(5)-C(10)-C(1) and C(4)-C(5)-C(10)-C(9), also deviate from the free ligand by *ca.* 3.5-7.0°.

The O(1)-S(1)···O(9) angle in **1c** is 81.00(1)° and the O(2)-S(1)···O(9) angle is 162.24(1)°. The O(1)-S(1)···O(9) angles are 78.20(1)° and 90.96(1)°, and the O(2)-S(1)···O(9) angles are 164.68(1)° and 154.31(1)° for **1a** and **1b**, respectively. Therefore, the angles seen in **1c** are intermediate between **1a** and **1b**. This falls into the pattern seen with other features of these complexes and we speculate that this is due to the competition between steric effects and intramolecular interactions, discussed earlier.

As already mentioned, in all three structures the 1,8-naphthosultone acts as a bidentate ligand, coordinating to the platinum via the sulfur and the oxygen atom to form a six-membered chelate ring. This six-membered $PtSOC_3$ ring can be described as having a twisted envelope type conformation with the S···O vector as the hinge (Figure 12). In **1a** and **1c**, C(1), C(10) and C(9) all lie in a plane but S(1) and O(9) are displaced above and/or below this plane, resulting in a non-planar, twisted $PtSOC_3$ ring. In **1b** the S(1) and O(9) atoms are located closer to the C_3 plane and subsequently the six-membered ring is less twisted. The displacement of Pt(1) from the mean O(9), S(1), C(1), C(10), C(9) plane is comparable for **1a** and **1c** with distances of 1.343(1) Å and 1.335(1) Å, respectively. Whereas, **1b** has a lower Pt(1) displacement of 1.149(1) Å. The angle of the hinge is also comparable for **1a** and **1c** with values of 54.22(1)° and 54.77(1)°, respectively. **1b** has a smaller hinge angle of 44.34(1)°. These differences are due to there being less distortion of the naphthalene backbone in **1b**.

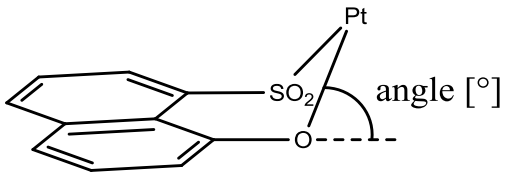

Figure 12 Diagram illustrating the twisted envelope type confirmation adopted by **1a**, **1b** and **1c**.

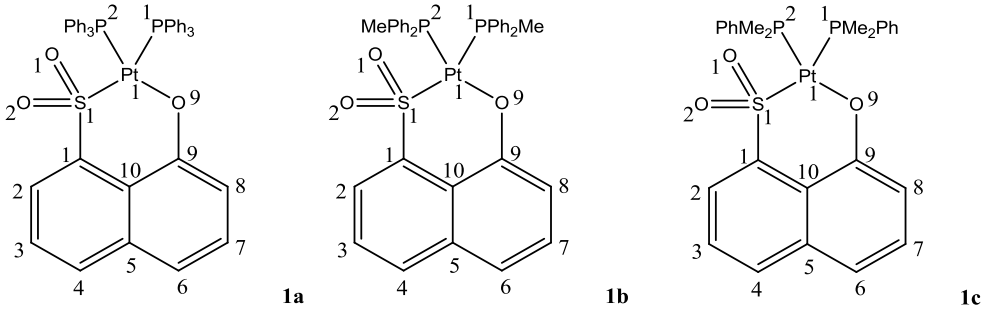

Figure 13 X-ray crystallography numbering scheme for **1a**, **1b** and **1c**.

Table 3 Selected Bond Lengths [Å] and Angles [°] of **1a** to **1c.**

Compound	**1a**	**1b**	**1c**
X-ray Code	afdw37	loud41r	ld072N
E, E'	SO_2, O	SO_2, O	SO_2, O
E(1), E(9)	S, O	S, O	S, O
Peri-region distance and sub-van der Waals contacts			
E(1)···E(9)	**2.842(3)**	**2.928(7)**	**2.889(6)**
Σr_{vdW} - E(1)···E(9); % Σr_{vdW}[a]	0.478;86	0.391; 88	0.431; 87
Naphthalene bond lengths			
C(1)-C(2)	1.373(8)	1.384(16)	1.36(3)
C(2)-C(3)	1.411(9)	1.388(18)	1.40(3)
C(3)-C(4)	1.354(9)	1.379(16)	1.34(3)
C(4)-C(5)	1.435(9)	1.437(18)	1.41(3)
C(5)-C(10)	1.430(8)	1.450(16)	1.44(3)
C(5)-C(6)	1.408(9)	1.433(16)	1.44(3)
C(6)-C(7)	1.370(9)	1.342(19)	1.37(3)
C(7)-C(8)	1.407(9)	1.415(18)	1.44(3)

C(8)-C(9)	1.380(9)	1.385(14)	1.40(3)
C(9)-C(10)	1.443(9)	1.414(16)	1.42(3)
C(1)-C(10)	1.422(9)	1.432(14)	1.415(18)
Peri-region bond angles			
E(1)-C(1)-C(10)	120.7(4)	124.8(9)	123.3(13)
C(1)-C(10)-C(9)	123.2(5)	124.9(10)	123.5(14)
E(9)-C(9)-C(10)	125.0(6)	123.5(9)	124.4(14)
∑ of bay angles	**368.9(9)**	**373.2(16)**	**371.2(24)**
Splay angle[b]	8.9	13.2	11.2
Bond angles			
C(4)-C(5)-C(6)	122.2(6)	119.7(11)	122.4(15)
O(1)-S(1)-O(2)	114.1(2)	113.9(4)	115.6(6)
O(1)-S(1)···O(9)	78.20(1)	90.96(1)	81.00(1)
O(2)-S(1)···O(9)	164.68(1)	154.31(1)	162.24(1)
C(1)-S(1)-O(1)	105.3(3)	105.2(5)	104.9(7)
C(1)-S(1)-O(2)	107.0(3)	104.6(5)	105.2(7)
Out of plane displacement			
E(1)	-0.426(1)	+0.057(1)	+0.379(1)
E(9)	+0.271(1)	+0.023(1)	-0.231(1)
Central naphthalene ring torsion angles			
C(6)-C(5)-C(10)-C(1)	174.4(5)	-178.7(10)	172.8(12)
C(4)-C(5)-C(10)-C(9)	173.4(6)	-178.8(10)	176.6(11)
Platinum geometry - bond lengths			
Pt(1)-P(1)	2.3319(15)	2.338(3)	2.325(4)
Pt(1)-P(2)	2.2480(16)	2.252(3)	2.234(4)
Pt(1)-E(1)	2.2764(15)	2.275(3)	2.291(4)
Pt(1)-E(9)	2.067(4)	2.074(7)	2.057(10)
Platinum geometry - bond angles			
E(1)-Pt(1)-E(9)	81.59(11)	84.5(2)	83.1(3)
E(1)-Pt(1)-P(1)	169.05(5)	166.09(10)	162.30(13)
E(1)-Pt(1)-P(2)	91.14(5)	92.91(11)	96.98(14)
E(9)-Pt(1)-P(1)	87.66(11)	85.7(2)	82.6(3)
E(9)-Pt(1)-P(2)	171.78(11)	167.7(2)	173.7(3)
P(1)-Pt(1)-P(2)	99.73(5)	98.71(11)	98.42(13)
Intramolecular Interactions			
Cg(C23-C28)····Cg(C29-C34)	3.605(1)	-	-
Cg(C25-C30)····H11-C11	-	3.697(1)	
Cg(C19-C24)····H18-C18	-	-	3.602(1)

[a] van der Waals radii used for calculations: r_{vdW}(S) 1.80 Å, r_{vdW}(O) 1.52 Å.[4]

[b] Splay angle: ∑ of the three bay region angles - 360.

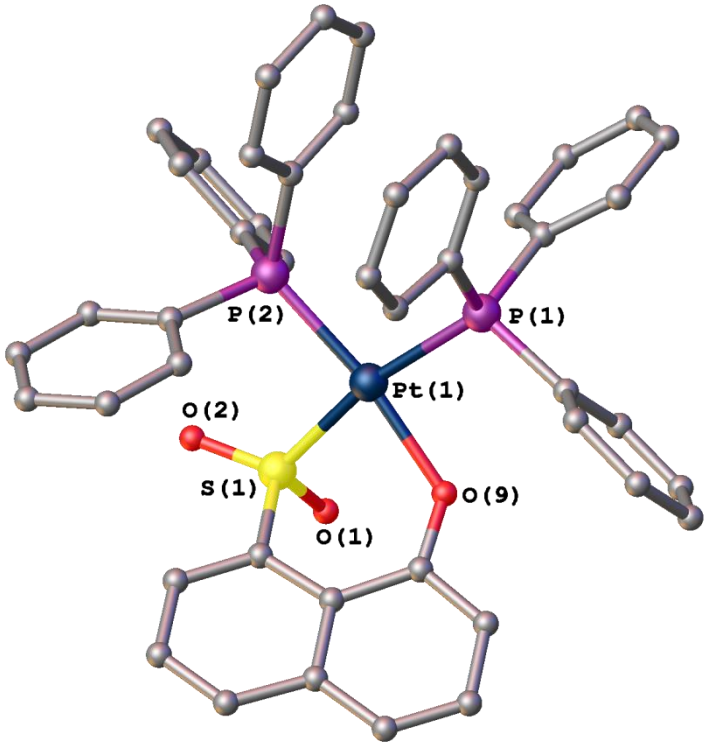

Figure 14 The molecular structure of **1a** with H atoms and solvent molecules omitted for clarity.

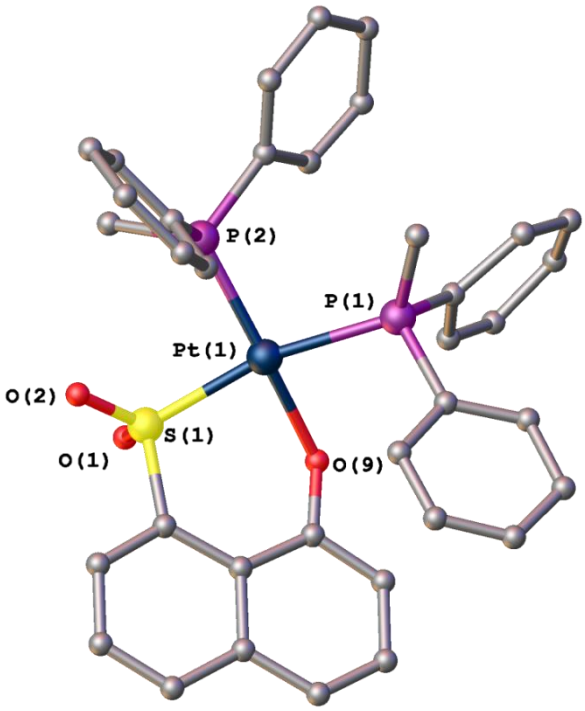

Figure 15 The molecular structure of **1b** with H atoms and solvent molecules omitted for clarity.

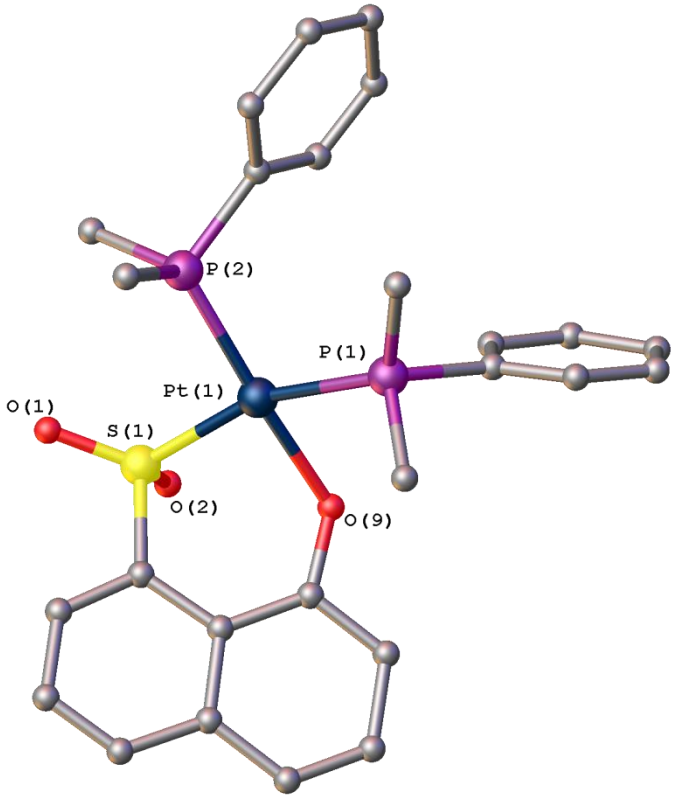

Figure 16 The molecular structure of **1c** with H atoms omitted for clarity.

Other work

The oxidative addition reaction utilised by the Woollins group involves reduction of the *cis*-dichloro*bis*(trimethylphosphine)platinum with two equivalents of lithium triethylborohydride or sodium naphthalide in THF under an ethene atmosphere to form, *in situ*, the zero-valent platinum-ethene derivative which is then reacted with the dichalcogenole naphthalene to give the desired product (Scheme 5).[11]

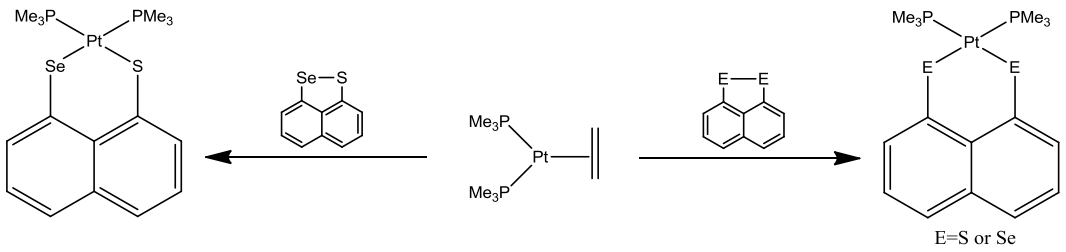

Scheme 5 Oxidative addition reactions of dichalcogen ligands with trimethylphosphine derivative.[11]

The metathesis reaction was used to prepare **1a**, **1b** and **1c** through reaction of the corresponding $[PtCl_2(PR_3)_2]$ with the dilithio-sultone species (Scheme 2).

Both the metathesis and oxidative addition reactions were utilised in attempts to prepare the sultone complex $[Pt(1\text{-}(SO_2),8\text{-}(O)\text{-nap})(PMe_3)_2]$. However, both reactions failed to yield the product. ^{31}P NMR revealed that the only phosphorus species present was *cis*-dichloro*bis*(trimethylphosphine)platinum. Reasons for this reaction being unsuccessful are unknown.

The metathesis reaction was attempted to prepare the sultone complex $[Pt(1\text{-}(SO_2),8\text{-}(O)\text{-nap})(COD)]$ *via* $[PtCl_2(COD)]$, again this reaction failed for unknown reasons. A search of the CCDC revealed only one compound where COD is bound via platinum to sulfur and oxygen. The complex $[Pt_2(\mu\text{-}SO_3)(\mu\text{-}SO_2)(C_8H_{12})_2]$ (Figure 17) formed as a result of $[Pt_2(\mu\text{-}SO_2)_2(C_8H_{12})_2]$ being slowly oxidised in the air.[20]

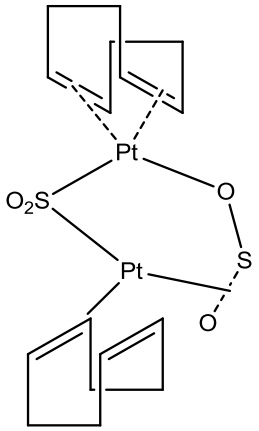

Figure 17 The $[Pt_2(\mu\text{-}SO_3)(\mu\text{-}SO_2)(C_8H_{12})_2]$ complex prepared by D. H. Farrar and R. R. Gukathasan.[20]

Platinum Complexes of 1,8-Naphthosultam

One equivalent of 1,8-naphthosultam was initially reacted with two equivalents of lithium triethylborohydride with the anticipation that it would reduce the sulfur-nitrogen bond and form the dilithio-species, which could then react with one equivalent of *cis*-dichloro*bis*(triphenylphosphine)platinum to form the $[Pt(1\text{-}(SO_2),8\text{-}(N)\text{-}nap)(PPh_3)_2]$ complex. This reaction has been successfully carried out previously within the Woollins' group on a variety of *peri*-substituted naphthalenes with success[11] and also proceeds as expected with 1,8-naphthosultone. However, it was found that with 1,8-naphthosultam, lithium triethylborohydride deprotonates the nitrogen and does not reduce the sulfur-nitrogen bond (Scheme 6). Instead the $[Pt(PPh_3)_2Cl_2]$ complex loses a chloride and complexes to the nitrogen to give mono-substituted $[Pt(1\text{-}(SO_2),8\text{-}(N)\text{-}nap)(PPh_3)_2(Cl)]$ (**mono-2a**).

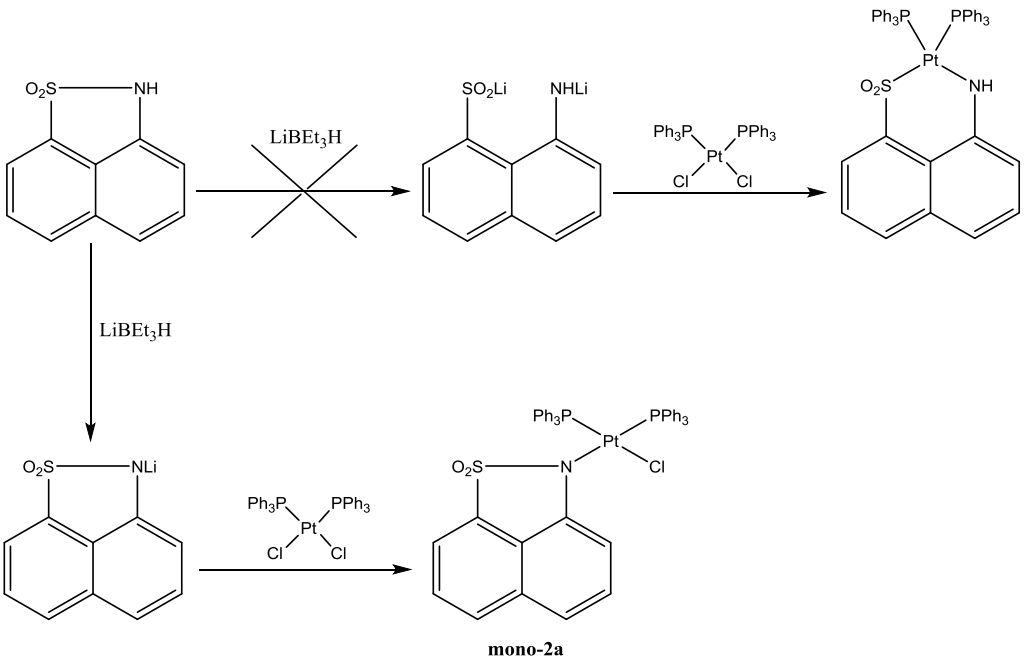

Scheme 6 Anticipated route of reaction and actual route of reaction for 1,8-naphthosultam and lithium triethylborohydride.

This can be rationalised by considering the influence the SO_2 group has on the acidity of the NH group; the basic lithium triethylborohydride would rather deprotonate the acidic nitrogen than reduce the sulfur-nitrogen bond.

This deprotonation reaction occurred with all *cis*-dichloro*bis*(phosphine)platinum species, resulting in a series of mono-substituted complexes: [Pt(1-(SO_2),8-(N)-nap)($PPh_2Me)_2$(Cl)] (**mono-2b**), [Pt(1-(SO_2),8-(N)-nap)($PPhMe_2)_2$(Cl)] (**mono-2c**) and [Pt(1-(SO_2),8-(N)-nap)($PMe_3)_2$(Cl)] (**mono-2d**). The reaction was also successful with (1,5-cyclooctadiene)platinum(II) dichloride to give [Pt(1-(SO_2),8-(N)-nap)(COD)(Cl)] (**mono-2e**) (Figure 18).

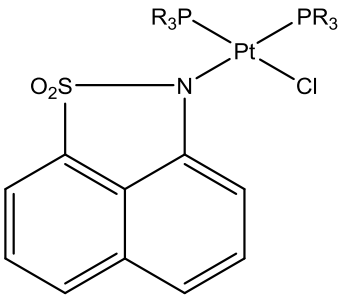

Where R_3 = Ph_3 (**mono-2a**),
Ph_2Me (**mono-2b**),
Me_2Ph (**mono-2c**),
Me_3 (**mono-2d**)

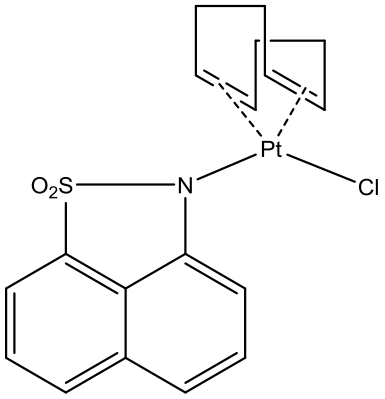

COD = **mono-2e**

Figure 18 1,8-naphthosultam mono-platinum complexes.

The $^{31}P\{^{1}H\}$ NMR ($CDCl_3$) data for the complexes (Table 4) are similar in that the spectra all have an AX pattern with appropriate platinum satellites. The phosphorus resonances and $^{1}J(^{31}P\text{-}^{195}Pt)$ coupling constants of complex **mono-2a** $\delta(P_A)$ = -16.3 ppm (3804 Hz) and $\delta(P_X)$ = 8.4 ppm (3328 Hz) are assigned to the phosphine groups *trans* to the nitrogen atom and the chlorine atom, respectively. In these complexes, the chlorine atom has a larger *trans* influence than the nitrogen atom and hence the smaller $^{1}J(^{31}P\text{-}^{195}Pt)$ coupling constant value has been assigned to the phosphine group *trans* to the chlorine. Following this, the resonances and coupling constants for the remaining complexes have been assigned.

Similar to the 1,8-naphthosultone complexes, a steady decrease in value for $^{1}J(^{31}P_A\text{-}^{195}Pt)$ coupling constant is seen as the phenyl groups are replaced by methyl groups. The same decrease is also seen for the $^{1}J(^{31}P_x\text{-}^{195}Pt)$ coupling constants. The $^{2}J(^{31}P_A\text{-}^{31}P_X)$ values of 19-21 Hz are indicative of un-symmetrically substituted *cis*-platinum diphosphine complexes.[11]

Table 4 Comparison of ^{31}P NMR data for products from lithium triethylborohydride reactions.

	Chemical Shifts [ppm]		Coupling Constants [Hz]		
Product	$\delta(^{31}P_A)$	$\delta(^{31}P_x)$	$^{1}J(P_A\text{-}Pt)$	$^{1}J(P_X\text{-}Pt)$	$^{2}J(P_A\text{-}P_X)$
mono-2a	-16.3	8.4	3804	3328	19
mono-2b	-2.8	-5.8	3698	3260	20
mono-2c	-10.9	-18.3	3577	3159	21
mono-2d	-26.1	-22.1	3507	3179	22

Unfortunately, ^{31}P NMR revealed that the reactions were not going to completion, with peaks seen for the corresponding *cis*-dichloro*bis*(phosphine)platinum reagent. It was therefore decided that instead of using lithium triethylborohydride we would use the non-nucleophilic base 1,8-diazabicyclo[5.4.0]undec-7-ene (DBU) to purposely deprotonate the nitrogen. Therefore, 1,8-naphthosultam was reacted with DBU and the corresponding *cis*-dichloro*bis*(phosphine)platinum in a 1:1:1 ratio.

The ^{31}P NMR data from the DBU reactions was in agreement with the data from the lithium triethylborohydride reactions indicating formation of the mono-platinum complexes (Figure 19). In addition, the crystal structure of the product obtained from the DBU reaction of *cis*-dichloro*bis*(triphenylphosphine)platinum was the same as that from the lithium triethylborohydride reaction, product **mono-2a**.

Table 5 Comparison of ^{31}P NMR data for products from DBU reactions.

	Chemical Shifts [ppm]		Coupling Constants [Hz]		
Product	$\delta(^{31}P_A)$	$\delta(^{31}P_x)$	$^{1}J(P_A\text{-}Pt)$	$^{1}J(P_X\text{-}Pt)$	$^{2}J(P_A\text{-}P_X)$
mono-2a	-16.3	8.4	3798	3338	19
mono-2b	2.4	-5.9	3708	3255	20
mono-2c	-10.9	-18.2	3594	3221	21
mono-2d	-26.2	-22.1	3508	3165	23

DBU reacted to give clean product with no unreacted *cis*-dichloro*bis*(triphenylphosphine)platinum peaks present. However, there were peaks for a secondary product (Product A) present at δ = 15.1 ppm and δ = 5.9 ppm, platinum satellites were hidden in the baseline and the coupling constants could not be determined (Figure 19).

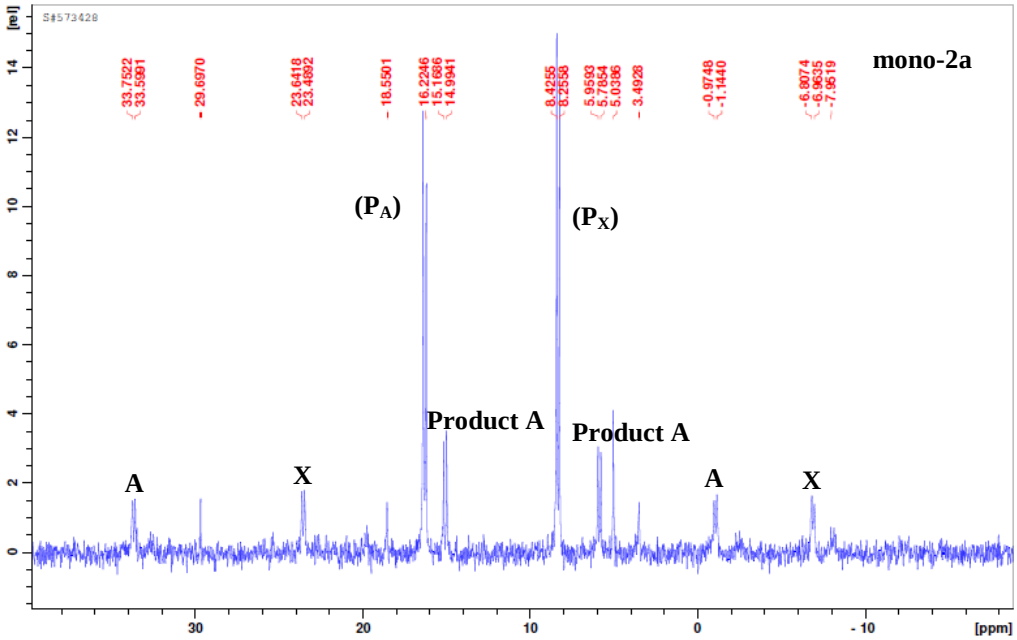

Figure 19 ^{31}P NMR spectrum for reaction of the 1,8-naphthosultam, DBU and *cis*-dichloro*bis*(triphenylphosphine)platinum.

It was suspected that the DBU was involved in a competitive side reaction with the *cis*-dichloro*bis*(triphenylphosphine)platinum. In order to confirm this, the reaction was repeated without 1,8-naphthosultam. Ammonium tetrafluoroborate was added to the reaction to balance the cationic charge of the suspected Pt-DBU complex (Figure 20).

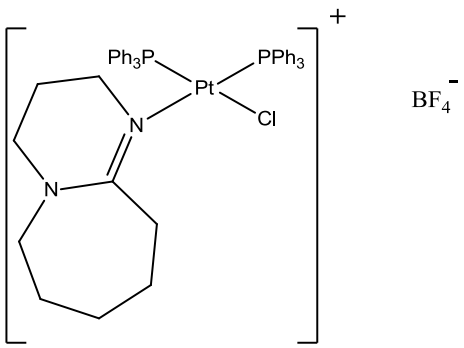

Figure 20 Anticipated structure of the Pt-DBU complex.

The phosphorus resonances and $^{1}J(^{31}P\text{-}^{195}Pt)$ coupling constants were at $\delta(P_A)$ = 14.5 ppm (3857 Hz) and $\delta(P_X)$ = 6.1 ppm (3056 Hz). These values are consistent with the secondary product found in the formation of **mono-2a**, confirming that DBU is indeed reacting with the dichloro*bis*(triphenylphosphine)platinum complex. Formation of the Pt-DBU complex was verified by mass spectrometry (Figure 21) and fluorine NMR. A peak for the cation $[Pt(Cl(PPh_3)_2DBU]^+$ was displayed at *m/z* 907.09 (100%) and a comparison of the fluorine NMR of ammonium tetrafluoroborate (δ = −150.7 to -150.8 ppm (m)) and the product (δ = −152.1(br s, $^{10}BF_4^-$), −152.2(br s, $^{11}BF_4^-$) showed minor differences. Unfortunately, attempts at crystallisation were unsuccessful.

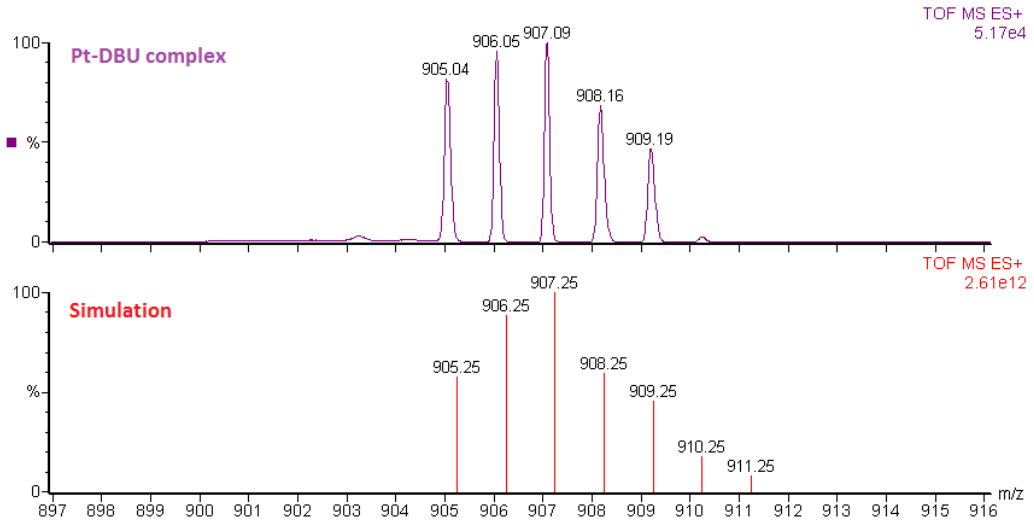

Figure 21 A comparison of the isotope pattern of the Pt-DBU complex and its simulation.

Although DBU reacted with each of the *cis*-dichloro*bis*(phosphine)platinum reagents to give clean product, removal of the Pt-DBU 'side' product proved to be problematic. Purification using column chromatography was not viable as both products elute with the same R_f value and crystallisation was only successful for [Pt(1-(SO_2),8-(N)-nap)(PPh_3)(Cl)] (**mono-2a**).

The unintentional use of lithium triethylborohydride as a base led to formation of product, but the reaction never went to completion; with unreacted *cis*-dichloro*bis*(phosphine)platinum seen in the ^{31}P NMR. This led to the use of DBU to purposely deprotonate the NH group of 1,8-naphthosultam and allow preparation of mono-platinum complexes of the type shown in Figure 18. Due to the delocalisation of the lone pair from one nitrogen atom onto the other, DBU can form a stable protonated amidinium ion (Scheme 7). This makes DBU a fairly moderate base, resulting in a pK_a of ≈ 12.5.[21]

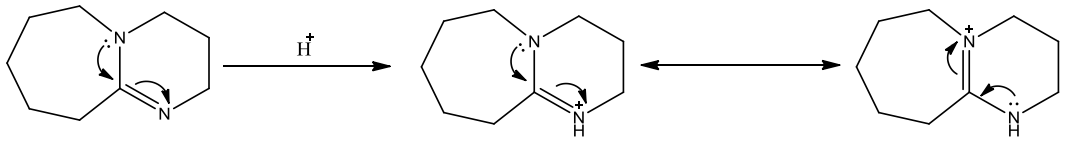

Scheme 7 Formation of the stable protonated amidinium ion.[21]

Due to the unwanted side reaction that occurs with DBU, it was decided to use a stronger base with the aim that deprotonation would occur cleanly. Sodium *tert*-butoxide, a stronger non-nucleophilic base with a pK_a ≈ 17.0 was chosen.[22] Therefore, 1,8-naphthosultam was reacted with sodium *tert*-butoxide and the corresponding *cis*-dichloro*bis*(phosphine)platinum in a 1:1:1 ratio.

The ^{31}P NMR data from the sodium *tert*-butoxide reactions (Table 6) was in agreement with the data from both the lithium triethylborohydride and DBU reactions. However, apart from the reaction of 1,8-naphthosultam and *cis*-dichloro*bis*(triphenylphosphine)platinum to yield **mono-2a**, the reactions did not go to completion with peaks for the corresponding *cis*-dichloro*bis*(phosphine)platinum complexes dominating the ^{31}P NMR. The presence of unreacted starting material was extremely high in the reactions for **mono-2c** and **mono-2d**, which prevented the $^{1}J(^{31}P\text{-}^{195}Pt)$ coupling constants from being measured.

Table 6 Comparison of ^{31}P NMR data for products from sodium tert-butoxide reactions.

	Chemical Shifts [ppm]		Coupling Constants [Hz]		
Product	$\delta(^{31}P_A)$	$\delta(^{31}P_x)$	$^{1}J(P_A\text{-}Pt)$	$^{1}J(P_X\text{-}Pt)$	$^{2}J(P_A\text{-}P_X)$
mono-2a	-16.4	8.4	3799	3331	19
mono-2b	2.5	-5.9	3699	3262	20
mono-2c	-10.9	-18.4	-	-	21
mono-2d	-26.3	-22.2	-	-	23

Unfortunately, this led back to the original problem of removing unreacted *cis*-dichloro*bis*(phosphine)platinum from the reaction mixture in order to yield pure mono-product. As discussed earlier this could not be achieved and due to time constraints the decision was made to proceed with other work.

It was however, observed that using a 1,8-naphthosultam: sodium *tert*-butoxide: *cis*-dichloro*bis*(diphenylmethylphosphine)platinum ratio of 2:2:1 instead of the aforementioned 1:1:1 led to 100% formation of the *bis*-complex [Pt(1-(SO_2),8-(N)-nap)$_2$(PPh_2Me)$_2$] (**bis-2b**). These reactions will be discussed later in this chapter.

X-ray Investigations

Single crystals were obtained for **mono-2a** and **mono-2e** from diffusion of hexane into a saturated solution of the product in dichloromethane. **mono-2a** crystallises with one molecule in the asymmetric unit whereas **mono-2e** crystallises with one dichloromethane molecule per molecule of product. The molecular structures of **mono-2a** and **mono-2e** are shown in Figures 25 and 26, respectively. Both structures possess the 1,8-naphthosultam system as a monodentate ligand, bonding through the nitrogen atom to a platinum centre, with the S-N-C_3 heterocycle remaining intact.

The sulfur-nitrogen *peri*-distances of 1.628(13) Å and 1.606(19) Å, for **mono-2a** and **mono-2e** respectively, appear at first glance shorter than that of 1,8-naphthosultam (1.676(9) Å). However, when the errors are considered they cannot be deemed statistically variant. Compression of the bond angles in the bay region is observed; 1,8-naphthosultam has a splay angle of -25.6° compared to -29.6° in **mono-2a** and -27.9° in **mono-2e**. One would expect that compression of

the angles in the bay region would result in a shortening of the *peri*-distance, but this is not condusively observed. There is minor distortion of the naphthalene system in 1,8-naphthosultam with torsion angles of 179.2(6)° and 177.8(7)°. This has not altered significantly in the complexes with both having torsion angles of *ca.* 177° and 179°. However, there is a noticeable change in out-of-plane displacement of the *peri*-atoms. In the free ligand the sulfur sits in the naphthyl plane with nitrogen 0.110(1) Å below. In both complexes the sulfur atom now lies *ca.* 0.250(1) Å below the naphthyl plane and the nitrogen lies on the naphthyl plane. Changes in the out-of-plane displacement can be accredited to the atoms moving to the optimum position for minimal distortion to the naphthalene geometry.

The square planar geometry around the platinum centre in complex **mono-2a** shows distortion with angles varying significantly from 90°. This was also seen in the corresponding triphenylphosphine platinum complex, **1a**, with 1,8-naphthosultone.

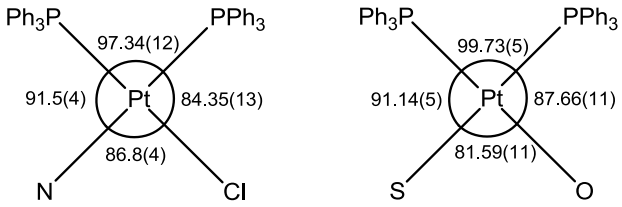

Figure 22 Comparison of the angles (°) associated with the square planar geometry of the platinum metal in complexes **mono-2a** (left) and **1a** (right).

Similar to complex **1a**, the P(1)-Pt(1)-P(2) angle of 97.34(12)° in **mono-2a** is enlarged to greater than the ideal 90° in order to accommodate the bulky triphenylphosphine groups. The N(9)-Pt(1)-Cl(1) angle of 86.8(4)° is larger than its sultone equivalent because only the nitrogen is tethered; whereas in **1a** both the sulfur and oxygen atoms are restricted by the naphthalene system. The P(1)-Pt(1)-N(9) angle is larger than the P(2)-Pt(1)-Cl(1) angle, this is comparable with the S(1)-Pt(1)-P(1) angles and the O(9)-Pt(1)-P(2) angles in **1a**. There are no significant differences between the Pt-P bond lengths, with Pt(1)-P(1) being 2.251(4) Å and Pt(1)-P(2) being 2.262(4) Å. The remaining bond lengths are similar to those in **1a**.

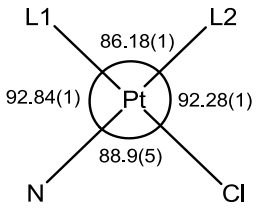

Figure 23 The angles (°) associated with the square planar geometry of the platinum metal in complex **mono-2e**.

In **mono-2e** the platinum also adopts a square planar geometry with the COD ligand binding to the platinum centre *via* centroids Cg(C11-C12) and Cg(C15-C16). For ease of comparison, Cg(C11-C12) and Cg(C15-C16) will be referred to as L1 and L2, respectively.

The L1-Pt(1)-L2 angle of 86.18(1)° is closer to the ideal 90° and much smaller than the corresponding P(1)-Pt(1)-P(2) angle of 97.34(12)° in **mono-2a**. The L(1)-Pt(1)-N(9) angle of 92.84(1)° is equal to the L(2)-Pt(1)-Cl(1) angle of 92.28(1)° whereas the P(1)-Pt(1)-N(9) angle is larger than the P(2)-Pt(1)-Cl(1) angle, 91.5(4)° and 84.35(13)°. The N(9)-Pt(1)-Cl(1) angles of 86.8(4)° and 88.9(5)°, in **mono-2a** and **mono-2e** respectively, are similar. These differences can be understood by the fact that triphenylphosphine is a monodentate ligand which means the two triphenylphosphine groups are independent of each other and therefore free to move to the most comfortable geometry. In comparison COD binds in a more restricted manner which leads to equal L(1)-Pt(1)-N(9) and L(2)-Pt(1)-Cl(1) angles, compression of L1-Pt(1)-L2 and subsequent widening of N(9)-Pt(1)-Cl(1).

There are no significant differences between the Pt(1)-N(9) and Pt(1)-Cl(1) bond lengths. However, there are differences seen in the other bond lengths.

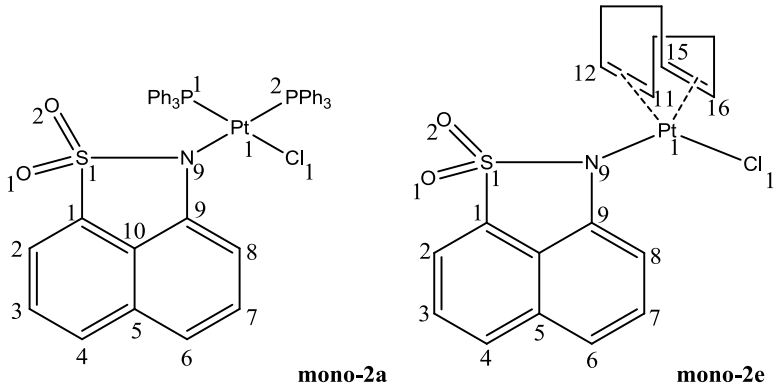

Figure 24 X-ray crystallography numbering scheme for **mono-2a** and **mono-2e**.

Table 7 Selected Bond Lengths [Å] and Angles [°] of **mono-2a** and **mono-2e.**

Compound	**mono-2a**	**mono-2e**
X-ray Code	loud43	112
S, N	SO_2, N[Pt(PPh_3)$_2$Cl]	SO_2, N[Pt(COD)Cl]
Peri-region distance		
S(1)-N(9)	**1.628(13)**	**1.606(19)**
Naphthalene bond lengths		
C(1)-C(2)	1.38(3)	1.36(3)
C(2)-C(3)	1.43(2)	1.41(3)
C(3)-C(4)	1.35(3)	1.39(4)
C(4)-C(5)	1.39(3)	1.41(4)
C(5)-C(10)	1.45(2)	1.40(3)
C(5)-C(6)	1.40(3)	1.48(4)
C(6)-C(7)	1.41(3)	1.33(3)
C(7)-C(8)	1.41(2)	1.43(3)
C(8)-C(9)	1.26(3)	1.41(3)
C(9)-C(10)	1.45(3)	1.37(3)
C(1)-C(10)	1.37(3)	1.44(3)
Peri-region bond angles		
S(1)-C(1)-C(10)	104.8(12)	104.1(14)
C(1)-C(10)-C(9)	119.3(13)	113.6(17)
N(9)-C(9)-C(10)	106.3(13)	114.4(18)
∑ of bay angles	**330.4(22)**	**332.1(28)**
Splay angle[a]	-29.6	-27.9
Bond angles		
C(4)-C(5)-C(6)	131.1(15)	130(2)
O(1)-S(1)-O(2)	116.4(7)	114.2(9)

C(1)-S(1)-O(1)	107.0(7)	115.2(10)
C(1)-S(1)-O(2)	115.5(7)	107.5(8)
Out of plane displacement		
S(1)	-0.250(1)	-0.242(1)
N(9)	+0.007(1)	+0.009(1)
Central naphthalene ring torsion angles		
C(6)-C(5)-C(10)-C(1)	-177.2(12)	178.5(17)
C(4)-C(5)-C(10)-C(9)	177.1(12)	180(2)
Platinum geometry - bond lengths		
Pt(1)-N(9)	2.056(11)	2.074(16)
Pt(1)-L(1)[b]	2.251(4)	2.060(1)
Pt(1)-L(2)[b]	2.262(4)	2.076(1)
Pt(1)-Cl(1)	2.341(4)	2.325(6)
Platinum geometry - bond angles		
N(9)-Pt(1)-Cl(1)	86.8(4)	88.9(5)
N(9)-Pt(1)-L(1)	91.5(4)	92.84(1)
N(9)-Pt(1)-L(2)	170.4(4)	177.91(1)
Cl(1)-Pt(1)-L(1)	178.30(13)	172.80(1)
Cl(1)-Pt(1)-L(2)	84.35(13)	92.28(1)
L(1)-Pt(1)-L(2)	97.34(12)	86.18(1)

[a] Splay angle: ∑ of the three bay region angles - 360; [b] L(1): P(1) for **mono-2a**, Cg(15,16) **mono-2e** L(2): P(2) for **mono-2a**, Cg(11,12) **mono-2e.**

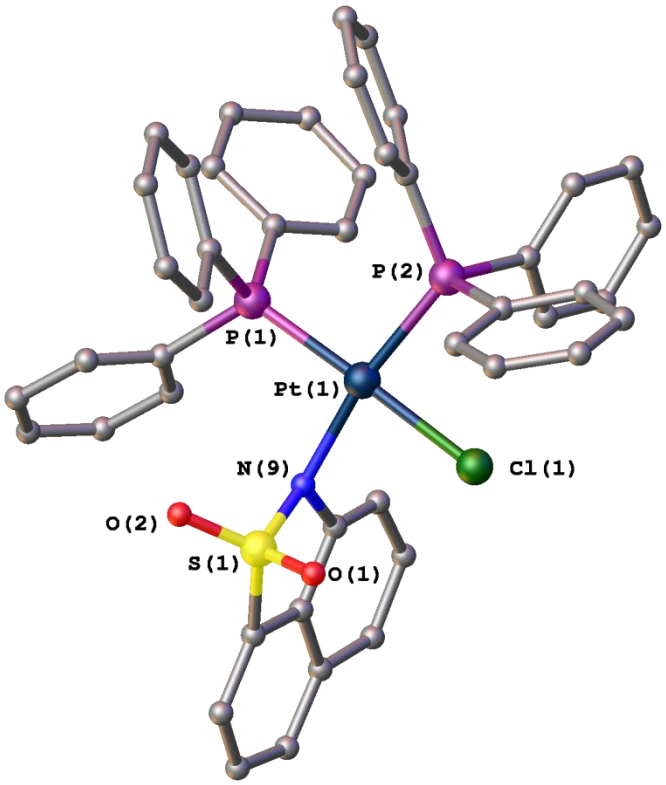

Figure 25 The molecular structure of **mono-2a** with H atoms omitted for clarity.

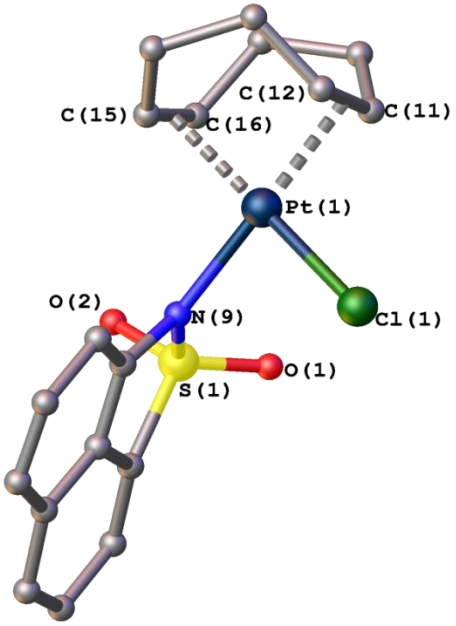

Figure 26 The molecular structure of **mono-2e** with H atoms and solvent molecules omitted for clarity.

As 1,8-naphthosultam reacts to give the mono-complexes previously described, it was decided to try and synthesise the corresponding bis-complexes. This was done by reacting two equivalents of 1,8-naphthosultam with two equivalents of sodium *tert*-butoxide to yield two equivalents of the deprotonated 1,8-naphthosultam species. The deprotonated species was then reacted with one equivalent of the appropriate *cis*-dichloro*bis*(phosphine)platinum to yield the desired bis-complex (Scheme 8).

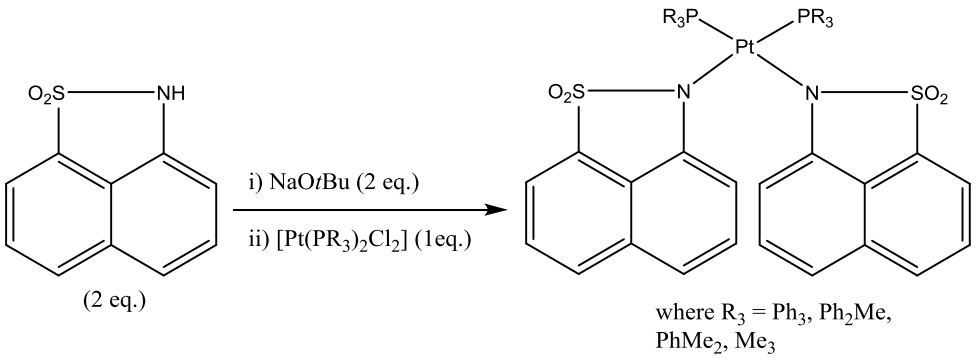

Scheme 8 Reaction route for synthesis of sultam bis-complexes.

This deprotonation reaction was successful with all *cis*-dichloro*bis*(phosphine)platinum species except *cis*-dichloro*bis*(triphenylphosphine)platinum, resulting in [Pt(1-(SO_2),8-(N)-nap)$_2$(PPh_2Me)$_2$] (**bis-2b**), [Pt(1-(SO_2),8-(N)-nap)$_2$($PPhMe_2$)$_2$] (**bis-2c**) and [Pt(1-(SO_2),8-(N)-nap)$_2$(PMe_3)$_2$] (**bis-2d**). The reaction was also successful with (1,5-cyclooctadiene)platinum(II) dichloride to give [Pt(1-(SO_2),8-(N)-nap)$_2$(η^4-COD)] (**bis-2e**) (Figure 27).

Density functional theory calculations were carried out using **mono-2a** (**A**) and the hypothetical complex **bis-2a** (**B**), in order to understand why only the mono product is obtained with *cis*-dichloro*bis*(triphenylphosphine)platinum. The distances at the PBE0/ECP1 level were collected (Table 8) and it was determined that there was no steric reason for **B** not being formed.

Table 8 Selected bond distances [Å] of Pt-sultam complexes.

Compound	Pt-P	Pt-N	Pt-Cl
A XRD[a]	2.262[b]/2.251	2.055	2.341
A DFT[c]	2.296[b]/2.271	2.073	2.375
B DFT[c]	2.295[d]	2.089[d]	n/a

[a]X-ray (this work); [b]Trans to N; [C]PBE0/ECP1 level; [d]Mean value.

Reaction enthalpies and free energies (in parentheses) were obtained at level M06/ECP2/PCM, in order to estimate the driving forces for the displacement of the chlorine ligands in the precursor $[Pt(PPh_3)_2Cl_2]$ (**C**). It was found that, formation of **A** and **B** from **C** and sultam anions is exothermic. There is therefore a substantial driving force for substitution of the second chlorine in **A**.

C + sultam$^-$ → **A** + Cl$^-$, ΔH = -7.7 kJ/mol (ΔG = +18.6 kJ/mol) (1)

C + 2 sultam$^-$ → **B** + 2 Cl$^-$, ΔH = -27.5 kJ/mol (ΔG = +24.4 kJ/mol) (2)

A + sultam$^-$ → **B** + Cl$^-$, ΔH = -19.8 kJ/mol (ΔG = +5.8 kJ/mol) (3)

It can be concluded from the calculations that there is no steric or thermodynamic reason for **bis-2a** not forming. It is proposed that the reason may be kinetic in origin. See Appendix for a more in depth explanation.

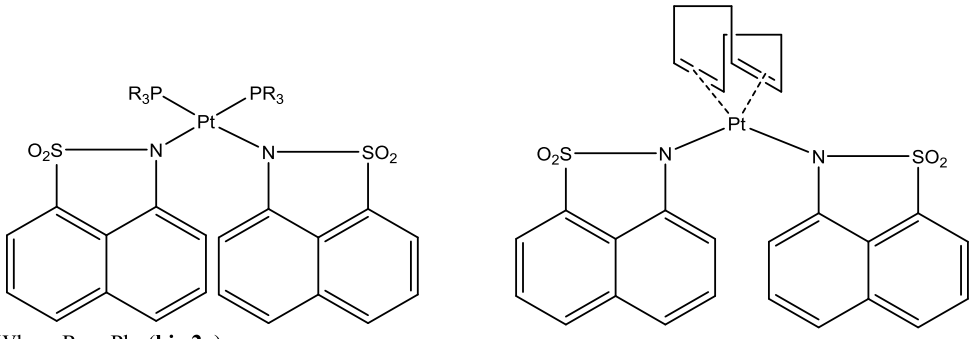

Where R_3 = Ph_3 (**bis-2a**), Ph_2Me (**bis-2b**), Me_2Ph (**bis-2c**), Me_3 (**bis-2d**)

COD = **bis-2e**

Figure 27 1,8-naphthosultam bis-platinum complexes; $[Pt(1\text{-}(SO_2),8\text{-}(N)\text{-}nap)_2(PPh_3)_2]$ (**bis-2a**), $[Pt(1\text{-}(SO_2),8\text{-}(N)\text{-}nap)_2(PPh_2Me)_2]$ (**bis-2b**), $[Pt(1\text{-}(SO_2),8\text{-}(N)\text{-}nap)_2(PPhMe_2)_2]$ (**bis-2c**), $[Pt(1\text{-}(SO_2),8\text{-}(N)\text{-}nap)_2(PMe_3)_2]$ (**bis-2d**) and $[Pt(1\text{-}(SO_2),8\text{-}(N)\text{-}nap)_2(COD)]$ (**bis-2e**).

The $^{31}P\{^{1}H\}$ NMR ($CDCl_3$) data for the complexes (Table 9) are similar in that the spectra all have an AX pattern with appropriate platinum satellites. A single phosphorus peak is seen due to the two phosphorus atoms being equivalent in these symmetrical bis-complexes. Similar to the 1,8-naphthosultam mono-complexes and the 1,8-naphthosultone complexes, a steady decrease in value for $^{1}J(^{31}P\text{-}^{195}Pt)$ coupling constant is seen as the phenyl groups are replaced by methyl groups.

Table 9 Comparison of ^{31}P NMR data for bis-complexes.

	Chemical Shifts [ppm]	**Coupling Constants [Hz]**
Product	**$\delta(^{31}P)$**	**^{1}J(P-Pt)**
bis-2a	-	-
bis-2b	-7.3	3348
bis-2c	-16.2	3305
bis-2d	-25.4	3216

Crystal structures for **bis-2b** to **2d** could not be obtained. However, single crystals were obtained for **bis-2e** from diffusion of hexane into a saturated solution of the product in dichloromethane. The molecular structure of **bis-2e** is shown in Figure 30. In **bis-2e** the two 1,8-naphthosultam ligands are monodentate, bonding through their nitrogen atom to a platinum centre, with their S-N-C_3 heterocycle remaining intact.

The *peri*-distance in **bis-2e** is statistically similar to that in **mono-2e** (1.648(11) Å and 1.606(19) Å). This is expected as the sulfur-nitrogen bond remains intact in both complexes. Due to the *peri*-bond remaining intact both complexes have a negative splay angle with values of -27.9° for **mono-2e** and -27.1° for **bis-2e**. In **bis-2e** both the sulfur and nitrogen atoms lie below the naphthyl plane at 0.032(1) Å and 0.078(1) Å, respectively. Whereas in **mono-2e** the sulfur atom lies 0.242(1) Å below the naphthyl plane and nitrogen atom lies on the plane. The observed differences in out-of-plane displacement are reflected in the torsion angles. The C(6)-(5)-(10)-(1) and C(4)-(5)-(10)-(9) torsion angles deviate from the ideal '180°' by *ca.* 3° in **bis-2e** and *ca.* 1.5° **mono-2e**. As the sulfur and nitrogen atoms show little out-of-plane distortion in **bis-2e** the naphthalene backbone distorts in-plane to relieve any geometrical constraints. The naphthalene backbone in **mono-2e** shows less in-plane distortion as the sulfur atom has been displaced to relieve the majority of the strain.

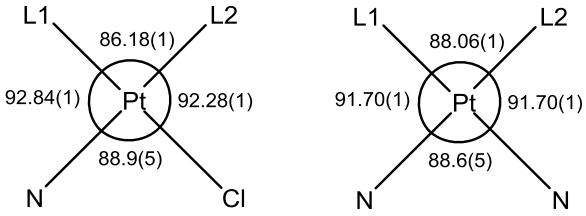

Figure 28 Comparison of the angles (°) associated with the square planar geometry of the platinum metal in complexes **mono-2e** (left) and **bis-2e** (right).

Both **mono-2e** and **bis-2e** show minor distortion from the 'ideal' square planar geometry with no significant differences seen in the bond angles or bond lengths between the two complexes.

It can be concluded that replacing a chlorine atom with another 1,8-naphthosultam ligand has a minimal effect on the geometry around the platinum centre and the overall complex.

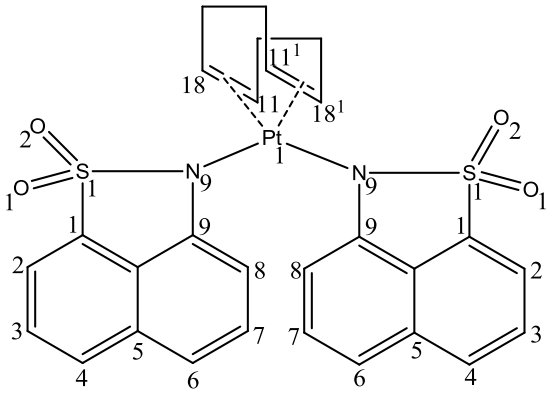

Figure 29 X-ray crystallography numbering scheme for **bis-2e**.

Table 10 Selected Bond Lengths [Å] and Angles [°] of **bis-2e**.

Compound	**bis-2e**
X-ray Code	**Loud6**
E, E'	SO_2, N
Peri-region distance	
S(1)-N(9)	**1.648(11)**
Naphthalene bond lengths	
C(1)-C(2)	1.36(2)
C(2)-C(3)	1.41(3)
C(3)-C(4)	1.35(3)
C(4)-C(5)	1.36(3)
C(5)-C(10)	1.428(18)

C(5)-C(6)	1.464(18)
C(6)-C(7)	1.35(3)
C(7)-C(8)	1.38(2)
C(8)-C(9)	1.391(17)
C(9)-C(10)	1.422(19)
C(1)-C(10)	1.391(16)
Peri-region bond angles	
S(1)-C(1)-C(10)	105.6(10)
C(1)-C(10)-C(9)	115.0(11)
N(9)-C(9)-C(10)	112.3(11)
∑ of bay angles	**332.9(18)**
Splay angle[a]	-27.1
Bond angles	
C(4)-C(5)-C(6)	130.7(14)
O(1)-S(1)-O(2)	114.9(7)
C(1)-S(1)-O(1)	111.9(8)
C(1)-S(1)-O(2)	110.3(7)
Out of plane displacement	
S(1)	-0.032(1)
N(9)	-0.078(1)
Central naphthalene ring torsion angles	
C(6)-C(5)-C(10)-C(1)	-177.1(11)
C(4)-C(5)-C(10)-C(9)	177.2(13)
Platinum geometry - bond lengths	
Pt(1)-N(9)	2.034(13)
Pt(1)-L(1)[b]	2.095(1)
Pt(1)-L(2)	2.095(1)
Platinum geometry - bond angles	
N(9)-Pt(1)-N(9)	88.6(5)
L(1)-Pt(1)-N(9)	91.70(1)
L(2)-Pt(1)-N(9)	91.70(1)
L(1)-Pt(1)-L(2)	88.06(1)

[a] Splay angle: ∑ of the three bay region angles - 360; [b] L(1): Cg(11,18), L(2): Cg(11^1,18^1).

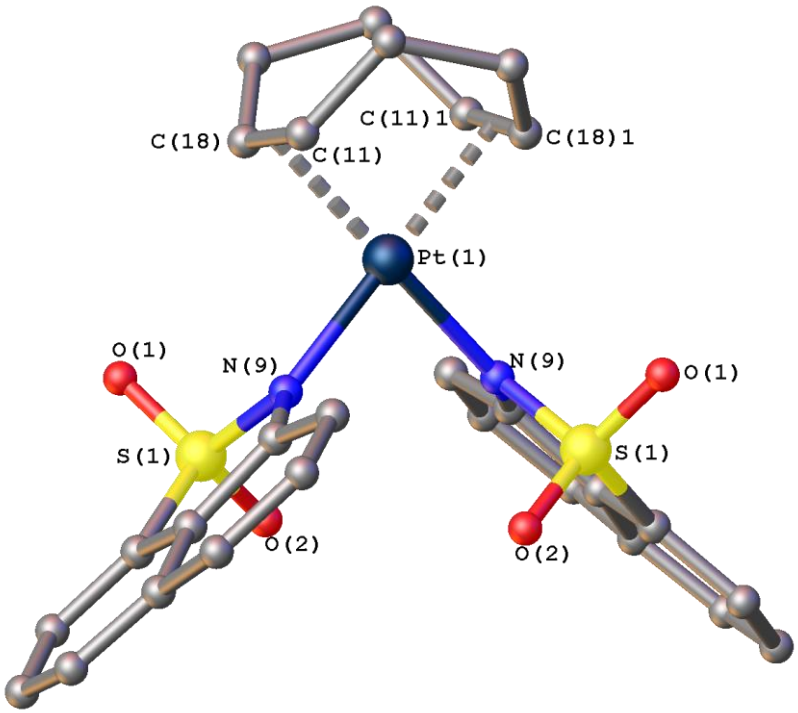

Figure 30 The molecular structure of **bis-2e** with H atoms omitted for clarity.

Other work

The nitrogen atom in 1,8-naphthosultam was deprotonated with sodium *tert*-butoxide to form the anionic species, which was then added to a suspension of *trans*-dichloro*bis*(triphenylphosphine)palladium in THF resulting in the complex [Pd(1-(SO_2),8-(N)-nap)(PPh_3)$_2$Cl] (**mono-3a**) (Scheme 9).

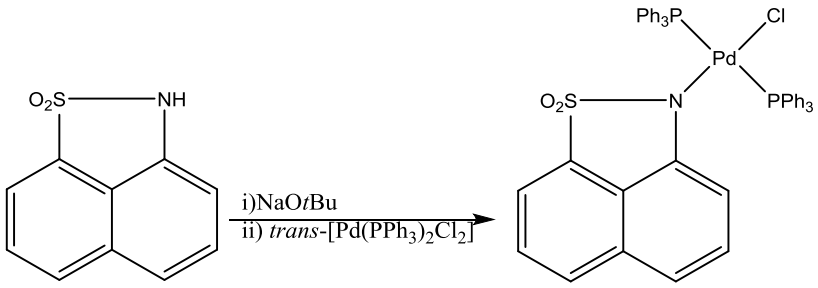

Scheme 9 Reaction route for synthesis of [Pd(1-(SO_2),8-(N)-nap)(PPh_3)$_2$Cl] (**mono-3a**).

The $^{31}P\{^{1}H\}$ NMR ($CDCl_3$) spectrum displays a single peak, due to the two phosphorus atoms being equivalent, at $\delta(^{31}P)$ = 23.1 ppm.

Single crystals were obtained for **mono-3a** by evaporation of a saturated solution of the compound in dichloromethane. The product crystallises with one dichloromethane molecule per molecule of product. The molecular structure of **mono-3a** is shown in Figure 33. As with the previously discussed 1,8-naphthosultam mono-complexes, the 1,8-naphthosultam behaves as a monodentate ligand binding to the palladium centre through the nitrogen atom leaving the *peri*-region intact. The central palladium metal adopts a distorted square planar geometry, with angles deviating from the ideal (90°).

The sulfur-nitrogen *peri*-distance of 1.640(9) Å in **mono-3a** is statistically equivalent to the *peri*-distance of 1.676(9) Å in the free ligand, which is expected as the *peri*-bond has remained intact. 1,8-naphthosultam and **mono-3a** both have negative splay angles of -25.6° and -26.8°, respectively. Small changes are seen in the out-of-plane displacement; the sulfur atom in the free ligand lies on the naphthyl plane and the nitrogen atom lies 0.110(1) Å below the plane whereas in **mono-3a** the sulfur atom moves to 0.026(1) Å above the plane and the nitrogen atom now lies 0.043(1) Å below the plane. These small changes are accompanied by changes to the torsion angles of the naphthalene backbone with the C(6)-(5)-(10)-(1) and C(4)-(5)-(10)-(9) torsion angles deviating from the ideal 180° by *ca.* 0.8-2.2° in the free ligand and *ca.* 0.1- 1.3° in **mono-3a**.

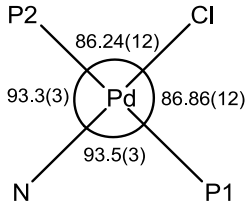

Figure 31 Comparison of the angles (°) associated with the square planar geometry of the palladium metal in **mono-3a**.

Like all heavy d^8 metals, palladium prefers to adopt a square planar geometry with all four angles around the metal centre equalling 90°. In **mono-3a** both P-Pd(1)-N(9) angles are equal, but greater than the ideal 90° (P(1)-Pd(1)-N(9) = 93.5(3)°, P(2)-Pd(1)-N(9) = 93.3°), this widening occurs to accommodate the bulky triphenylphosphine groups. The P(1)-Pd(1)-Cl(1) angle of

86.86(12)° is statistically equal to the P(2)-Pd(1)-Cl(1) angle of 86.24(12)°. The P-Pd(1)-Cl(1) angles have been compressed to compensate for the widening of the P-Pd(1)-N(9) angles and to keep the geometry around the palladium centre as square planar.

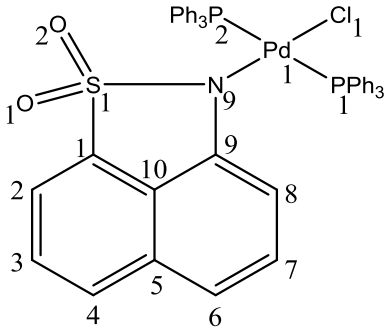

Figure 32 X-ray crystallography numbering scheme for **mono-3a**.

Table 11 Selected Bond Lengths [Å] and Angles [°] of **mono-3a**.

Compound	**mono-3a**
X-ray Code	124
S, N	SO_2, N[Pd(COD)Cl]
Peri-region distance	
S(1)-N(9)	**1.640(9)**
Naphthalene bond lengths	
C(1)-C(2)	1.374(16)
C(2)-C(3)	1.42(2)
C(3)-C(4)	1.40(2)
C(4)-C(5)	1.404(18)
C(5)-C(10)	1.42(2)
C(5)-C(6)	1.436(19)
C(6)-C(7)	1.362(19)
C(7)-C(8)	1.42(2)
C(8)-C(9)	1.402(15)
C(9)-C(10)	1.418(16)
C(1)-C(10)	1.372(17)
Peri-region bond angles	
S(1)-C(1)-C(10)	106.2(9)
C(1)-C(10)-C(9)	114.5(12)

N(9)-C(9)-C(10)	112.5(10)
∑ of bay angles	**333.2(18)**
Splay angle[a]	-26.8
Bond angles	
C(4)-C(5)-C(6)	127.7(15)
O(1)-S(1)-O(2)	115.7(6)
C(1)-S(1)-O(1)	111.7(6)
C(1)-S(1)-O(2)	109.5(6)
Out of plane displacement	
S(1)	+0.026(1)
N(9)	-0.043(1)
Central naphthalene ring torsion angles	
C(6)-C(5)-C(10)-C(1)	-179.9(10)
C(4)-C(5)-C(10)-C(9)	-178.7(11)
Palladium geometry - bond lengths	
Pd(1)-N(9)	2.039(10)
Pd(1)-P(1)	2.376(3)
Pd(1)-P(2)	2.362(3)
Pd(1)-Cl(1)	2.300(3)
Palladium geometry - bond angles	
P(1)-Pd(1)-Cl(1)	86.86(12)
P(2)-Pd(1)-Cl(1)	86.24(12)
N(9)-Pd(1)-P(1)	93.5(3)
N(9)-Pd(1)-P(2)	93.3(3)

[a] Splay angle: ∑ of the three bay region angles - 360.

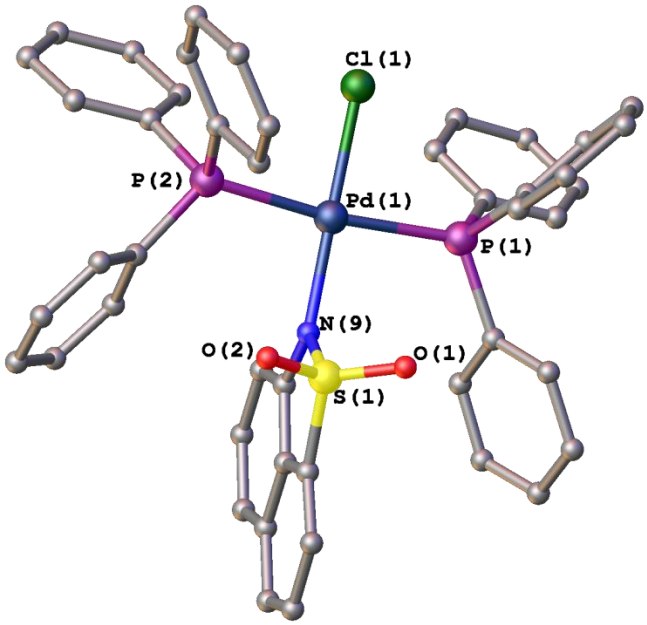

Figure 33 The molecular structure of **mono-3a** with H atoms and solvent molecules omitted for clarity.

As reducing agents preferentially deprotonate the nitrogen atom in 1,8-naphthosultam instead of reducing the sulfur-nitrogen bond it was decided to replace the hydrogen atom on the nitrogen with a methyl group. It was thought that this would allow the reducing agent to reduce the sulfur-nitrogen bond. In order to do this an aqueous solution of sodium hydroxide was added to a solution of 1,8-naphthosultam in dimethylacetamide. Iodomethane was then added to the mixture and this was left to stir overnight. The resulting dark brown solution was filtered. Water was added to the filtrate with vigorous stirring to yield N-methyl-1,8-naphthosultam as a cream solid (Scheme 10).[23]

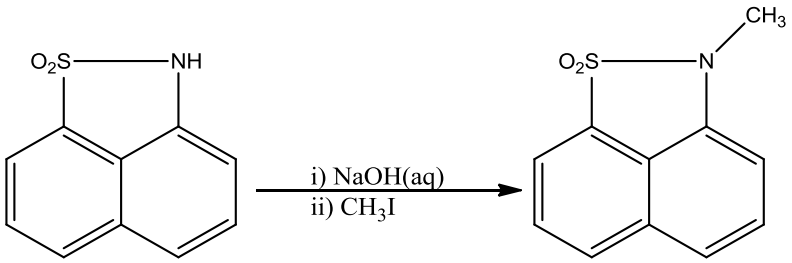

Scheme 10 Synthetic route to N-methyl-1,8-naphthosultam.[23]

N-methyl-1,8-naphthosultam is a known compound, however the crystal structure has not been reported. For comparison purposes with the 1,8-naphthosultam ligand (**2**) I will refer to N-methyl-1,8-naphthosultam as **2Me**. Single crystals were obtained for **2Me** from diffusion of hexane into a saturated solution of the product in dichloromethane. The product crystallises with two molecules in the asymmetric unit. The molecular structure of **2Me** is shown in Figure 35.

The crystal structure of **2** shows a *peri* sulfur-nitrogen bond distance of 1.676(9) Å. The *peri*-distance in **2Me** is statistically the same with values of 1.674(5) Å [1.659(5) Å]. The sum of the bay angles in **2** and **2Me** are 334.4(12)° and 334.0(8)° [333.0(8)°], respectively resulting in splay angles of -25.6° and -26.0° [-27.0°] which confirms a favourable interaction is occurring between the *peri*-atoms. There is little distortion to the geometry of the naphthalene carbon skeleton with torsion angles deviating from the 'ideal' 180° by 0.8-2.2° in **2** and 0.7-2.0° [0.1-0.2°] in **2Me**. Minor out of plane displacement is observed in both ligands. The sulfur atom in **2** lies on the naphthyl plane and the nitrogen atom lies below the plane by 0.110(1) Å whereas in **2Me** the sulfur atom lies 0.033(1) Å [0.078(1) Å] below the plane and the nitrogen atom lies on the plane. It can be concluded that replacing the hydrogen atom on the nitrogen with a methyl group has not had an effect on the overall geometry of the ligand.

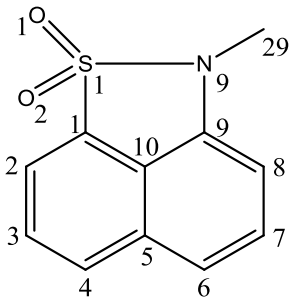

Figure 34 X-ray crystallography numbering scheme for **2Me**.

Table 12 Selected Bond Lengths [Å] and Angles [°] for **2** and **2Me** [values in parentheses are for independent molecules].

Compound	**2**	**2Me**
X-ray code	afdw23	LDO-91-1
E, E'	SO_2, NH	SO_2, NMe
E(1), E(9)	S, N	S, N
Peri-region distance		
E(1)-E(9)	**1.676(9)**	**1.674(5), [1.659(5)]**
Bond lengths		

C(1)-S(1)	1.756(9)	1.769(6), [1.766(6)]
C(9)-E(9)	1.374(11)	1.419(7), [1.397(7)]
S(1)-O(1)	1.440(6)	1.441(4), [1.442(5)]
S(1)-O(2)	1.431(6)	1.446(4), [1.432(5)]
C(1)-C(2)	1.319(13)	1.342(9), [1.376(8)]
C(2)-C(3)	1.420(15)	1.405(9), [1.405(9)]
C(3)-C(4)	1.387(16)	1.384(9), [1.367(10)]
C(4)-C(5)	1.484(14)	1.412(9), [1.416(9)]
C(5)-C(10)	1.392(11)	1.406(8), [1.398(8)]
C(5)-C(6)	1.398(17)	1.418(8), [1.405(10)]
C(6)-C(7)	1.34(3)	1.351(10), [1.371(9)]
C(7)-C(8)	1.402(15)	1.414(8), [1.419(9)]
C(8)-C(9)	1.388(12)	1.374(8), [1.350(9)]
C(9)-C(10)	1.443(11)	1.394(9), [1.421(8)]
C(1)-C(10)	1.348(12)	1.407(8), [1.390(9)]
Peri-region bond angles		
E(1)-C(1)-C(10)	110.2(7)	106.3(4), [107.6(4)]
C(1)-C(10)-C(9)	113.4(7)	115.9(5), [114.7(5)]
E(9)-C(9)-C(10)	110.8(7)	111.8(5), [110.7(5)]
∑ of bay angles	**334.4(12)**	**334.0(8), [333.0(8)]**
Splay angle[a]	-25.6	-26.0, [-27.0]
Bond angles		
C(4)-C(5)-C(6)	129.0(10)	127.9(5), [128.0(6)]
E(9)-E(1)-C(1)	92.1(4)	94.9(3), [93.6(3)]
E(1)-E(9)-C(9)	113.0(7)	111.0(4), [112.9(4)]
O(1)-S(1)-O(2)	116.3(3)	116.2(2), 116.0(3)]
O(1)-S(1)-E(9)	109.41(1)	110.2(3), [111.4(3)]
O(2)-S(1)-E(9)	108.06(1)	109.3(3), [109.2(3)]
C(1)-S(1)-O(1)	113.9(4)	112.9(3), [111.1(3)]
C(1)-S(1)-O(2)	114.1(4)	111.3(3), [113.4(3)]
Out of plane displacement		
E(1)	+0.003(1)	-0.033(1), [-0.078(1)]
E(9)	-0.110(1)	+0.005(1), [+0.039(1)]
Central naphthalene ring torsion angles		
C(6)-C(5)-C(10)-C(1)	177.8(7)	179.3(5), [-179.9(5)]
C(4)-C(5)-C(10)-C(9)	179.2(6)	-178.0(5), [-179.8(5)]

[a]Splay angle: ∑ of the three bay region angles - 360.

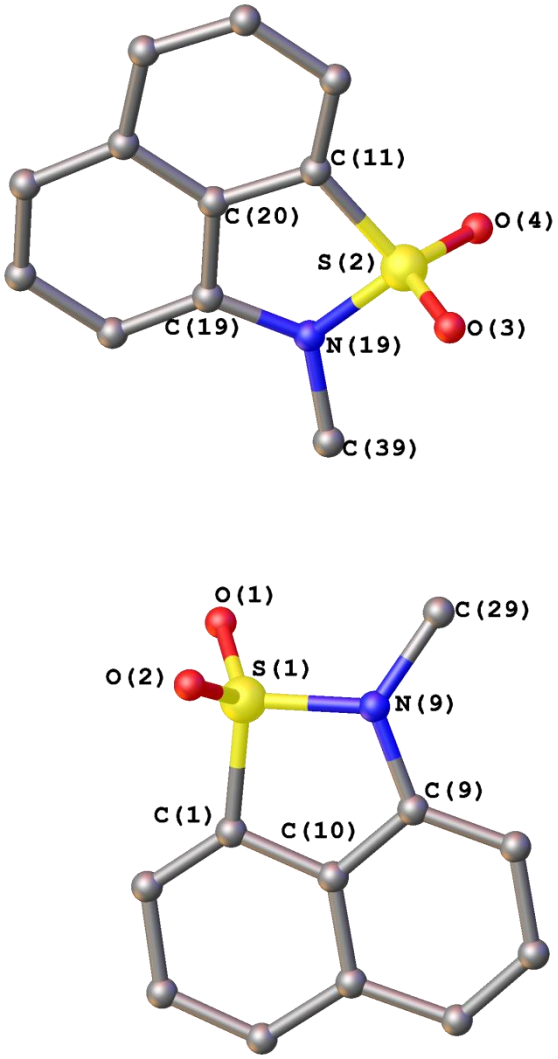

Figure 35 The molecular structure of N-methyl-1,8-naphthosultam (**2Me**) with H atoms omitted for clarity.

N-methyl-1,8-naphthosultam was then reacted with two equivalents of lithium triethylborohydride with the anticipation that without the hydrogen atom it would reduce the sulfur-nitrogen bond and form the dilithio-species, which could then react with *cis*-dichloro*bis*(triphenylphosphine)platinum to form the [Pt(1-(SO_2),8-(N)-nap)(PPh_3)$_2$] complex. This reaction did not proceed, with ^{31}P NMR showing peaks for the starting materials only.

Experimental

All experiments, except that of **2Me**, were carried out under an oxygen- and moisture-free nitrogen atmosphere using standard Schlenk techniques and glassware. Reagents were obtained from commercial sources and used as received. Dry solvents were collected from a MBraun solvent system. Elemental analyses were performed by Stephen Boyer at the London Metropolitan University. Infra-red spectra were recorded for solids as KBr discs in the range 4000-300 cm^{-1} on a Perkin-Elmer System 2000 Fourier transform spectrometer. ^{1}H and ^{13}C NMR spectra were recorded on a Bruker Avance 300 MHz spectrometer with δ(H) and δ(C) referenced to external tetramethylsilane. ^{31}P were recorded on a Jeol GSX 110 MHz spectrometer with δ(P) referenced to external phosphoric acid. All measurements were performed at 25 °C. All values reported for NMR spectroscopy are in parts per million (ppm). Coupling constants (*J*) are given in Hertz (Hz). Mass spectrometry was performed by the University of St. Andrews Mass Spectrometry Service. Electrospray Mass Spectrometry (ESMS) was carried out on a Micromass LCT orthogonal accelerator time of flight mass spectrometer. DFT calculations were carried out by Michael Bühl at the University of St Andrews. All *cis*-dichloro*bis*(phosphine)platinum reagents were prepared following standard literature procedures.[24,25,26]

Platinum Complexes of 1,8-Naphthosultone

[Pt(1-(SO_2),8-(O)-nap)(PPh_3)$_2$] (1a): Lithium triethylborohydride (1.50 mL of a 1.0 M solution in THF, 1.50 mmol) was added to a solution of 1,8-naphthosultone (0.16 g, 0.78 mmol) in THF (20 mL). An immediate colour change occurred from colourless to pale yellow. After stirring for 30 min, the resulting solution was transferred *via* a stainless steel cannula to a suspension of *cis*-dichloro*bis*(triphenylphosphine)platinum (0.31 g, 0.39 mmol) in THF (10 mL). The mixture was stirred for 24 hours resulting in a yellow solution. The solution was evaporated to dryness under reduced pressure and re-dissolved in the minimum amount of dichloromethane. The product was purified by column chromatography using a dichloromethane/ hexane/ ethyl acetate eluent to yield a yellow solid (0.22 g, 61%); mp 184-186 °C (decomp.); elemental analysis (Found: C, 57.8; H, 3.2. Calc. for $C_{46}H_{36}O_3P_2PtS.1/2CH_2Cl_2$: C, 57.9; H, 3.8%); IR (KBr disc) ν_{max} cm^{-1} 3464w, 3052w, 1619w, 1555s, 1482s, 1436vs, 1368s, 1316w, 1275s, 1207s, 1188s, 1164w, 1100vs, 1066vs, 1029w, 999w, 912w, 821w, 787w, 745s, 693vs, 645w, 617w, 585w, 542vs, 524vs; δ_H(300 MHz; $CDCl_3$; 25 °C; Me_4Si) 8.05 (1 H, dd, $^{3}J_{HH}$ 6.9 Hz, $^{4}J_{HH}$ 0.6 Hz, Nap 4-H), 7.87 (1 H, dd, $^{3}J_{HH}$ 8.1 Hz, $^{4}J_{HH}$

0.8 Hz, Nap 2-H), 7.52-7.45 (6 H, m, P-Phenyl), 7.41-7.35 (1 H, m, Nap 3-H), 7.34-7.24 (11 H, m, P-Phenyl), 7.15-7.04 (13 H, m, Nap 5-H, P-Phenyl), 6.81-6.75 (1 H, m, Nap 6-H), 5.43 (1 H, d, $^{3}J_{HH}$ 7.2 Hz, Nap 7-H); δ_C(75.5 MHz; $CDCl_3$; 25 °C; Me_4Si) 134.6 (d, $^{2}J_{CP}$ 11.4 Hz), 134.2 (d, $^{2}J_{CP}$ 11.4 Hz), 131.7(s), 131.0 (d, $^{4}J_{CP}$ 2.1 Hz), 130.7 (d, $^{4}J_{CP}$ 2.1 Hz), 128.5-128.2 (m), 127.7(s), 124.2(s), 119.8(s), 116.3(s), 115.6(s); δ_P(110 MHz; $CDCl_3$; 25 °C; H_3PO_4) 10.6 (d, $^{1}J_{PPt}$ 3876 Hz, $^{2}J_{PPt}$ 19 Hz), 19.1 (d, $^{1}J_{PPt}$ 2504 Hz, $^{2}J_{PPt}$ 19 Hz); MS (ES^+): *m/z* 947.95 (100%, M^+ + Na).

The other 1,8-naphthosultone complexes were similarly prepared and the physical and spectral data are as follows.

[Pt(1-(SO_2),8-(O)-nap)(PPh_2Me)$_2$] (1b): From 1,8-naphthosultone (0.16 g, 0.79 mmol), lithium triethylborohydride (1.50 mL of a 1.0 M solution in THF, 1.50 mmol), and *cis*-dichloro*bis*(diphenylmethylphosphine)platinum (0.26 g, 0.39 mmol) to yield a yellow solid (0.06 g, 19%); mp 194-196 °C (decomp.); elemental analysis (Found: C, 53.8; H, 4.0. Calc. for $C_{36}H_{32}O_3P_2PtS$: C, 53.9; H, 4.0%); IR (KBr disc) ν_{max} cm^{-1} 3438s, 3052w, 2369w, 2345w, 1555s, 1495w, 1437vs, 1369vs, 1280s, 1201s, 1105vs, 1060vs, 892s, 821w, 788w, 739s, 693s, 645w, 587w, 534s, 516s; δ_H(300 MHz; $CDCl_3$; 25 °C; Me_4Si) 8.14 (1 H, dd, $^{3}J_{HH}$ 7.3 Hz, $^{4}J_{HH}$ 1.1 Hz, Nap 4-H), 7.84 (1 H, dd, $^{3}J_{HH}$ 8.2 Hz, $^{4}J_{HH}$ 1.0 Hz, Nap 2-H), 7.44-7.37 (6 H, m, Nap 3-H, P-Phenyl), 7.31-7.24 (8 H, m, Nap 5-H, P-Phenyl), 7.17-7.12 (8 H, m, P-Phenyl), 6.85-6.79 (1 H, m, Nap 6-H), 5.85 (1 H, d, $^{3}J_{HH}$ 7.5 Hz, Nap 7-H), 2.38 (3 H, d, $^{2}J_{HH}$ 11.1 Hz, P-CH_3), 1.26 (3 H, $^{2}J_{HH}$ 10.0 Hz, P-CH_3); δ_C(75.5 MHz; $CDCl_3$; 25 °C; Me_4Si); 132.9 (d, $^{2}J_{CP}$ 3.3 Hz), 132.8 (d, $^{2}J_{CP}$ 3.1 Hz), 132.2(s), 131.6 (d, $^{4}J_{CP}$ 2.1 Hz), 131.1 (d, $^{4}J_{CP}$ 2.2 Hz), 129.2 (d, $^{3}J_{CP}$ 2.8 Hz), 129.0 (d, $^{3}J_{CP}$ 3.3 Hz), 128.0(s), 124.7(s), 119.7(s), 116.6(s), 115.6(s), 16.0 (d, $^{1}J_{CP}$ 43.2 Hz), 11.6 (d, $^{1}J_{CP}$ 34.5 Hz); δ_P(110 MHz; $CDCl_3$; 25 °C; H_3PO_4) 3.0 (d, $^{1}J_{PPt}$ 2537 Hz, $^{2}J_{PPt}$ 19 Hz), -2.4 (d, $^{1}J_{PPt}$ 3700 Hz, $^{2}J_{PPt}$ 19 Hz); MS (ES^+): *m/z* 823.50 (20%, M^+ + Na).

[Pt(1-(SO_2),8-(O)-nap)(PMe_2Ph)$_2$] (1c): From 1,8-naphthosultone (0.16 g, 0.80 mmol), lithium triethylborohydride (1.50 mL of a 1.0 M solution in THF, 1.50 mmol) and *cis*-dichloro*bis*(dimethylphenylphosphine)platinum (0.22 g, 0.41 mmol) to yield a yellow solid (0.05 g, 17%); mp 186-188 °C (decomp.); elemental analysis (Found: C, 46.2; H, 4.3. Calc. for $C_{26}H_{28}O_3P_2PtS$: C, 46.1; H, 4.2%); IR (KBr disc) ν_{max} cm^{-1} 3426w, 3052w, 2963w, 2917w, 1555s, 1496w, 1439vs, 1370vs, 1284vs, 1263s, 1187vs, 1106vs, 1055vs, 1031s, 954s, 912s, 847w, 824s, 789s, 746s, 719w, 694s, 646w, 618w, 585s, 534s; δ_H(300 MHz; $CDCl_3$; 25 °C; Me_4Si) 8.30 (1 H, dd,

$^{3}J_{HH}$ 7.2 Hz, $^{4}J_{HH}$ 0.8 Hz, Nap 4-H), 7.89 (1 H, dd, $^{3}J_{HH}$ 8.2 Hz, $^{4}J_{HH}$ 0.8 Hz, Nap 2-H), 7.91-7.88 (1 H, m, Nap 3-H), 7.48-7.08 (12 H, m, Nap 5-H, Nap 6-H, P-Phenyl), 6.91 (1 H, d, $^{3}J_{HH}$ 7.0 Hz, Nap 7-H), 1.88 (3 H, d, $^{2}J_{HH}$ 11.5 Hz, P-CH_3), 1.30 (3 H, $^{2}J_{HH}$ 10.7 Hz, P-CH_3); δ_C(75.5 MHz; $CDCl_3$; 25 °C; Me_4Si) 132.5 (s), 131.4-130.7 (m), 129.3 (d, $^{3}J_{CP}$ 10.6 Hz), 129.1 (d, $^{3}J_{CP}$ 10.8 Hz), 128.1(s), 125.0(s), 119.6(s), 117.1(s), 115.3 (s), 14.9 (d, $^{1}J_{CP}$ 43.2 Hz), 11.1 (d, $^{1}J_{CP}$ 34.7 Hz); δ_P(110 MHz; $CDCl_3$; 25 °C; H_3PO_4) -9.6 (d, $^{1}J_{PPt}$ 2504 Hz, $^{2}J_{PPt}$ 21 Hz), -17.6 (d, $^{1}J_{PPt}$ 3603 Hz, $^{2}J_{PPt}$ 21 Hz); MS (ES^+): *m/z* 699.59 (45%, M^+ + Na).

Platinum Complexes of 1,8-Naphthosultam

[Pt(1-(SO_2),8-(N)-nap)(PPh_3)$_2$(Cl)] (mono-2a): *Method A:* Lithium triethylborohydride (0.75 mL of a 1.0 M solution in THF, 0.75 mmol) was added to a solution of 1,8-naphthosultam (0.08 g, 0.38 mmol) in THF (10 mL). An immediate colour change occurred from clear, orange to clear, yellow. After stirring for 30 min, the resulting solution was transferred *via* a stainless steel cannula to a suspension of *cis*-dichloro*bis*(triphenylphosphine)platinum (0.30 g, 0.37 mmol) in THF (10 mL). The mixture was stirred for 24 hours resulting in a creamy yellow solution. The solution was then filtered through a layer of silica and eluted with dichloromethane (100 mL). The filtrate was evaporated to dryness under reduced pressure and was re-dissolved in dichloromethane (5 mL). Hexane (50 mL) was slowly added to induce precipitation, followed by diethyl ether (50 mL). The impure yellow solid was collected by suction filtration, washed with diethyl ether (25 mL) and dried *in vacuo*. The product was recrystallised from dichloromethane/hexane; δ_P(110 MHz; $CDCl_3$; 25 °C; H_3PO_4) 8.34 (d, $^{1}J_{PPt}$ 3328 Hz, $^{2}J_{PPt}$ 19 Hz), -16.3 (d, $^{1}J_{PPt}$ 3804 Hz, $^{2}J_{PPt}$ 19 Hz).

Method B: DBU (0.06 mL, 0.40 mmol) was added to a solution of 1,8-naphthosultam (0.08 g, 0.38 mmol) in THF (10 mL). An immediate colour change occurred from clear orange to clear yellow. After stirring for 30 min, the resulting solution was transferred *via* a stainless steel cannula to a suspension of *cis*-dichloro*bis*(triphenylphosphine)platinum (0.30 g, 0.38 mmol) in THF (10 mL). The mixture was stirred for 24 hours resulting in a clear dark yellow solution. The solution was then filtered through a layer of silica and eluted with dichloromethane (100 mL). The filtrate was evaporated to dryness under reduced pressure, to give a yellow oil and this was re-dissolved in dichloromethane (5 mL). Hexane (50 mL) was slowly added to induce precipitation, followed by diethyl ether (25 mL). The impure yellow solid was collected by suction filtration, washed with

diethyl ether (25 mL) and dried *in vacuo*; δ_P(110 MHz; $CDCl_3$; 25 °C; H_3PO_4) 8.4 (d, $^1J_{PPt}$ 3331 Hz, $^2J_{PPt}$ 19 Hz), -16.4 (d, $^1J_{P\text{-}Pt}$ 3799 Hz, $^2J_{PPt}$ 19 Hz).

Method C: Sodium *tert*-butoxide (0.08 g, 0.82 mmol) was added to a solution of 1,8-naphthosultam (0.16 g, 0.78 mmol) in THF (20 mL). An immediate colour change occurred from clear, orange to dark, yellow. After stirring for 30 min, the resulting solution was transferred *via* a stainless steel cannula to a suspension of *cis*-dichloro*bis*(triphenylphosphine)platinum (0.30 g, 0.38 mmol) in THF (10 mL). The mixture was stirred for 24 hours resulting in a cloudy yellow solution. The solution was then filtered and the filtrate was evaporated to dryness under reduced pressure, to give a yellow solid which was dried *in vacuo* (0.15 g, 40%); mp 155-157 °C (decomp.); elemental analysis (Found: C, 57.4; H, 3.9; N, 1.4. Calc. for $C_{46}H_{36}ClNO_2P_2PtS$: C, 57.6; H, 3.8; N, 1.5%); IR (KBr disc) ν_{max} cm^{-1} 3054w, 1621w, 1582s, 1482s, 1436vs, 1374s, 1281vs, 1211w, 1156vs, 1134vs, 1095vs, 1000w, 879w, 808s, 744s, 692vs, 604w, 568s, 548s, 526vs, 497s; δ_H(300 MHz; $CDCl_3$; 25 °C; Me_4Si) 7.52-7.39 (12 H, m, Nap 2, 4-H, P-Phenyl), 7.31-7.13 (6 H, m, Nap 3, 5, 6-H, P-Phenyl), 7.09-7.05 (6 H, m, P-Phenyl), 7.00-6.95 (6 H, m, P-Phenyl), 6.90-6.83 (6 H, m, P-Phenyl), 6.77 (1 H, d, $^3J_{HH}$ 7.2 Hz, Nap 7-H); δ_C(75.5 MHz; $CDCl_3$; 25 °C; Me_4Si) 135.7 (d, $^2J_{CP}$ 10.1 Hz), 134.9 (d, $^2J_{CP}$ 10.9 Hz), 131.1 (br s), 129.6(s), 129.2(s), 128.4 (d, $^3J_{CP}$ 11.2 Hz), 128.0 (d, $^3J_{CP}$ 11.5 Hz), 126.6(s), 118.2(s), 114.2(s), 104.9(s); δ_P(110 MHz; $CDCl_3$; 25 °C; H_3PO_4) 8.4 (d, $^1J_{PPt}$ 3331 Hz, $^2J_{PPt}$ 19 Hz), -16.4 (d, $^1J_{PPt}$ 3799 Hz, $^2J_{PPt}$ 19 Hz); MS (ES^+): *m/z* 923.06 (100%, M^+ - Cl).

The other 1,8-naphthosultam mono-complexes were prepared using methods A to C, except **mono-2e** and **mono-3a** which were prepared using method C only.

[Pt(1-(SO_2),8-(N)-nap)(PPh_2Me)$_2$(Cl)] (mono-2b): *Method A*: From 1,8-naphthosultam (0.08 g, 0.38 mmol), lithium triethylborohydride (0.75 mL of a 1.0 M solution in THF, 0.75 mmol) and *cis*-dichloro*bis*(diphenylmethylphosphine)platinum (0.18 g, 0.26 mmol); δ_P(110 MHz; $CDCl_3$; 25 °C; H_3PO_4) -5.8 (d, $^1J_{PPt}$ 3260 Hz, $^2J_{PPt}$ 20 Hz), -2.8 (d, $^1J_{PPt}$ 3698 Hz, $^2J_{PPt}$ 20 Hz).

Method B: From 1,8-naphthosultam (0.08 g, 0.40 mmol), DBU (0.06 mL, 0.39 mmol) and *cis*-dichloro*bis*(diphenylmethylphosphine)platinum (0.17 g, 0.26 mmol); δ_P(110 MHz; $CDCl_3$; 25 °C; H_3PO_4) -5.9 (d, $^1J_{PPt}$ 3255 Hz, $^2J_{PPt}$ 20 Hz), 2.4 (d, $^1J_{PPt}$ 3708 Hz, $^2J_{PPt}$ 20 Hz).

Method C: From 1,8-naphthosultam (0.08 g, 0.38 mmol), sodium *tert*-butoxide (0.04 g, 0.41 mmol) and *cis*-dichloro*bis*(diphenylmethylphosphine)platinum (0.26 g, 0.39 mmol); δ_P(110 MHz; $CDCl_3$; 25 °C; H_3PO_4) -5.9 (d, $^1J_{PPt}$ 3262 Hz, $^2J_{PPt}$ 20 Hz), 2.5 (d, $^1J_{PPt}$ 3699 Hz, $^2J_{PPt}$ 20 Hz).

[Pt(1-(SO_2),8-(N)-nap)($PPhMe_2$)$_2$(Cl)] (mono-2c): *Method A*: From 1,8-naphthosultam (0.08 g, 0.40 mmol), lithium triethylborohydride (0.75 mL of a 1.0 M solution in THF, 0.75 mmol) and *cis*-dichloro*bis*(dimethylphenylphosphine)platinum (0.15 g, 0.28 mmol); δ_P(110 MHz; $CDCl_3$; 25 °C; H_3PO_4) -18.3 (d, $^1J_{PPt}$ 3159 Hz, $^2J_{PPt}$ 21 Hz), -10.9 (d, $^1J_{PPt}$ 3577 Hz, $^2J_{PPt}$ 21 Hz).

Method B: From 1,8-naphthosultam (0.08 g, 0.39 mmol), DBU (0.06 mL, 0.39 mmol) and *cis*-dichloro*bis*(dimethylphenylphosphine)platinum (0.16 g, 0.30 mmol); δ_P(110 MHz; $CDCl_3$; 25 °C; H_3PO_4) -18.2 (d, $^1J_{PPt}$ 3221 Hz, $^2J_{PPt}$ 21 Hz), -10.9 (d, $^1J_{PPt}$ 3594 Hz, $^2J_{PPt}$ 21 Hz).

Method C: From 1,8-naphthosultam (0.08 g, 0.39 mmol), sodium *tert*-butoxide (0.04 g, 0.41 mmol) and *cis*-dichloro*bis*(dimethylphenylphosphine)platinum (0.21 g, 0.39 mmol); δ_P(110 MHz; $CDCl_3$; 25 °C; H_3PO_4) -18.4 (d, $^2J_{PPt}$ 21 Hz), -10.9 (d, $^2J_{PPt}$ 21 Hz).

[Pt(1-(SO_2),8-(N)-nap)(PMe_3)$_2$(Cl)] (mono-2d): *Method A*: From 1,8-naphthosultam (0.08 g, 0.41 mmol), lithium triethylborohydride (0.78 mL of a 1.0 M solution in THF, 0.78 mmol) and *cis*-dichloro*bis*(trimethylphosphine)platinum (0.16 g, 0.39 mmol); δ_P(110 MHz; $CDCl_3$; 25 °C; H_3PO_4) -22.1 (d, $^1J_{PPt}$ 3179 Hz, $^2J_{PPt}$ 22 Hz), -26.1 (d, $^1J_{PPt}$ 3507 Hz, $^2J_{PPt}$ 22 Hz).

Method B: From 1,8-naphthosultam (0.08 g, 0.39 mmol), DBU (0.06 mL, 0.39 mmol) and *cis*-dichloro*bis*(trimethylphosphine)platinum (0.16 g, 0.39 mmol); δ_P(110 MHz; $CDCl_3$; 25 °C; H_3PO_4) -22.2 (d, $^1J_{PPt}$ 3165 Hz, $^2J_{PPt}$ 23 Hz), -26.2 (d, $^1J_{PPt}$ 3508 Hz, $^2J_{PPt}$ 23 Hz).

Method C: From 1,8-naphthosultam (0.08 g, 0.38 mmol), sodium *tert*-butoxide (0.04 g, 0.39 mmol) and *cis*-dichloro*bis*(trimethylphosphine)platinum (0.17 g, 0.42 mmol); δ_P(110 MHz; $CDCl_3$; 25 °C; H_3PO_4) -22.2 (d, $^2J_{PPt}$ 23 Hz), -26.3 (d, $^2J_{PPt}$ 23 Hz).

[Pt(1-(SO_2),8-(N)-nap)(COD)(Cl)] (mono-2e): *Method C*: From 1,8-naphthosultam (0.08 g, 0.40 mmol), sodium *tert*-butoxide (0.04 g, 0.42 mmol) and (1,5-cyclooctadiene)platinum(II) dichloride (0.16 g, 0.43 mmol) to yield an off-brown solid (0.13 g, 61%); mp 134-136 °C (decomp.);

elemental analysis (Found: C, 39.6; H, 3.4; N, 2.7. Calc. for $C_{18}H_{18}ClNO_2PtS$: C, 39.8; H, 3.3; N, 2.6%); IR (KBr disc) ν_{max} cm^{-1} 3229w, 3008w, 2961w, 2363w, 2345w, 1625w, 1583w, 1492w, 1475w, 1460w, 1450s, 1424w, 1371s, 1339s, 1311s, 1178s, 1157vs, 1138vs, 1029w, 1009s, 910w, 872s, 832s, 811vs, 765s, 695w, 604s, 570s, 555w, 527s, 503w, 474s; δ_H(300 MHz; $CDCl_3$; 25 °C; Me_4Si) 8.00 (1 H, d, $^3J_{HH}$ 8.2 Hz, Nap 4-H), 7.88 (1 H, d, $^3J_{HH}$ 7.0 Hz, Nap 2-H), 7.70-7.65 (1 H, m, Nap 3-H), 7.44-7.42 (2 H, m, Nap 5, 6-H), 6.86 (1 H, dd, $^3J_{HH}$ 6.2 Hz, $^4J_{HH}$ 1.8 Hz, Nap 5-H), 5.51 (4 H, s, $^2J_{PtH}$ 66.7 Hz, COD-CH_2), 2.61-2.57 (4 H, m, COD-CH_2), 2.20-2.13 (4 H, m, COD-CH_2); δ_C(75.5 MHz; $CDCl_3$; 25 °C; Me_4Si) 131.6(s), 129.8(s), 128.6(s), 120.2(s), 120.0(s), 107.4(s), 100.7 (s, $^1J_{PtC}$ 152.6 Hz), 31.3 (s); MS (ES^+): *m/z* 564.91 (35%, M^+ + Na).

[Pd(1-(SO_2),8-(N)-nap)(PPh_3)$_2$(Cl)] (mono-3a): *Method C*: From 1,8-naphthosultam (0.09 g, 0.42 mmol), sodium *tert*-butoxide (0.04 g, 0.37 mmol) and *trans*-dichloro*bis*(triphenylphosphine)palladium, to yield a cream solid (0.14 g, 45%); mp 157-159 °C; elemental analysis (Found: C, 63.3; H, 4.2; N, 1.7. Calc. for $C_{46}H_{36}ClNO_2P_2PdS$: C, 63.5; H, 4.2; N, 1.6%); IR (KBr disc) ν_{max} cm^{-1} 3448s, 3054w, 2361s, 2342s, 1773w, 1619w, 1581s, 1482w, 1448s, 1435vs, 1375s, 1333w, 1277s, 1186w, 1156vs, 1131vs, 1096s, 1028w, 998w, 875w, 809s, 767w, 745s, 722s, 667vs, 669w, 606w, 568s, 540s, 520vs, 511vs, 457w, 350w; δ_H(300 MHz; $CDCl_3$; 25 °C; Me_4Si) 7.68-7.60 (12 H, m, P-Phenyl), 7.53-7.50 (1 H, m, Nap 4-H), 7.31-7.21 (2 H, m, Nap 2, 3-H), 7.21-7.14 (6 H, P-Phenyl), 7.11-7.02 (12 H, m, P-Phenyl), 6.98-6.92 (1 H, m, Nap 6-H), 6.72 (1 H, d, $^3J_{HH}$ 8.3 Hz, Nap 7-H), 6.26 (1 H, d, $^3J_{HH}$ 7.2 Hz, Nap 5-H); δ_C(75.5 MHz; $CDCl_3$; 25 °C; Me_4Si) 135.4-135.3 (m, P-Phenyl), 130.8(s, P-Phenyl), 129.0(s), 128.9(s), 128.3-128.1 (m, P-phenyl), 126.5(s), 118.7(s), 113.6(s), 103.7(s); δ_P(110 MHz; $CDCl_3$; 25 °C; H_3PO_4) 23.1 (s); MS (ES^+): *m/z* 857.25 (100%, M^+ + Na-Cl). Due to impurities ^1H and ^{13}C NMR peaks have been tentatively assigned based on prior knowledge of structurally similar compounds.

[Pt(1-(SO_2),8-(N)-nap)$_2$(PPh_2Me)$_2$] (bis-2b): Sodium *tert*-butoxide (0.08 g, 0.84 mmol) was added to a solution of 1,8-naphthosultam (0.16 g, 0.80 mmol) in THF (20 mL). An immediate colour change occurred from clear orange to dark yellow. After stirring for 30 min, the resulting solution was transferred *via* a stainless steel cannula to a suspension of *cis*-dichloro*bis*(diphenylmethylphosphine)platinum (0.27 g, 0.40 mmol) in THF (10 mL). The mixture was stirred for 24 hours resulting in a cloudy yellow solution. The solution was then filtered and the filtrate was evaporated to dryness under reduced pressure, to give a yellow solid which was dried *in vacuo* (0.14 g, 34%); mp 179-181 °C; elemental analysis (Found: C, 54.8; H, 3.9; N, 2.7.

Calc. for $C_{46}H_{38}N_2O_4P_2PtS_2$: C, 55.0; H, 3.8; N, 2.8%); IR (KBr disc) ν_{max} cm^{-1} 3053w, 2923w, 1621w, 1582s, 1489s, 1448vs, 1373vs, 1335w, 1273vs, 1211s, 1157vs, 1133vs, 1104s, 1022w, 884s, 810s, 766s, 736s, 692s, 606w, 568s, 510s, 454w, 353w; δ_H(300 MHz; $CDCl_3$; 25 °C; Me_4Si) 7.57 (1 H, d, $^3J_{HH}$ 8.1 Hz, Nap 4-H), 7.45 (1 H, d, $^3J_{HH}$ 7.1 Hz, Nap 2-H), 7.40-7.38 (4 H, m, P-Phenyl 10, 14 H), 7.32-7.24 (2 H, m, Nap 3, 6-H), 7.19-7.17 (1 H, m, Nap 5-H), 7.06-6.98 (6 H, m, P-Phenyl 11-13-H), 6.93 (1 H, d, $^3J_{HH}$ 8.4 Hz, Nap 7-H), 1.70 (6 H, d, $^1J_{HH}$ 10.5 Hz, CH_3 x 2); δ_C(75.5 MHz; $CDCl_3$; 25 °C; Me_4Si); 133.6-133.1 (m, P-Phenyl), 131.4 (br s), 131.1 (br s), 129.8(s), 129.4(s), 128.4-128.3 (m, P-Phenyl), 126.7(s), 118.2(s), 114.6(s), 106.6(s), 30.7(s, P-Methyl); δ_P(110 MHz; $CDCl_3$; 25 °C; H_3PO_4) -7.3 (s, $^1J_{PPt}$ 3348 Hz); MS (ES^+): *m/z* 1025.98 (100%, M^+ + Na), 798.99 (80%, M^+ - Cl).

The other 1,8-naphthosultam *bis*-complexes were prepared using the same method.

[Pt(1-(SO_2),8-(N)-nap)$_2$($PPhMe_2$)$_2$] (bis-2c): From 1,8-naphthosultam (0.16 g, 0.78 mmol), sodium *tert*-butoxide (0.08 g, 0.82 mmol) and *cis*-dichloro*bis*(dimethylphenylphosphine)platinum (0.21 g, 0.37 mmol) to yield a yellow solid (0.24 g, 76%); mp 171-173 °C (decomp.); elemental analysis (Found: C, 41.4; H, 3.6; N, 2.8. Calc. for $C_{36}H_{34}N_2O_4P_2PtS_2$: C, 49.1; H, 3.9; N, 3.2%); IR (KBr disc) ν_{max} cm^{-1} 2919w, 1621s, 1581s, 1490s, 1449vs, 1372vs, 1335w, 1273vs, 1211w, 1157vs, 1132vs, 1109s, 950s, 926s, 880s, 811s, 745s, 694s, 606w, 568s, 534s, 490w, 449w, 350w; δ_H(300 MHz; $CDCl_3$; 25 °C; Me_4Si) 7.74 (2 H, d, $^3J_{HH}$ 8.0 Hz, Nap 4-H), 7.66 (2H, d, $^3J_{HH}$ 6.8 Hz, Nap 2-H), 7.46-7.33 (16 H, m, Nap 3, 5, 6-H, P-Phenyl), 7.01 (1 H, dd, $^3J_{HH}$ 7.8 Hz, $^4J_{HH}$ 1.1 Hz, Nap 7-H), 1.27-1.18 (12 H, m, CH_3 x 4); δ_C(75.5 MHz; $CDCl_3$; 25 °C; Me_4Si); 132.1(s), 131.6-131.5 (m, P-Phenyl), 130.1(s), 129.5-129.3 (m, P-phenyl), 127.2(s), 118.8(s), 114.6(s), 106.5(s), 16.1 (d, $^1J_{PC}$ 43.0 Hz), 10.6 (d, $^1J_{PC}$ 40.0 Hz); δ_P(110 MHz; $CDCl_3$; 25 °C; H_3PO_4) -16.2 (s, $^1J_{PPt}$ 3305 Hz); MS (ES^+): *m/z* 901.89 (100%, M^+ + Na), 674.95 (70%, M^+ - Cl). NB. Elemental analysis was submitted multiple times with no success.

[Pt(1-(SO_2),8-(N)-nap)$_2$(PMe_3)$_2$] (bis-2d): From 1,8-naphthosultam (0.16 g, 0.79 mmol), sodium *tert*-butoxide (0.08 g, 0.81 mmol) and *cis*-dichloro*bis*(trimethylphosphine)platinum (0.17 g, 0.40 mmol) to yield an impure yellow solid; δ_P(110 MHz; $CDCl_3$; 25 °C; H_3PO_4) -25.4 (s, $^1J_{PPt}$ 3216 Hz).

[Pt(1-(SO_2),8-(N)-nap)$_2$(COD)] (bis-2e): From 1,8-naphthosultam (0.16 g, 0.78 mmol), sodium *tert*-butoxide (0.08 g, 0.84 mmol) and (1,5-cyclooctadiene)platinum(II) dichloride (0.15 g, 0.41 mmol) to yield a yellow solid (0.07 g, 24%); mp 180-182 °C (decomp.); elemental analysis (Found:

C, 37.95; H, 3.3; N, 2.9. Calc. for $C_{28}H_{24}N_2O_4PtS_2$: C, 47.3; H, 3.4; N, 3.9%); IR (KBr disc) ν_{max} cm^{-1} 3434s, 1622s, 1582s, 1491w, 1450s, 1372s, 1281s, 1157vs, 1134vs, 880s, 813s, 606s, 571s, 534s; δ_H(300 MHz; $CDCl_3$; 25 °C; Me_4Si) 7.71 (1 H, d, $^3J_{HH}$ 6.8 Hz, Nap 4-H), 7.62 (1 H, d, $^3J_{HH}$ 8.1 Hz, Nap 2-H), 7.46-7.41 (1 H, m, Nap 3-H), 7.23-7.16 (2 H, m, Nap 5, 6-H), 6.69-6.60 (1 H, m, Nap 7-H), 5.82 (4 H, s, COD-CH_2), 2.77-2.72 (4 H, m, COD-CH_2), 2.34-2.30 (4 H, m, COD-CH_2); δ_C(75.5 MHz; $CDCl_3$; 25 °C; Me_4Si) 130.4(s), 129.1(s), 118.6(s), 116.1(s), 107.8(s), 104.7(s), 31.0(s); MS (ES^+): *m/z* 734.05 (50%, M^+ + Na). NB. Elemental analysis was submitted multiple times with no success.

Pt-DBU Complex: DBU (0.03 mL, 0.20 mmol) was added to a suspension of *cis*-dichloro*bis*(triphenylphosphine)platinum (0.15 g, 0.19 mmol) and ammonium tetrafluoroborate (0.03 g, 0.25 mmol) in THF (10 mL). The mixture was stirred overnight resulting in a clear, colourless solution. The solution was then filtered through a layer of silica and eluted with dichloromethane (100 mL). The filtrate was evaporated to dryness under reduced pressure and was re-dissolved in dichloromethane (5 mL). Hexane (25 mL) was slowly added to induce precipitation, followed by diethyl ether (25 mL). A white solid was collected by suction filtration, washed with diethyl ether (25 mL) and dried *in vacuo* (0.10 g, 54%); mp 145-147 °C (decomp.); elemental analysis (Found: C, 51.6; H, 4.5; N, 2.8. Calc. for $C_{45}H_{46}BClF_4N_2P_2Pt.CH_2Cl_2$: C, 51.2; H, 4.5; N, 2.6%); IR (KBr disc) ν_{max} cm^{-1} 3056w, 2934w, 2861w, 1602vs, 1482w, 1437s, 1377w, 1319s, 1190w, 1161w, 1095vs, 1056vs, 999w, 842w, 749s, 696vs, 550s, 527vs, 499s, 424w; δ_H(300 MHz; $CDCl_3$; 25 °C; Me_4Si) 7.58-7.50 (3 H, m, P-Phenyl), 7.44-7.33 (5 H, m, P-Phenyl), 7.26-7.20 (2 H, m, P-Phenyl), 3.79-3.64 (2 H, m, DBU-CH_2), 3.52-3.40 (3 H, m, DBU-CH_2), 3.17-3.09 (1 H, m, DBU-CH_2), 2.98-2.90 (1 H, m, DBU-CH_2), 2.77-2.54 (3 H, m, DBU-CH_2), 2.39 (1 H, br s), 1.70-1.53 (4 H, m, DBU-CH_2), 1.28-1.20 (1 H, m, DBU-CH_2); δ_C(75.5 MHz; $CDCl_3$; 25 °C; Me_4Si); 135.3 (d, $^2J_{CP}$ 10.1 Hz), 134.4 (d, $^2J_{CP}$ 11.0 Hz), 132.7 (d, $^4J_{CP}$ 2.3 Hz), 131.7 (d, $^4J_{CP}$ 2.8 Hz), 129.4 (d, $^3J_{CP}$ 11.3 Hz), 128.7 (d, $^3J_{CP}$ 11.2 Hz), 54.8(s), 48.1(s), 47.4(s), 39.9(s), 29.1(s), 27.6(s), 23.7(s), 21.9(s); δ_P(110 MHz; $CDCl_3$; 25 °C; H_3PO_4) 14.5 (d, $^1J_{PPt}$ 3857 Hz, $^2J_{PPt}$ 19 Hz), 6.1 (d, $^1J_{PPt}$ 3056 Hz, $^2J_{PPt}$ 19 Hz); δ_F (376.5 MHz, $(CD_3)_2CO$, 25 °C, CCl_3F) −152.1(br s, $^{10}BF_4^-$), −152.2(br s, $^{11}BF_4^-$); MS (ES^+): *m/z* 907.09 (100%, M^+).

N-methyl-1,8-naphthosultam (2Me):[23] A solution of sodium hydroxide (0.44 g, 11.0 mmol) in water (10 mL) was added to a stirred solution of 1,8-naphthosultam (2.06 g, 10.0 mmol) in dimethylacetamide (10 mL). Heat was produced during addition, upon cooling to room temperature iodomethane (0.65 mL, 10.5 mmol) was added and the solution was left to stir overnight. The resulting dark brown solution was filtered and the filtrate was added slowly to

water (150 mL) with vigorous stirring to yield a cream solid. The solid was collected and dried *in vacuo*. (1.21 g, 55%). ^{1}H NMR data was in agreement with literature values.

References

[1] E. G. Cox, D. W. J. Cruickshank and J. A. S. Smith, *Proc. Roy. Soc. (London)*., 1958, **A247**, 1.

[2] C. A. Coulson, R. Daudel and J. M. Robertson, *Proc. Roy. Soc. (London).,* 1951, **A207**, 306; D. W. J. Cruickshank, *Acta. Crystallogr.,* 1957, **10**, 504.

[3] V. Balasubramaniyan, *Chem. Rev.,* 1966, **66**, 567.

[4] A. Bondi, *J. Phys. Chem.,* 1964, **68**, 441.

[5] F. R. Knight, A. L. Fuller, M. Bühl, A. M. Z. Slawin and J. D. Woollins, *Chem. Eur. J.,* 2010, **16**, 7503 and the references therein.

[6] R. W. Alder, P. S. Bowman, W. R. S. Steele and D. R. Winterman, *Chem. Commun.,* 1968, 723; R. W. Alder, M. R. Bryce, N. C. Goode, N. Miller and J. Owen, *J. Chem. Soc., Perkin Trans. 1,* 1981, 2840.

[7] J. D. Hoefelmeyer, M. Schulte, M. Tschinkl and F. P. Gabbai, *Coord. Chem. Rev.,* 2002, **235**, 93.

[8] P. Kilian, F. R. Knight and J. D. Woollins, *Chem. Eur. J.,* 2011, **17**, 2302.

[9] P. Kilian, F. R. Knight and J. D. Woollins, *Coord. Chem. Rev.,* 2011, **255**, 1387.

[10] B. K. Teo, F. Wudl, J. H. Marshall and A. Krugger, *J. Am. Chem. Soc.,* 1977, **99**, 2349; B. K. Teo, P. A. Snyder-Robinson, *Inorg. Chem.,* 1978, **17**, 3489; B. K. Teo, P. A. Snyder-Robinson, *Inorg. Chem.,* 1979, **18**, 1490; B. K. Teo, P. A. Snyder-Robinson, *Inorg. Chem.,* 1981, **20**, 4235.

[11] S. M. Aucott, H. L. Milton, S. D. Robertson, A. M. Z. Slawin, G. D. Walker and J. D. Woollins, *Chem. Eur. J.,* 2004, **10**, 1666; S. D. Robertson, PhD Thesis, University of St Andrews (UK), 2005. and the references therein.

[12] F. H. Allen, O. Kennard, D. G. Watson, L. Brammer, A. G. Orpen and R. Taylor, *J. Chem. Soc. Perkin Trans II*, 1987, S1.

[13] H. G. Wallace, J. G. Stark, M. L. McGlashan, *Chemistry Data Book Second in S.I.,* 2nd ed., John Murray Ltd, London, 1982.

[14] N. N. Greenwood, A. Earnshaw, *Chemistry of the Elements*, 2nd ed., Elsevier Butterworth-Heinemann, Oxford, 1997.

[15] All images of molecular structures were generated using OLEX2: O. V. Dolomanov, L. J. Bourhis, R. J. Gildea, J. A. K. Howard and H. Puschmann, *J. Appl. Cryst*., 2009, **42**, 339.

[16] B. J. Coe and S. J. Glenwright*, Coord. Chem. Re*v.*,* 2000, **203**, 5; T. G. Appleton, H. C. Clark and L. E. Manzer, *Coord. Chem. Rev.*, 1973, **10**, 335; A. Pidcock, R. E. Richards and L. M. Venanzi, *J. Chem. Soc. A*, 1966, 1707, F. R. Knight, A. L. Fuller, A. M. Z. Slawin and J. D. Woollins, *Polyhedron*, 2010, **29 (8)**, 1956.

[17] D. F. Shriver and P. W. Atkins, *Inorganic Chemistry,* 3rd ed., Oxford University Press, Oxford, 1999.

[18] P. G. Waddell, PhD Thesis, University of St Andrews (UK), 2010. and the references therein.

[19] C. A. Tolman, *Chem. Rev*., 1977, **77 (3)**, 313.

[20] D. H. Farrar and R. R. Gukathasan, *J. Chem. Soc. Dalton Trans*., 1989, 557.

[21] Clayden, Greeves, Warren and Wothers, *Organic Chemistry*, Oxford University Press, Oxford, 2001.

[22] D. S. Surry and S. L. Buchwald, *Chem. Sci*., 2011, **2 (1)**, 27.

[23] P. Maslak, A. Chopra, C. R. Moylan, R. Wortmann, S. Lebus, A. L. Rheingold and G. P. A. Yap, *J. Am. Chem. Soc.*, 1996, **118**, 1471.

[24] D. Drew and J. R. Doyle, *Inorg. Synth.,* 1972, **13**, 47.

[25] F. J. Ramos-Lima, A. G. Quiroga, J. M. Pérez, M. Font-Bardía, X. Solans and C. Navarro-Ranninger, *Eur. J. Inorg. Chem.,* 2003, **8**, 1591.

[26] J. Bailar and H. Itatani, *Inorg. Chem.,* 1965, **4**, 1618.

Chapter 3

A literature review of *peri*-substituted acenaphthylenes and acenaphthenes

Introduction

The chemistry of *peri*-substituted acenaphthylenes is much less developed than that of the naphthalenes or acenaphthenes, though there are many occurrences in the literature regarding mono- and poly- substitution of the acenaphthene and acenaphthylene ring systems and substitution across the ethane/ethene backbones. These types of reactions will not be discussed here, as the scope of this work is focussed on *peri*-substitution.

***Peri*-Substituted Acenaphthylenes**

A literature search of *peri*-substituted acenaphthylenes shows that Petrenko and Tel'nyuk[1] were the first group to prepare compounds of this type. Although information is limited, from 1966 to 1967 the group synthesised many halogen derivatives of acenaphthylene (Figure 1).

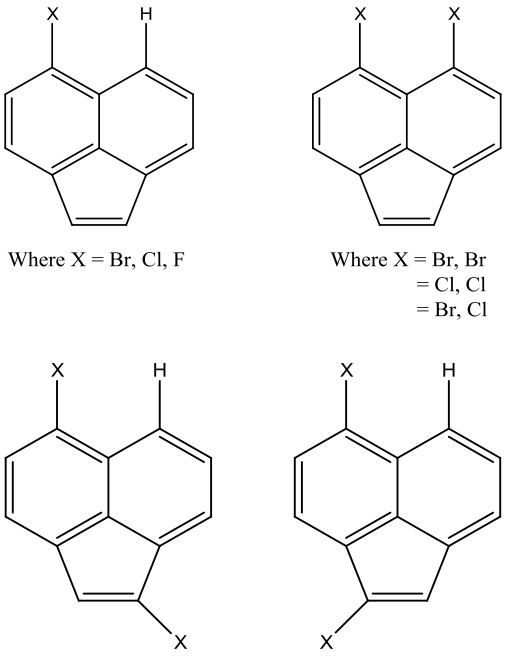

Figure 1 Examples of halogen derivatives synthesised by Petrenko and Teln'yuk.[1]

Chiang and Meinwald[2] described Petrenko's route to 5,6-dibromacenaphthylene as "lengthy and inefficient" and thus improved it. Their goal was to prepare chalcogen-bridged acenaphthylenes

via 5,6-dilithioacenaphthylene and therefore required an efficient route to 5,6-dibromoacenaphthylene. The first step in the synthetic route involves the bromination of acenaphthene using two equivalents of N-bromosuccinimide (NBS) to give 5,6-dibromoacenaphthene in a 25% yield. Bromination with a further two equivalents of NBS results in a mixture of the *cis* and *trans* isomers of 1,2,5,6-tetrabromoacenaphthene in a 84% yield. In the final step, 1,2,5,6-tetrabromoacenaphthene is debrominated using zinc dust in ethanol to yield 73% of the desired product (Scheme 1).

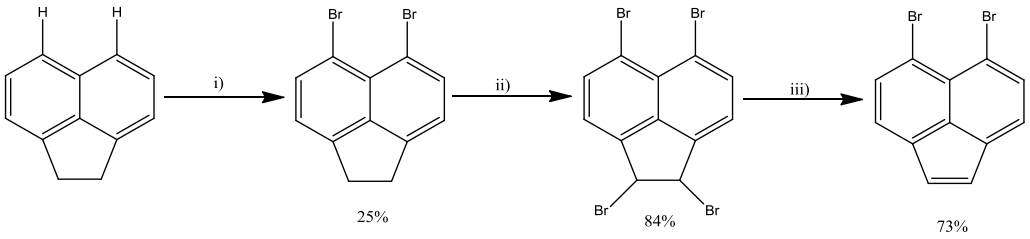

Scheme 1 Synthetic route to 5,6-dibromoacenaphthylene with yields shown for each stage: i) NBS (2 eq.), $C_4H_6O_3$, <25 °C; ii) NBS (2 eq.), CCl_4, $(C_6H_5CO_2)_2$); iii) Zn dust, EtOH.[2]

In 1992, Mitchell and co-workers prepared 5,6-dibromoacenaphthylene through a simpler route.[3] A solution of 5,6-dibromoacenaphthene and one and a half equivalents of 2,3-dichloro-5,6-dicyano-1,4-benzoquinone (DDQ) in dry benzene was heated to reflux for thirty hours. Once the solution was cooled to room temperature, pentane was added and the solution was filtered. The filtrate was then passed through a short column of basic alumina. Evaporation afforded the product in a 75% yield (Scheme 2).The group prepared 5,6-dibromoacenaphthylene with the intention of using it to form dicyclopenta[1,2,3-*cd*:1',2',3'-*lm*]perylene (Figure 2) through a coupling reaction. However, the reaction mixture was found to contain thirteen different products and the desired one could not be isolated. Dicyclopenta[1,2,3-*cd*:1',2',3'-*lm*]perylene was eventually prepared by treating diaceperylene with DDQ.

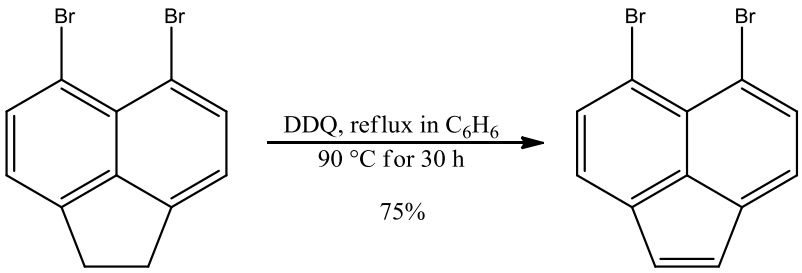

Scheme 2 Mitchell and co-workers synthetic route to 5,6-dibromoacenaphthylene.[3]

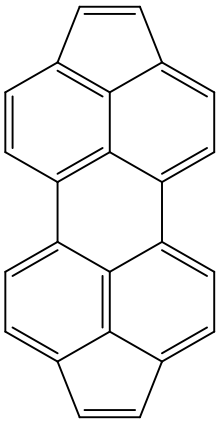

Figure 2 Dicyclopenta[1,2,3-*cd*:1',2',3'-*lm*]perylene.

After Petrenko and Tel'nyuk,[1] Koziar and Cowan[4] were the first to prepare 5,6-dichloroacenaphthylene. They used DDQ to dehydrogenate 5,6-dichloroacenaphthene in a similar procedure to that discussed previously for the synthesis of 5,6-dibromoacenaphthylene, yielding 34% of pure product.

Ogura *et al.*[5] also prepared 5,6-dichloroacenaphthylene for use as a precursor for preparing 3,4-dichacogen-bridged fluoranthenes, which the group were using to develop new electron donors. Ogura *et al.* utilised both synthetic routes previously discussed. They produced 5,6-dichloroacenaphthylene in a 37% yield *via* dehydrogenation with DDQ and in a 51% yield *via* bromination with NBS and further reaction with zinc dust and ethanol (Scheme 3).

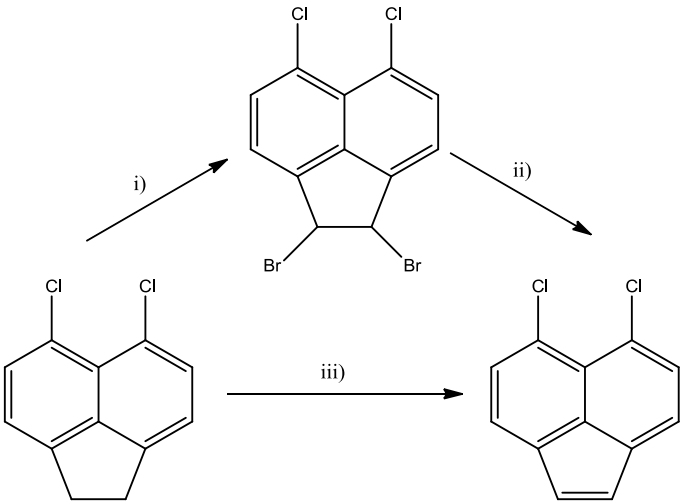

Scheme 3 The preparation of 5,6-dichloroacenaphthene: i) NBS, CCl_4, reflux; ii)Zn dust, EtOH, reflux; iii) DDQ, C_6H_6, reflux.[5]

The first known fluorine analogue of acenaphthylene was octafluoroacenaphthylene which was prepared in 1963 by Harrison and colleagues.[6] Surprisingly, it was years later in 2000, that the *peri*-substituted 5,6-difluoroacenaphthylene was synthesised. Mallory and co-workers[7] prepared eighteen compounds, including 5,6-difluroacenaphthylene, that were structurally similar to 1,8-difluoronaphthalene in order to study nuclear spin-spin coupling *via* non-bonded interactions. 5,6-difluoroacenaphthylene was synthesised by refluxing a mixture of 5,6-difluoroacenaphthene and nickel peroxide hydrate in benzene for twenty nine hours. Upon cooling to room temperature the reaction mixture was diluted with benzene and then filtered through Celite. Evaporation of the filtrate under reduced pressure yielded 56% of the product (Scheme 4).

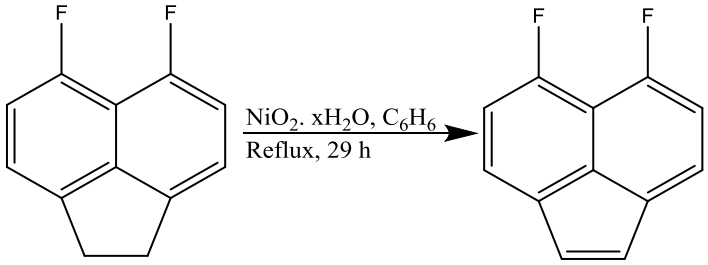

Scheme 4 The preparation of 5,6-difluoroacenaphthylene.[7]

A literature search for 5,6-diiodoacenaphthylene revealed that it has not been reported. The only iodine derivatives of acenaphthylene to have been reported are 1-iodoacenaphthylene and 1,2-diiodoacenaphthylene. These were synthesised by Dunoguès and co-workers[8] during a study of regioselective electrophilic substitution of silylated acenaphthenes and acenaphthylenes. The monoiodination reaction involved adding iodine monochloride, in carbon tetrachloride, dropwise at 0 °C to a solution of 1-(trimethylsilyl)acenaphthylene in carbon tetrachloride. The reaction was stirred for three hours at 0 °C, then for one hour at room temperature. The reaction mixture was washed with an aqueous solution of sodium thiosulfate and then water. The mixture was then dried over sodium sulfate and the carbon tetrachloride was evaporated. The crude product was purified using a silica column with a pentane eluent. The resulting 1-iodoacenaphthylene was collected in a 50-60% yield (Scheme 5). 1,2-Diiodoacenaphthylene was synthesised using the same procedure, but with two equivalents of iodine monochloride to give a 73% yield.

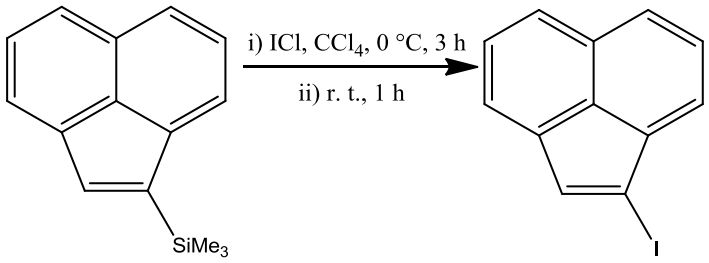

Scheme 5 The preparation of 1-iodocenaphthylene.[8]

In recent years acenaphthylenes have been used along with acenaphthenes to form proton sponges. In 2000, Ozeryanskii *et al.*[9] synthesised 5,6-*bis*(dimethylamino)acenaphthylene which is an analogue of the first known proton sponge 1,8-*bis*(dimethylamino)naphthalene.[10] 5,6-*bis*(dimethylamino)acenaphthylene was synthesised by reacting 5,6-diaminoacenaphthene with excess methyl iodide in a mixture of dimethyl sulfoxide (DMSO) and potassium hydroxide to give 5,6-*bis*(dimethylamino)acenaphthene; this was then dehydrogenated by reaction with chloranil in boiling benzene for thirty minutes (Scheme 6).

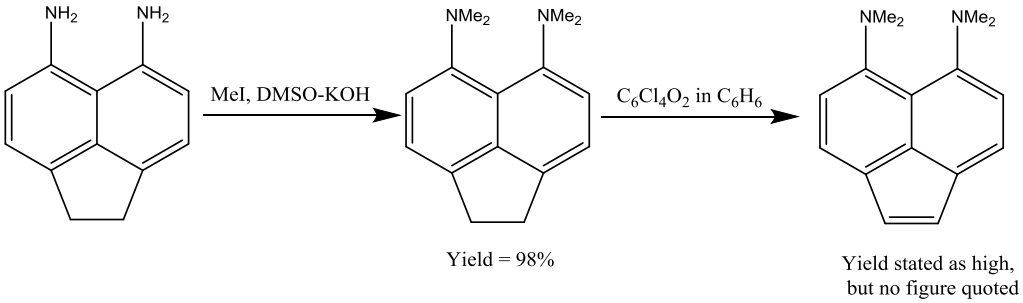

Scheme 6 The preparation of 5,6-*bis*(dimethylamino)acenaphthylene.[9]

The basicity constants (pK_a) of the two compounds measured in DMSO were very different, with 5,6-*bis*(dimethylamino)acenaphthene having a value of 7.7, similar to 5,6-*bis*(dimethylamino)naphthalene (pK_a of 7.5 in DMSO[11]), but the shorter carbon-carbon bridge causes the proton sponge 5,6-*bis*(dimethylamino)acenaphthylene to be less basic having a value of 5.7.

The authors[9] thought it possible that the slightly higher pK_a value of 7.7 for the acenaphthene analogue could be caused by the electron-donating effect of the ethane linker. Whereas the considerably lower pK_a value of 5.7 for the acenaphthylene analogue was due to more than just the weak dative properties of the ethene linker. It was concluded that the presence of the rigid five-membered ring in acenaphthene and acenaphthylene alters the geometry of the naphthalene core by compressing the angle at the bottom of the ring and widening the *peri*-region angle at the top. This widening causes an increase in the distance between the two NMe_2 substituents which in turn minimises their steric interaction. This decrease in interaction may result in a lowering of basicity because the activity of the nitrogen lone pairs is weakened due to more effective conjugation between the NMe_2 groups and the naphthalene π-system. This is much more apparent in the acenaphthylene analogue than the acenaphthene.[9]

It was found that the oxidation-reduction process for 5,6-*bis*(dimethylamino)acenaphthene to 5,6-*bis*(dimethylamino)acenaphthylene is easily reversible. Catalytic hydrogenation of 5,6-*bis*(dimethylamino)acenaphthylene using hydrogen gas and 2% palladium on charcoal at 20 °C for ten minutes results in 5,6-*bis*(dimethylamino)acenaphthene in a quantitative yield. This ability of a proton sponge to switch basicity through redox is the first of its kind to be reported and may prove useful in the field of molecular electronics.[9]

In 2002, Ozeryanskii *et al.*[12] continued their studies exploring the lowered basicity of 5,6-*bis*(dimethylamino)acenaphthylene. Comparison of the molecular structures of 5,6-*bis*(dimethylamino)acenaphthene and 5,6-*bis*(dimethylamino)acenaphthylene confirmed the authors previous assumptions that the shortening of the carbon-carbon bridge was having a profound effect on the chemistry of the acenaphthylene derivative. Substantial conjugation between the NMe_2 substituents and the aromatic acenaphthylene functionality can be deemed accountable for the significant reduction in basicity.

Ozeryanskii and co-workers spent the next few years studying the reactivity of 5,6-*bis*(dimethylamino)acenaphthylene. They found it can be used to form new "proton sponges" with the diazafluoroanthene backbone by reacting it in [4+2] cycloaddition reactions with *symm*-tetrazine derivatives.[13] It was also found that 5,6-*bis*(dimethylamino)acenaphthylene acts as both an electron-rich alkene or arene and a proton sponge.[14]

In the early part of the twentieth century, Dziewonski and Rapalski[15] discovered that when a solution of acenaphthylene was exposed to sunlight, dimerization occurred. The outcome of this dimerization reaction is two isomeric cyclobutane dimers, the yields of which depend greatly on the solvent and acenaphthylene concentration (Scheme 7).

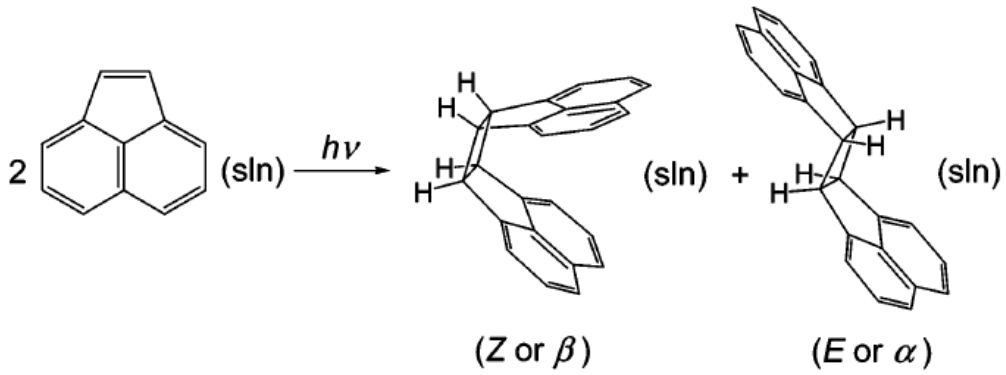

Scheme 7 The photodimerization of acenaphthylene yielding the Z and E isomers of cyclobutane.[15]

Koziar and Cowan studied internal heavy-atom effects on the photodimerization of acenaphthylene.[4] During this study they observed that 5,6-dichloroacenaphthylene behaves the

same way photochemically as acenaphthylene. In some solvents the *trans*cyclobutane dimer is the major product and the *cis*cyclobutane dimer the minor.

From 2006 to 2011, Mezheritskii and co-workers studied various aspects of *peri*-substituted acenaphthylenes. In 2006 they reported the first *peri*-amino ketone of acenaphthylene.[16] The groups aim was to create a structure which had a hydroxy or amino group in the *peri*-position adjacent to a carbonyl group across the *peri*-gap, thus allowing the substituents to be conjugated through the π system. *Peri*-substituents that are conjugated into the aromatic system are unusual and the group were hoping this would create new reactivity.

N-(6-Acetylacenaphthylen-5-yl)acetamide was prepared, in a 13% yield, by adding chloranil to a solution of *N*-(6-acetylacenaphthen-5-yl)acetamide in *o*-dichlorobenzene. The mixture was refluxed for two hours using a Vigreaux column. Upon cooling the solvent was removed and the remaining solid was redissolved in chloroform and purified using an alumina column (Scheme 8).

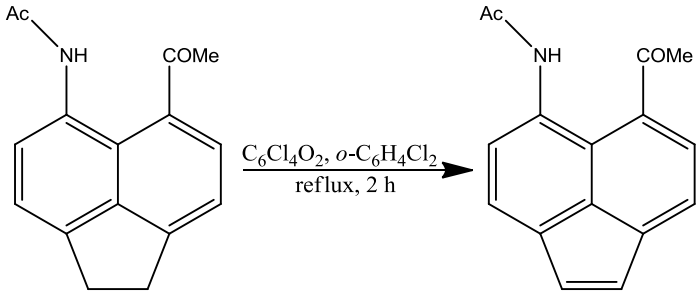

Scheme 8 Synthetic route for *N*-(6-acetylacenaphthylen-5-yl)acetamide.[16]

The acenaphthene analogue displays a sharp peak in the ^{1}H NMR spectrum for the NH proton in the acetylamino substituent, shifted strongly downfield to 9.7 ppm (DMSO-d_6). This downfield shift is due to the electron-withdrawing effect of the acetyl group on the nitrogen atom, which strengthens the intramolecular hydrogen bond. The peak for the NH proton at 10.1 ppm (DMSO-d_6) in the acenaphthylene is a sharp singlet and shows a further downfield shift implying that the intramolecular hydrogen bond is even stronger in this compound.[16]

The following year Mezheritskii and co-workers prepared the first known *peri*-hydroxyacylacenaphthylene, 5-acetyl-6-hydroxyacenaphthylene.[17] The synthetic route carried out was multi-step; the first step was dehydration of 5-acetyl-6-benzoyloxyacenaphthene with chloranil, this resulted in a 1:1 mixture of the starting acenaphthene and the desired acenaphthylene, 5-acetyl-6-benzoyloxyacenaphthylene. The group failed to separate these two compounds using chromatography as they possessed identical R_f values of 0.8. Despite this inability to separate the two compounds they proceeded with the second step of the reaction which involved cleavage of the ester group at the *peri*-position to yield the desired *peri*-hydroxyketone. A mixture of 5-acetyl-6-hydroxyacenaphthylene (44%) and 5-acetyl-6-hydroxyacenaphthene (48%) resulted and these compounds were successfully separated on a silica column with a chloroform eluent (Scheme 9).[17]

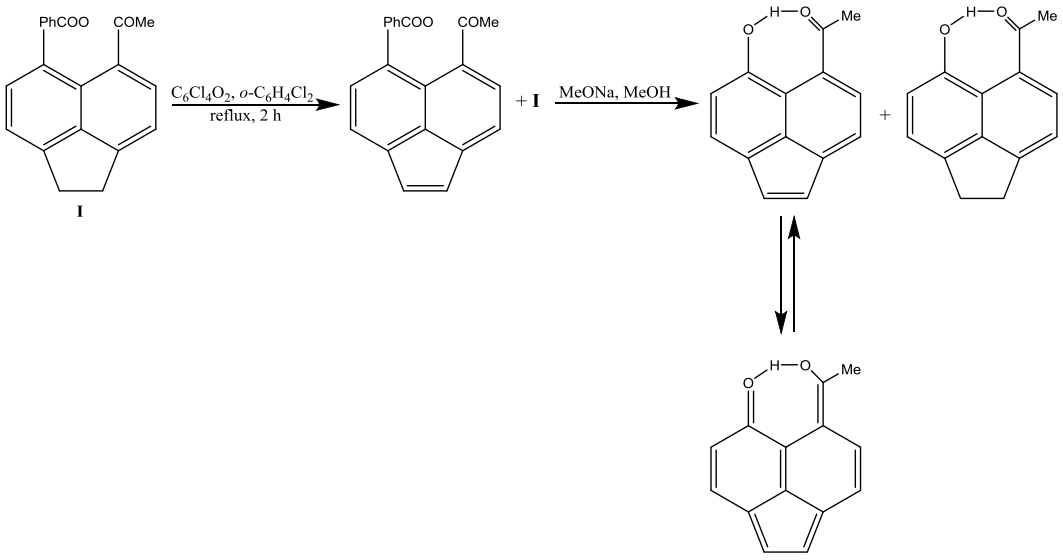

Scheme 9 The preparation of 5-acetyl-6-hydroxyacenaphthylene.[17]

In addition to preparing 5-acetyl-6-hydroxyacenaphthylene, Mezheritskii and co-workers chose to react it with acetic anhydride in pyridine (Scheme 10). This resulted in another novel acenaphthylene, 5-acetyl-6-acetoxyacenaphthylene.[17]

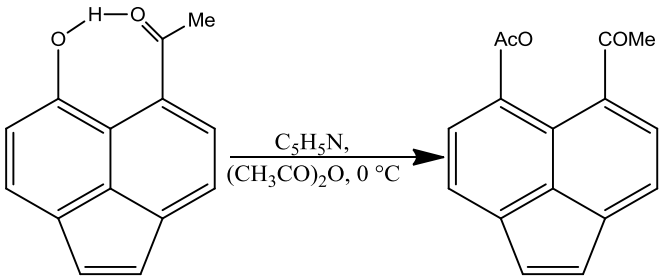

Scheme 10 The preparation of 5-acetyl-6-acetoxyacenaphthylene; with a 70% yield.[17]

The group then went on to prepare acenaphthopyridazine, 1,3-dimethyl-1*H*-6,7-dihydroacenaphtho[5,6-*de*]pyridazine, by heating 6-acetyl-5-hydroxyacenaphthene with methyl hydrazine in ethanol. The acenaphthopyridazine was then dehydrogenated with *p*-chloranil to yield 1,3-dimethyl-1*H*-indeno[6,7,1-*def*]cinnoline (Scheme 11).[18]

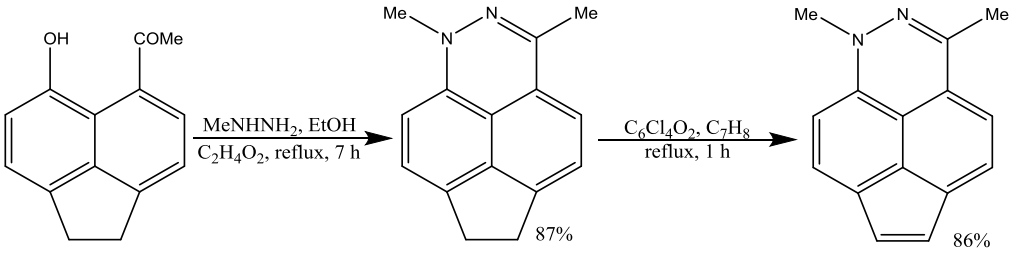

Scheme 11 The preparation of 1,3-dimethyl-1*H*-indeno[6,7,1-*def*]cinnoline via acenaphthopyridazine.[18]

Mezheritskii and colleagues[19] further studied the strength of intramolecular interactions between the *peri*-substituents in hydroxy and methoxy aldehydes and ketones of naphthalene, acenaphthene and acenaphthylene compounds (Figure 3). They wanted to determine what effect the ethane and ethene linkers had on the rigidity of the backbone and in turn how this affected the strength of intramolecular interactions between the *peri*-substituents.

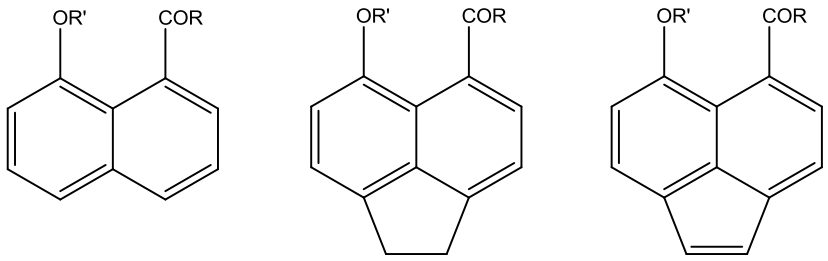

1a-d 2a-d 3a-d

Figure 3 Naphthalene, acenaphthene and acenaphthylene compounds studied where: R = R'= H (a); R = H, R' = Me (b); R = Me, R' = H (c); R = R' = Me (d).[19]

The group discovered that the addition of the ethane and ethene bridges causes the backbone to become more rigid and that the strength of the intramolecular hydrogen bond that occurs between the *peri*-hydroxy carbonyl substituents increases.[19]

Further investigation into intra- and intermolecular interactions were carried out using *peri*-amino-substituted methyl and aryl ketones of acenaphthene and acenaphthylene. The acenaphthenes and acenaphthylenes underwent protonation and acylation at the nitrogen atom, dehydrogenation and were reacted with aldehydes as part of the studies.[20]

Peri-fused pyran derivatives were discovered to have antibacterial properties comparable to known strong antibiotics.[21] With this in mind, Mezheritskii *et al.* prepared two pyran derivatives where the pyran ring is *peri*-fused to acenaphthene and acenaphthylene backbones (Scheme 12).[22] Further investigation is now required to determine their antibacterial properties.

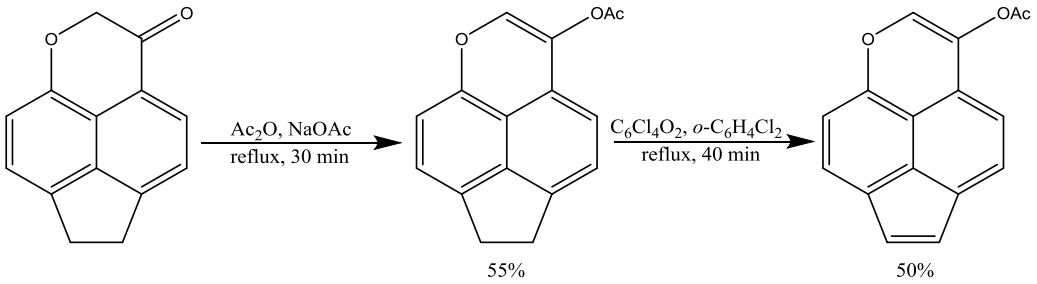

55% 50%

Scheme 12 Preparative route to 6,7-dihydroindeno[6,7,1-*def*]chromen-3-yl acetate and indeno[6,7,1-*def*]chromen-3-yl acetate.[22]

Flowerday, Perkins and Arthur[23] previously prepared a triazine version of acenaphthylene (Figure 4) that had surprising stability. This prompted them to investigate improving its synthesis and also to synthesise other electronically related heterocycles (Scheme 13 and 14).

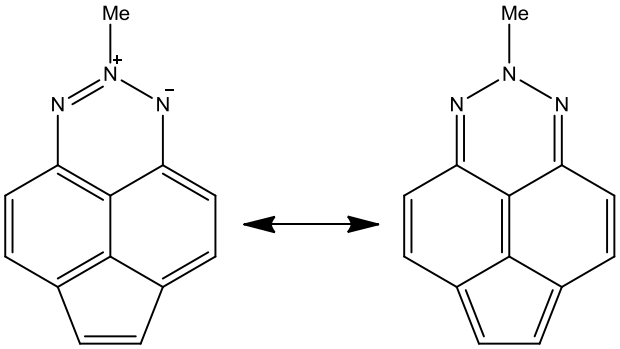

Figure 4 A triazineversion of acenaphthylene and its resonance structure.[23]

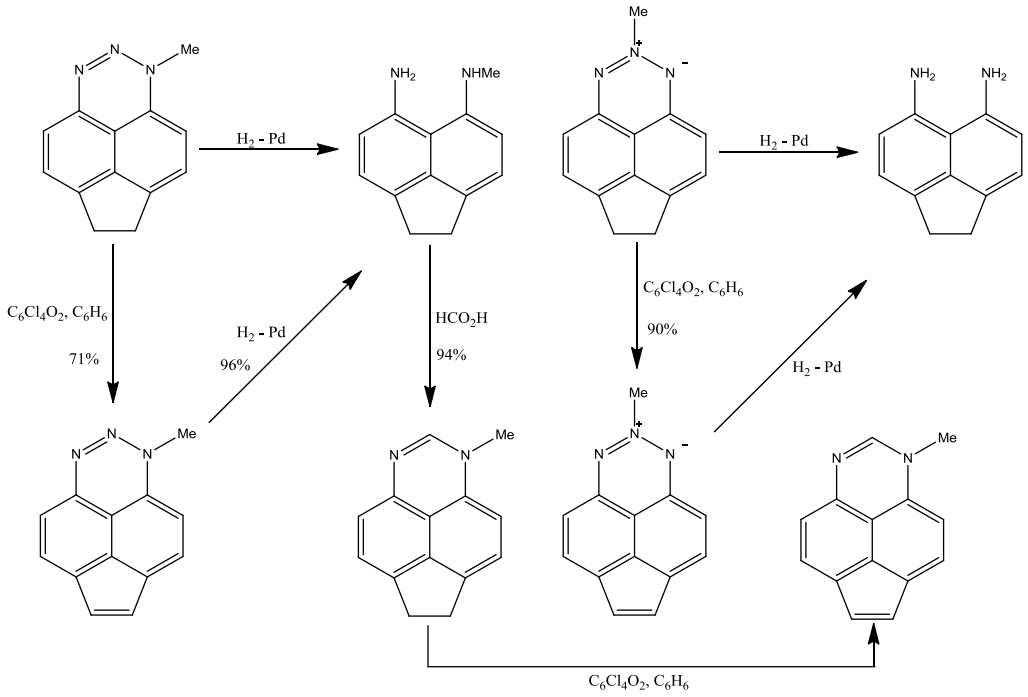

Scheme 13 Various synthetic procedures carried out by Perkins *et al*. with available yields quoted.[23]

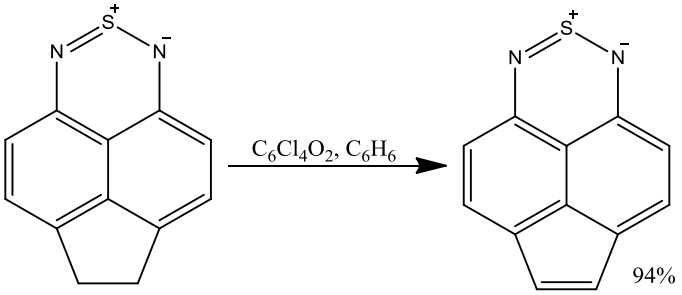

Scheme 14 Synthesis of the violet acenaphtho[5,6-*c,d*][1,2,6]thiadiazine by dehydrogenation of the blue 6,7-dihydroacenaphtho[5,6-*c,d*][1,2,6]thiadiazine.[23]

The spectra of the new acenaphthylene based heterocycles displayed significant differences when compared to their acenaphthene precursors. The aromaticity of the heterocycles is clear from the NMR chemical shift data; with the acenaphthylene ring protons showing a distinct decrease in shielding which is associated with increased aromaticity. The chemical properties of these new heterocycles were not fully investigated, although a brief look into electrophilic substitution did occur.[23]

As discussed earlier, Chiang and Meinwald[2] used 5,6-dibromoacenaphthylene to prepare the intermediate 5,6-dilithioacenaphthylene, which they then used to synthesise the dichalcogen-bridged acenaphthylenes (Scheme 15); acenaphtho[5,6-*cd*]-1,2-dithiole (28%), acenaphtho[5,6-*cd*]-1,2-diselenole (22%) and acenaphtho[5,6-*cd*]-1,2-ditellurole (14%).

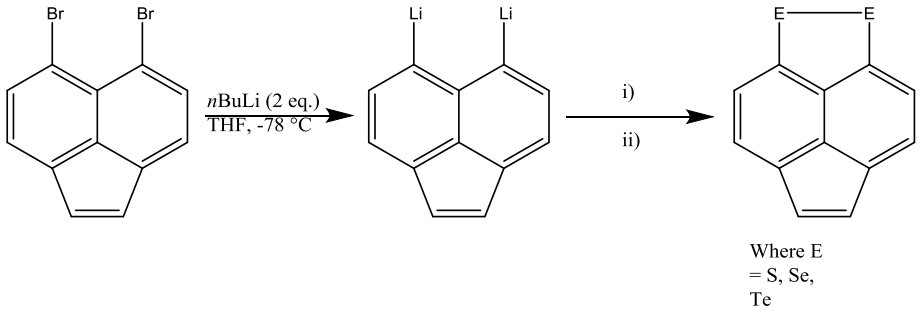

Scheme 15 Synthetic route to dichalcogen-bridged acenaphthylenes: i) E, -78 °C (-30 °C for Te); 25% AcOH in THF; ii) r.t., [O], 1 h.[2]

Dunoguès and co-workers prepared silylated derivatives of acenaphthene and acenaphthylene.[8] However, only one of these derivatives involved silylation at the *peri*-position, 5-(trimethylsilyl)acenaphthylene. 5-(trimethylsilyl)acenaphthylene was synthesised through two routes; the first route involved dehydrogenation of the acenaphthene analogue and the second route involved reacting 4,5-*bis*(trimethylsilyl)-4,5-dihydroacenaphthene using the Harvey's method (Scheme 16). Preparation of 5-(trimethylsilyl)acenaphthylene using *p*-chloranil did not go to completion implying that it was not a strong enough oxidising agent.

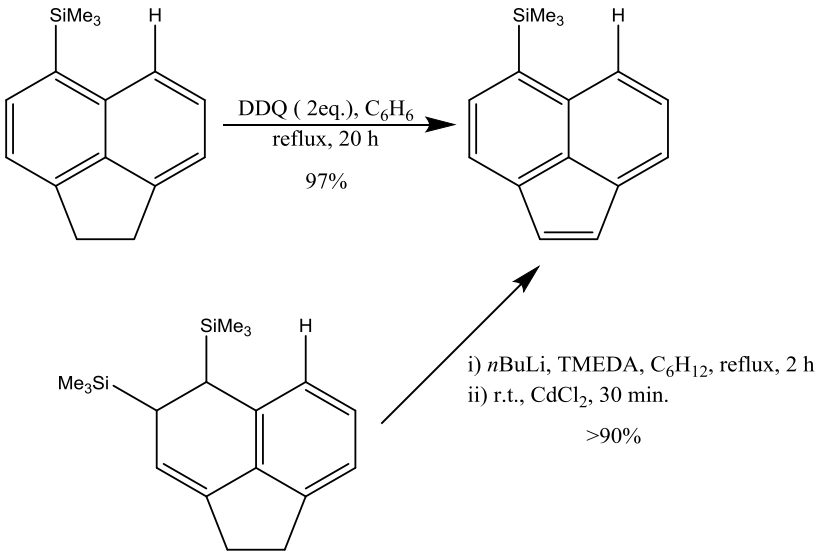

Scheme 16 The two synthetic routes to 5-(trimethylsilyl)acenaphthylene with yields.[8]

The authors tried to use 5-(trimethylsilyl)acenaphthylene in electrophilic substitution reactions to produce 5-functionalised acenaphthylenes. However, the ethene double bond is highly reactive towards electrophiles, which prevents the reaction from proceeding as desired.[8]

Most recently in 2009, Matano and colleagues[24] studied the ring-fusion effects on the electron-accepting and electron-donating abilities of [*c*]-fused phosphole *P*-oxides. For this study, they chose naphthalene as the fused framework due to the ease of altering the π-system through substitution. They then compared the naphthalene, acenaphthene and acenaphthylene fused phosphole derivatives using optical and electrochemical properties. The fused phosphole derivatives were prepared by employing a Ti^{II}-mediated cyclisation of the dialkynylated parent

compound (Scheme 17). The acenaphthylene-fused phosphole derivative shown was also prepared through dehydrogenation of the acenaphthene analogue with a much lower 39% yield.

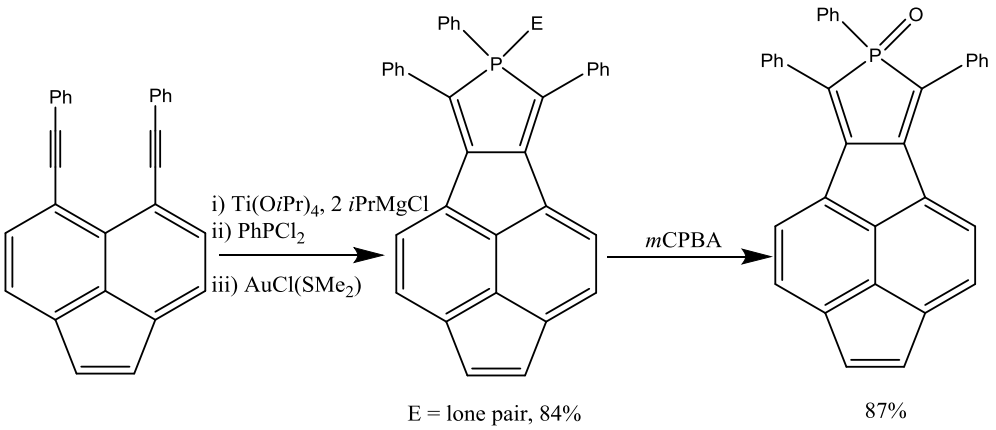

Scheme 17 Synthesis of acenaphthylene-fused phosphole derivative; naphthalene and acenaphthene derivatives follow similar route.[24]

The optical properties of the naphthalene- and acenaphthene-fused phosphole derivatives were found to be different from those of the acenaphthylene analogues. It was also found that out of the three backbones used, the naphthalene- and acenaphthene-fused *P*-oxides displayed substantial thermal stability. The electron mobility of the naphthalene-fused phosphole *P*-oxide is one order higher than that of *tris*(8-hydroxyquinoline)aluminium(III), which is an important component in organic light-emitting diodes, at any given electric field. It was concluded from this study that the [*c*]-fusion of the naphthalene ring into the phosphole platform could help develop a new group of phosphol based π-systems with great electron mobility.[24]

Peri-Substituted Acenaphthenes

Peri-substituted acenaphthenes are becoming more commonly used in studies that utilise rigid backbones. This is due to the synthesis of 5,6-dibromoacenaphthene being much easier than that of its naphthalene analogue. The majority of published material in which the naphthalene scaffold has been replaced with acenaphthene has been carried out by the Woollins and Kilian groups in St Andrews.

A literature search of *peri*-substituted dihalogen acenaphthenes revealed that Dashevskii and Karishin first prepared 5,6-dibromoacenaphthene[25] and 5,6-dichloroacenaphthene[26] back in 1937.

A while later, Letsinger, Gilpin and Vullo[27] modified Dashevskii and Karishin's procedure to yield 10% of 5,6-dibromoacenaphthene. Acenaphthene was refluxed in ethanol; bromine was then swept by a stream of nitrogen into the solution and the mixture was refluxed for a further two hours. The solvent was removed, leaving behind a residue. Purification of the residue using first column chromatography and then recrystallisation from ethanol resulted in 5,6-dibromoacenaphthene.

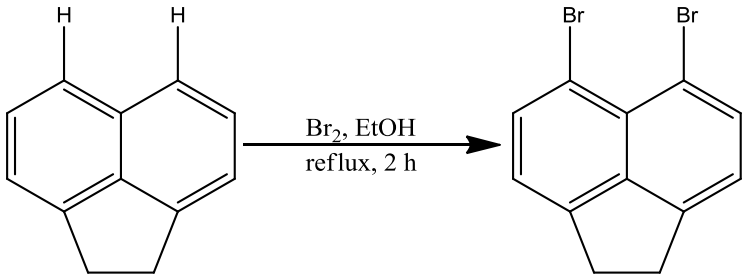

Scheme 18 Early synthetic route to 5,6-dibromoacenaphthene.[27]

The procedure used today to form this important precursor involves adding a suspension of N-bromosuccinimide in dimethylformamide (2 eq.) dropwise to an ice-cooled suspension of acenaphthene in dimethylformamide. After stirring for twelve hours the mixture is warmed to room temperature. The precipitate is removed, washed with ethanol and then purified by refluxing in ethanol overnight.[28]

In 1954, Goto and Nagai developed a more efficient synthesis of the dichloro analogue, obtaining 5,6-dichloroacenaphthene in a 53% yield using chlorine with a zinc powder catalyst and a 58% yield using sulfuryl chloride with an iodine catalyst.[29] The next year Dashevskii and Petrenko improved upon their yields (75-78%) by using an aluminium chloride catalyst and sulfuryl chloride.[30]

A decade later, 5,6-diiodoacenaphthene was prepared by diazotization of 5-iodo-6-aminoacenaphthene in sulfuric acid (10%) and subsequent treatment with potassium iodide

(58%).[31] 5,6-diiodoacenaphthene can also be prepared, in a 62% yield, from reaction of 5,6-dilithioacenaphthene with iodine in diethyl ether at -10 to 0 °C.[32]

Karishin and co-workers were the first to prepare and study the reactions of 5,6-difluoroacenaphthene; the synthetic route is multistep starting from 5-fluoroacenaphthene as shown in Scheme 19.[33]

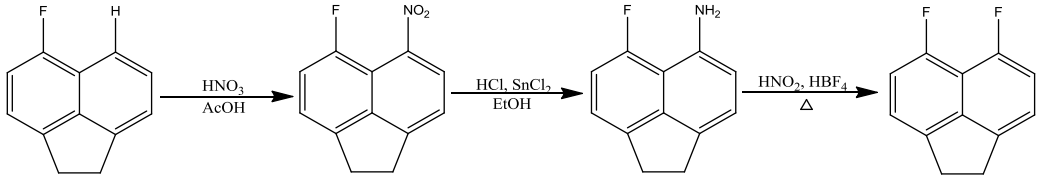

Scheme 19 Preparation of 5,6-difluoroacenaphthene utilised by Karishin and co-workers.[33]

The same group also prepared a series of mixed halogen-halogen *peri*-substituted acenaphthenes (Figure 5),[34] with 5-fluoro-6-chloroacenaphthene additionally prepared by Ivanova and Yagupol'skii.[35]

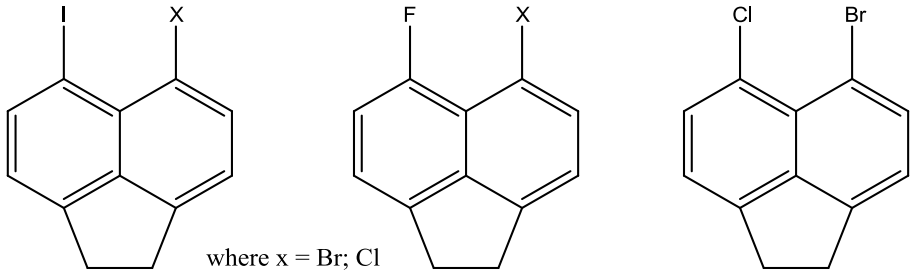

Figure 5 Known mixed halogen-halogen *peri*-substituted acenaphthenes.[34,35]

In 1969 Constantine, Deady and Topsom studied electrophilic substitution in acenaphthenes, performing bromination and chlorination reactions of 3- and 5- monosubstituted bromo- and chloro-acenaphthenes.

In their study Constantine and co-workers concluded that the 3-halo compounds undergo further substitution at the 6-position, whilst reaction of sulfuryl chloride with 5-bromo- and 5-chloroacenaphthenes yields the 5,6-dihalo derivative as the major product. Small amounts of 3,5- and 3,6-dibromoacenaphthene were produced through reaction of 5-bromoacenaphthene with

bromine vapour, whereas 5,6-dibromoacenaphthene is the major product when hypobromous acid is used.[36]

Vernon and Wilson synthesised some derivatives of acenaphthene as part of their investigation into halogenated phenols.[37] The only *peri*-acenaphthene synthesised was 5-bromo-6-nitroacenaphthene. This was prepared by adding a mixture of nitric acid and acetic acid to a solution of 5-bromoacenaphthene in acetic acid. After twelve hours a precipitate of 5-bromo-6-nitroacenaphthene had formed (Scheme 20).

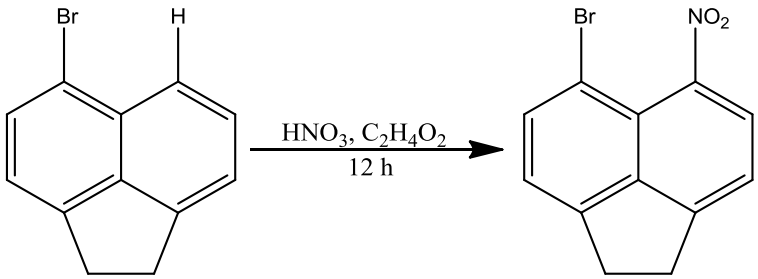

Scheme 20 Synthesis of 5-bromo-6-nitroacenaphthene.[37]

Deady, Gray and Topsom developed their study of electrophilic substitution reactions through acetylation of monosubstituted acenaphthenes. 5-acetyl-6-fluoroacenaphthene was the only *peri*-substituted acenaphthene to be synthesised. Acetylation occurred solely in the 6 position with 3-acetyl-, 3-bromo-, 3-chloro- and 3-nitroacenaphthene and primarily in the 6 position with 3-*tert*-butylacenaphthene. 5-Acetyl- and 5-acetamidoacenaphthene react at the 8 position, whereas 5-*tert*-butyl- and 5-methylacenaphthene react mainly at the 3 position. Finally, 5-fluoro-, 5-chloro-, 5-bromo- and 5-iodoacenaphthene reacted to give mixtures of the 3- and 8-acetylated acenaphthenes, with the ratio of isomers depending on the 5-halogen.[38]

Roberts and co-workers prepared the sterically crowded *peri*-diphenylacenaphthene, in a 78% yield, by a nickel catalysed aryl-aryl coupling reaction between 5,6-diiodoacenaphthene and phenylmagnesiumiodide. *Peri*-diphenylacenaphthene was then compared to 1,8-diphenylnaphthalene and 1,4,5,8-tetraphenylnaphthalene. The authors chose to compare *peri*-diphenylacenaphthene to these two compounds because overall they represent a series which differ only by the groups at the 4 and 5 positions (Figure 6).[39]

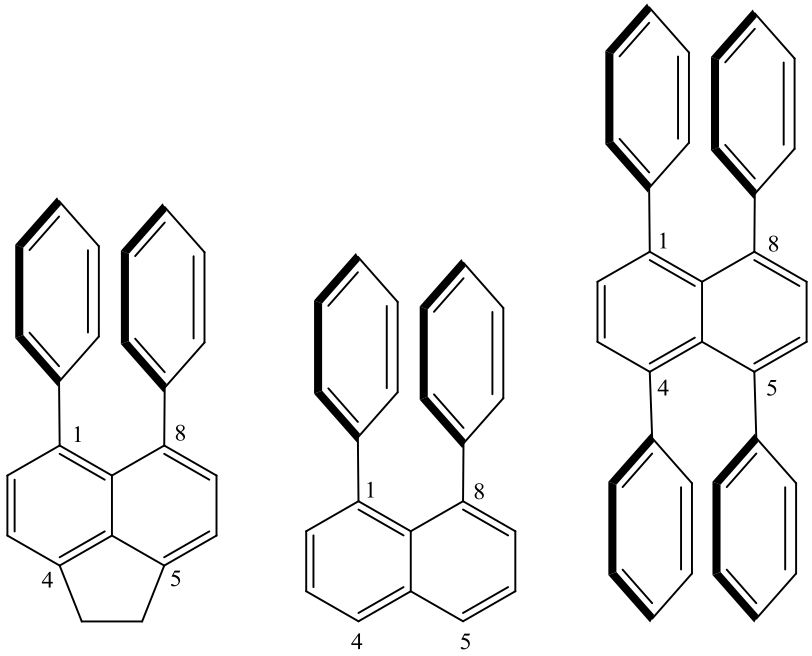

Figure 6 *Peri*-diphenylacenaphthene, 1,8-diphenylnaphthalene and 1,4,5,8-tetraphenylnaphthalene with the important positions numbered.[39]

It was found through crystal structure analysis that the addition of the ethane bridge in *peri*-diphenylacenaphthene causes compression of the C4-C10-C5 angle at the bottom of the ring by 2°. This decrease effectively increases the distortion that is already found in the naphthalene analogue. In comparison the 1,4,5,8-tetraphenylnaphthalene has bond distances and angles close to that of unsubstituted naphthalene because the in-plane distortion that occurs at both ends of the naphthalene backbone effectively cancel each other out.[39]

The complex 5,6-dilithioacenaphthene-N,N,N',N'-tetramethyl-1,2-ethanediamine is a key intermediate for many reactions and was introduced in 1981 by Tanaka and Kasai.[32] The complex is synthesised from reaction of 5,6-dibromoacenaphthene with *n*-butyllithium and N,N,N',N'-tetramethyl-1,2-ethanediamine (TMEDA) in diethyl ether at -10 to 0 °C. The complex was reacted with iodine and carbon dioxide affording 5,6-diiodoacenaphthene and 5,6-acenaphthenedicarboxylic anhydride, respectively (Scheme 21).

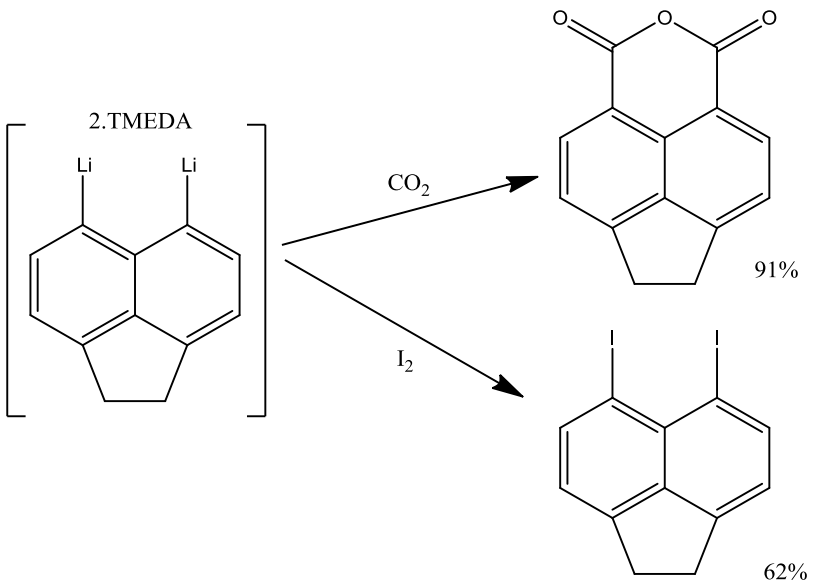

Scheme 21 Reaction of 5,6-dilithioacenaphthene.2TMEDA with I_2 and CO_2.[32]

Reaction of 5,6-dilithioacenaphthene.2TMEDA with biacetyl resulted in only the *cis* isomer of 1,2,5,6-tetrahydro-1,2-dimethylcyclopent[*fg*]-acenaphthylene-1,2-diol. In contrast the reaction of pyracenequinone with methyl magnesium bromide gave both the *cis*- and *trans*- isomers. *Cis*-diols resulted from the reaction of the complex with acenaphthenequinone and pyracenequinone and they were subsequently reacted with phenylboronic acid to give the respective cyclic ester (Scheme 22).[32]

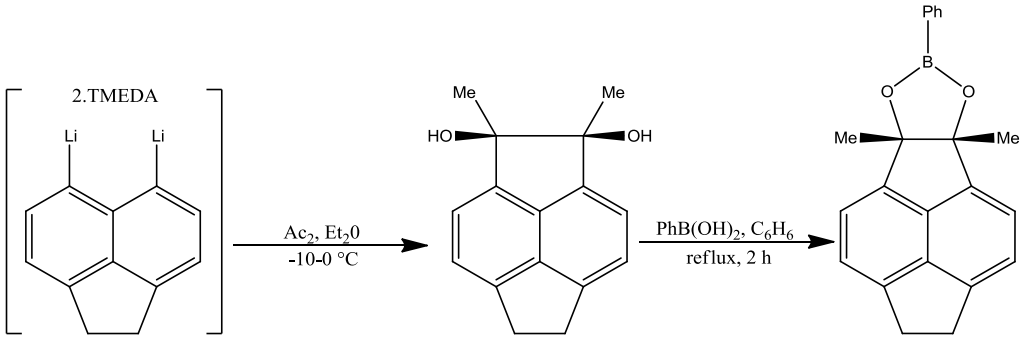

Scheme 22 Synthetic route for production of cyclic ester 1,2,4b,7a-tetrahydro-4b,7a-dimethyl-6-phenylcyclopent[5,6]-acenaphtho[1,2-*d*][1,3,2]dioxaborole.[32]

Whiting *et al.* used theoretical and experimental methods to study a series of 5,6-diarylacenaphthenes (Figure 7) in order to understand the process of atropisomer interconversion.[40]

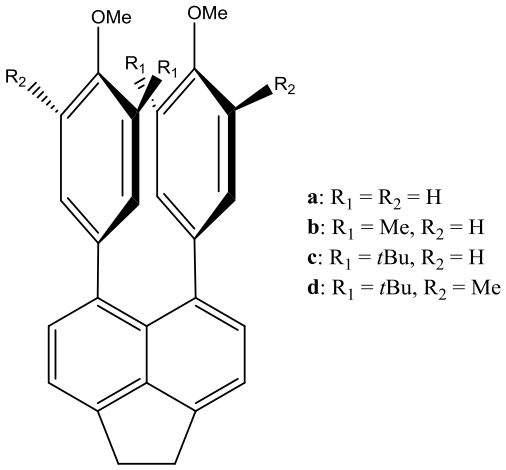

Figure 7 5,6-diarylacenaphthenes prepared by Whiting *et al.*[40]

It was found through calculations and NMR studies that the energy difference between the *syn*- and *anti*- atropisomers was small. However, in the three molecular structures determined only one atropisomer was found i.e. *syn*-**b**, *anti*-**c** and *anti*-**d**. The authors believe that the reason behind only one form being crystallised is as follows; when the major form of atropisomer in solution begins to crystallise, it upsets the *anti-syn* equilibrium, which causes the minor form to be converted to the major form to restore the equilibrium. Calculations of the transition state structures for rotation show that the acenaphthene ring system has significant flexibility and that bulky substituents in the *meta*-positions of the *peri*-phenyl rings are not able to stabilise a single atropisomeric form. However, calculations revealed that substituents in the 4 and 7 positions of the acenaphthene backbone may be able to prevent atropisomer interconversion. Further investigation is needed.[40]

As discussed earlier, Mezheritskii and co-workers studied some derivatives of acenaphthylene which they synthesised through dehydrogenation of the relevant acenaphthene analogue. In 2008, the group focussed on acenaphthene alone by developing a new synthetic route to *peri*-hydroxyacenaphthoyl compounds.[41] The new procedure (Scheme 23) involves acid-catalysed acylation of esters prepared from 5-hydroxyacenaphthene. Esters were utilised as they prevent

acylation from occurring at the *ortho*-position with respect to the hydroxy group. However, the procedure did enable formation of the corresponding 3- and 8-acyl-substituted isomers. Unfortunately despite this new procedure the only acetylation product the group were able to isolate was compound **3a**, in a 33% yield.[41]

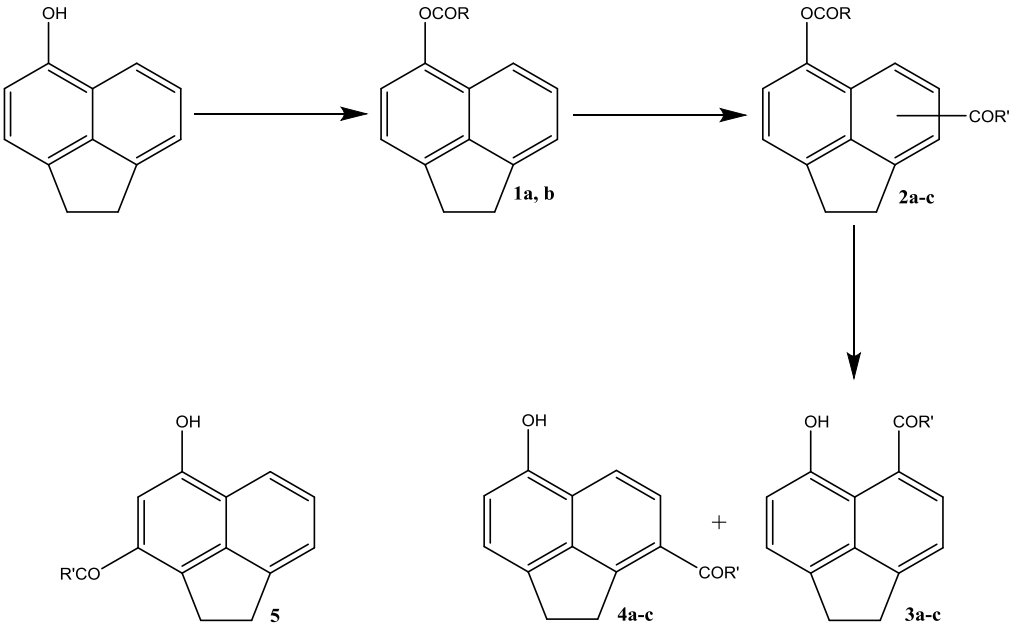

1a R = Me, **b** R = Ph; **2a** R = R' = Me, **b** R = R' = Ph, **c** R = Ph, R' = Me; **3/4a** R' = Me, **b** R' = Ph, **c** R' = H; **5** R' = Ph.

Scheme 23 Mezheritskii and co-workers new synthetic route to *peri*-hydroxyacenaphthoyl compounds.[41]

In their work, Kilian *et al.*[42] chose to use 5,6-dibromoacenaphthene[28] instead of 1,8-dibromonaphthalene[43] as the *peri*-backbone because it is much easier to synthesise. They took 5,6-dibromoacenaphthene and lithiated it to obtain 5,6-dilithioacenaphthene, which they then reacted with various dichlorophosphines $RPCl_2$ (R = alkyl, aryl). However, instead of the desired phosphorus *peri*-bridged acenaphthene a complex mixture of products was attained.

In order to obtain pure product, Kilian *et al*. developed a new synthetic route (Scheme 24) which involved first mono-lithiating 5,6-dibromoacenaphthene, **a**, and then reacting it with alkyl or aryl dichlorophosphine to give intermediates **b** and **c**. Methyllithium (**b**) or *tert*-butyllithium (**c**) was slowly added to the relevant intermediate, leading to an internal halogen-lithium exchange reaction which resulted in subsequent ring-closing to give **e** and **f**. It was found that the

alkyllithium used has an effect on the ring-closing step. If methyllithium is reacted with **b** then this yields pure **e**. However, if methyllithium is reacted with **c** this yields similar amounts of non-cyclic **d** and cyclic **f**. If *tert*-butyllithium is reacted with **c**, pure **f** is obtained (Scheme 24). The phosphorus *peri*-bridged acenaphthenes, **e** and **f**, are moisture resistant and display good donor properties which the authors believe makes them hopeful ligands for metal centre catalysed reactions.[42]

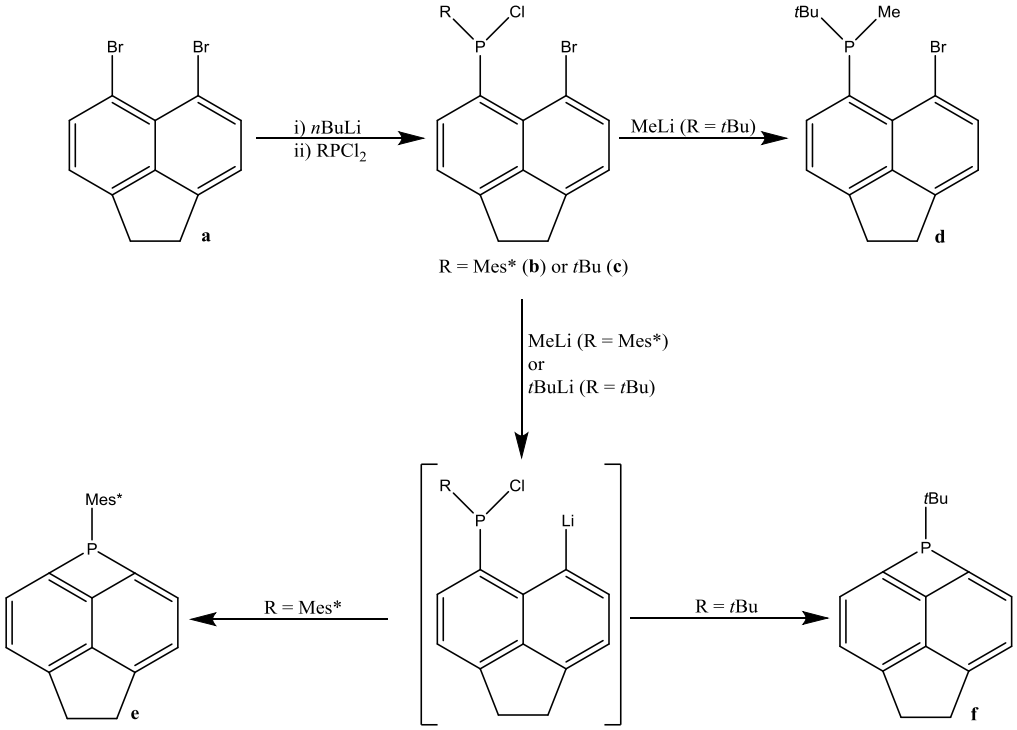

Scheme 24 Synthetic route to phosphorus *peri*-bridged acenaphthenes, developed by Kilian *et al*.[42]

In 2009, Kilian and co-workers prepared the first room temperature stable intramolecular donor-acceptor phosphonium-phosphoranide complex.[44] 5-diphenoxyphosphanyl-6-diisopropylphosphinoacenaphthene was reacted with chlorotrimethylsilane to yield a phosphonium-phosphine compound, which had four phosphorus atoms connected in a chain (Scheme 25). After obtaining the phosphonium-phosphine compound, the remaining filtrate was left to stand and crystals formed within. X-ray diffraction identified these crystals to be 5-dichlorophosphino-6-diisopropylphosphinoacenaphthene. Kilian and co-workers proposed that this compound was an intermediate in the formation of the phosphonium-phosphine compound and tried to synthesise it on its own (Scheme 26).[44]

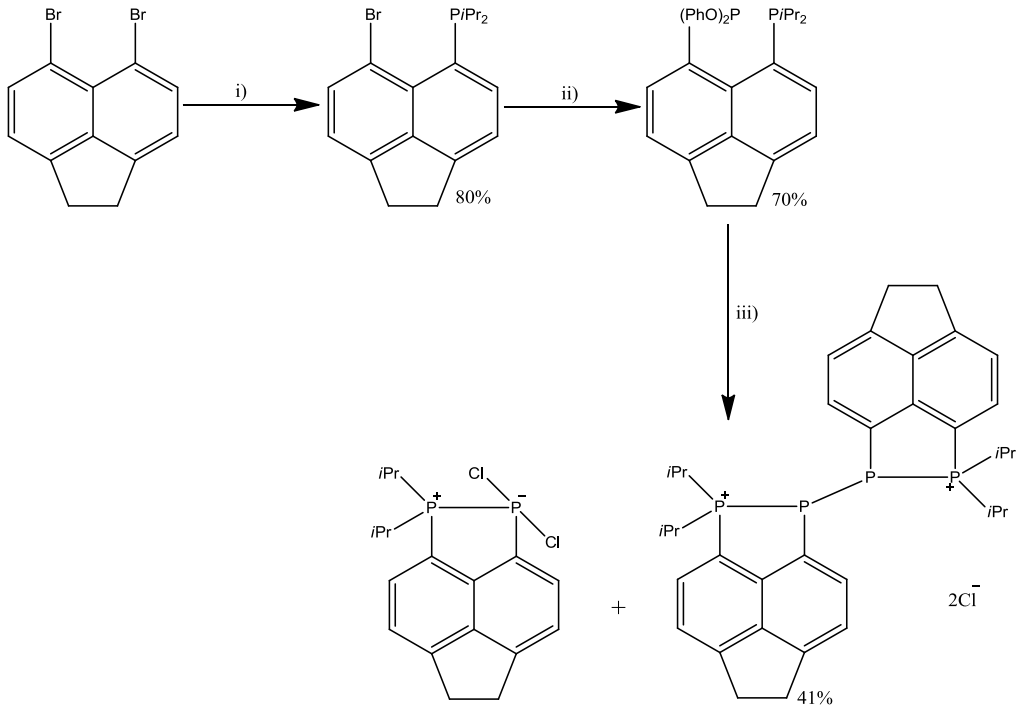

Scheme 25 Preparation of phosphonium-phosphine compound: i) *n*BuLi, THF, -78 °C, then Cl*P*iPr_2, -78 °C to r. t.; ii) *n*BuLi, THF, -78 °C, then $P(OPh)_3$, -78 °C to r.t.; iii) $ClSiMe_3$, THF, -78 °C to r.t.[44]

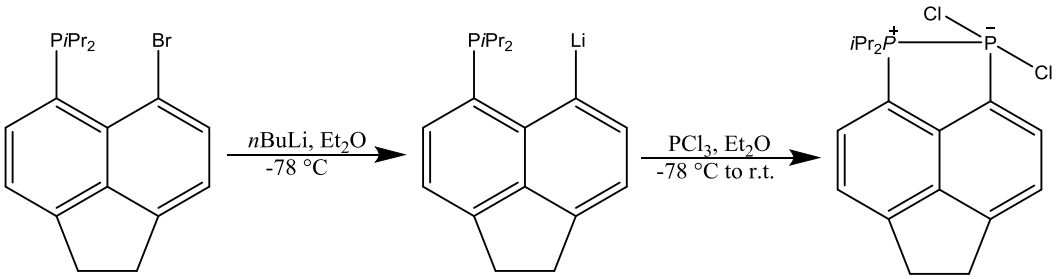

Scheme 26 Synthetic route to 5-dichlorophosphino-6-diisopropylphosphinoacenaphthene.[44]

In 5-dichlorophosphino-6-diisopropylphosphinoacenaphthene the two phosphine environments form an intramolecular donor-acceptor (phosphonium-phosphoranide) complex. A σ P-P bond forms because the isopropylphosphino substituent is σ-donating and the chloride groups are σ-accepting. This phosphonium-phosphoranide complex was found to be stable, in the solid state, at room temperature and as a solution in some solvents. Kilian and co-workers carried out a ^{31}P

NMR mechanistic study and revealed that the phosphonium-phosphoranide complex is unstable in the presence of nucleophiles and will change into the phosphonium-phosphine dimer.[44]

After the Kilian group synthesised 5-dichlorophosphino-6-diisopropylphosphinoacenaphthene they were interested in synthesising more heteroleptic *peri*-substituted acenaphthenes. Due to compounds with the P-Cl bond being very reactive, they aimed to replace these with the more stable trifluoromethyl groups. The group tried to synthesise *bis*(trifluoromethyl)phosphino *peri*-substituted acenaphthene intermediates, but despite trying various synthetic routes they were unable to attach the second phosphorus group at the *peri*-position. This was found to be due to the $ArP(CF_3)_2$ (Ar = acenaphthene) being incompatible with organolithium. Instead they synthesised two new mono-substituted acenaphthenes (Scheme 27).[45]

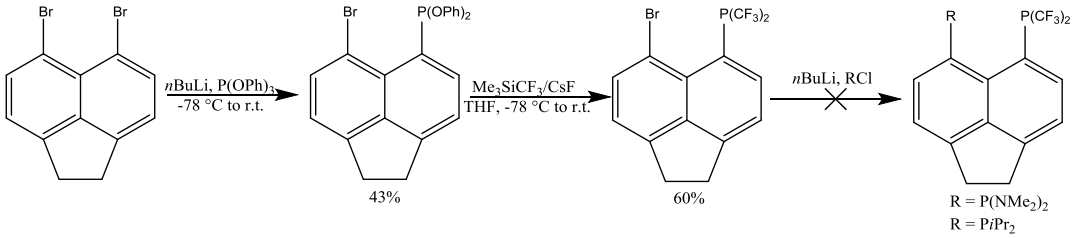

Scheme 27 Attempted synthesis of *bis*(trifluoromethyl)phosphine *peri*-substituted acenaphthenes.[45]

In 2012, Kilian and co-workers investigated the chemistry of the previously synthesised room temperature stable phosphine-phosphine donor-acceptor complex[44] and found that it led to an isolable phosphanylidene phosphorane with a sterically accessible two-coordinate phosphorus atom.[46] Reaction of the donor-acceptor complex with a dimethyl sulfide borane complex led to the *bis*(borane) compound (Scheme 28),which was the first *bis*(borane) push-pull phosphinidene system to be structurally characterised. It was found that the *bis*(borane) compound was extremely stable and no decomposition occurred when it was stored in air at room temperature for many weeks. Reaction of the *bis*(borane) compound with dimethylamine (Scheme 28) yielded the phosphanylidene phosphorane which was highly air sensitive. [46]

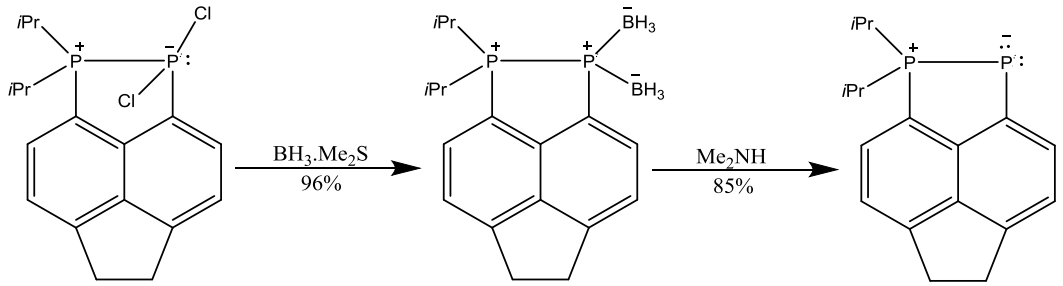

Scheme 28 Synthesis of the phosphanylidene phosphorane.[46]

The following year, Kilian and co-workers studied the synthesis and reactivity of *peri*-substituted phosphino-phosphonium salts (Scheme 29).[47]

Reaction of 5-bromo-6-(diisopropylphosphino)acenaphthene with *n*BuLi gave the 5-lithio-6-(diisopropylphosphino) acenaphthene, which was then reacted with dichlorophosphines $RPCl_2$ (R = Ph, Fc, NMe_2, *i*Pr) to give the *peri*-substituted phosphino-phosphonium salts **2**-**5**. The salts were found to maintain their ionic structure in solution (^{31}P NMR chemical shifts) and in the solid state (X-ray diffraction data).

Salts **2** and **3** underwent further reaction; first with lithium aluminium hydride in tetrahydrofuran to yield the heteroleptic *bis*(phosphines) **6** and **7** and secondly with an excess of neat methyl trifluoromethanesulfonate to yield the chiral 1,2-diphosphonium salts **8** and **9**. The 1,2-diphosphoniums **8** and **9** were then reduced with lithium aluminium hydride in tetrahydrofuran to give the heteroleptic *bis*(phosphines) **10** and **11**.

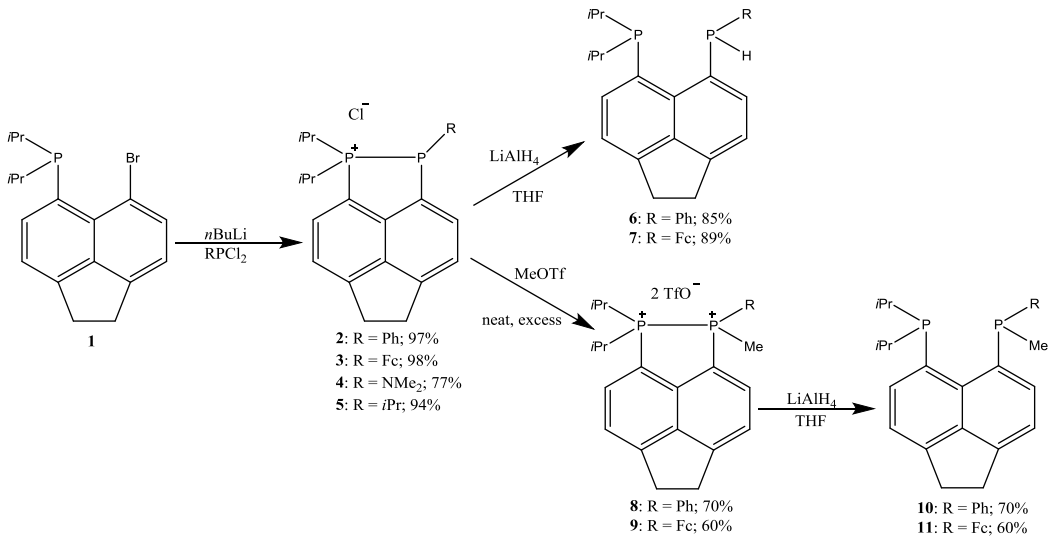

Scheme 29 Synthesis of compounds **2**-**11** used by Kilian and co-workers.[47]

The Kilian group concluded from this study, that the procedure used to produce compounds **2**-**5** could be used to synthesise a broad range of "heteroleptic" phosphino-phosphonium salts. They also established the use of these salts as precursors for the formation of mixed tertiary/secondary *bis*(phosphines) and heteroleptic 1,2-diphosphonium salts.[47]

The first geminally *bis*(*peri*-substituted) tridentate phosphine was synthesised in 2013 by Kilian and colleagues.[48] 5-bromo-6-(diisopropylphosphino)acenaphthene underwent a lithium-halogen exchange at -78 °C to yield 5-lithio-6-(diisopropylphosphino)acenaphthene. This was then reacted with half an equivalent of dichloroisopropyl phosphine at -78 °C. After work-up, the tridentate phosphine was isolated in a 68% yield (Scheme 30).

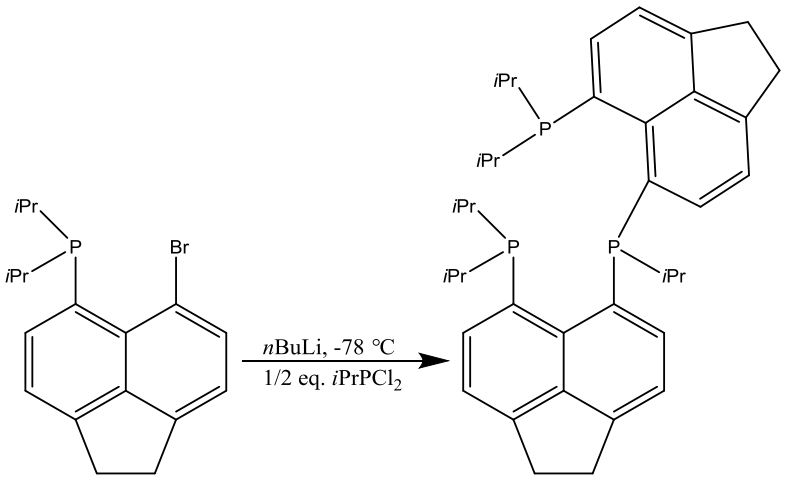

Scheme 30 Procedure for the first geminally *bis(peri*-substituted) tridentate phosphine.[48]

The amount of steric crowding in the previously synthesised *bis*(phosphino)naphthalenes was established through their reactivity with chalcogens. Kilian and colleagues decided to react the *bis*(*peri*-substituted) tridentate phosphine with elemental sulfur and selenium in order to determine the effect the additional crowding has on the sterics of the phosphorus centres.[48]

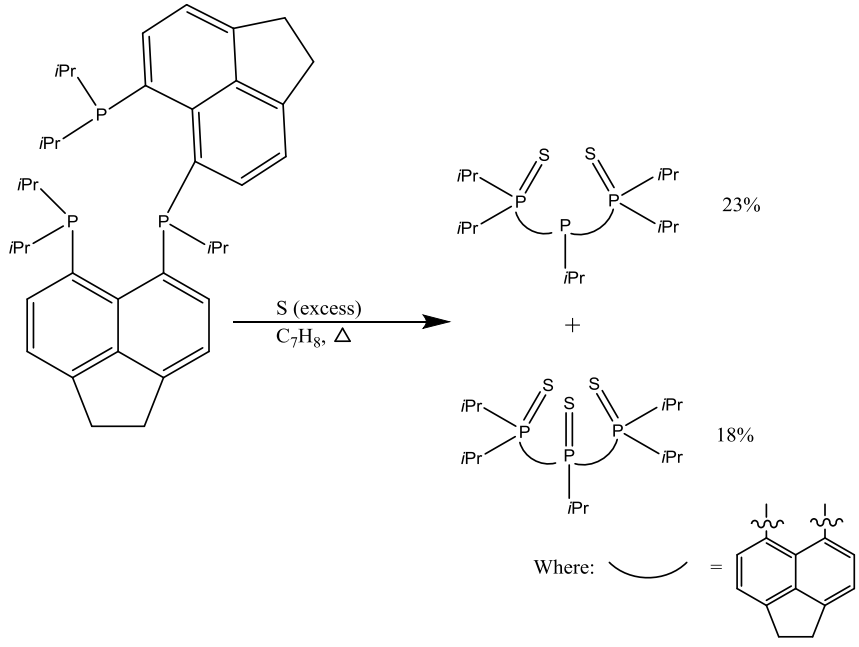

Scheme 31 Reaction of the *bis*(*peri*-substituted) tridentate phosphine with elemental sulfur.[48]

The reaction of the tridentate phosphine with sulfur yields two strained *bis*- and *tris*(sulfides). The *bis*(sulfide) is much more strained than the tridentate phosphine precursor due to the thionation of two phosphorus atoms increasing the steric bulk. The *tris*(sulfide) shows further strain due to thionation of all three phosphorus atoms.

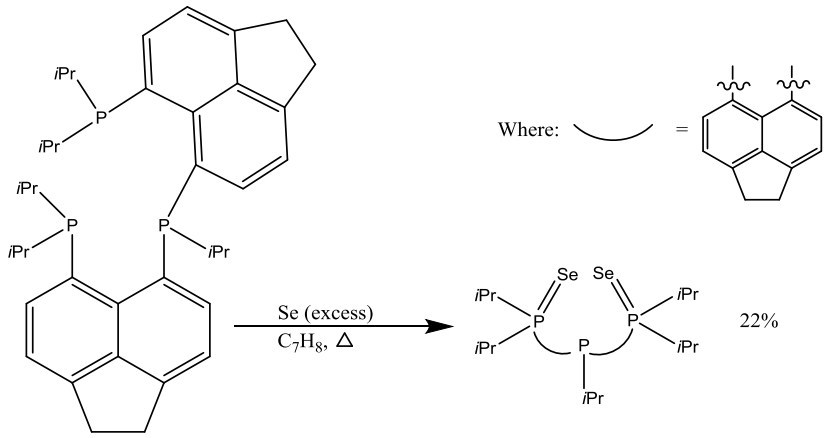

Scheme 32 Reaction of the *bis*(*peri*-substituted) tridentate phosphine with elemental selenium.[48]

Reaction of the tridentate phosphine with elemental selenium resulted in a complex mixture. Recrystallisation of the crude product from hexane gave the *bis*(selenide). The *tris*(selenide) was not isolated, indicating that there was insufficient space to fit three selenium atoms.

The *bis*(*peri*-substituted) tridentate phosphine was then reacted with transition metals to form transition-metal complexes, this will be discussed later in this review.

Ogura and co-workers synthesised 5,6-dichalcogen-bridged acenaphthenes and studied their properties as electron donors.[49] Consecutive reactions of 5,6-dibromoacenaphthene with one equivalent of *n*-butyllithium and one equivalent of elemental chalcogen, then oxidation in air yielded 5,6-dihydroacenaphtho[5,6-*c*,*d*]-1,2-dithiole and 5,6-dihydroacenaphtho[5,6-*c*,*d*]-1,2-diselenole (Scheme 33), however 5,6-dihydroacenaphtho[5,6-*c*,*d*]-1,2-ditellurole could not be prepared using this method. Instead it was synthesised by reacting 5,6-dichloroacenaphthene with sodium ditelluride in hexamethylphosphoric triamide (HMPA) (Scheme 33). It was also found that reaction of 5,6-dichloroacenaphthene with sodium diselenide in HMPA produced 5,6-dihydroacenaphtho[5,6-*c*,*d*]-1,2-diselenole with a 10% increase in yield.[49]

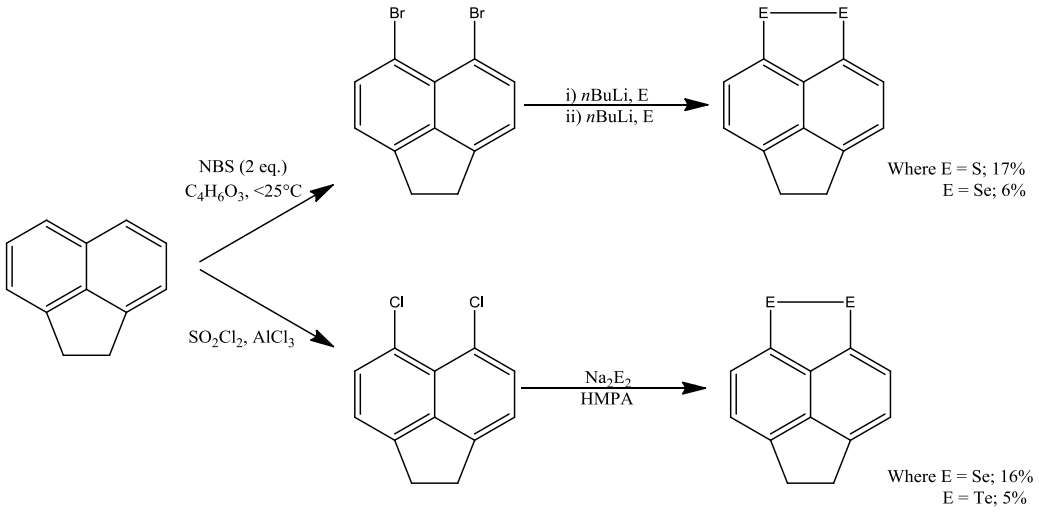

Scheme 33 Synthetic route to 5,6-dichalcogen-bridged acenaphthenes.[49]

It was observed by Ogura and co-workers[49] that the dichalcogen-bridged acenaphthenes had noticeably enhanced donor character compared to their dichalcogen-bridged naphthalene analogues. Charge-transfer complexes with tetracyanoquinodimethane (TCNQ) were formed and it was determined that their electrical conductivities increased in order of polarisable chalcogen.

Woollins *et al*.[50] have previously synthesised *peri*-substituted acenaphthenes with *bis*-chalcogen, halogen-chalcogen and mixed chalcogen-chalcogen moieties and compared them to their previously prepared naphthalene analogues.[51,52] The acenaphthenes were prepared through a series of halogen-lithium exchange reactions involving 5,6-dibromoacenaphthene, 5,6-diiodoacenaphthene and the complex 5,6-dilithioacenaphthene.2TMEDA (Schemes 34-37). They found that the level of distortion observed for the *peri*-substituted acenaphthene compounds follows that of the naphthalene analogues.

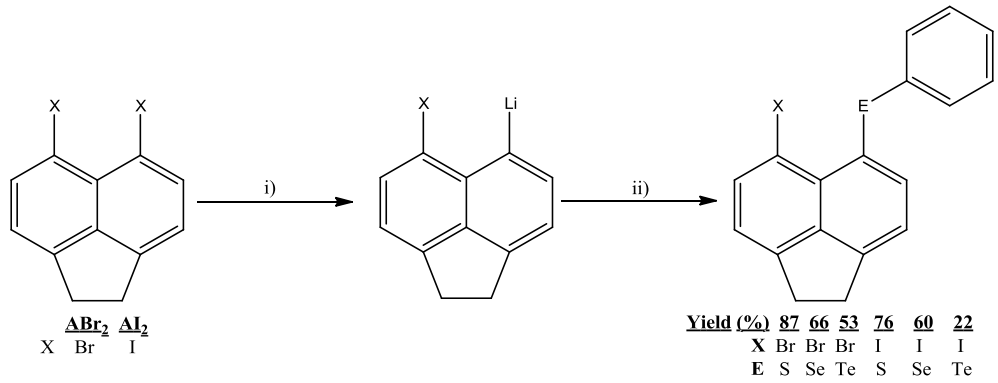

Scheme 34 The preparation of 5-halo-6-(phenylchalcogeno)acenaphthenes from ABr_2 and AI_2: i) *n*BuLi, Et_2O, -78 °C, 1h; ii) PhEEPh, Et_2O, -78 °C, 1h.[50]

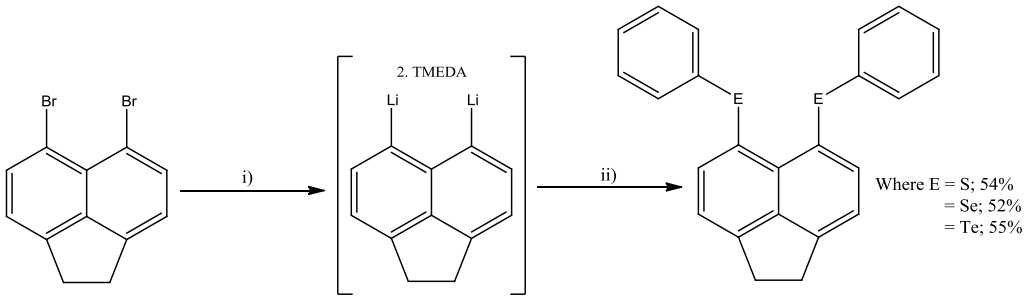

Scheme 35 The preparation of 5,6-*bis*(phenylchalcogeno)acenaphthenes *via* 5,6-dilithioacenaphthene-TMEDA complex: i) TMEDA, *n*BuLi, Et_2O, -10-0 °C, 1 h; ii)PhEEPh, Et_2O, -78 °C, 2 h.[50]

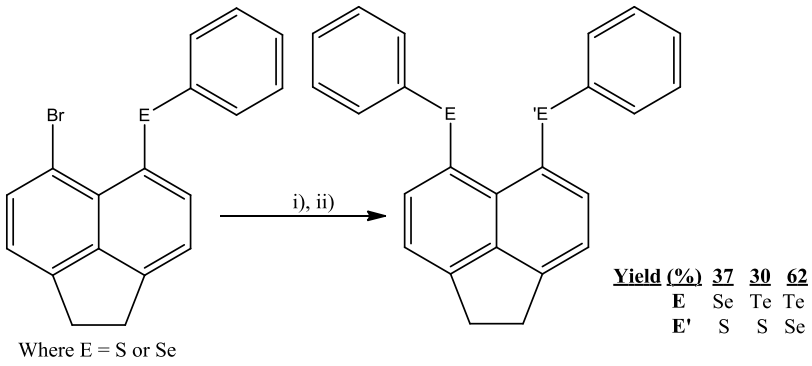

Scheme 36 The preparation of mixed 5,6-(phenylchalcogeno)acenaphthenes: i) *n*BuLi, Et_2O, -78 °C, 1h; ii) PhEEPh, Et_2O, -78 °C, 1h.[50]

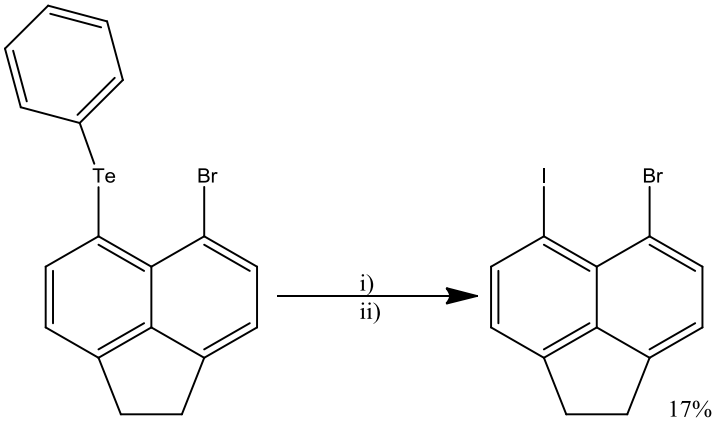

Scheme 37 The preparation of 5-iodo-6-bromoacenaphthene:
i) *n*BuLi, Et_2O, -78 °C, 1h; ii) I_2, Et_2O, -10-0 °C, 1h.[50]

Woollins and co-workers used some of the acenaphthene compounds prepared above to study hypervalency and three-centre, four-electron bonding interactions.[53] They used the following donors (**D1**-**D7**), [Acenap(EPh)(Br) E = Se, Te; Acenap(SePh)(EPh) E = Se, S and Acenap(TePh)(EPh) E = S, Se, Te] which they reacted with bromine and iodine to yield a variety of addition products (**1**-**12**) (Scheme 38-41).

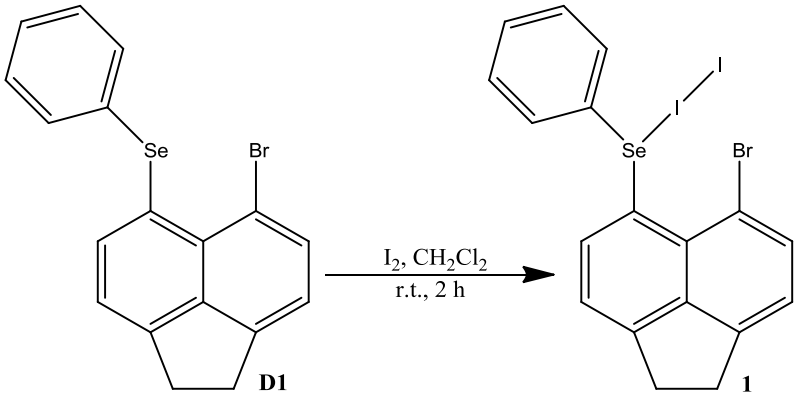

Scheme 38 Reaction of Acenap(SePh)(Br) **D1** with iodine to give the neutral charge adduct **1**.[53]

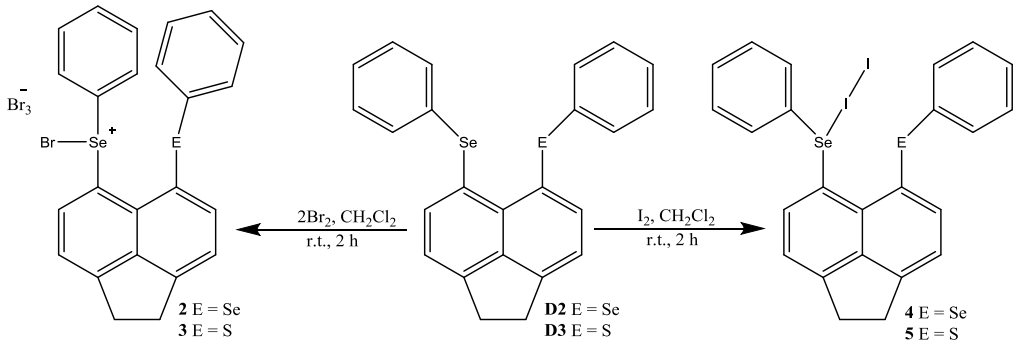

Scheme 39 Reactions of **D2** and **D3** with iodine and bromine.[53]

It was observed that reaction of iodine with the selenium donors **D1**-**D3** resulted in formation of neutral charge-transfer compounds (**1**, **4** and **5**) which have *hypervalent* three-body Se-I-I linear fragments.[53] Differing results were seen when **D2** and **D3** were reacted with bromine. Instead of forming neutral-charge transfer compounds, two tribromide salts were formed which contained bromoselanyl cations $[R_2Se\text{-}Br]^+$.[53]

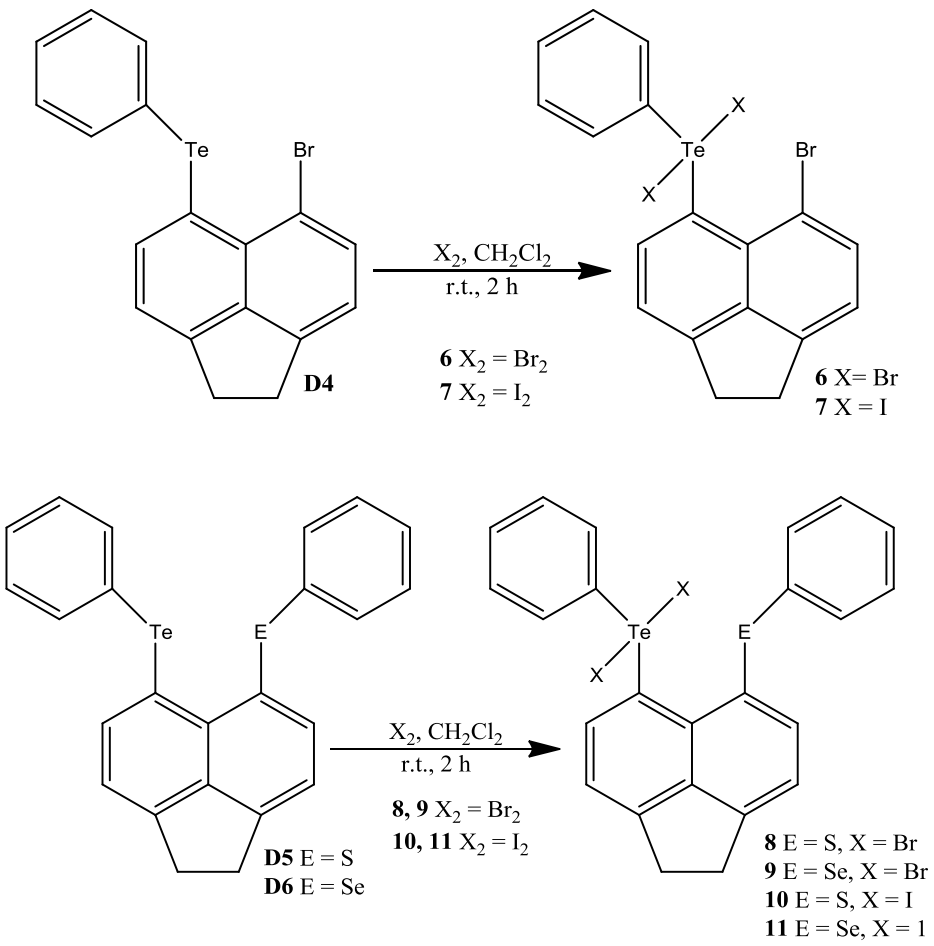

Scheme 40 Reaction of tellurium donors **D4**-**D6** with iodine and bromine.[53]

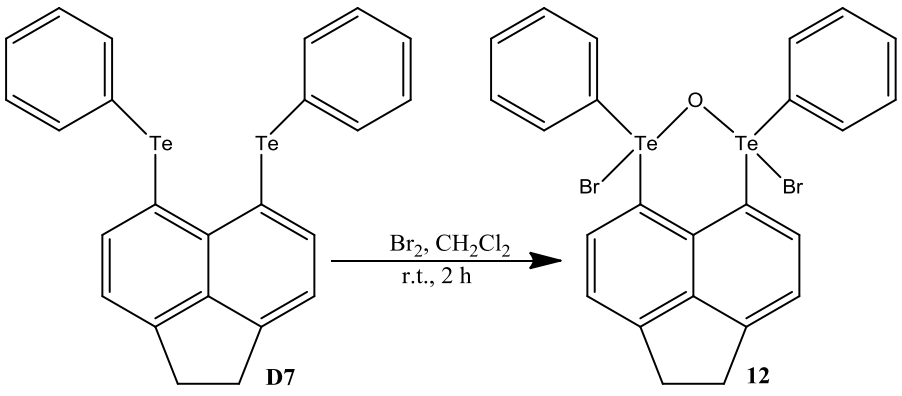

Scheme 41 Reaction of ditellurium donor **D7** with bromine.[53]

Reaction of the tellurium based donors **D4**-**D6** with iodine and bromine resulted in a series of compounds containing *quasi*-linear *hypervalent* X-Te-X groups. The ditellurium donor **D7** displayed differing behaviour to the other donors; reaction with bromine yielded an oxygenated derivative (**12**). Compound **12** contained a Te-O-Te bridge and two Br-Te-O *quasi*-linear fragments.[53]

Sterically crowded tin acenaphthenes have also been prepared by the Woollins group. For their synthesis they reacted 5,6-dibromoacenaphthene with one equivalent of *n*-butyllithium at -40 °C to yield 5-bromo-6-lithioacenaphthene. The corresponding organotin reagent was then added at 0 °C; this resulted in 5-bromo-6-(triphenylstannyl)acenaphthene (**1**), 5-bromo-6-(chlorodiphenylstannyl)acenaphthene (**2**), *bis*(6-bromoacenaphthen-5-yl)diphenylstannane (**3**), *bis*(6-bromoacenaphthen-5-yl)dibenzylstannane (**4**), *bis*(6-bromoacenaphthen-5-yl)dibutylstannane (**6**) and *bis*(6-bromoacenaphthen-5-yl)dichlorostannane (**7**) (Scheme 42 and 43).[54]

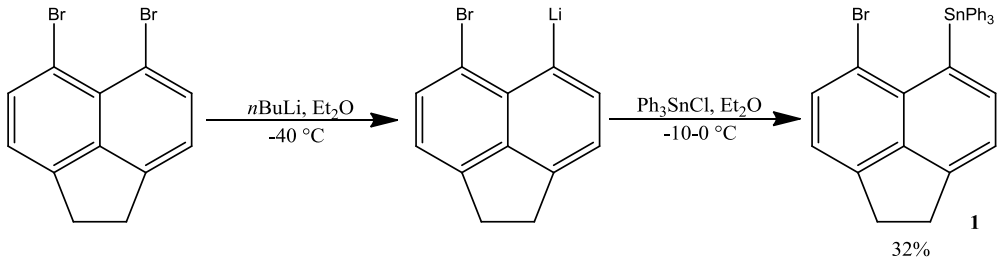

Scheme 42 Synthesis of 5-bromo-6-(triphenylstannyl)acenaphthene.[54]

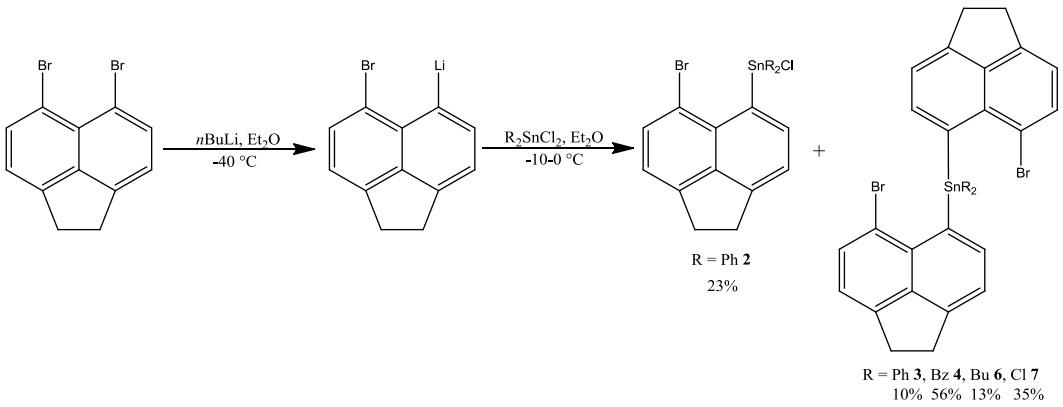

Scheme 43 Synthesis of sterically crowded tin acenaphthenes.[54]

The Woollins group found that stirring *bis*(6-bromoacenaphthen-5-yl)dibenzylstannane (**4**) overnight in chloroform with excess iodine resulted in 5-iodo-6-bromoacenaphthene (**5**). The formation of **5** was confirmed by X-ray crystallography, but no further analysis was carried out as the compound had been previously studied by the group.[50] 5-bromo-6-(dichlorobenzylstannyl)acenaphthene (**8**) was also prepared (Scheme 44).

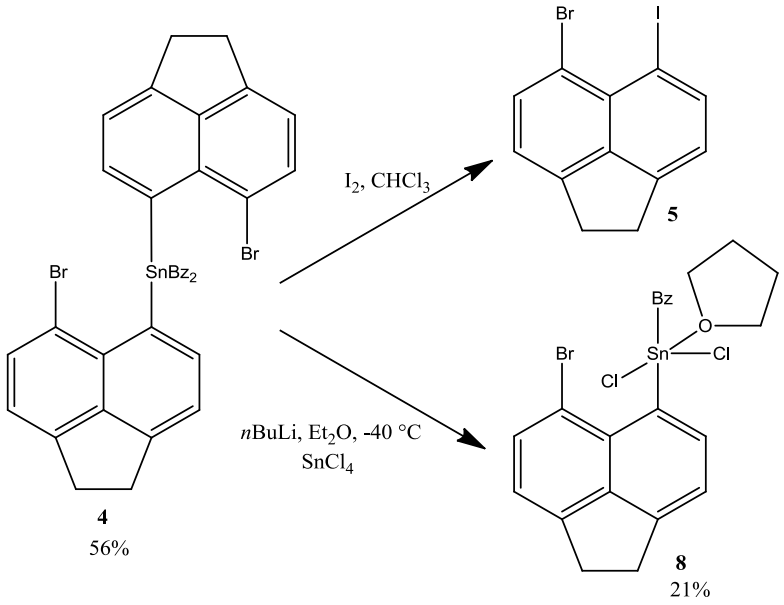

Scheme 44 Synthesis of 5-iodo-6-bromoacenaphthene (**5**) and 5-bromo-6-(dichlorobenzylstannyl)acenaphthene (**8**) from *bis*(6-bromoacenaphthen-5-yl)dibenzykstannane (**4**).[54]

Woollins and co-workers prepared monocation chalconium salts **1**-**9** (Figure 8) by reacting acenaphthenes [Acenap (Z)(EPh)] (Acenap = acenaphthene-5,6-diyl; Z = Br, SPh, SePh, TePh; E = S, Se, Te) with one equivalent of methyl trifluoromethanesulfonate (MeOTf).[55]

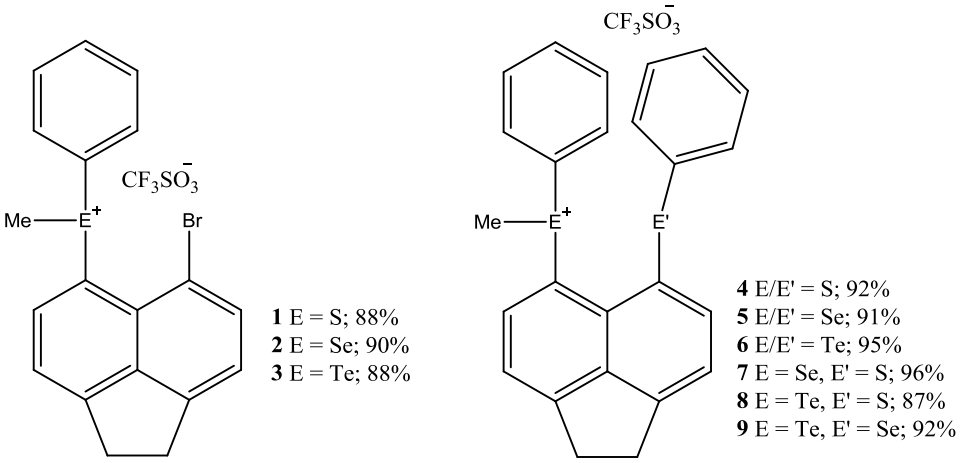

Figure 8 Monocation chalconium salts of acenaphthene **1**-**9**.[55]

The only compound to produce a dication chalconium salt when reacted with two equivalents of MeOTf was 5,6-*bis*(phenyltelluro)acenaphthene (Figure 9).

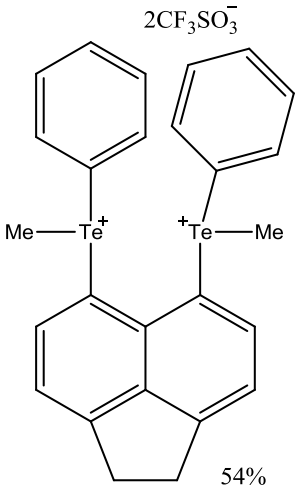

Figure 9 Dication chalconium salt $[\{Acenap(TePhMe)_2\}^{2+}\ \{(CF_3SO_3)_2\}^{2-}]$.[55]

When more than one methylation site is possible, such as in the mixed-chalcogen and bromo-chalcogen acenaphthenes, it was found that reaction will take place at the least electronegative chalcogen atom in the mixed derivatives or only at the chalcogen atom in the bromo-chalcogen derivatives.[55]

The molecular structures of the salts were varied and significantly different to their precursor acenaphthenes. It was found that most of the salts had an equatorial alignment of the E-C_{Me} bond which resulted in a *quasi*-linear three-body fragment, C_{Me}-E···Z (E = Te, Se, S; Z = Br/E). Density functional studies confirmed the presence of E···Z attractive interactions and suggested that under the correct geometric conditions the onset of three-centre, four-electron-type bonding would occur.[55]

Bühl, Woollins and co-workers used NMR and DFT techniques to study weak tellurium-tellurium interactions. They used a series of *peri*-substituted naphthalene and acenaphthene ditellurides (Figure 10) for the study. These compounds were chosen because the rigid naphthalene and acenaphthene frameworks force the tellurium atoms to sit in close proximity which results in non-bonded distances shorter than the sum of their van der Waals radii. These close non-bonded distances have been associated with weak donor-acceptor interactions and the onset of three-centre, four-electron bonding.[56]

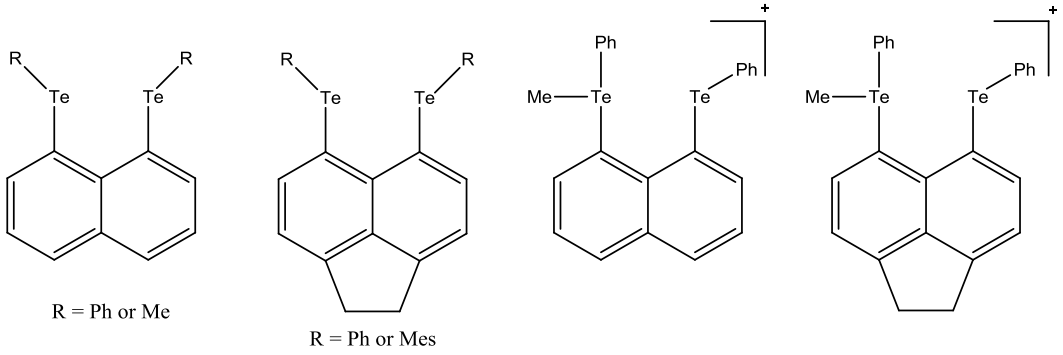

Figure 10 *Peri*-naphthalene and *peri*-acenaphthene ditellurides.[56]

From their study Bühl *et al.* found that the weak donor-acceptor interactions which lead to the onset of three-centre, four-electron bonding strengthen the tellurium-tellurium couplings and consequently result in large $J(^{125}Te, ^{125}Te)$ values. They also discovered that the coupling values can be used to determine the electronic structure behind the bonding and the structural conformation. Further studies are underway (see Chapter 5).[56]

Most recently, Woollins *et al.* have prepared a tellurium dication using the electrochemically informed synthesis of 5,6-*bis*(phenyltelluro)acenaphthene with one-electron oxidising agents silver(I) tetrafluoroborate ($AgBF_4$) and silver(I) trifluoromethanesulfonate (AgOTf) (Scheme 45).

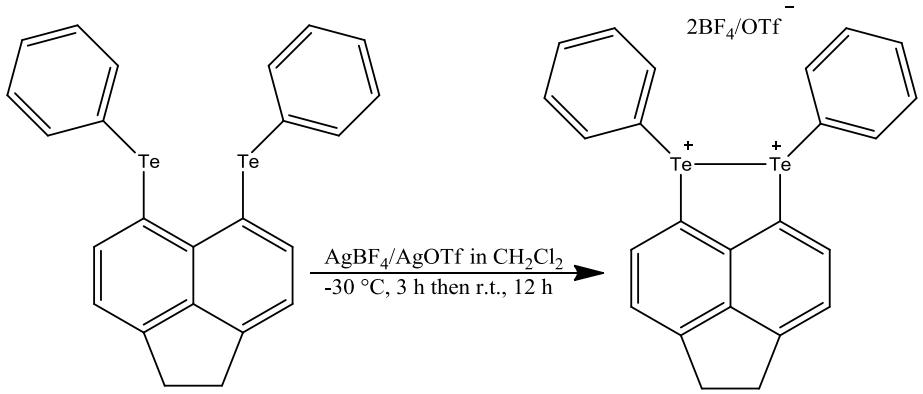

Scheme 45 Electrochemically informed synthesis of tellurium dication.[57]

The sulfur and selenium analogues, 5,6-*bis*(phenylsulfanyl)acenaphthene and 5,6-*bis*(phenylselanyl)acenaphthene, were also reacted with $AgBF_4$. Instead of undergoing oxidation they coordinated to the silver, resulting in two isomorphous three-dimensional silver(I) supramolecular coordination networks.[57]

During their studies of platinum complexes of naphthalene-1,8-dichalcogenole ligands[58], Woollins and co-workers also prepared platinum complexes of other dithiole ligands involving acenaphthene, phenanthrene and *tert*-butyl-substituted naphthalene. The acenaphthene derivative, [Pt(1,2-S_2-acenap)(PPh_3)$_2$], was prepared in a 94% yield by oxidative addition of 5,6-*bis*(phenylsulfanyl)acenaphthene to *tetrakis*(triphenylphosphine)platinum in toluene at room temperature. This is the first known *peri*-substituted acenaphthene metal complex found in the literature.[58, 59]

Woollins and colleagues continued their studies into metal complexes of *peri*-substituted compounds by looking at *bis*(cyclopentadienyl)titanium complexes of naphthalene-1,8-dithiolates and related ligands.[59, 60] They chose to prepare an acenaphthene derivative of titanocene 1,8-dithiolato-naphthalene in order to examine what effect changing the backbone would have on the complex (Scheme 46).

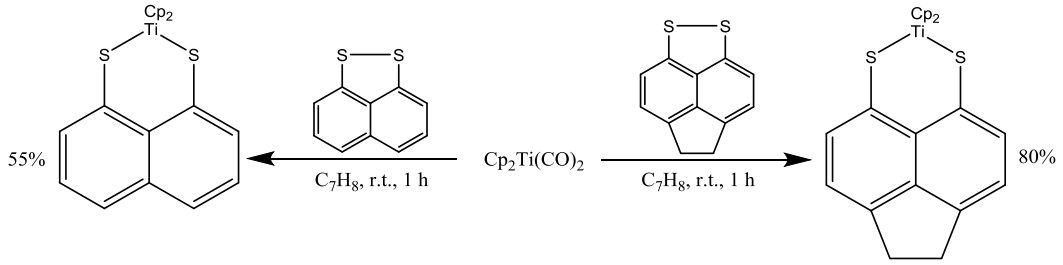

Scheme 46 Oxidative addition reactions of disulfide ligands to titanocene dicarbonyl.[60]

It was found using X-ray crystallography that altering the backbone from naphthalene to acenaphthene has little effect on the overall structure of the complex with data collected for both complexes being similar.[60]

The previously discussed phosphanylidene phosphorane[46], prepared by Kilian *et al.*, was reacted with *tetrakis*(triphenylphosphine)palladium to yield a transition metal complex (Scheme 47) in a 70% yield. The formation of this complex highlights the phosphine-phosphinidene donor-acceptor bonding feature of the phosphanylidene phosphorane.

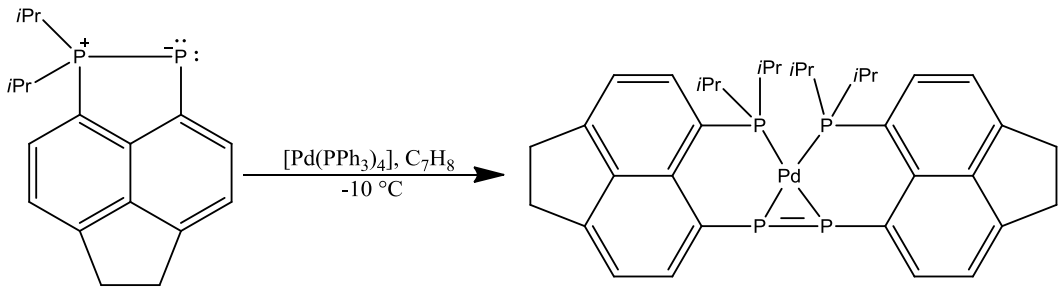

Scheme 47 Reaction of Kilian's phosphanylidene phosphorane with $[Pd(PPh_3)_4]$.[46]

Mixed chalcogen-chalcogen *peri*-substituted acenaphthenes **L** [Acenap(EPh)(E'Ph)] (where Acenap = acenaphthene-5,6-diyl; E/E' = S, Se, Te) were reacted with one equivalent of silver tetrafluoroborate in dichloromethane to produce silver(I) complexes in yields of 88-97%. The same reaction was repeated using one equivalent of silver triflate, resulting in product yields of

67-70%. It was found that many factors affected the structure of the resulting silver(I) complexes such as the recrystallisation solvent, the nature of the donor atoms and the coordinating properties of the tetrafluoroborate and triflate anions. Due to these factors a variety of monomeric silver(I) complexes were produced; $[Ag(BF_4(L)_2]$, $[AgBF_4(L)_3]$ and $[AgOTf(L)_3]$. A one-dimensional polymeric chain was also formed with the [AgOTf(**L3**)]*n* monomer unit. Within these complexes the silver atom is at the centre of a tetrahedral or trigonal planar motif with the ligands **L1**-**L3** binding in a variety of different ways.[61]

Further work was carried out into silver(I) coordination complexes using 5-bromo-6-(phenylchalcogeno)acenaphthene ligands **L1** [Acenap(Br)(EPh)] (where Acenap = acenaphthene-5,6-diyl; E = S, Se, Te) under the same reaction conditions used in the previous study. Again a variety of structures were synthesised; a monomeric dinuclear complex $[(AgBF_4(\mathbf{L1})_2)_2]$, two monomeric, mononuclear, two-coordinate complexes $[AgBF_4(\mathbf{L1})_2]$, a monomeric, three-coordinate complex $[AgOTf(\mathbf{L1})_2]$, a monomeric four-coordinate complex $[AgOTf(\mathbf{L1})_3]$ and a one-dimensional extended helical chain polymer with [AgOTf(**L1**)*n*] as the monomer unit. Unlike the mixed chalcogen-chalcogen *peri*-substituted acenaphthene ligands, these ligands only bind to the silver atom in a monodentate fashion. Linear, trigonal planar, see-saw and tetrahedral coordination geometries around the silver atom are observed.[62]

An initial look at the coordination chemistry of the *bis*(phosphines) **6** and **7**, prepared by Kilian *et al.*,[47] was carried out due to their promising capabilities as new P-chiral heteroleptic chelating ligands. The *bis*(phosphines) were each reacted with dichloro(1,5-cyclooctadiene)platinum(II) in dichloromethane at room temperature. Both reaction mixtures were then evaporated under reduced pressure to yield **6a** and **7a** in quantitative yield (Scheme 48).

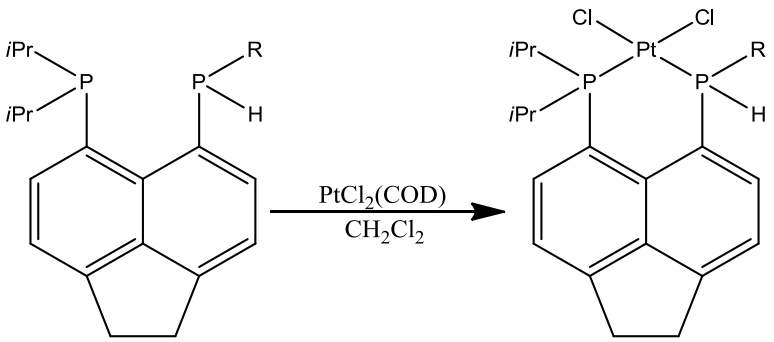

6: R = Ph; 85%
7: R = Fc; 89%

6a: R = Ph;100%
7a: R = Fc; 100%

Scheme 48 Synthesis of the platinum(II) complexes of *bis*(phosphines) **6** and **7**.[47]

Kilian *et al.*[47] also reacted the crude heteroleptic *bis*(phosphines) **10** and **11** with [Mo(CO)$_4$(nor)] (where nor = norbornadiene) in dichloromethane to form the molybdenum(0) complexes **10a** and **11a** (Scheme 49).

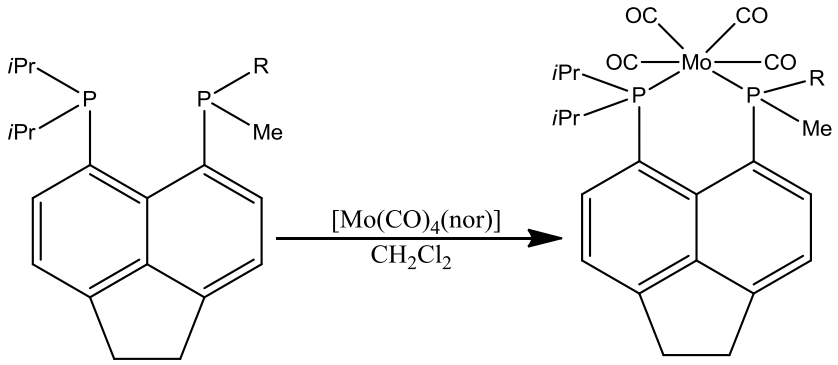

10: R = Ph; 70%
11: R = Fc; 60%

10a: R = Ph; 23%
11a: R = Fc; 23%

Scheme 49 Synthesis of the molybdenum(0) complexes of *bis*(phosphines) **10** and **11**.[47]

The synthesis of *bis*(*peri*-substituted) tridentate phosphine (**1**) (Figure 11) by Kilian and co-workers was discussed earlier in this review.[48] The chemistry of this compound will be further discussed by examining its coordination chemistry.

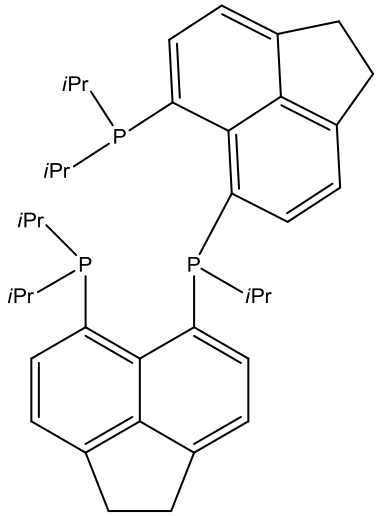

Figure 11 The *bis*(*peri*-substituted) tridentate phosphine (**1**) synthesised by Kilian *et al*.[48]

It was observed that the three phosphorus atoms in the tridentate phosphine (**1**) are arranged in such a way that reaction with a transition metal centre would result in a "well-defined coordination pocket."[48] The group were successful in using (**1**) as a tridentate ligand and prepared tetrahedral [(**1**)Cu(MeCN)][BF_4] (100%), square planar [(**1**)PtCl][Cl] (100%), trigonal bipyramidal [(**1**)$FeCl_2$] (92%) and octahedral *fac*-[(**1**)$Mo(CO)_3$] metal complexes. It was observed from X-ray crystallography data that in the four metal complexes, all three M-P bonds differ slightly in length due to the rigidity of the tridentate phosphine ligand.[48]

The most recent metal complexes of *peri*-substituted acenaphthenes to be prepared are the platinum complexes of 5,6-dihydroacenaphtho[5,6-*cd*]-1,2-dichalcogenoles.[63] Six complexes were synthesised by metathesis reactions of *cis*-[$PtCl_2(PR_3)_2$] (R_3 = Ph_3, Ph_2Me, $PhMe_2$) with the dilithium salts of the ligand 5,6-dihydroacenaphtho[5,6-*cd*]-1,2-dichalcogenoles (AcenapE_2, where E = S or Se) (Scheme 50).

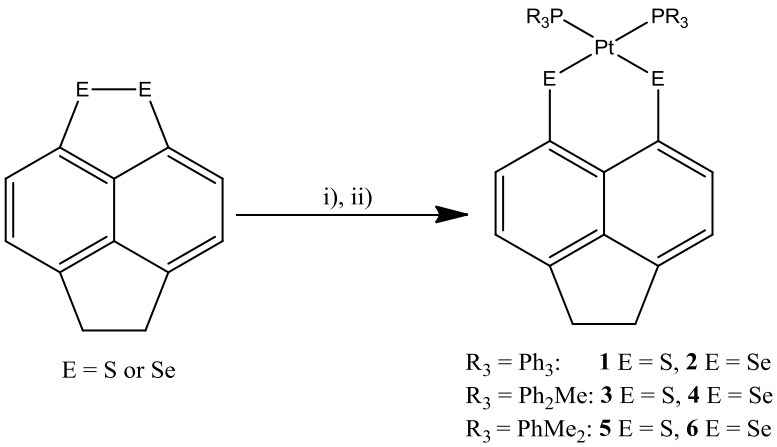

Scheme 50 Reaction scheme for platinum complexes of 5,6-dihydroacenaphtho[5,6-*cd*]-1,2-dichalcogenoles: i) $LiBEt_3H$ (2 eq.), THF, r.t. ii) $[PtCl_2(PR_3)_2]$, THF.[63]

References

[1] G. P. Petrenko and E. N. Tel'nyuk, *Zh. Obshch. Khim*., 1966, **2(4)**, 722; G. P. Petrenko and E. N. Tel'nyuk, *Zh. Org. Chim*., 1967, **3(1)**, 180; G. P. Petrenko and E. N. Tel'nyuk., *Zh. Org. Khim*., 1967, **3(5)**, 927.

[2] L-Y. Chiang and J. Meinwald, *Tetrahedron Lett*., 1980, **21**, 4565.

[3] R. H. Mitchell, M. Chaudhary, R. V. Williams, R. Fyles, J. Gibson, M. J. Ashwood-Smith and A. J. Fry, *Can. J. Chem*., 1992, **70**, 1015.

[4] J. C. Koziar and O. Cowan, *J. Am. Chem. Soc*., 1976, **98(4)**, 1001.

[5] F. Ogura, H. Miyamoto, K. Yui, Y. Aso and T. Otsubo, *Tetrahedron Lett*. 1986, **18**, 2011.

[6] D. Harrison, M. Stacey, R. Stephens and J. C. Tattrow, *Tetrahedron*, 1963, **19**, 1893.

[7] F. B. Mallory, C. W. Mallory, K. E. Butler, M. B. Lewis, A. Q. Xia, E. D. Luzik Jr., L. E. Fredenburgh, M. M. Ramanjulu, Q. N. Van, M. M. Francl, D. A. Freed, C. C. Wray, C. Hann, M. Nerz-Stormes, P. J. Carroll and L. E. Chirlian, *J. Am. Chem. Soc*., 2000, **122**, 4108.

[8] G. Felix, M. Laguerre, J. Dunoguès and R. Calas, *J. Org. Chem*., 1982, **47**, 1423.

[9] V. A. Ozeryanskii, A. F. Pozharskii, G. R. Milgizina and S. T. Howard, *J. Org. Chem*., 2000, **65**, 7707.

[10] R. W. Alder, *Chem Rev*., 1989, **89**, 1215.

[11] R. L. Benoit, D. Lefebvre and M. Frechette, *Can. J. Chem*., 1987, **65**, 996.

[12] A. F. Pozharskii, V. A. Ozeryanskii and Z. A. Starikova, *J. Chem. Soc., Perkin Trans. 2*, 2002, 318.

[13] A. F. Pozharskii, V. A. Ozeryanskii and N. V. Vistorobskii, *Russian Chemical Bulletin, International Edition*, 2003, **52**, 218.

[14] M. A. Mekh, V. A. Ozeryanskii and A. F. Pozharskii, *Tetrahedron*, 2006, **62**, 12288.

[15] K. Dziewonski and G. Rapalski, *Chem. Ber*., 1912, **45**, 2491; K. Dziewonski and G. Rapalski, *Chem. Ber*., 1913, **46**, 1986.

[16] A. N. Antonov, R. V. Tyurin, L. G. Minyaeva and V. V. Mezheritskii, *Russ. J. Org. Chem*., 2006, **42(10)**, 1576.

[17] A. N. Bezuglov, L. G. Minyaeva, R. V. Tyurin and V. V. Mezheritskii, Russ. J. Org. Chem., 2007, **43(8)**, 1256.

[18] V. V. Mezheritskii, L. G. Minyaeva and R. V. Tyurin, *Russian Chemical Bulletin, International Edition*, 2003, **54(3)**, 792.

[19] V. V. Mezheritskii, A. N. Bezuglov, L. G. Minyaeva, K. A. Lysenko, Y. V. Revinskii and A. A. Milov, *Russ. J. Org. Chem*., 2010, **46(1)**, 98.

[20] V. V. Mezheritskii, A. N. Antonov, A. A. Milov and K. A. Lysenko, *Russ. J. Org. Chem*., 2010, **46(6)**, 844.

[21] Y. G. Suh, S. N. Kim, D. Y. Shin, S. S. Hyun, D. S. Lee, K. H. Min, S. M. Choi, F. Li, E. C. Choi and S. H. Choi, *Bioorg. Med. Chem. Lett*., 2006, **16**, 142; D. Y. Shin, S. N. Kim, J. H. Chae, S. S. Hyun, S. Y. Seo, Y. S. Lee, K. O. Lee, S. H. Kim, Y.S. Lee, J.M. Jeong, N. S. Choi and Y. G. Suh, Bioorg. *Med. Chem. Lett*., 2004, **14**, 4519.

[22] I. A. Abdulaeva, L. G. Minyaeva and V. V. Mezheritskii, *Russ. J. Org. Chem*., 2011, **47(3)**, 385.

[23] P. Flowerday, M. J. Perkins and A. R. J. Arthur, *J. Chem. Soc. C*, 1970, **2**, 290.

[24] A. Saito, T. Miyajima, M. Nakashima, T. Fukushima, H. Kaji, Y. Matano and H. Imahori, *Chem. Eur. J*., 2009, **15**, 10000.

[25] M. M. Dashevskii and A. P. Karishin, *Prom. Org. Khimi*, 1937, **4**, 406.

[26] M. M. Dashevskii and A. P. Karishin, *Prom. Org. Khimi*, 1937, **4**, 109.

[27] R. L. Letsinger, J. A. Gilpin and W. J. Vullo, *J. Org. Chem*., 1962, **27**, 672.

[28] W. Dietrich Neudorff, D. Lentz, M. Anibarro and A. Dieter Schlüter, *Chem. Eur. J*., 2003, **9**, 2745.

[29] N. Goto and Y. Nagai, *Chem. Soc. Jpn, Ind. Chem. Sect*., 1954, **57**, 236.

[30] M. M. Dashevskii and G. P. Petrenko, *Ukrains'kii Khemichnii Zhurnal*, 1955, **21**, 370.

[31] A. P. Karishin and D. M. Kustol, *Zh. Obshch. Khim*., 1964, **34(3)**, 1001.

[32] N. Tanaka and T. Kasai, *Bull. Chem, Soc. Jpn*., 1981, **54**, 3020.

[33] A. P. Karishin, V. Yu. Samusenko and N. V. Krivoshapko, *Zh. Obshch. Khim.,* 1969, **39(9)**, 2098.

[34]A. P. Karishin, *Ukrains'kii Khemichnii Zhurnal*, 1952, **18**, 504; A. P. Karishin and D. M. Kustol, *Zh. Obshch. Khim*., 1964, **34(4)**, 924; A. P. Karishin and D. M. Kustol, *Zh. Obshch. Khim*., 1964, **34(4)**, 1292; N. G. Krivoshapko, A. P. Karishin, V. Yu. Samusenko, T. F. Dryanitsa and V. P. Lykho, *Ukrainskii Khimicheskii Zhurnal*, 1973, **39(8)**, 802.

[35] L. M. Yagupol'skii and M. Zh. Ivanova, *Zh. Obshch. Khim*., 1957, **27**, 2273.

[36] P. R. Constantine, L. W. Deady and R. D. Topsom, *J. Org. Chem*., 1969, **34(4)**, 1113.

[37] F. Vernon and R. D. Wilson, *Tetrahedron*, 1965, **21**, 2719.

[38] L. W. Deady, P. M. Gray and R. D. Topsom, *J. Org. Chem*., 1972, **21**, 3335.

[39] R. L. Clough, W. J. Kung, R. E. Marsh and J. D. Roberts, *J. Org. Chem*., 1976, **41**, 3603.

[40] W. Cross, G. E. Hawkes, R. T. Kroemer, K. R. Liedl, T. Loerting, R. Nasser, R. G. Pritchard, M. Steele, M. Watkinson and A. Whiting, *J. Chem. Soc., Perkin Trans. 2*, 2001, 459.

[41] A. N. Bezuglov, L. G. Minyaeva and V. V. Mezheritskii, *Russ. J. Org. Chem*., 2008, **44(3)**, 353.

[42] P. Wawrzyniak, A. M. Z. Slawin, A. L. Fuller, J. D. Woollins and P. Kilian, *Dalton Trans*., 2009, 7883.

[43] D. Seyferth and S. C. Vick, *J. Org. Chem*., 1977, **141**, 173.

[44] P. Wawrzyniak, A. L. Fuller, A. M. Z. Slawin and P. Kilian, *Inorg. Chem*., 2009, **48**, 2500.

[45] P. Wawrzyniak, A. M. Z. Slawin, J. D. Woollins and P. Kilian, *Dalton Trans*., 2010, **39**, 85.

[46] B. A. Surgenor, M. Bühl, A. M. Z. Slawin, J. D. Woollins and P. Kilian, Angew. *Chem. Int. Ed*., 2012, **51**, 10150.

[47] M. J. Ray, A. M. Z. Slawin, M. Bühl and P. Kilian, *Organometallics*, 2013, **32**, 3481.

[48] M. J. Ray, R. A. M. Randall, K. S. Athukorala Arachchige, A. M. Z. Slawin, M. Bühl, T. Lebl and P. Kilian, *Inorg. Chem*., 2013, **52**, 4346.

[49] Y. Aso, K. Yui, T. Miyoshi, T. Otsubo, F. Ogura and J. Tanaka, *Bull. Chem. Soc. Jpn*., 1988, **61**, 2013.

[50] L. K. Aschenbach, F. R. Knight, R. A. M. Randall, D. B. Cordes, A. Baggott, M. Bühl, A. M. Z. Slawin and J. D. Woollins, *Dalton Trans*., 2012, **41**, 3141.

[51] F. R. Knight, A. L. Fuller, M. Bühl, A. M. Z. Slawin and J. D. Woollins, *Chem. Eur. J*., 2010, **16**, 7503.

[52] F. R. Knight, A. L. Fuller, M. Bühl, A. M. Z. Slawin and J. D. Woollins, *Chem. Eur. J*., 2010, **16**, 7605.

[53] F. R. Knight, K. S. Athukorala Arachchige, R. A. M. Randall, M. Bühl, A. M. Z. Slawin and J. D. Woollins, *Dalton Trans*., 2012, **41**, 3154.

[54] M-L. Lechner, K. S. Athukorala Arachchige, R. A. M. Randall, F. R. Knight, M. Bühl, A. M. Z. Slawin and J. D. Woollins, *Organometallics*, 2012, **31**, 2922.

[55] F. R. Knight, R. A. M. Randall, K. S. Athukorala Arachchige, L. Wakefield, J. M. Griffin, S. E. Ashbrook, M. Bühl, A. M. Z. Slawin and J. D. Woollins*, Inorg. Chem*., 2012, **51**, 11087.

[56] M. Bühl, F. R. Knight, A. Křístová, I. Malkin Ondík, O. L. Malkina, R. A. M. Randall, A. M. Z. Slawin and J. D. Woollins, *Angew. Chem. Int. Ed*., 2013, **52**, 2495.

[57] F. R. Knight, R. A. M. Randall, T. L. Roemmele, R. T. Boeré, B. E. Bode, L. Crawford, M. Bühl, A. M. Z. Slawin and J. D. Woollins, *ChemPhysChem*, 2013, **14**, 3199.

[58] S. M. Aucott, H. L. Milton, S. D. Robertson, A. M. Z. Slawin, G. D. Walker and J. D. Woollins, *Chem. Eur. J*., 2004, **10**, 1666.

[59] P. Kilian, F. R. Knight and J. D. Woollins, Coord. *Chem. Rev*., 2011, **255**, 1387.

[60] S. M. Aucott, P. Kilian, H. L. Milton, S. D. Robertson, A. M. Z. Slawin and J. D. Woollins, *Inorg. Chem*., 2005, **44**, 2710.

[61] F. R. Knight, R. A. M. Randall, L. Wakefield, A. M. Z. Slawin and J. D. Woollins, *Molecules*, 2012, **17**, 13307.

[62] F. R. Knight, R. A. M. Randall, L. Wakefield, A. M. Z. Slawin and J. D. Woollins, *Dalton Trans*., 2013, **42**, 143.

[63] C. G. M. Benson, C. M. Schofield, R. A. M. Randall, L. Wakefield, F. R. Knight, A. M. Z. Slawin and J. D. Woollins, *Eur. J. Inorg. Chem*., 2013, 427.

Chapter 4

Peri-substituted acenaphthylenes

Introduction

The published manuscript: L. M. Diamond, F. R. Knight, K. S. Athukorala Arachchige, R. A. M. Randall, M. Bühl. A. M. Z. Slawin and J. D. Woollins, *Eur. J. Inorg. Chem*., 2014, **9**, 1512. was drafted from this chapter (see Collaboration Statement).

The family of polycyclic aromatic hydrocarbons naphthalene, acenaphthene and acenaphthylene, containing rigid organic backbones, allow the study of non-bonded intramolecular interactions.[1, 2, 3] Heteroatoms that are substituted at the *peri*-positions (positions 1- and 8- of the naphthalene ring and positions 5- and 6- of the acenaphthene and acenaphthylene rings) are forced to occupy space that is closer than the sum of their van der Waals radii, resulting in unique interactions. Naphthalene has a planar structure with all internal angles *ca*. 120°. Consequently the hydrogen atoms attached to C1 and C8 align in a parallel manner and have a non-bonded distance of 2.44 Å.[1] In acenaphthene the planarity is altered by the addition of the ethane bridge at the opposite side of the naphthalene ring with the internal angles becoming unequal and varying from 111-127°. The C1-C1a-C2 angle becomes compressed and in turn the C5-C5a-C6 angle becomes enlarged. The reduction in planarity causes the exocyclic *peri*-atom bonds to lie non-parallel in the plane, which increases the *peri*-distance to *ca*. 2.7 Å.[2] In acenaphthylene the ethene bridge causes further alteration in the planarity with internal angles varying from 107-136°. Like acenaphthene the C1-C1a-C2 angle becomes compressed and in turn the C5-C5a-C6 angle is enlarged. This change is much less drastic than that observed between naphthalene and acenaphthene with the *peri*-distance only increasing to *ca.* 2.73 Å.[3]

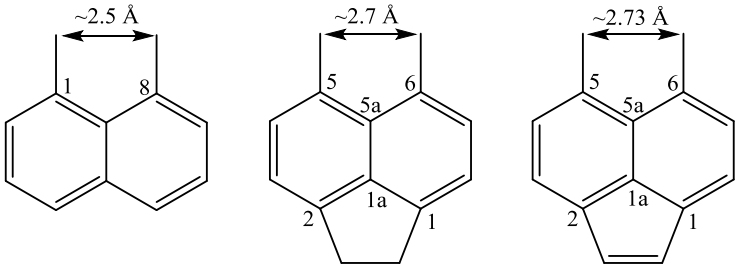

Figure 1 *Peri*-substitution in naphthalene, acenaphthene and acenaphthylene.

In all three parent systems the *peri*-substituents sit significantly closer together than is typical for ortho-substitution (see Chapter 1). If the substituents bound to the *peri*-carbon atoms are hydrogen atoms they can still be accommodated with ease. This is because the non-bonded hydrogen distances in naphthalene, acenaphthene and acenaphthylene (2.44 Å, 2.7 Å, 2.73 Å) are still greater than the sum of the van der Waals radii for two hydrogen atoms (Σr_{vdw} = 2.18 Å).[4] If these *peri*-hydrogens are replaced with larger substituents, steric hindrance is expected as there is not enough space for the larger groups to be accommodated without a significant overlap of orbitals.[5]

Although steric strain occurs when the hydrogen atoms are replaced by larger heteroatoms, a great array of *peri*-substituted naphthalenes[6] have been prepared. However, although some *peri*-substituted acenaphthenes[7] have been prepared they have received much less attention than naphthalenes. Preparation is possible because of the 'naphthalene' unit's ability to relieve strain through distortion. The rigid backbone in both systems forces the *peri*-substituents to occupy the limited space; in turn they experience steric strain as a consequence of sub van der Waals contacts.[8] This strain, however, can be alleviated in two ways allowing the larger *peri*-substituents to remain. Firstly, attractive interactions can occur which relieve the strain by causing formation of weak or strong bonds between the substituents.[5,6,8] Secondly, repulsive interactions cause the *peri*-bonds to distort in-plane or out-of-plane or distort the naphthalene backbone away from its normal geometry.[5,6,8] X-ray crystallography plays a key part in understanding these repulsive and attractive interactions (see Chapter 1). In comparison to *peri*-substituted naphthalenes and acenaphthenes, *peri*-substituted acenaphthylenes have received less consideration with only a handful of compounds known (see Chapter 3).

The preparation and structural study of two acenaphthylene series containing chalcogen-chalcogen moieties at the 5,6-positions in **Ay1**-**Ay6** (Acenapyl[EPh][E'Ph]) (Acenapyl = acenaphthylene-5,6-diyl; E/E' = S, Se, Te) and chalcogen-halogen moieties at the 5,6-positions in **Ay7**-**Ay12** (Acenapyl[X][EPh]) (Acenapyl = acenaphthylene-5,6-diyl; X = Br, I; E = S, Se, Te) is reported. The molecular structures of **Ay2-Ay4, Ay8, Ay9, Ay11** and **Ay12** are compared to the previously reported analogous naphthalene compounds **N2-N4, N8, N9, N11** and **N12**[8,9] and acenaphthene compounds **A2-A4, A8, A9, A11** and **A12**.[10] The synthesis and structural study of acenaphthene **ABr_4** (AcenapBr_2[Br_2]) (Acenap = acenaphthene-5,6-diyl) and acenaphthylenes **$AyBr_2$** and **AyI_2** (Acenapyl[X][X'])(XX' = BrBr, II) is also reported.

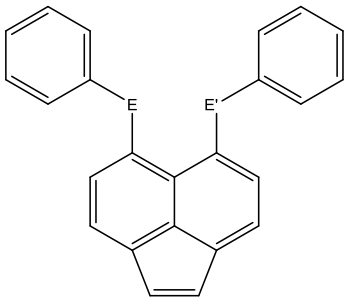

	Ay1	**Ay2**	**Ay3**	**Ay4**	**Ay5**	**Ay6**
E	S	Se	Te	S	Te	Te
E'	S	Se	Te	Se	S	Se

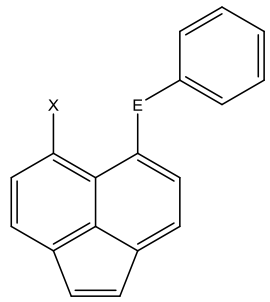

	Ay7	**Ay8**	**Ay9**	**Ay10**	**Ay11**	**Ay12**
X	Br	Br	Br	I	I	I
E	S	Se	Te	S	Se	Te

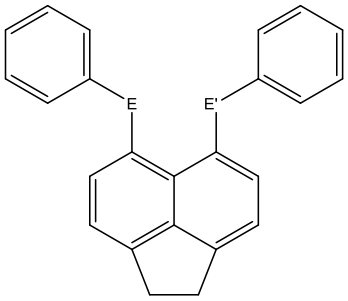

	A1	**A2**	**A3**	**A4**	**A5**	**A6**
E	S	Se	Te	S	Te	Te
E'	S	Se	Te	Se	S	Se

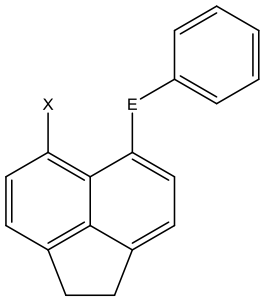

	A7	**A8**	**A9**	**A10**	**A11**	**A12**
X	Br	Br	Br	I	I	I
E	S	Se	Te	S	Se	Te

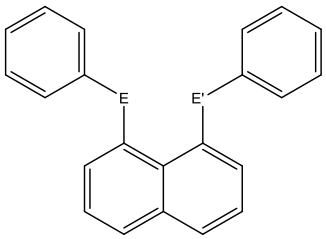

	N1	**N2**	**N3**	**N4**	**N5**	**N6**
E	S	Se	Te	S	Te	Te
E'	S	Se	Te	Se	S	Se

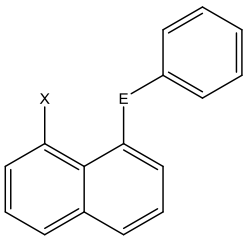

	N7	**N8**	**N9**	**N10**	**N11**	**N12**
X	Br	Br	Br	I	I	I
E	S	Se	Te	S	Se	Te

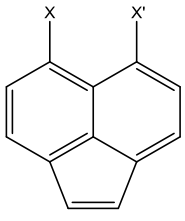

	$AyBr_2$	**AyI_2**
X	Br	I
X'	Br	I

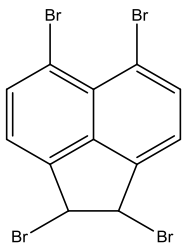

ABr_4

Figure 2 Naphthalenes **N1**-**N12**, acenaphthenes **A1**-**A12**, **ABr_4**, acenaphthylenes **Ay1**-**Ay12**, **$AyBr_2$** and **AyI_2**.

Results and Discussion

Compounds **($AyBr_2$, ABr_4, AyI_2 and Ay1-Ay12)** were synthesised and crystal structures were determined for **$AyBr_2$, ABr_4, Ay2-Ay4, Ay8, Ay9, Ay11** and **Ay12**.

5,6-dibromoacenaphthylene (**$AyBr_2$**) was prepared via two routes, as shown in Scheme 1. Both routes are slight modifications of the procedures taken from the literature.[11]

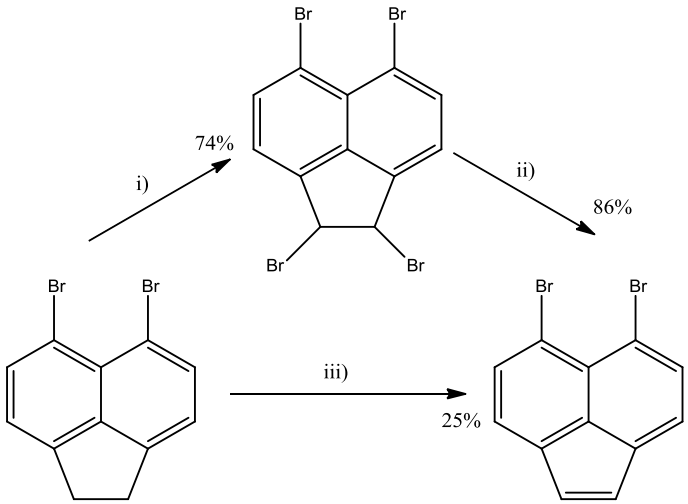

Scheme 1 The preparation of **$AyBr_2$** with corresponding yields: i) N-bromosuccinimide, benzoyl peroxide, chloroform, 80 °C, 5 h; ii) zinc powder, glacial acetic acid, 120 °C, 4 h; iii) 2,3-dichloro-5,6-dicyano-1,4-benzoquinone, benzene, 90 °C, 24 h.

Initially **$AyBr_2$** was prepared as follows; a chloroform solution of 5,6-dibromoacenaphthene (**ABr_2**), N-bromosuccinimide (NBS) (2.2 eq.) and benzoyl peroxide (0.22 eq.) was heated to reflux, under a nitrogen atmosphere, for five hours. After work-up, intermediate 1,2,5,6-tetrabromoacenaphthene **ABr_4** was isolated and fully characterised. For the second step of this route, a solution of **ABr_4** and zinc powder (5 eq.) in glacial acetic acid was heated to reflux for four hours, then cooled and filtered. The yellow filtrate was washed with saturated aqueous sodium hydrogen carbonate, dried, filtered and concentrated under reduced pressure to give 5,6-dibromoacenaphthylene (**$AyBr_2$**) as an orange solid in 86% yield.

The decision was made to try the second route using 2,3-dichloro-5,6-dicyano-1,4-benzoquinone (DDQ) because it gave a direct path from **ABr_2** to **$AyBr_2$**. A solution of **ABr_2** and DDQ (1.5 eq) in benzene was heated to reflux, under a nitrogen atmosphere, for twenty four hours. Once the solution was cooled to room temperature, pentane was added resulting in precipitation of a brown solid. The solution was filtered and the filtrate passed through a short silica column with a pentane eluent. The collected yellow solution was concentrated under reduced pressure to yield **$AyBr_2$** as a yellow solid in 20% yield.

Although the first routes' overall yield 64% of **$AyBr_2$** and the second route only 20%, the second route is more favourable due to it being less time consuming, more cost efficient and requires less purification of the product.

$AyBr_2$ was initially prepared for use as a precursor for the formation of a series of *peri*-substituted acenaphthylenes, containing chalcogen-chalcogen and mixed halogen-chalcogen moieties at the *peri*-positions, analogous to those already prepared using the naphthalene and acenaphthene backbones.[8,9,10] The initial attempt at preparing 5,6-*bis*(phenylsulfanyl)acenaphthylene (**Ay1**) followed the literature method used for synthesising 5,6-*bis*(phenylsulfanyl)acenaphthene (**A1**) from **ABr_2**.[10] A solution of **$AyBr_2$** in diethyl ether was cooled to -10-0 °C and a solution of N,N,N',N'-tetramethyl-1,2-ethanediamine (TMEDA) (2.7 eq.) was added. After fifteen minutes of stirring, a solution of *n*-butyllithium (*n*BuLi) (2.4 eq.) was added dropwise and the mixture was left to stir for one hour at -10 °C. The temperature was then lowered to -78 °C and a solution of diphenyl disulfide (2 eq.) in diethyl ether was added. After two hours of stirring the mixture was worked up resulting in an orange oil. ^{1}H NMR revealed that **$AyBr_2$** had reacted; however, the desired product peaks were not present. Purification of the mixture using column chromatography was unsuccessful.

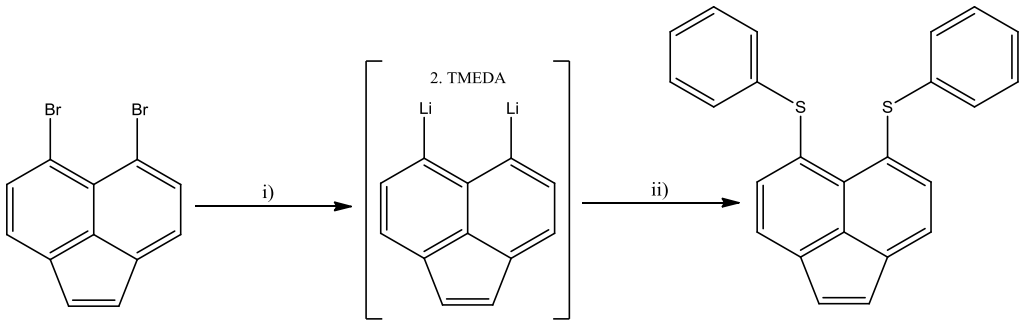

Scheme 2 The attempted preparation of 5,6-*bis*(phenylsulfanyl)acenaphthylene: i) TMEDA, *n*BuLi, diethyl ether,-10-0 °C, 1 h; ii) diphenyl disulfide, diethyl ether, -78 °C, 2 h.[10]

The initial unsuccessful attempt at synthesising **Ay1** from **$AyBr_2$** led us to investigate alternative routes to the chalcogen-substituted acenaphthylenes. Prompted by the successful transformation of **ABr_2** into **$AyBr_2$** with DDQ, it was decided to first prepare the desired acenaphthene and then react it with DDQ to achieve the corresponding acenaphthylene. All acenaphthenes were prepared following known literature procedures;[10] **ABr_2** was reacted with TMEDA (2.7 eq.) and *n*BuLi (2.4 eq.) to create a 5,6-dilithioacenaphthene.2TMEDA complex. This complex was then reacted with the respective diphenyl dichalcogenide (diphenyl disulfide, diphenyl diselenide, diphenyl ditelluride; 2 eq.) to yield a series of 5,6-*bis*(phenylchalcogeno)acenaphthenes **A1**-**A3**.[10]

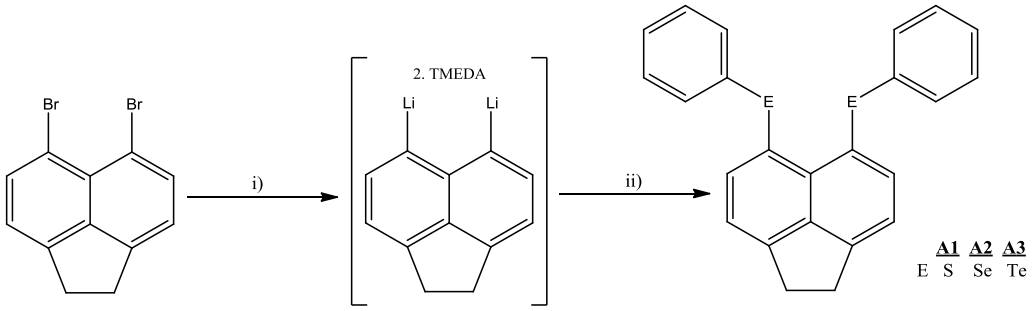

Scheme 3 The preparation of 5,6-*bis*(phenylchalcogeno)acenaphthenes **A1**-**A3** *via* 5,6-dilithioacenaphthene-TMEDA complex: i) TMEDA, *n*BuLi, diethyl ether, -10-0 °C, 1 h; ii)PhEEPh, diethyl ether, -78 °C, 2 h.[10]

The synthesis of 5-bromo-6-(phenylchalcogeno)acenaphthenes results from the reaction of **ABr_2** with *n*BuLi (1 eq.) to afford 5-bromo-6-(lithioacenaphthene), which is then treated with the

corresponding diphenyl dichalcogenide (diphenyl disulfide, diphenyl diselenide, diphenyl ditelluride; 1 eq.) to yield **A7**-**A9**. The 5-iodo-6-(phenylchalcogeno)acenaphthenes **A10**-**A12** were prepared following the same procedure with 5,6-diiodoacenaphthene (**AI_2**) as the precursor (Scheme 4).[10]

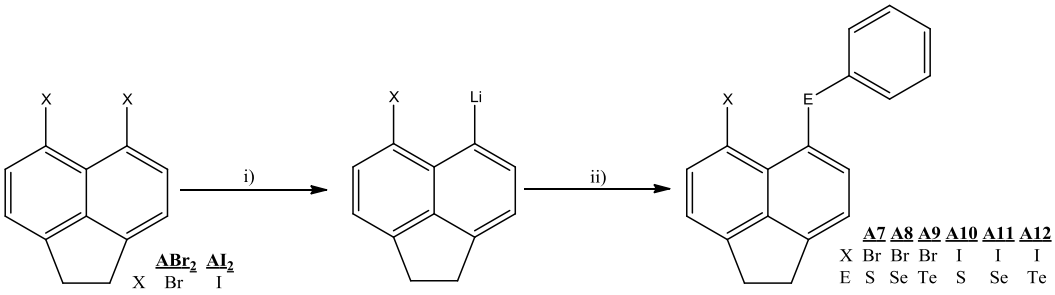

Scheme 4 The preparation of 5-halo-6-(phenylchalcogeno)acenaphthenes **A7**-**A12** from **ABr_2** and **AI_2**: i) *n*BuLi, diethyl ether, -78 °C, 1h; ii) PhEEPh, diethyl ether, -78 °C, 1h.[10]

The mixed 5,6-(phenylchalcogeno)acenaphthenes were synthesised from further reaction of the corresponding 5-halo-6-(phenylchalcogeno)acenaphthene (**A7** and **A8**) with *n*BuLi (1 eq.) and diphenyl dichalogenide (diphenyl disulfide, diphenyl diselenide, diphenyl ditelluride; 1 eq.).

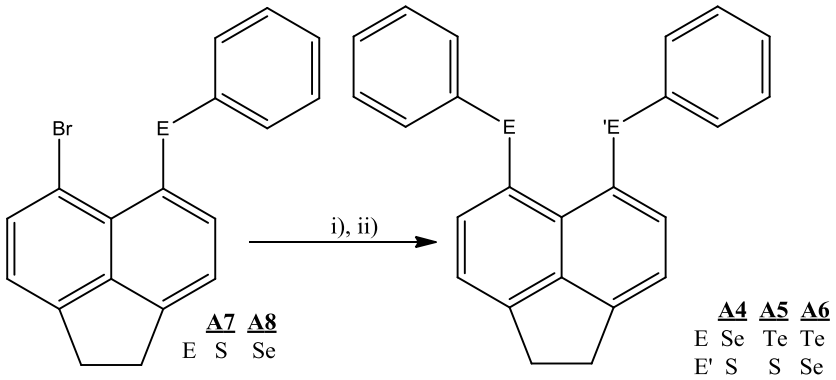

Scheme 5 The preparation of mixed 5,6-(phenylchalcogeno)acenaphthenes **A4**-**A6**: *i) n*BuLi, diethyl ether, -78 °C, 1h; ii) PhEEPh, diethyl ether, -78 °C, 1h.[10]

The acenaphthenes **A1**-**A12** and **AI_2** were reacted with DDQ (1.5 eq.) to achieve the desired acenaphthylenes **Ay1**-**Ay5**, **Ay7**-**Ay12** and **AyI_2**, following the same procedure as for the preparation of **$AyBr_2$**.[11]

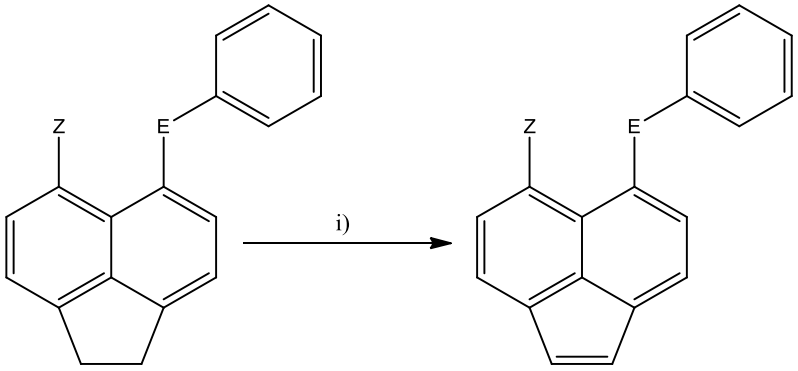

	Ay1	**Ay2**	**Ay3**	**Ay4**	**Ay5**	**Ay6**	**Ay7**	**Ay8**	**Ay9**	**Ay10**	**Ay11**	**Ay12**
Z	SPh	SePh	TePh	SePh	TePh	TePh	Br	Br	Br	I	I	I
E	S	Se	Te	S	S	Se	S	Se	Te	S	Se	Te
Yield (%)	58	53	45	31	12	/	48	18	23	37	34	71

Scheme 6 The preparation and yields of acenaphthylenes **Ay1**-**Ay12**: i) DDQ, benzene, 90 °C, 24 h.

Unlike the analogous acenaphthylenes, attempts to prepare **Ay6** using the above reaction were unsuccessful. ^{1}H NMR revealed that the reaction had formed an unsymmetrical acenaphthylene, as the characteristic pair of doublets which represent the two C*H* peaks of the ethene double bond were present (6.94 (1 H, d, $^{3}J_{HH}$ 5.2 Hz, C*H*), 6.91 (1 H, d, $^{3}J_{HH}$ 5.2 Hz, C*H*)). However, ^{1}H NMR and HSQC revealed that only one set of peaks were present for a phenyl group, indicating that only one chalcogen-phenyl group remained. This was confirmed when ^{125}Te NMR displayed no peaks and ^{77}Se NMR displayed a singlet at 446.1 ppm. Mass spectrometry confirmed the presence of a mono-substituted selenium-phenyl acenaphthylene with a *m/z* peak at 307.0 with a 70% abundance. Attempts to recrystallise the unknown product were unsuccessful. A density functional theory (DFT) calculation on the expected product determined that it should be successfully formed.

^{77}Se and ^{125}Te NMR spectroscopic data for the series of acenaphthylenes and their acenaphthene[10] and naphthalene[8,9] equivalents are shown below in Table 1. Previously, it was found that compared to the naphthalene analogues the acenaphthene NMR signals lie at lower

chemical shift values, indicating that the nuclei have greater shielding.[10] The acenaphthylenes display chemical shift values close to those of their corresponding naphthalene system, with the exception of **Ay5** which has a significantly higher chemical shift. We do not have a ready explanation for this difference.

Table 1 ^{77}Se and ^{125}Te NMR spectroscopic data.[8,9,10]

***peri*-atoms**		**Se, Se**	**Te, Te**	**Se, S**	**Te, S**	**Br, Se**	**Br, Te**	**I, Se**	**I, Te**
		Ay2	**Ay3**	**Ay4**	**Ay5**	**Ay8**	**Ay9**	**Ay11**	**Ay12**
Acenaphthylene	**^{77}Se NMR**	**427.1**	**-**	**456.3**	**-**	**447.7**	**-**	**426.6**	**-**
	^{125} Te NMR	**-**	**618.3**	**-**	**951.4**	**-**	**723.4**	**-**	**686.8**
		A2	*A3*	*A4*	*A5*	*A8*	*A9*	*A11*	*A12*
Acenaphthene	*^{77}Se NMR*	*408.3*	*-*	*433.7*	*-*	*423.7*	*-*	*400.9*	*-*
	^{125} Te NMR	*-*	*585.9*	*-*	*689.4*	*-*	*696.0*	*-*	*662.0*
		N2	*N3*	*N4*	*N5*	*N8*	*N9*	*N11*	*N12*
Naphthalene	*^{77}Se NMR*	*428.6*	*-*	*455.3*	*-*	*447.8*	*-*	*430.8*	*-*
	^{125} Te NMR	*-*	*619.7*	*-*	*715.2*	*-*	*731.2*	*-*	*698.3*

All spectra run in $CDCl_3$; δ (ppm)

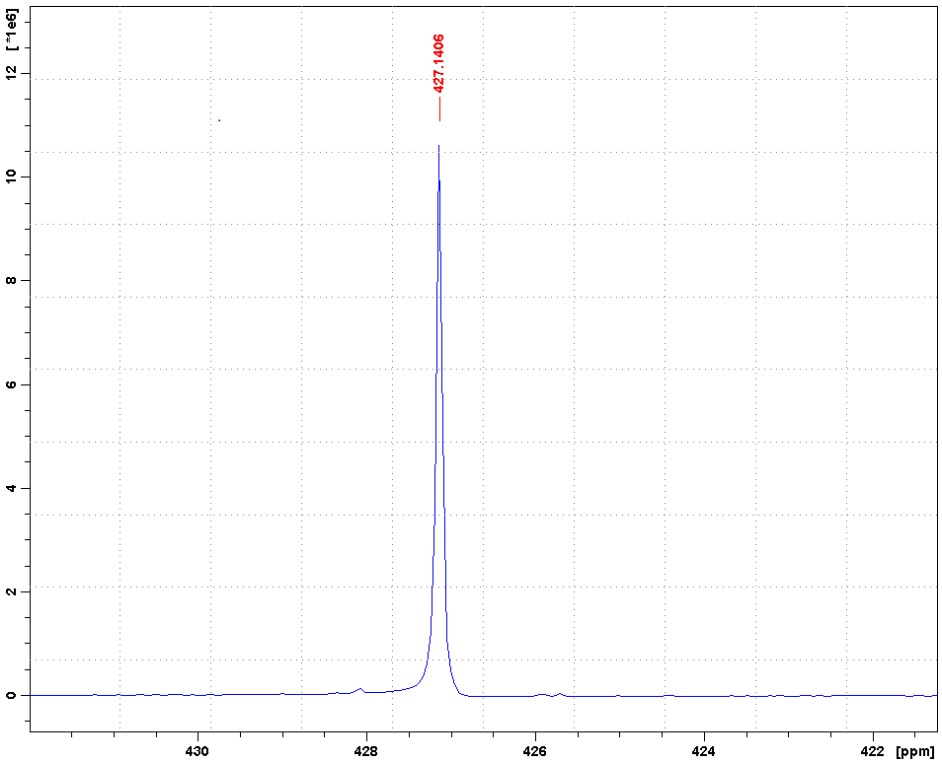

Figure 3 A typical ^{77}Se NMR spectrum with ^{13}C satellites e.g. shown for **Ay2**.

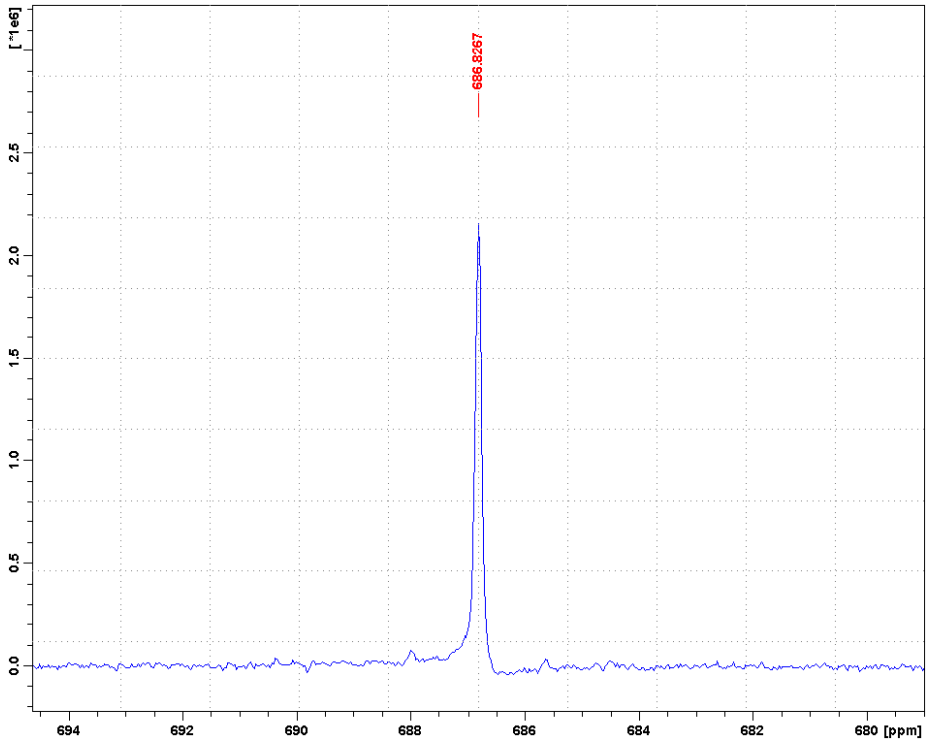

Figure 4 A typical ^{125}Te NMR spectrum with ^{13}C satellites e.g. shown for **Ay12**.

X-ray Investigations

Single crystals of **Ay2**, **Ay8**, **Ay9**, **Ay11** and **Ay12** were obtained by diffusion of hexane into a saturated solution of the compound in dichloromethane. Through the same method, **$AyBr_2$** crystallised with two nearly identical independent molecules in the asymmetric unit. Single crystals of **Ay3** and **Ay4** were obtained by evaporation of a saturated solution of the compound in dichloromethane. Single crystals were also attained for **ABr_4** by recrystallisation from hexane. In the following sections the molecular structures of **Ay2-4**, **Ay8**, **Ay9**, **Ay11** and **Ay12** are analysed and compared to the previously reported analogous structures that contain the naphthalene[8,9] and acenaphthene[10] backbones. The molecular structures of **ABr_4** and **ABr_2** are also discussed. The structures of **Ay8** and **Ay9**; **Ay11** and **Ay12**; **Ay2** and **Ay3**; **Ay4**; **$AyBr_2$** and **$AyBr_4$** are shown in Figures 8, 9, 13, 14, 18 and 19 respectively. Selected bond lengths, angles and torsion angles are recorded in Tables 2, 3, 4, 5 and 13.

The molecular structures of **Ay2-4**, **Ay8**, **Ay9**, **Ay11** and **Ay12** present both similarities and differences to their naphthalene[8,9] and acenaphthene[10] equivalents. The addition of the ethane bridge on the organic backbone of acenaphthene causes a reduction in the planarity of the system compared to naphthalene. This reduction is accompanied by the exocyclic *peri*-atom bonds shifting in opposite directions in the plane, increasing the *peri*-distance from *ca.* 2.5 Å in naphthalene to *ca*. 2.7 Å in acenaphthene.[2] As expected the change from an ethane to an ethene bridge has little effect on the planarity of acenaphthylene compared to acenaphthene, resulting in a small increase in the *peri*-distance to *ca.* 2.73 Å.[3] Despite the minor increase in *peri*-distance, acenaphthylene still cannot accommodate the halogen and chalcogen groups in **Ay2-4**, **Ay8**, **Ay9**, **Ay11** and **Ay12** with ease, resulting in deviations from the ideal acenaphthylene geometry. The deviations observed are similar to those observed in the acenaphthene analogues, but less than those observed in the naphthalene analogues.

In previous studies it was found that the naphthalene analogues, **N2-4**, **N8**, **N9**, **N11** and **N12**, relieve the strain caused from overcrowding at the *peri*-positions by increasing the C1-C10-C9 angle (ideal 121.0° compared to mean 128.1°) and stretching the bonds around C10 (ideal 1.420 Å compared to mean 1.436 Å). The C4-C5-C6 angle at the bottom of the naphthalene ring experiences compression (average of 118.3° compared to ideal 121.0°) and the C5-C10 central bond stretches (ideal 1.395 Å to an average of 1.436 Å).[1,8,9] The acenaphthene analogues **A2-4**,

A8, **A9**, **A11** and **A12** also experience widening of the C1-C10-C9 angle (average 131.2° compared to ideal 127.0°); however, the bonds around C5 and C10 do not elongate greatly from their ideal length (averages of 1.415 Å and 1.437 Å compared to ideal averages of 1.418 Å and 1.423 Å). In the acenaphthenes the C5-C10 bond also lengthens when compared to that of the ideal structure (1.428 Å mean compared to 1.39 Å in the ideal), but the C4-C5-C6 angle remains the same as the ideal at 111.3°.[2,10] The acenaphthylenes, **Ay2-4**, **Ay8**, **Ay9**, **Ay11** and **Ay12**, experience an increase in the C1-C10-C9 angle (mean 131.6° compared to ideal 127.8°), but the C4-C5-C6 angle shows negligible change (mean 108.9° compared to ideal 108.5°). The C5-C10 central bond stretches (mean 1.413 Å compared to ideal 1.386 Å), whereas the bonds around C5 compress (average 1.421 Å compared to ideal 1.441 Å) and the bonds around C10 remain close to the ideal (average 1.435 Å compared to ideal 1.433 Å).[3]

The observed bond lengthening and angle widening is not enough to relieve the strain that occurs from substituting bulky halogen and chacogen groups onto the acenaphthylene backbone. Akin to their naphthalene and acenaphthene analogues, acenaphthylenes experience additional distortion through in-plane tilting of the exocyclic *peri*-bonds and out-of-plane displacement of the *peri*-atoms. Out-of-plane displacement varies from 0.18-0.42 Å with displacement increasing as the bulk of the *peri*-substituents increases. Strain is also relieved by deformation of the 'naphthalene' ring with torsion angles varying from 172-180°. The ideal C1-C10-C9 angle increases from 121.6° in naphthalene[1], to 126.9° in acenaphthene[2] and to 127.8° in acenaphthylene[3] due to the addition of the ethane and ethene bridges at the bottom of the 'naphthalene' ring. As a consequence, increased splay angles and in turn *peri*-distances observed going from naphthalene to acenaphthylene in the series; 3.06-3.31 Å in **N2-4**, **N8**, **N9**, **N11** and **N12**, 3.11-3.38 Å in **A2-4**, **A8**, **A9**, **A11** and **A12** and 3.14-3.39 Å in **Ay2-4**, **Ay8**, **Ay9**, **Ay11** and **Ay12**. However, these *peri*-distances are still shorter than the sum of the van der Waals radii for the two corresponding atoms (3.70-4.12 Å).[4]

The configurations adopted by the 5-halo-6-(phenylchalcogeno)acenaphthylenes are classified using the method which was first outlined by Nakanishi *et al.*[12] and Nagy *et al.*[13] Classification is derived by examining the manner in which the acenaphthylene and phenyl rings align with respect to the C(ar)-E-C(ar) planes.[13] The same method also applies to the naphthalene and acenaphthene derivatives. Torsion angles θ and γ are calculated as shown in Figure 5 in order to determine the conformation. The rotation around the E-$C_{Acenapyl}$ bond is described by θ and the

rotation around the E-C_{Ph} bond is described by γ. If θ and γ are near 90°, the orientation is termed axial and if they near 180° it is termed equatorial. There are three conformations; types A, B and C (Figure 6). Type A is an axial conformation where the E-C_{Ph} bond is perpendicular to the acenaphthylene plane.[12,13] Type B is an equatorial conformation where the E-C_{Ph} bond lies on or close to the acenaphthylene plane.[12,13] Type C is intermediate of A and B where the E-C_{Ph} bond is neither axial or equatorial.[12,13]

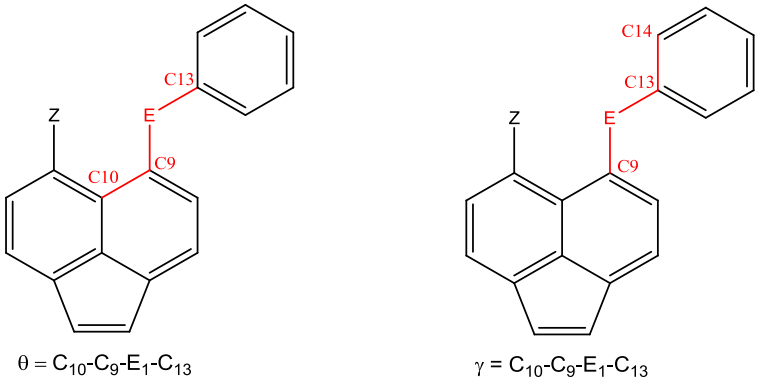

Figure 5 Conformation of the acenaphthylene aromatic rings is calculated from torsion angles: θ defines rotation around E-$C_{Acenapyl}$ bond; γ defines rotation around E-C_{Ph} bond.

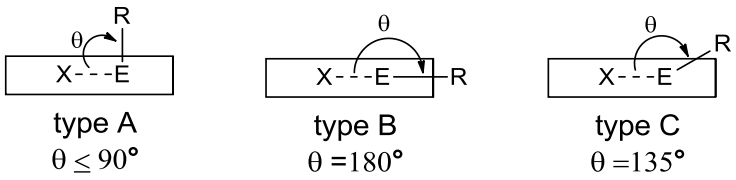

Figure 6 The three conformation types that can be adopted by 5-(halo)-6-(phenyl)acenaphthylenes.

The 5-halo-6(phenylchalcogeno)acenaphthylenes **Ay8**, **Ay9**, **Ay11** and **Ay12** show the same B type conformations (Table 2, Figures 8 and 9) as their respective acenaphthenes and naphthalenes.[8,9,10] The E-C_{Ph} bond aligns along the acenaphthylene plane resulting in a three-body fragment with X···E-C_{Ph} angles (ψ) in the range 169-177°. From **Ay8** to **Ay12** there is an increase in the *peri*-atom size which results in the bay region becoming more congested. In order to relieve this compression a steady increase in *peri*-distance is observed from 3.189(2) Å in **Ay8** to 3.366(3) Å in **Ay12**. The *peri*-distances in **Ay8** to **Ay12** are still shorter than the sum of their respective van der Waals radii by 14-17%. A variation in splay angle is observed between the four

compounds; a decrease is seen from 16.5° in **Ay8** to 14.9° in **Ay9,** whereas **Ay11** and **Ay12** have similar splay angles of 19.3° and 19.4°, respectively. Out-of-plane distortion also varies between the four compounds. The bromine atom shows similar distortion in **Ay8** and **Ay9,** lying 0.217(1) Å and 0.255(1) Å below the acenaphthylene plane. However, in contrast, the selenium atom in **Ay8** lies 0.190(1) Å above the plane whereas the tellurium atom lies above the plane in **Ay9** by 0.388(1) Å. There is greater out-of-plane displacement observed in **Ay9** because there is an increase in *peri*-distance, but a decrease in splay angle; this causes the *peri* atoms to move in/out of plane to relieve the distortion. **Ay11** and **Ay12** have differing out-of-plane distortion with **Ay12** showing greater distortion than **Ay11**. The iodine atom in **Ay11** lies below the plane (0.245(1) Å) and the selenium atom above the plane (0.183(1) Å). In **Ay12** by comparison the iodine atom lies above the plane (0.357(1) Å) and the tellurium atom lies below the plane (0.417(1) Å). **Ay12** displays greater out-of-plane distortion than **Ay11** because there is an increase in *peri*-distance, but negligible difference in the splay angle. The strain this causes on the system is relieved by the *peri*-atoms distorting in/out of the acenaphthylene plane. In all four compounds the acenaphthylene backbone displays distortion with selected C-C(5)-C(10)-C torsion angles deviating from the planar 180° by 0.2-7.6°.

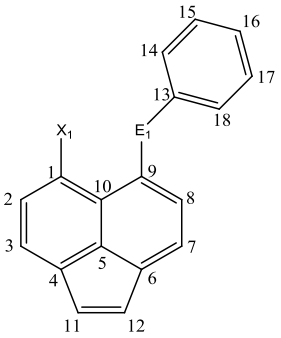

Figure 7 X-ray crystallography numbering scheme for 5-(halo)-6-(phenyl)acenaphthylenes.

Table 2 Selected interatomic distances [Å] and angles [°] for compounds **Ay8**, **Ay9**, **Ay11** and **Ay12**.

Compound	**Ay8**	**Ay9**	**Ay11**	**Ay12**
X-ray Code	LouD47B	LMD0-26-2	LMD039	LMD092-1OFF
X, EPh	Br,SePh	Br,TePh	I,SePh	I,TePh
Peri-region-distances				
X(1)···E(1)	**3.189(2)**	**3.260(4)**	**3.3324(9)**	**3.366(3)**
Σr_{vdW} - X···E[a]	0.561	0.650	0.5476	0.674
% Σr_{vdW}[a]	85	83	86	83

X(1)-C(1)	1.881(11)	1.89(3)	2.101(4)	2.072(18)
E(1)-C(9)	1.920(10)	2.17(3)	1.929(5)	2.127(18)
Acenaphthylene bond lengths				
C(1)-C(2)	1.401(15)	1.41(4)	1.386(6)	1.40(3)
C(2)-C(3)	1.401(16)	1.33(5)	1.392(7)	1.43(4)
C(3)-C(4)	1.367(15)	1.42(4)	1.367(6)	1.36(4)
C(4)-C(5)	1.401(15)	1.35(4)	1.417(6)	1.44(4)
C(5)-C(10)	1.416(14)	1.41(4)	1.404(6)	1.42(3)
C(5)-C(6)	1.418(14)	1.46(4)	1.419(6)	1.37(3)
C(6)-C(7)	1.375(15)	1.40(4)	1.356(6)	1.39(4)
C(7)-C(8)	1.415(15)	1.37(4)	1.411(6)	1.39(3)
C(8)-C(9)	1.391(14)	1.33(4)	1.381(6)	1.40(3)
C(9)-C(10)	1.442(14)	1.52(4)	1.442(6)	1.41(3)
C(10)-C(1)	1.428(14)	1.38(4)	1.432(6)	1.43(3)
C(4)-C(11)	1.460(16)	1.43(4)	1.481(6)	1.44(4)
C(11)-C(12)	1.341(16)	1.39(4)	1.341(7)	1.36(4)
C(12)-C(6)	1.474(15)	1.36(4)	1.463(6)	1.47(4)
Peri-region bond angles				
X(1)-C(1)-C(10)	124.0(8)	122.6(18)	125.4(3)	121.2(12)
C(1)-C(10)-C(9)	131.3(9)	134.0(3)	132.2(4)	131.7(17)
E(1)-C(9)-C(10)	121.2(7)	118.0(18)	121.7(3)	126.5(14)
Σ of bay angles	**376.5(14)**	**374.6(26)**	**379.3(6)**	**379.4(25)**
Splay angle[b]	16.5	14.6	19.3	19.4
C(4)-C(5)-C(6)	109.0(9)	109.0(3)	109.5(4)	109.0(2)
X(1)-E(1)-C(13)	177.07(1)	169.40(1)	174.72(1)	170.03(1)
Out-of-plane displacement				
X(1)	-0.217(1)	-0.258(1)	-0.245(1)	0.357(1)
E(1)	0.190(1)	0.382(1)	0.183(1)	-0.417(1)
Central naphthalene ring torsion angles				
C:(6)-(5)-(10)-(1)	-175.1(8)	-174.0(2)	-175.6(4)	177.4(19)
C:(4)-(5)-(10)-(9)	179.8(8)	-178.0(2)	-179.7(4)	172.4(19)

[a] van der Waals radii used for calculations: r_{vdW}(Se) 1.90 Å, r_{vdW}(Te) 2.06 Å, r_{vdW}(Br) 1.85 Å, r_{vdW}(I) 1.98 Å.[4]

[b] Splay angle: Σ of the three bay region angles – 360.

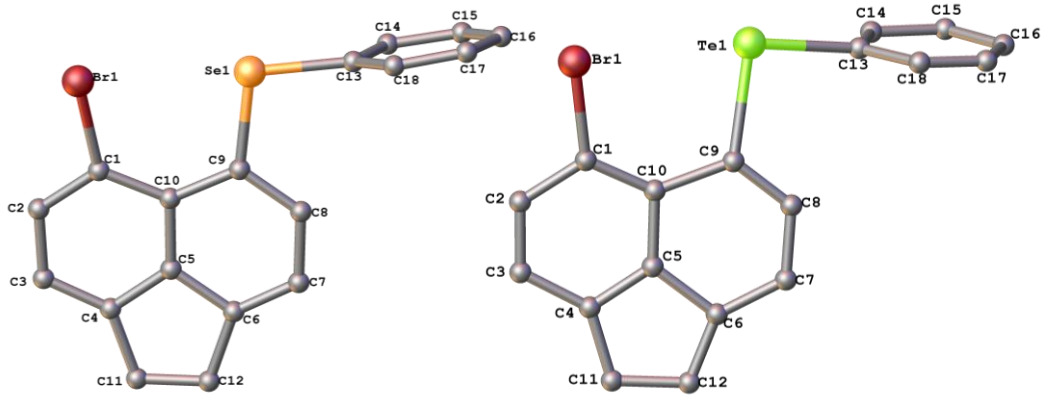

Figure 8 The molecular structures of **Ay8** and **Ay9** with H atoms omitted for clarity.[14]

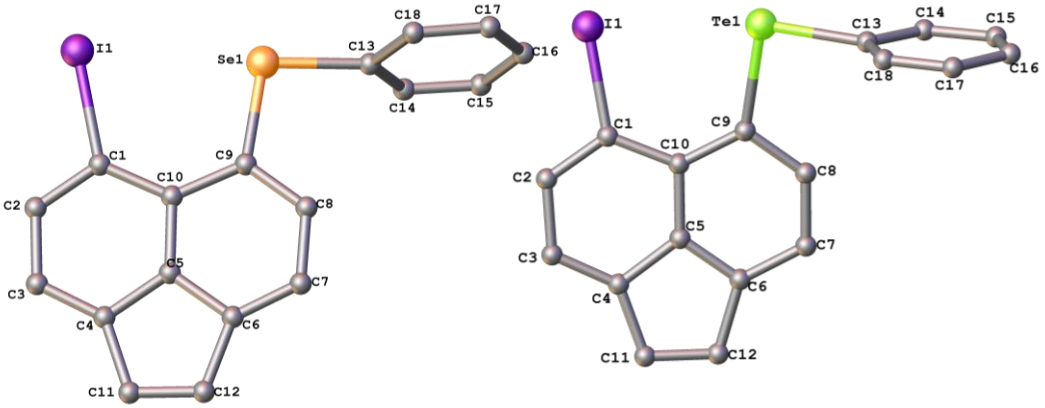

Figure 9 The molecular structures of **Ay11** and **Ay12** with H atoms omitted for clarity.

Table 3 Torsion angles [°] categorising the acenaphthylene and phenyl ring conformations in **Ay8**, **Ay9**, **Ay11** and **Ay12**.

Compound	***Acenaphthylene ring conformations***		***Phenyl ring conformations***	
Torsion angle	**C(10)-C(9)-E(1)-C(13)**	**Conformation**	**C(9)-E(1)-C(13)-C(14)**	**Conformation**
Ay8	θ_1 -167.8(7)	$Acenapyl_1$[a]: equatorial[d]	γ_1 84.8(7)	Ph_1[b]: axial[c]
Ay9	θ_1 -161.2(13)	$Acenapyl_1$: equatorial	γ_1 100.5(14)	Ph_1: axial
Ay11	θ_1 -167.7(3)	$Acenapyl_1$: equatorial	γ_1 84.4(3)	Ph_1: axial
Ay12	θ_1 162.8(15)	$Acenapyl_1$: equatorial	γ_1 89.5(12)	Ph_1: axial

[a]**$Acenapyl_1$**: [a]acenaphthylene ring E(1); [b]**Ph_1**: E(1) phenyl ring; [c]**axial**: perpendicular to C(ar)-E-C(ar) plane; [d]**equatorial**: coplanar with C(ar)-E-C(ar) plane.

The conformations adopted by the 5,6-*bis*(phenylchalcogeno)acenaphthylenes are classified in a similar manner to the 5-halo-6(phenylchalcogeno)acenaphthylenes. As before they are based on the way in which the acenaphthylene and phenyl rings align with respect to the C(ar)-E-C(ar) planes.[13] Torsion angles θ and γ are calculated as shown in Figure 5 in order to determine the conformation. There are four conformations; type AA, AB, BB and CC (Figure 10 and 11). Type AA is an axial conformation where both the E-C_{Ph} bonds are perpendicular to the acenaphthylene plane.[12,13] Type AB is a combination of equatorial and axial conformation where one E-C_{Ph} bond lies on or close to the acenaphthylene plane and the other E-C_{Ph} bond lies perpendicular to the plane.[12,13] Type BB is an equatorial conformation where both the E-C_{Ph} bonds lie on or close to the acenaphthylene plane. Type CC is intermediate of AA and BB where the E-C_{Ph} bonds are neither axial or equatorial and it is deemed a twist conformation.[12,13] Type AA, AB and CC can also be described as having a *cis* or *trans* conformation which is denoted by, for e.g. AA*t* and AA*c* for *trans* and *cis* respectively. If both phenyl rings are displaced to the same side of the mean acenaphthylene plane this would be a *cis* conformation. *Trans* is therefore defined as both phenyl rings being displaced to opposite sides of the mean acenaphthylene plane (see Figure 11).

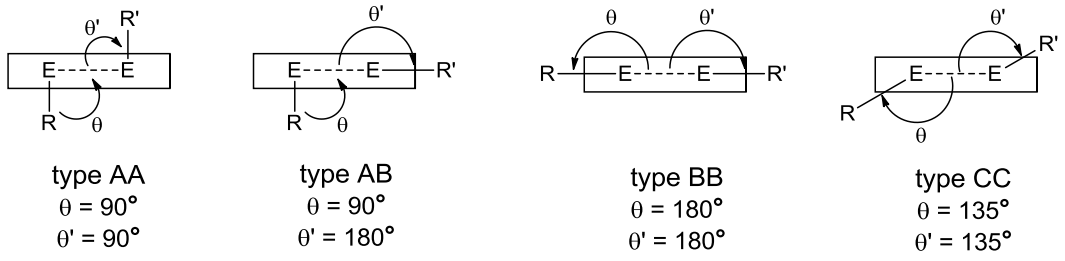

Figure 10 The four conformation types that can be adopted by 5,6-*bis*(phenylchalcogeno)acenaphthylenes.

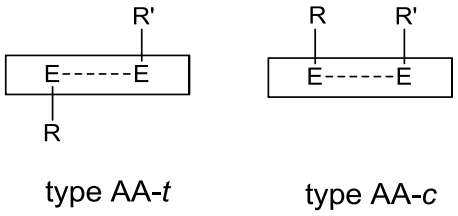

Figure 11 Type AA displaying *cis* and *trans* conformations.

Compounds **Ay2**-**Ay4** adopt AB type configurations (Table 4, Figures 13 and 14) with one E-C_{Ph} bond lying perpendicular to the acenaphthylene plane and the other E-C_{Ph} bond lying close to the acenaphthylene plane. In all three compounds the phenyl rings are displaced to opposite sides of

the mean acenaphthylene plane making them type AB*t*. The analogous acenaphthene derivatives **A2**-**A4** also have AB type configurations, but only the *bis*-telluride **A3** has the phenyl rings displaced to opposite sides of the mean acenaphthene plane. **A2** and **A4** have the phenyl rings displaced to the same side (AB*c*).[10] The naphthalene derivatives adopt similar conformations to the acenaphthene derivatives with the exception of the *bis*-telluride **N3** which has a CC*c* orientation.[8]

In all three compounds one of the E-C_{Ph} bonds aligns along the acenaphthylene plane resulting in a three-body fragment with E···E'-C_{Ph} angles (ψ) in the range 172-177°. Replacement of selenium atoms with tellurium atoms results in an expected increase in *peri*-distance from 3.191(3) Å in **Ay2** to 3.393(3) Å in **Ay3**, but still 16 and 18% shorter than the sum of their respective van der Waals radii. **Ay4** has a shorter *peri*-distance, 3.144(3) Å, than **Ay2** and **Ay3** which is expected as one of the selenium atoms has been replaced with the smaller sulfur atom. The *peri*-distance in **Ay4** is shorter than the sum of the van der Waals radii by 15%. There is a steady widening of the splay angle with increasing atom size at the *peri*-positions with angles of 15.7°, 16.4° and 19.8° for **Ay4**, **Ay2** and **Ay3** respectively. Out-of-plane distortion varies between the three compounds with distances in the range of 0.21 to 0.39 Å. **Ay3** shows the greatest out-of-plane distortion with **Ay2** showing the least. In all three compounds the acenaphthylene backbone displays distortion with C-C-C-C torsion angles deviating from the planar 180° by 1.5-4.8°. As with out-of-plane distortion it is **Ay3** that has the greatest deviation, but it differs in that **Ay4** shows the least deviation.

Ay3 behaves like its acenaphthene analogue **A3**[10] by forming short intermolecular contacts between the Te atoms of neighbouring molecules to form a Te_4 parallelogram (Figure 15). The planar Te_4 parallelogram has internal angles totalling 360° and two unequal Te···Te non-bonded distances. The intramolecular *peri*-distance of 3.393(3) Å is shorter than the intermolecular Te···Te distance of 3.843(1) Å, however both distances are still shorter than the sum of the van der Waals radii for two tellurium atoms (4.12 Å).[4] Formation of these short intermolecular contacts is only observed for the TeTe analogues with no such behaviour seen for the SeSe or SeS naphthalene or acenaphthene derivatives.

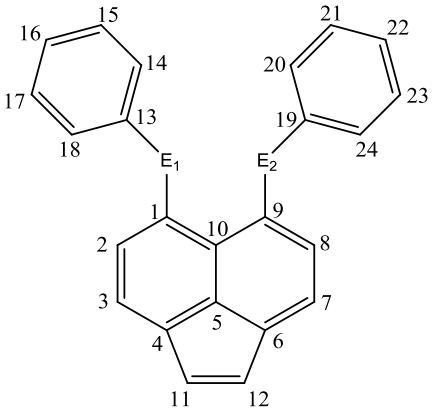

Figure 12 X-ray crystallography numbering scheme for 5,6-*bis*(phenylchalcogeno)acenaphthylenes.

Table 4 Selected interatomic distances [Å] and angles [°] for compounds **Ay2**-**Ay4**.

Compound	Ay2	Ay3	Ay4
X-ray Code	LMD011_off	LMD0-15	LMD0-53
E(1)Ph, E(2)Ph	SePh,SePh	TePh,TePh	SePh,SPh
Peri-region-distances			
E(1)···E(2)	**3.191(3)**	**3.393(3)**	**3.144(3)**
Σr_{vdW} - E(1)···E(2)[a]	0.609	0.727	0.556
%Σr_{vdW}[a]	84	82	85
E(1)-C(1)	1.926(13)	2.123(15)	1.932(7)
E(2)-C(9)	1.905(13)	2.151(14)	1.781(8)
Acenaphthylene bond lengths			
C(1)-C(2)	1.42(3)	1.394(19)	1.397(11)
C(2)-C(3)	1.40(2)	1.40(3)	1.443(11)
C(3)-C(4)	1.40(3)	1.383(19)	1.357(10)
C(4)-C(5)	1.44(3)	1.422(19)	1.441(11)
C(5)-C(10)	1.437(18)	1.40(2)	1.402(9)
C(5)-C(6)	1.45(3)	1.43(2)	1.421(9)
C(6)-C(7)	1.33(3)	1.387(19)	1.375(11)
C(7)-C(8)	1.42(2)	1.40(3)	1.401(10)
C(8)-C(9)	1.41(3)	1.41(2)	1.388(9)
C(9)-C(10)	1.46(3)	1.434(17)	1.428(10)
C(10)-C(1)	1.43(3)	1.425(19)	1.433(8)
C(4)-C(11)	1.47(2)	1.46(3)	1.470(9)
C(11)-C(12)	1.37(3)	1.37(2)	1.360(11)
C(12)-C(6)	1.45(2)	1.48(2)	1.458(11)
Peri-region bond angles			
E(1)-C(1)-C(10)	123.4(11)	124.5(10)	122.8(6)
C(1)-C(10)-C(9)	130.5(12)	131.2(13)	129.9(6)
E(2)-C(9)-C(10)	122.5(12)	124.1(10)	123.0(5)

Σ of bay angles	**376.4(20)**	**379.8(19)**	**375.7(10)**
Splay angle[b]	16.4	19.8	15.7
C(4)-C(5)-C(6)	109.0(12)	108.7(13)	108.4(6)
E(2)-E(1)-C(13)	84.47(1)	92.99(1)	172.72(1)
E(1)-E(2)-C(19)	176.6(1)	174.06(1)	94.35(1)
Out-of-plane displacement			
E(1)	-0.213(1)	0.306(1)	0.276(1)
E(2)	0.245(1)	-0.387(1)	-0.260(1)
Central naphthalene ring torsion angles			
C:(6)-(5)-(10)-(1)	-177.1(14)	177.5(8)	178.5(6)
C:(4)-(5)-(10)-(9)	-177.0(14)	175.2(8)	177.4(6)

[a] van der Waals radii used for calculations: r_{vdW}(S) 1.80 Å, r_{vdW}(Se) 1.90 Å, r_{vdW}(Te) 2.06 Å.[4]

[b] Splay angle: Σ of the three bay region angles – 360.

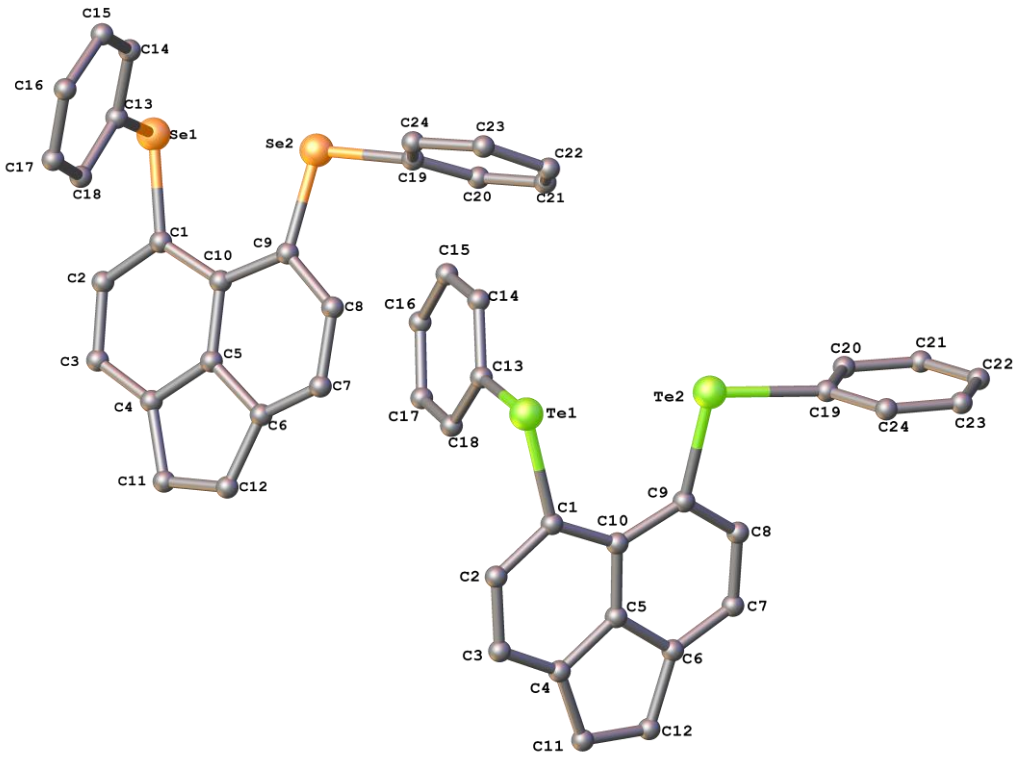

Figure 13 The molecular structures of **Ay2** and **Ay3** with H atoms omitted for clarity.

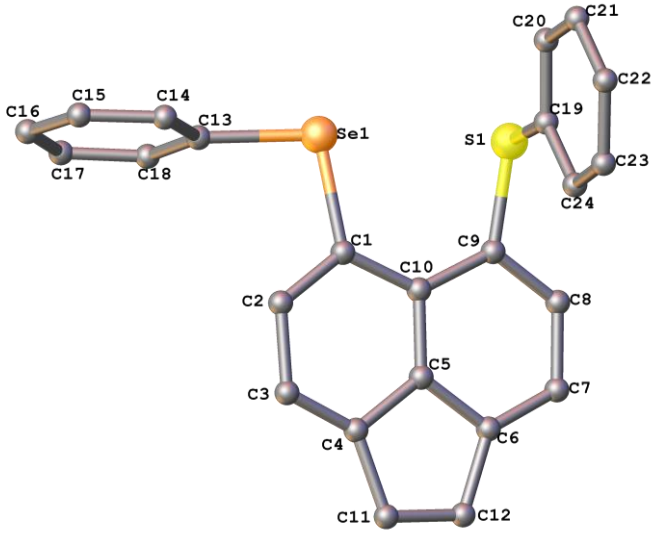

Figure 14 The molecular structure of **Ay4** with H atoms omitted for clarity.

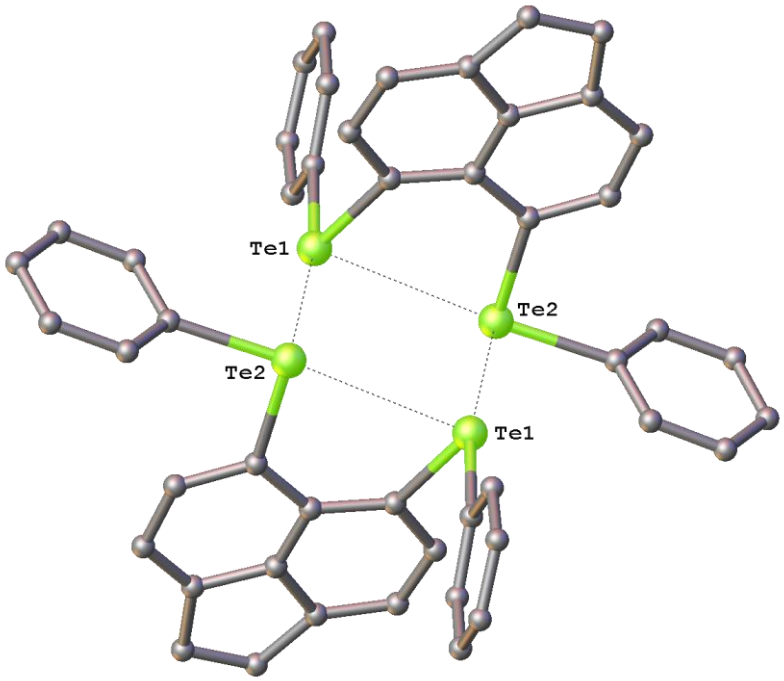

Figure 15 Short intermolecular contacts are observed in **Ay3** resulting in Te_4 parallelograms.

Table 5 Torsion angles [°] categorising the acenaphthylene and phenyl ring conformations in **Ay2**-**Ay4**.

Compound	***Acenaphthylene ring conformations***		***Phenyl ring conformations***	
Torsion angle	**C(10)-C(1)-E(1)-C(13)**	**C(10)-C(9)-E(2)-C(19)**	**C(1)-E(1)-C(13)-C(14)**	**C(9)-E(2)-C(19)-C(20)**
Ay2	θ_1 -75.7(13)	θ_2 -174.0(12)	γ_1 156.2(14)	γ_2 84.6(10)
	$Acenapyl_1$[a]: axial[e]	$Acenapyl_2$[b]: equatorial[f]	Ph_1[c]: equatorial	Ph_2[d]: axial
Ay3	θ_1 78.8(7)	θ_2 166.2(7)	γ_1 -159.2(8)	γ_2 86.1(10)
	$Acenapyl_1$: axial	$Acenapyl_2$: equatorial	Ph_1: equatorial	Ph_2: axial
Ay4	θ_1 161.9(5)	θ_2 82.1(5)	γ_1 99.2(6)	γ_2 -165.8(5)
	$Acenap_1$: equatorial	$Acenap_2$: axial	Ph_1: axial	Ph_2: equatorial

[a]**Acenapyl1**: acenaphthylene ring E(1); [b]**Acenapyl2**: acenaphthylene ring E(2); [c]**Ph1**: E(1) phenyl ring; [d]**Ph2**: E(2) phenyl ring; [e] **axial**: perpendicular to C(ar)-E-C(ar) plane; [f]**equatorial**: coplanar with C(ar)-E-C(ar) plane

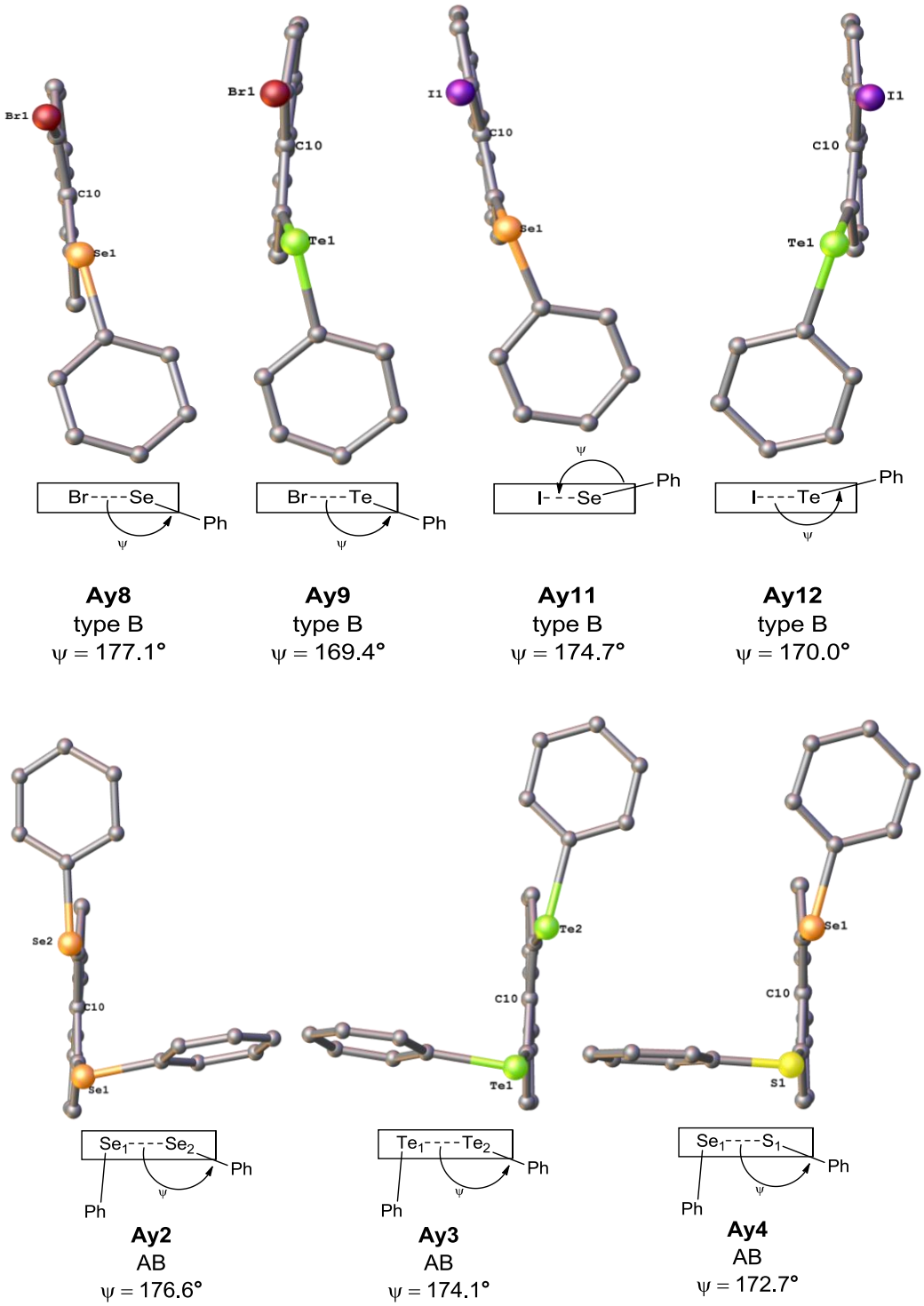

Figure 16 The orientation of the E(Ph) groups, the three-linear fragment arrangements and structural conformations for **Ay2**-**4**, **Ay8**, **Ay9**, **Ay11** and **Ay12**.

A2[10] and **Ay2** display similar characteristics, with **N2**[8] being the 'odd one out'. **A2** and **Ay2** have similar *peri*-distances (3.1834(10) Å and 3.191(3) Å, respectively) which are shorter than the sum of their van der Waals radii by 16%. In comparison **N2** has a *peri*-distance of 3.1332(9) Å which is 18% shorter than the sum of the van der Waals radii of two selenium atoms. Splay angles of 16.5° and 16.4° are observed in **A2** and **Ay2**, whereas a value of 13.9° is seen in **N2**. These differences can be explained by the addition of the ethane bridge (1.570(12) Å) in acenaphthene and the ethene bridge (1.37(3) Å) in acenaphthylene. The addition of the bridge at the bottom of the naphthalene ring compresses the C4-C5-C6 angle from 117.3(6)° in **N2** to 110.5(7)° in **A2** and 109.0(12)° in **Ay2**. This compression at the bottom of the naphthalene ring is accompanied by an increase in the splay angle at the top of the ring. The selenium atoms in **N2** sit 0.468(9) Å above and 0.327(9) Å below the mean naphthalene plane. In **A2** the atoms sit 0.176(1) Å above and 0.193(1) Å below the plane of the ring and in **Ay2** they sit 0.245(1) Å above and 0.213(1) Å below. All three compounds display 'naphthalene' backbone distortion with C-C-C-C torsion angles deviating from planar 180° by 5.4-6.5° in **N2**, 0.8-1.6° in **A2** and 2.9-3.0° in **Ay2**. **N2** displays greater distortion of the backbone and larger out-of-plane displacement of the selenium atoms than **A2** and **Ay2** because the acenaphthene and acenaphthylene ring systems are more rigid than the naphthalene. The natural rigidity of the naphthalene backbone is enhanced with the addition of the ethane/ethene linker which lessens the system's ability to relieve strain *via* buckling.

Table 6 Selected interatomic distances [Å] and angles [°] for compounds **N2,**[8] **A2**[10] and **Ay2**

Compound	**N2**	**A2**	**Ay2**
E(1)Ph, E(2)Ph	SePh,SePh	SePh,SePh	SePh,SePh
Peri-region-distances			
E(1)···E(2)	**3.1332(9)**	**3.1834(10)**	**3.191(3)**
Σr_{vdW} - X···E[a]	0.67	0.6166	0.609
$\%\Sigma r_{vdW}$[a]	82	84	84
E(1)-C(1)	1.922(7)	1.928(9)	1.926(13)
E(2)-C(9)	1.930(7)	1.932(8)	1.905(13)
"Naphthalene" bond lengths			
C(1)-C(2)	1.381(10)	1.372(12)	1.42(3)
C(2)-C(3)	1.400(11)	1.411(12)	1.40(2)
C(3)-C(4)	1.357(11)	1.371(12)	1.40(3)
C(4)-C(5)	1.420(10)	1.420(12)	1.44(3)
C(5)-C(10)	1.423(10)	1.423(12)	1.437(18)
C(5)-C(6)	1.436(10)	1.425(12)	1.45(3)

C(6)-C(7)	1.371(10)	1.364(12)	1.33(3)
C(7)-C(8)	1.381(12)	1.412(12)	1.42(2)
C(8)-C(9)	1.368(10)	1.372(12)	1.41(3)
C(9)-C(10)	1.436(9)	1.444(12)	1.46(3)
C(10)-C(1)	1.461(9)	1.425(12)	1.43(3)
C(4)-C(11)	-	1.520(12)	1.47(2)
C(11)-C(12)	-	1.570(12)	1.37(3)
C(12)-C(6)	-	1.509(12)	1.45(2)
Peri-region bond angles			
E(1)-C(1)-C(10)	123.5(5)	123.4(6)	123.4(11)
C(1)-C(10)-C(9)	126.6(6)	131.1(8)	130.5(12)
E(2)-C(9)-C(10)	123.8(5)	122.0(6)	122.5(12)
Σ of bay angles	**373.9(9)**	**376.5(13)**	**376.4(20)**
Splay angle[b]	13.9	16.5	16.4
C(4)-C(5)-C(6)	117.3(6)	110.5(7)	109.0(12)
E(2)-E(1)-C(13)	-	171.28(1)	84.47 (1)
E(1)-E(2)-C(19)	-	91.48(1)	176.6(1)
Out-of-plane displacement			
E(1)	0.468(9)	0.176(1)	-0.213(1)
E(2)	-0.327(9)	-0.193(1)	0.245(1)
Central naphthalene ring torsion angles			
C:(6)-(5)-(10)-(1)	173.5(6)	178.40(1)	-177.1(14)
C:(4)-(5)-(10)-(9)	174.6(6)	179.23(1)	-177.0(14)

[a] van der Waals radii used for calculations: r_{vdW}(Se) 1.90 Å.[4]

[b] Splay angle: Σ of the three bay region angles – 360.

N3,[8] **A3**,[10] and **Ay3** all have differing characteristics, unlike their selenium analogues. An increase in the *peri*-distances is observed from 3.287(1) Å in **N3,** to 3.3674(19) Å in **A3**, to 3.393(3) Å in **Ay3**. The *peri*-distances are shorter than the sum of the van der Waals radii of two tellurium atoms by 20% for **N3** and 18% for **A3** and **Ay3**. An increase in splay angle is also observed from 15.0° in **N3**, to 18.4° in **A3**, to 19.8° in **Ay3**. The C4-C5-C6 angle decreases from 118.0(1)° in **N3**, to 113.3(14)° in **A3**, to 108.7(13)° in **Ay3**. These trends are expected due to the addition of ethane (1.545(18) Å) in **A3** and the shorter ethene (1.37(2) Å) in **Ay3** to the naphthalene ring. This causes a steady decrease in the C4-C5-C6 angle which in turn widens the splay angle and increases the space available for the tellurium atoms, lengthening the *peri*-distance. The tellurium atoms in **A3** and **Ay3** have similar out-of-plane distortion, with the atoms sitting 0.310(1) Å above the plane and 0.404(1) Å below the plane in **A3**, and 0.306(1) Å above and 0.387(1) Å below in **Ay3**. **N3** displays significantly greater out-of-plane distortion than its analogues **A3** and **Ay3** with the

tellurium atoms sitting 0.51(1) Å below the plane and 0.57(1) Å above the plane. All three compounds display 'naphthalene' backbone distortion with C-C-C-C torsion angles deviating from the planar 180° by 4.9-5.8° in **N3**, 1.0-3.8° in **A3** and 2.5-4.8° in **Ay3**. **N3** displays greater distortion of the backbone and larger out-of-plane displacement of the tellurium atoms than **A3** and **Ay3** because the acenaphthene and acenaphthylene ring systems are more rigid than the naphthalene. The lack of the linker bridge in naphthalene allows the system to be more 'flexible' in order to relieve the strain caused by forcing the tellurium atoms to occupy a space smaller than the sum of their van der Waals radii.

N3, **A3** and **Ay3** show a steady increase in *peri*-distance and splay angle whereas **A2** and **Ay2** are similar, with **N2** being the 'odd one out'. These differences in trend can be attributed to the C4-C5-C6 bond angle. In **A2** the C4-C5-C6 bond angle is 110.5(7)° which is close to the 109.0(12)° seen in **Ay2**. However, in **A3** the C4-C5-C6 bond angle is 113.3(14)° and in **Ay3** it is 108.7(13)°. The fact that the C4-C5-C6 angle is similar in **A2** and **Ay2** leads them to have similar characteristics in the bay region. In comparison **A3** and **Ay3** will have more diverse characteristics.

Table 7 Selected interatomic distances [Å] and angles [°] for compounds **N3**,[8] **A3**[10] and **Ay3**.

Compound	**N3**	**A3**	**Ay3**
E(1)Ph, E(2)Ph	TePh,TePh	TePh,TePh	TePh,TePh
Peri-region-distances			
E(1)···E(2)	**3.287(1)**	**3.3674(19)**	**3.393(3)**
Σr_{vdW} - X···E[a]	0.83	0.7526	0.727
$\%\Sigma r_{vdW}$[a]	80	82	82
E(1)-C(1)	2.14(1)	2.180(17)	2.123(15)
E(2)-C(9)	2.14(2)	2.155(17)	2.151(14)
"Naphthalene" bond lengths			
C(1)-C(2)	1.34(1)	1.367(19)	1.394(19)
C(2)-C(3)	1.38(1)	1.43(3)	1.40(3)
C(3)-C(4)	1.34(1)	1.36(2)	1.383(19)
C(4)-C(5)	1.46(1)	1.410(17)	1.422(19)
C(5)-C(10)	1.42(1)	1.43(2)	1.40(2)
C(5)-C(6)	1.39(1)	1.443(20)	1.43(2)
C(6)-C(7)	1.35(1)	1.318(19)	1.387(19)
C(7)-C(8)	1.38(1)	1.42(3)	1.40(3)
C(8)-C(9)	1.37(1)	1.38(2)	1.41(2)
C(9)-C(10)	1.41(2)	1.430(18)	1.434(17)
C(10)-C(1)	1.45(1)	1.43(2)	1.425(19)

C(4)-C(11)	-	1.50(2)	1.46(3)
C(11)-C(12)	-	1.545(18)	1.37(2)
C(12)-C(6)	-	1.55(2)	1.48(2)
Peri-region bond angles			
E(1)-C(1)-C(10)	123(1)	123.9(10)	124.5(10)
C(1)-C(10)-C(9)	128(1)	131.7(16)	131.2(13)
E(2)-C(9)-C(10)	124(1)	122.8(12)	124.1(10)
Σ of bay angles	**375.0(2)**	**378.4(24)**	**379.8(19)**
Splay angle[b]	15.0	18.4	19.8
C(4)-C(5)-C(6)	118.0(1)	113.3(14)	108.7(13)
E(2)-E(1)-C(13)	-	174.0(4)	92.99(1)
E(1)-E(2)-C(19)	-	94.1(4)	174.06(1)
Out-of-plane displacement			
E(1)	-0.51(1)	0.310(1)	0.306(1)
E(2)	0.57(1)	-0.404(1)	-0.387(1)
Central naphthalene ring torsion angles			
C:(6)-(5)-(10)-(1)	174.2(1)	176.19(1)	177.5(8)
C:(4)-(5)-(10)-(9)	175.1(1)	179.03(1)	175.2(8)

[a] van der Waals radii used for calculations: r_{vdW}(Te) 2.06 Å.[4]

[b] Splay angle: Σ of the three bay region angles – 360.

N4,[8] **A4**[10] and **Ay4** behave in a similar fashion to **N3**, **A3** and **Ay3** in that they display a trend. Lengthening of the *peri*-distance occurs from 3.063(2) Å in **N4,** to 3.113(4) Å in **A4**, to 3.144(3) Å in **Ay4**. The *peri*-distances are shorter than the sum of van der Waals radii by 17% in **N4**, 16% in **A4** and 15% in **Ay4**. An increase in splay angle is observed from 12.4° in **N4**, to 12.7° in **A4**, to 15.7° in **Ay4**. Correspondingly, the C4-C5-C6 angle decreases from 117.6(8)° in **N4**, to 113.4(9)° in **A4**, to 108.4(6)° in **Ay4**. These trends are expected because the addition of the ethane linker (1.568(17) Å) in **A4** and the shorter ethene linker (1.360(11) Å) in **Ay4** cause a steady decrease in the C4-C5-C6 angle which in turn widens the splay angle and hence increases the *peri*-distance. The *peri* atoms in all three compounds experience out-of-plane displacement with **N4** showing the greatest distortion. In **N4** the selenium atom lies 0.432(11) Å above the plane of the ring and the sulfur atom lies 0.320(11) Å below it. The selenium atoms lie 0.274(1) Å and 0.276(1) Å above the plane in **A4** and **Ay4**, respectively, whilst the sulfur atoms lie 0.416(1) Å and 0.260(1) Å below the plane. C-C-C-C torsion angles deviate from the planar 180° by 4.8-5.5° in **N4**, 4.9-5.4° in **A4** and 1.5-2.6° in **Ay4** indicating varying degrees of 'naphthalene' backbone distortion. Like **N2** and

N3, **N4** shows greater out-of-plane distortion and naphthalene backbone distortion than its acenaphthene and acenaphthylene analogues.

Table 8 Selected interatomic distances [Å] and angles [°] for compounds **N4**,[8] **A4**[10] and **Ay4**.

Compound	**N4**	**A4**	**Ay4**
E(1)Ph, E(2)Ph	SePh,SPh	SePh,SPh	SePh,SPh
Peri-region-distances			
E(1)···E(2)	**3.063(2)**	**3.113(4)**	**3.144(3)**
Σr_{vdW} - X···E[a]	0.64	0.5870	0.556
$\%\Sigma r_{vdW}$[a]	83	84	85
E(1)-C(1)	1.907(9)	1.953(10)	1.932(7)
E(2)-C(9)	1.813(8)	1.798(11)	1.781(8)
"Naphthalene" bond lengths			
C(1)-C(2)	1.367(12)	1.393(15)	1.397(11)
C(2)-C(3)	1.372(14)	1.424(14)	1.443(11)
C(3)-C(4)	1.375(15)	1.350(16)	1.357(10)
C(4)-C(5)	1.426(14)	1.404(15)	1.441(11)
C(5)-C(10)	1.435(12)	1.450(14)	1.402(9)
C(5)-C(6)	1.413(14)	1.423(16)	1.421(9)
C(6)-C(7)	1.363(15)	1.367(16)	1.375(11)
C(7)-C(8)	1.435(14)	1.406(15)	1.401(10)
C(8)-C(9)	1.381(13)	1.361(17)	1.388(9)
C(9)-C(10)	1.423(12)	1.451(15)	1.428(10)
C(10)-C(1)	1.447(12)	1.434(16)	1.433(8)
C(4)-C(11)	-	1.522(15)	1.470(9)
C(11)-C(12)	-	1.568(17)	1.360(11)
C(12)-C(6)	-	1.525(15)	1.458(11)
Peri-region bond angles			
E(1)-C(1)-C(10)	122.3(6)	120.7(7)	122.8(6)
C(1)-C(10)-C(9)	127.8(7)	131.3(9)	129.9(6)
E(2)-C(9)-C(10)	122.3(6)	120.7(8)	123.0(5)
Σ of bay angles	**372.4(11)**	**372.7(16)**	**375.7(10)**
Splay angle[b]	12.4	12.7	15.7
C(4)-C(5)-C(6)	177.6(8)	113.4(9)	108.4(6)
E(2)-E(1)-C(13)	-	167.95(1)	172.72(1)
E(1)-E(2)-C(19)	-	86.58(1)	94.35(1)
Out-of-plane displacement			
E(1)	0.432(11)	0.274(1)	0.276(1)
E(2)	-0.320(11)	-0.416(1)	-0.260(1)
Central naphthalene ring torsion angles			
C:(6)-(5)-(10)-(1)	-175.2(8)	175.14(1)	178.5(6)

C:(4)-(5)-(10)-(9)	-174.5(8)	174.65(1)	177.4(6)

[a] van der Waals radii used for calculations: r_{vdW}(S) 1.80 Å , r_{vdW}(Se) 1.90 Å.[4]

[b] Splay angle: Σ of the three bay region angles – 360.

The bromo-selenium analogues **N8**,[9] **A8**[10] and **Ay8**, display a clear trend in the levels of distortion moving from the naphthalene compound through to the acenaphthylene. An increase in the *peri*-distance is observed from 3.1136(6) Å in **N8,** to 3.1588(16) Å in **A8**, to 3.189(2) Å in **Ay8**. The *peri*-distances are shorter than the sum of the van der Waals radii of bromine and selenium by 17% for **N8**, 16% for **A8** and 15% for **Ay8**. Consequently an increase in splay angle is also observed from 13.0° in **N8**, to 14.6° in **A8**, to 16.5° in **Ay8** and the C4-C5-C6 angle decreases from 118.5(3)° in **N8**, to 111.4(5)° in **A8**, to 109.0(9)° in **Ay8**. These trends are anticipated because the addition of the ethane bridge (1.562(9) Å) in **A8** and the shorter ethene bridge (1.341(16) Å) in **Ay8** cause a steady decrease in the C4-C5-C6 angle, which in turn widens the splay angle and increases the space available for the *peri*-atoms, lengthening the *peri*-distance. The bromine atoms lie 0.40(1) Å and 0.287(1) Å above the plane in **N8** and **A8**, respectively, whilst the selenium atoms lie 0.42(1) Å and 0.359(1) Å below the plane. In **Ay8** the bromine atom lies below the plane (0.217(1) Å) and the selenium atom lies on top (0.190(1) Å). All three compounds display significant 'naphthalene' backbone distortion with the least buckling of the ring system occurring in **Ay8**. C-C-C-C torsion angles diverge from the planar 180° by 4.2-6.2° in **N8**, 2.8-4.7° in **A8** and 0.2-4.9° in **Ay8**. **N8** adopts the most distorted conformation of the three compounds. This is in agreement with the previously discussed compounds.

Table 9 Selected interatomic distances [Å] and angles [°] for compounds **N8**,[9] **A8**[10] and **Ay8**.

Compound	**N8**	**A8**	**Ay8**
X, EPh	Br,SePh	Br,SePh	Br,SePh
Peri-region-distances			
X(1)···E(1)	**3.1136(6)**	**3.1588(16)**	**3.189(2)**
Σr_{vdW} - X···E[a]	0.6364	0.5912	0.561
%Σr_{vdW}[a]	83	84	85
X(1)-C(1)	1.919(3)	1.905(5)	1.881(11)
E(1)-C(9)	1.948(3)	1.943(5)	1.920(10)
"Naphthalene" bond lengths			
C(1)-C(2)	1.363(6)	1.361(8)	1.401(15)
C(2)-C(3)	1.402(5)	1.429(8)	1.401(16)
C(3)-C(4)	1.354(5)	1.362(8)	1.367(15)
C(4)-C(5)	1.436(6)	1.416(8)	1.401(15)
C(5)-C(10)	1.433(5)	1.423(7)	1.416(14)

C(5)-C(6)	1.420(5)	1.405(8)	1.418(14)
C(6)-C(7)	1.373(6)	1.367(8)	1.375(15)
C(7)-C(8)	1.395(5)	1.405(8)	1.415(15)
C(8)-C(9)	1.384(5)	1.377(8)	1.391(14)
C(9)-C(10)	1.434(6)	1.438(8)	1.442(14)
C(10)-C(1)	1.431(5)	1.431(8)	1.428(14)
C(4)-C(11)	-	1.514(8)	1.460(16)
C(11)-C(12)	-	1.562(9)	1.341(16)
C(12)-C(6)	-	1.510(8)	1.474(15)
Peri-region bond angles			
X(1)-C(1)-C(10)	122.1(3)	121.8(4)	124.0(8)
C(1)-C(10)-C(9)	128.3(3)	131.4(5)	131.3(9)
E(1)-C(9)-C(10)	122.6(2)	121.4(4)	121.2(7)
Σ of bay angles	**373.0(6)**	**374.6(9)**	**376.5(14)**
Splay angle[b]	13.0	14.6	16.5
C(4)-C(5)-C(6)	118.5(3)	111.4(5)	109.0(9)
X(1)-E(1)-C(13)	-	172.83(1)	177.07(1)
Out-of-plane displacement			
X(1)	0.40(1)	0.287(1)	-0.217(1)
E(1)	-0.42(1)	-0.359(1)	0.190(1)
Central naphthalene ring torsion angles			
C:(6)-(5)-(10)-(1)	175.8(3)	175.27(1)	-175.1(8)
C:(4)-(5)-(10)-(9)	173.8(3)	177.24(1)	179.8(8)

[a] van der Waals radii used for calculations: r_{vdW}(Se) 1.90 Å, r_{vdW}(Br) 1.85 Å.[4]

[b] Splay angle: Σ of the three bay region angles – 360.

A9[10] and **Ay9** have *peri*-distances which are statistically the same (3.2503(14) Å and 3.259(4) Å, respectively) and which are shorter than the sum of their van der Waals radii by 17%. In comparison **N9**[9] has a *peri*-distance of 3.1909(10) Å which is 18% shorter than the sum of the van der Waals radii. The trend in splay angle varies in these compounds compared to their selenium analogues. Instead of the acenaphthylene, it is the acenaphthene, **A9**, which has the largest splay angle of 16.8°. **N9** has a splay angle of 13.6° and **Ay9** has one of 14.9°. The splay angle widens due to a decrease in the C4-C5-C6 angle. Compression of the C4-C5-C6 angle is still seen in these compounds due to the addition of the ethane (1.538(17) Å) and ethene (1.39(4) Å) linkers at the bottom of the naphthalene ring. The C4-C5-C6 angles range from 118.9(6)° in **N9** to 110.8(9)° in **A9** and 108.9(18)° in **Ay9**. Although the C4-C5-C6 angles show a steady decrease from **N9** to **Ay9**, a corresponding increase in the splay angles is not observed. The reason behind this is not clear. The bromine atoms lie 0.4058(84) Å and 0.307(1) Å above the plane in **N9** and **A9**, respectively,

whilst the tellurium atoms lie 0.529(88) Å and 0.298(1) Å below the plane. In **Ay9** the bromine atom lies below the plane instead of above (0.255(1) Å) in turn forcing the tellurium atom to lie on top (0.388(1) Å). The same behaviour is seen in **Ay8** where the bromine and selenium atoms change their orientation in/out of the plane. 'Naphthalene' backbone distortion is observed in all three compounds with **A9** showing the least and **N9** showing the most. C-C-C-C torsion angles diverge from the planar 180° by 5.2-6.6° in **N9**, 1.8-3.6° in **A9** and 1.8-6.1° in **Ay9**.

Table 10 Selected interatomic distances [Å] and angles [°] for compounds **N9**,[9] **A9**[10] and **Ay9**.

Compound	**N9**	**A9**	**Ay9**
X, EPh	Br,TePh	Br,TePh	Br,TePh
Peri-region-distances			
X(1)···E(1)	**3.1909(10)**	**3.2503(14)**	**3.260(4)**
Σr_{vdW} - X···E[a]	0.7191	0.6597	0.650
$\%\Sigma r_{vdW}$[a]	82	83	83
X(1)-C(1)	1.917(6)	1.919(10)	1.89(3)
E(1)-C(9)	2.153(6)	2.148(10)	2.17(3)
"Naphthalene" bond lengths			
C(1)-C(2)	1.382(12)	1.369(14)	1.41(4)
C(2)-C(3)	1.387(11)	1.389(16)	1.33(5)
C(3)-C(4)	1.352(10)	1.376(16)	1.42(4)
C(4)-C(5)	1.417(12)	1.415(14)	1.35(4)
C(5)-C(10)	1.440(9)	1.434(14)	1.41(4)
C(5)-C(6)	1.422(9)	1.420(15)	1.46(4)
C(6)-C(7)	1.399(13)	1.364(15)	1.40(4)
C(7)-C(8)	1.363(10)	1.409(14	1.37(4)
C(8)-C(9)	1.384(9)	1.396(14)	1.33(4)
C(9)-C(10)	1.433(11)	1.434(13)	1.52(4)
C(10)-C(1)	1.419(9)	1.411(13)	1.38(4)
C(4)-C(11)	-	1.505(15)	1.43(4)
C(11)-C(12)	-	1.538(17)	1.39(4)
C(12)-C(6)	-	1.488(17)	1.36(4)
Peri-region bond angles			
X(1)-C(1)-C(10)	121.7(6)	121.6(7)	122.6(18)
C(1)-C(10)-C(9)	128.6(6)	131.7(9)	134.0(3)
E(1)-C(9)-C(10)	123.3(4)	123.5(7)	118.0(18)
Σ of bay angles	**373.6(10)**	**376.8(15)**	**374.6(26)**
Splay angle[b]	13.6	16.8	14.6
C(4)-C(5)-C(6)	118.9(6)	110.8(9)	109.0(3)
X(1)-E(1)-C(13)	-	169.0(1)	169.4(1)
Out-of-plane displacement			

X(1)	0.4058(84)	0.307(1)	-0.258(1)
E(1)	-0.529(88)	-0.298(1)	0.382(1)
Central naphthalene ring torsion angles			
C:(6)-(5)-(10)-(1)	174.8(6)	178.17(1)	-174.0(2)
C:(4)-(5)-(10)-(9)	173.4(6)	176.39(1)	-178.0(2)

[a] van der Waals radii used for calculations: r_{vdW}(Te) 2.06 Å, r_{vdW}(Br) 1.85 Å.[4]

[b] Splay angle: Σ of the three bay region angles – 360.

A11[10] and **Ay11** have similar *peri*-distances (3.3291(11) Å and 3.3324(9) Å, respectively) which are shorter than the sum of their van der Waals radii by 14%. In comparison **N11**[9] has a *peri*-distance of 3.2524(8) Å which is 16% shorter than the sum of the van der Waals radii. An increase in the splay angles is observed, with values of 14.9°, 17.5° and 19.3° for **N11**, **A11** and **Ay11**, respectively. The increase in splay angle can be related to the addition of the ethane bridge (1.545(11) Å) in acenaphthene and the ethene bridge (1.341(7) Å) in acenaphthylene. The addition of the bridge at the bottom of the naphthalene ring compresses the C4-C5-C6 angle from 118.8(4)° in **N11** to 111.1(6)° in **A11** and 109.5(4)° in **Ay11**. This compression at the bottom of the naphthalene ring is relieved by an increase in the splay angle at the top of the ring. The selenium atoms lie 0.364(1) Å and 0.183(1) Å above the plane in **A11** and **Ay11**, respectively, whilst the iodine atoms lie 0.439(1) Å and 0.245(1) Å below the plane. In **N11** the selenium atom lies below the plane (0.42(1) Å) and iodine atom lies above (0.50(1) Å). Significant buckling of the usually planar 'naphthalene' backbone observed in all three compounds with values deviating from 180° by 5.1-5.4° in **N11**, 2.1-5.7° in **A11** and 0.3-4.4° in **Ay11**. **N11** displays the largest distortion of the backbone and out-of-plane displacement of the *peri*-atoms because the acenaphthene and acenaphthylene ring systems in **A11** and **Ay11** are more rigid than the naphthalene. The natural rigidity of the naphthalene backbone is improved with the addition of the ethane/ethene linker which lessens the system's ability to relieve strain *via* deformation.

Table 11 Selected interatomic distances [Å] and angles [°] for compounds **N11**,[9] **A11**[10] and **Ay11**.

Compound	**N11**	**A11**	**Ay11**
X, EPh	I,SePh	I,SePh	I,SePh
Peri-region-distances			
X(1)···E(1)	**3.2524(8)**	**3.3291(11)**	**3.3324(9)**
Σr_{vdW} - X···E[a]	0.6276	0.5509	0.5476
$\%\Sigma r_{vdW}$[a]	84	86	86
X(1)-C(1)	2.122(4)	2.110(7)	2.101(4)
E(1)-C(9)	1.958(4)	1.930(7)	1.929(5)
"Naphthalene" bond lengths			
C(1)-C(2)	1.373(7)	1.360(10)	1.386(6)
C(2)-C(3)	1.402(7)	1.407(11)	1.392(7)
C(3)-C(4)	1.372(9)	1.368(11)	1.367(6)
C(4)-C(5)	1.418(7)	1.401(9)	1.417(6)
C(5)-C(10)	1.449(6)	1.417(9)	1.404(6)
C(5)-C(6)	1.414(9)	1.428(9)	1.419(6)
C(6)-C(7)	1.372(8)	1.361(10)	1.356(6)
C(7)-C(8)	1.416(7)	1.390(10)	1.411(6)
C(8)-C(9)	1.366(8)	1.391(10)	1.381(6)
C(9)-C(10)	1.452(7)	1.444(9)	1.442(6)
C(10)-C(1)	1.437(8)	1.433(10)	1.432(6)
C(4)-C(11)	-	1.513(10)	1.481(6)
C(11)-C(12)	-	1.545(11)	1.341(7)
C(12)-C(6)	-	1.510(10)	1.463(6)
Peri-region bond angles			
X(1)-C(1)-C(10)	124.2(3)	123.8(5)	125.4(3)
C(1)-C(10)-C(9)	128.3(4)	131.4(6)	132.2(4)
E(1)-C(9)-C(10)	122.4(4)	122.3(5)	121.7(3)
Σ of bay angles	**374.9(7)**	**377.5(11)**	**379.3(6)**
Splay angle[b]	14.9	17.5	19.3
C(4)-C(5)-C(6)	118.8(4)	111.1(6)	109.5(4)
X(1)-E(1)-C(13)	-	177.69(1)	174.72(1)
Out-of-plane displacement			
X(1)	0.50(1)	-0.439(1)	-0.245(1)
E(1)	-0.42(1)	0.364(1)	0.183(1)
Central naphthalene ring torsion angles			
C:(6)-(5)-(10)-(1)	174.9(5)	174.34(1)	-175.6(4)
C:(4)-(5)-(10)-(9)	174.6(5)	177.91(1)	-179.7(4)

[a] van der Waals radii used for calculations: r_{vdW}(Se) 1.90 Å, r_{vdW}(I) 1.98 Å.[4]

[b] Splay angle: Σ of the three bay region angles – 360.

The *peri*-distances in **N12**,[9] **A12**[10] and **Ay12** display different behaviour compared to the previously discussed compounds. Instead of the acenaphthylene, it is the acenaphthene, **A12**, that has the longest *peri*-distance at 3.3721(17) Å [3.3774 (17) Å]. 17% [16%] shorter than the sum of van der Waals. **N12** and **Ay12** have *peri*-distances of 3.3146(6) Å and 3.366(3) Å, respectively, which are 18% and 17% shorter than the sum of the van der Waals radii. There is an increase in splay angle from 16.2° in **N12**, to 18.3° [18.4°] in **A12**, to 19.4° in **Ay12** and a decrease in C4-C5-C6 angle from 118.9(6)° in **N11**, to 110.4(15)° [109.8(14)°] in **A11**, to 109.0(2)° in **Ay11**. These changes are expected due to the addition of the ethane linker (1.48(3) Å [1.53(3)°]) in **A12** and the shorter ethene linker (1.36(4) Å) in **Ay12**, as observed previously. This reduction causes the bay angles at the top of the ring to widen. The iodine atom in **N12** lies 0.4152(86) Å below the plane and the tellurium atom lies 0.5355(86) Å above the plane. **A12** crystallises with two nearly identical molecules in the asymmetric unit; in bulk molecules the iodine atom lies 0.425(1) Å below the plane and the tellurium atom lies 0.334(1) Å above the plane. In **Ay12** the iodine atom lies above the plane (0.357(1) Å) and the tellurium atom lies below (0.417(1) Å). C-C-C-C torsion angles differ from the planar 180° by 4.9-5.5° in **N12**, 2.7-4.4° [1.9-4.2°] in **A12** and 2.6-7.6° in **Ay12**. **N12** adopts the most distorted C-C-C-C torsion angles and out-of-plane displacement of the three compounds. This is in agreement with the previously discussed compounds.

Table 12 Selected interatomic distances [Å] and angles [°] for compounds **N12**,[9] **A12**[10] and **Ay12**.

Compound	**N12**	**A12**	**Ay12**
X, EPh	I,TePh	I,TePh	I,TePh
Peri-region-distances			
X(1)···E(1)	**3.3146(6)**	**3.3721(17) [3.3774(17)]**	**3.366(3)**
Σr_{vdW} - X···E[a]	0.7254	0.6679 [0.6626]	0.674
%Σr_{vdW}[a]	82	83 [84]	83
X(1)-C(1)	2.108(6)	2.058(16) [2.067(16)]	2.072(18)
E(1)-C(9)	2.151(6)	2.176(17) [2.151(18)]	2.127(18)
"Naphthalene" bond lengths			
C(1)-C(2)	1.382(12)	1.37(2) [1.40(2)]	1.40(3)
C(2)-C(3)	1.389(10)	1.37(3) [1.37(3)]	1.43(4)
C(3)-C(4)	1.356(10)	1.39(3) [1.45(2)]	1.36(4)
C(4)-C(5)	1.400(11)	1.41(2) [1.39(2)]	1.44(4)
C(5)-C(10)	1.454(8)	1.43(2) [1.42(2)]	1.42(3)
C(5)-C(6)	1.411(9)	1.42(2) [1.40(2)]	1.37(3)
C(6)-C(7)	1.379(12)	1.40(2) [1.37(2)]	1.39(4)
C(7)-C(8)	1.365(10)	1.44(2) [1.39(2)]	1.39(3)
C(8)-C(9)	1.346(9)	1.34(2) [1.38(2)]	1.40(3)

C(9)-C(10)	1.443(11)	1.44(2) [1.47(2)]	1.41(3)
C(10)-C(1)	1.418(9)	1.44(2) [1.43(2)]	1.43(3)
C(4)-C(11)	-	1.50(3) [1.50(2)]	1.44(4)
C(11)-C(12)	-	1.48(3) [1.53(3)]	1.36(4)
C(12)-C(6)	-	1.45(2) [1.52(2)]	1.47(4)
Peri-region bond angles			
X(1)-C(1)-C(10)	123.4(5)	124.6(12) [123.7(11)]	121.2(12)
C(1)-C(10)-C(9)	129.2(5)	130.5(15) [130.3(14)]	131.7(17)
E(1)-C(9)-C(10)	123.6(4)	123.2(12) [124.4(10)]	126.5(14)
Σ of bay angles	**376.2(9)**	378.3(32) [378.4(28)]	**379.4(25)**
Splay angle[b]	16.2	18.3 [18.4]	19.4
C(4)-C(5)-C(6)	118.9(6)	110.4(15) [109.8(14)]	109.0(2)
X(1)-E(1)-C(13)	175.1(1)	171.31(1) [171.48(1)]	170.03(1)
Out-of-plane displacement			
X(1)	-0.4152(86)	-0.425(1) [0.333(1)]	0.357(1)
E(1)	0.5355(86)	0.334(1) [-0.395(1)]	-0.417(1)
Central naphthalene ring torsion angles			
C:(6)-(5)-(10)-(1)	-174.5(6)	175.29(1) [175.81(1)]	177.4(19)
C:(4)-(5)-(10)-(9)	-175.1(6)	-177.33(1) [178.08(1)]	172.4(19)

[a] van der Waals radii used for calculations: r_{vdW}(Te) 2.06 Å, r_{vdW}(I) 1.98 Å.[4]

[b] Splay angle: Σ of the three bay region angles – 360.

AyBr$_2$ and **ABr$_4$** were first prepared by G. P. Pretenko *et al.*[15] in 1967 and despite their use in the years to follow; no molecular structure data has been published. Single crystal data have been obtained in the course of this work.

ABr$_4$ has a *peri*-distance of 3.462(3) Å which is shorter than the sum of the van der Waals radii of two bromine atoms by only 6%. In comparison, **AyBr$_2$** has a smaller *peri*-distance of 3.3387(6) Å [3.3195(6) Å] which is shorter than the sum of the van der Waals radii by 10% [10%]. The splay angle in **ABr$_4$** is 22.0° whereas in **AyBr$_2$** it is 21.7° [20.7°]. The C4-C5-C6 angle decreases from 118.5(12)° in **ABr$_4$** to 109.5(2)° [109.5(3) Å] in **AyBr$_2$**. These trends are unexpected because the dehydrogenation of the ethane linker (1.59(2) Å) in **ABr$_4$** to form the shorter ethene linker (1.322(5) Å) [1.359(5) Å] in **AyBr$_2$** results in compression of the C4-C5-C6 angle which in turn should widen the splay angle and increases the space available for the *peri*-atoms, lengthening the *peri*-distance. The bromine atoms in **AyBr$_2$** show much less out-of-plane distortion than those in **ABr$_4$**. In **AyBr$_2$** one bromine atom essentially lies on the plane 0.006(1) Å [0.011(1) Å] and the other sits 0.042(1) Å [0.029(1) Å] above. In **ABr$_4$** out of plane distortion is more distinct, with one

bromine atom sitting 0.192(1) Å above the plane and the other sitting 0.196(1) Å below. Both compounds demonstrate minor distortion of the 'naphthalene' backbone with C-C-C-C torsion angles differing from the planar 180° by 0.6-0.7° in **ABr_4** and 1.3-1.9° [0.3-1.5°] in **$AyBr_2$**.

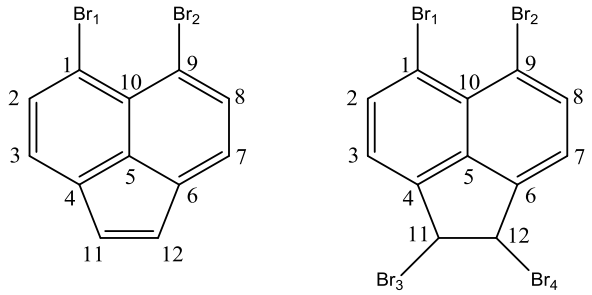

Figure 17 X-ray crystallography numbering scheme for **$AyBr_2$** and **ABr_4**.

Table 13 Selected interatomic distances [Å] and angles [°] for compounds **$AyBr_2$** and **ABr_4** [values in parentheses are for independent molecules].

Compound	**$AyBr_2$**	**ABr_4**
X-ray Code	LouD09-3	LouD42-13
X(1), X(2)	Br, Br	Br, Br
Peri-region-distances		
X(1)···X(2)	**3.3387(6) [3.3195(6)]**	**3.462(3)**
Σr_{vdW} - X(1)···X(2)[a]	0.3613 [0.3805]	0.238
$\%\Sigma r_{vdW}$[a]	90 [90]	94
X(1)-C(1)	1.910(3) [1.907(3)]	1.724(17)
X(2)-C(9)	1.901(3) [1.885(3)]	1.694(14)
'Naphthalene' bond lengths		
C(1)-C(2)	1.384(4) [1.369(4)]	1.35(3)
C(2)-C(3)	1.406(4) [1.413(5)]	1.27(2)
C(3)-C(4)	1.352(5) [1.350(4)]	1.43(2)
C(4)-C(5)	1.414(4) [1.419(4)]	1.37(2)
C(5)-C(10)	1.410(4) [1.417(5)]	1.239(18)
C(5)-C(6)	1.417(4) [1.422(5)]	1.42(2)
C(6)-C(7)	1.353(4) [1.371(5)]	1.40(2)
C(7)-C(8)	1.414(4) [1.413(5)]	1.22(2)
C(8)-C(9)	1.373(4) [1.367(5)]	1.40(3)
C(9)-C(10)	1.423(4) [1.440(4)]	1.46(3)
C(10)-C(1)	1.429(4) [1.430(4)]	1.49(3)
C(4)-C(11)	1.469(4) [1.481(5)]	1.372(19)
C(11)-C(12)	1.322(5) [1.359(5)]	1.59(2)

C(12)-C(6)	1.476(4) [1.473(5)]	1.35(2)
Br(3)-C(11)	-	2.066(15)
Br(4)-C(12)	-	2.078(14)
Peri-region bond angles		
X(1)-C(1)-C(10)	124.0(2) [123.6(2)]	120.2(12)
C(1)-C(10)-C(9)	133.3(3) [133.6(3)]	142.2(13)
X(2)-C(9)-C(10)	124.44(19) [123.5(3)]	119.6(11)
Σ of bay angles	**381.74(19) [380.7(5)]**	**382.0(21)**
Splay angle[b]	21.74 [20.7]	22.0
C(4)-C(5)-C(6)	109.5(2) [109.5(3)]	118.5(12)
Out-of-plane displacement		
X(1)	-0.006(1) [-0.011(1)]	0.192(1)
X(2)	0.042(1) [0.029(1)]	-0.196(1)
Central naphthalene ring torsion angles		
C:(6)-(5)-(10)-(1)	178.7(3) [-178.5(2)]	179.3(12)
C:(4)-(5)-(10)-(9)	-178.1(3) [179.7(2)]	179.4(13)

[a] van der Waals radii used for calculations: r_{vdW}(Br) 1.85 Å.[4]

[b] Splay angle: Σ of the three bay region angles – 360.

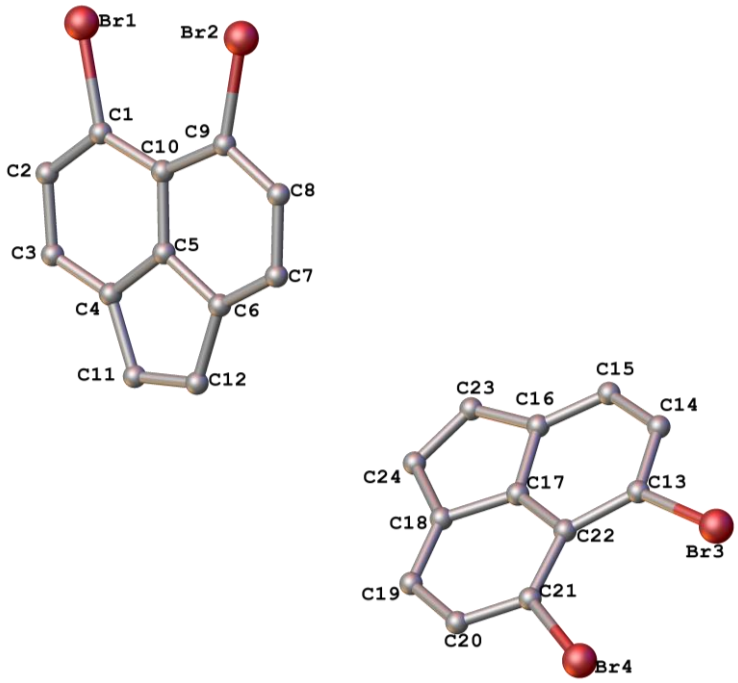

Figure 18 The molecular structure of **AyBr$_2$** with H atoms omitted for clarity.

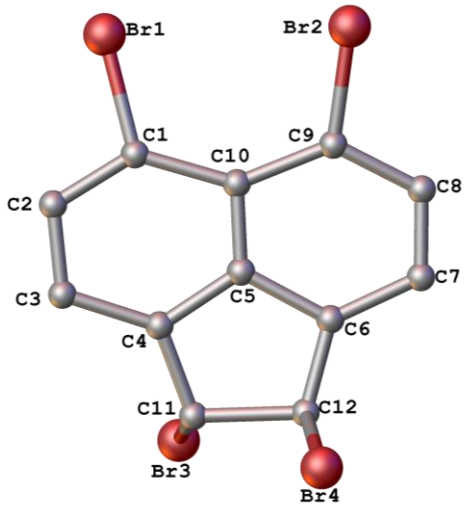

Figure 19 The molecular structure of **ABr_4** with H atoms omitted for clarity.

In the presence of light, solutions of acenaphthylenes are known to undergo photodimerisation *via* 2 + 2 cycloaddition reactions.[16] This was demonstrated when a solution of **$AyBr_2$** in chloroform was left exposed to daylight for one week resulting in crystallisation of the dimer.

The *peri*-distances in the dimer (Br(1)-Br(2) and 3.306(4) Å for Br(3)-Br(4)) are statistically similar to those in the monomer (3.3387(6) Å [3.3195(6)]). The splay angles observed in the dimer are 19.6° and 21.1°, which again are similar to that of 21.7° [20.7°] in the monomer. The C(4)-C(5)-C(6) angle has increased to 111.6(18)° (C(16)-C(17)-C(18) is 111.9(19)°) compared to 109.5(2)° [109.5(3)°], this is expected due to the loss of the ethene double bond.

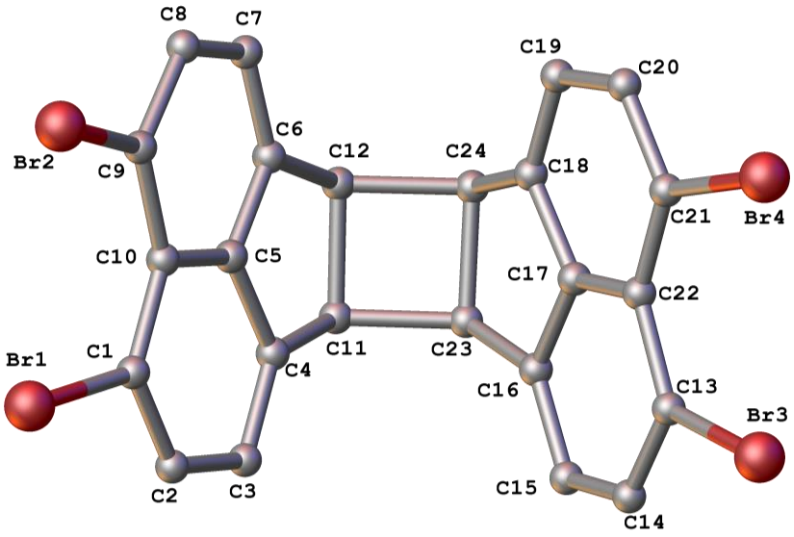

Figure 20 The molecular structure of the **$AyBr_2$** dimer with H atoms omitted for clarity.

Crystal structures could not be obtained for **Ay1**, **Ay5**, **Ay10** and **AyI_2**. A crystal structure was obtained for **Ay7**; however, the data is not of publishable quality. The structure was not as expected, though like **$AyBr_2$**, exposure to light could explain the formation of the dimer.

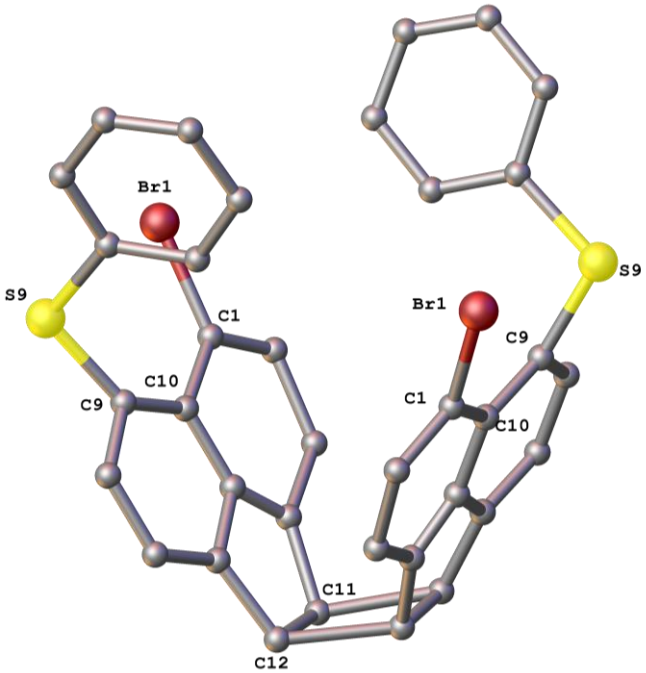

Figure 21 The molecular structure of **Ay7** with H atoms omitted for clarity.

In past studies of the naphthalenes **N1**-**N12** and the acenaphthenes **A1**-**A12** it was observed that the conformation of the aromatic ring systems and the subsequent location and interaction of the chalcogen and halogen lone-pairs determined the geometry of the *peri*-region.[8,9,10] Larger *peri*-distances are observed for A/AA configurations due to there being greater repulsion between the *p*-type lone pairs. If the B/AB configuration is observed there is less repulsion between the *p*-type lone pairs and therefore shorter *peri*-distances.[8,9,10,12,13] In the B/AB configuration the 'naphthalene' ring has an equatorial conformation resulting in torsion angles (θ) close to the ideal '180°' and the axis of the *p*-orbitals aligns parallel and vertical to the 'naphthalene' system.[13] As well as there being less repulsive interactions in the B/AB configuration there is an additional attractive interaction due to the existence of a *quasi*-linear G···E-C_{Ph} (where G = Br, I, S, Se, Te) three-body fragment. Density functional studies confirmed that an attractive three-centre four-electron (3c-4e) type interaction was occurring in type AB conformers due to the delocalisation of a *p*-type lone pair (G) to the antibonding σ*(E-C) orbital.[8,9,10] The 3c-4e type interaction become more dominant throughout the series as heavier congeners were used, with Wiberg bond index (WBI)[17] values increasing, up to a value of 0.14 for **A9**.[8,9,10] Similar, attractive donor-acceptor 3c-4e type interactions were expected to occur in the B/AB configured acenaphthylenes **Ay2**, **Ay3**, **Ay5**, **Ay6** and **Ay8**-**10**. DFT calculations confirmed that the same trends are observed (see Table 14).

Table 14 Relative energies, interatomic distances [Å] and WBIs for selected conformers of compounds **Ay2**, **Ay3**, **Ay4**, **Ay5**, **Ay8-12** and their naphthalene and acenaphthene analogues.[10]

Conformer-Compound	**A-N2**	**B-N2**	**A-A2**	**B-A2**	**A-Ay2**	**B-Ay2**
E_{rel}, kJ/mol	9.9	0.0	6.1	0.0	11.4	0.0
Br···Se, Å	3.369	3.173	3.430	3.223	3.451	3.232
WBI	0.009	0.045	0.008	0.041	0.008	0.041
Confomer-Compound		**B-N3**	**A-A3**	**B-A3**	**A-Ay3**	**B-Ay3**
E_{rel}, kJ/mol		n.a[b]	15.1	0.0	19.0	0.0
Br···Te, Å		3.266	3.563	3.319	3.580	3.327
WBI		0.068	0.011	0.062	0.011	0.061
Conformer-Compound		**C-N5**	**A-A5**	**B-A5**	**A-Ay5**	**B-Ay5**
E_{rel}, kJ/mol		n.a[b]	4.8	0.0	10.1	0.0
I···Se, Å		3.336	3.565	3.384	3.585	3.380
WBI		0.057	0.014	0.050	0.014	0.052

Conformer-Compound		**B-N6**	**A-A6**	**B-A6**	**A-Ay6**	**B-Ay6**
E_{rel}, kJ/mol		n.a[b]	15.1	0.0	19.3	0.0
I···Te, Å		3.425	3.705	3.455	3.722	3.465
WBI		0.087	0.018	0.084	0.017	0.087
Conformer - Compound	**CCt-N8**[a]	**AB-N8**	**AAt-A8**	**AB-A8**	**CCt-Ay8**	**AB-Ay8**
E_{rel}, kJ/mol	0.00	1.5	11.00	0.00	1.2	0.0
Se···Se, Å	3.117	3.152	3.4720	3.2170	3.179	3.237
WBI	0.082	0.081	0.0123	0.0660	0.064	0.062
Conformer-Compound	**AAt-N10**	**BA-N10**	**AAt-A10**	**BA-A10**[c]		**BA-Ay10**
E_{rel}, kJ/mol	15.1	0.0	11.53	0.00		n.a[b]
Se···S, Å	3.333	3.057	3.3946	3.1313		3.147
WBI	0.012	0.068	0.0107	0.056		0.055
Conformer-Compound		**BA-N11**	**AAt-A11**	**BA-A11**		**BA-Ay11**
E_{rel}, kJ/mol		n.a[b]	22.7	0.00		n.a[b]
Te···S, Å		3.120	3.508	3.191		3.206
WBI		0.103	0.015	0.091		0.087
Conformer-Compound		**BA-N12**	**AAt-A12**	**BA-A12**		**BA-Ay12**
E_{rel}, kJ/mol		n.a[b]	23.9	0.0		n.a[b]
Te···Se, Å		3.204	3.586	3.267		3.284
WBI		0.130	0.018	0.116		0.109

[a] From reference[10] [b] Only minimum found. [c] A(Se)···B(S) isomer higher in energy.

Conclusion

A series of *bis*-chalcogen (**Ay1**-**Ay3**), mixed chalcogen-chalcogen (**Ay4**-**Ay5**) and mixed halogen-chalcogen (**Ay7**-**Ay12**) acenaphthylenes have been prepared by dehydrogenation of the parent acenaphthene with DDQ. **$AyBr_2$**, **AyI_2** and **ABr_4** were also prepared. The molecular structures of **Ay2**-**Ay4, Ay8, Ay9, Ay11** and **Ay12** were compared with the naphthalene[8,9] and acenaphthene[10] analogues. Overall the naphthalene structures display the greatest molecular distortion. The acenaphthene and acenaphthylene structures display less molecular distortion due to two main features; the first is the natural *peri*-distance in these systems is longer and the second is the addition of the ethane/ethene bridge which lessens the system's ability to relieve strain *via* buckling. The acenaphthene and acenaphthylene structures varied in behaviour, with some having similar *peri*-distances and others showing a small increase in *peri*-distance when going from the acenaphthene to the acenaphthylene derivative.

Ay8, Ay9, Ay11 and **Ay12** display the same trends as the naphthalene and acenaphthene analogues. All compounds adopt the B type configuration and a steady increase in *peri*-distance is observed as the atoms occupying the *peri*-positions increase. **Ay2**-**Ay4** adopt the AB*t* type configuration and an increase in *peri*-distance is also observed as the *peri*-atoms become larger. In comparison the acenaphthene compounds, **A2**-**A4**, and naphthalene compounds, **N2**-**N4**, do not all adopt the same configuration, with the *bis*-telluride derivative being the 'odd one out' in both cases. **A2** and **A4** adopt the AB*c* configuration whereas **A3** adopts the AB*t* configuration. **N2** and **N4** also adopt the AB*c* configuration; however **N3** adopts a CC*c* configuration.

Overall the series of acenaphthylenes is unremarkable showing similar trends to the acenaphthene derivatives.

Experimental

All experiments were carried out under an oxygen- and moisture-free nitrogen atmosphere using standard Schlenk techniques and glassware. Reagents were obtained from commercial sources and used as received. Dry solvents were collected from a MBraun solvent system. Elemental analyses were performed by Stephen Boyer at the London Metropolitan University. Infra-red spectra were recorded for solids as KBr discs and oils on NaCl plates in the range 4000-300 cm^{-1} on a Perkin-Elmer System 2000 Fourier transform spectrometer. ^{1}H and ^{13}C NMR spectra were recorded on a Bruker Avance 300 MHz spectrometer with δ(H) and δ(C) referenced to external tetramethylsilane. ^{77}Se, ^{125}Te and ^{123}Te NMR spectra were recorded on a Jeol GSX 270 MHz spectrometer with δ(Se) and δ(Te) referenced to external Me_2Se and Me_2Te respectively, with a secondary reference for δ(Te) to diphenyl ditelluride (δ(Te) = 428 ppm). NB. All J_{TeTe} values listed in the experimental are derived from experimentally obtained $^{1}J(^{123}Te,^{125}Te)$ SSCCs. Assignments of ^{13}C and ^{1}H NMR spectra were made with the help of H-H COSY and HSQC experiments. All measurements were performed at 25 °C. All values reported for NMR spectroscopy are in parts per million (ppm). Coupling constants (*J*) are given in Hertz (Hz). Mass spectrometry was performed by the University of St. Andrews Mass Spectrometry Service for **Ay1-Ay12 and ABr_4**. Electrospray Mass Spectrometry (ESMS) was carried out on a Micromass LCT orthogonal accelerator time of flight mass spectrometer. Mass spectrometry for **$AyBr_2$ and AyI_2** was carried out at EPSRC National Mass Spectrometry Service in Swansea. All acenaphthene precursors (**A1-A12**, dibromoacenaphthene and diiodoacenaphthene) were prepared following standard literature procedures.[10]

Compounds **Ay1-Ay12, $AyBr_2$, ABr_4 and AyI_2** were prepared using a modification of the procedure described for the formation of 5,6-dibromoacenaphthylene by Mitchell and co-workers.[11]

For example **[Acenapyl($SPh)_2$] (Ay1)**: DDQ (0.93 g, 4.11 mmol) was added to a stirred solution of 5,6-*bis*(phenylsulfanyl)acenaphthene (1.04 g, 2.81 mmol) in benzene (200 mL) and the mixture was heated under reflux for 24 h. After cooling to room temperature, pentane (200 mL) was added and the mixture was filtered. The filtrate was passed through a short column of silica with a pentane eluent. The resulting solution was then evaporated under reduced pressure to yield the title compound as a dark yellow solid (0.61 g, 58%); mp 169-171 °C; elemental analysis (Found: C, 78.1; H, 4.5. Calc. for $C_{24}H_{16}S_2$: C, 78.2; H, 4.4%); IR (KBr disk) ν_{max} cm^{-1} 3054w, 2951w, 1578s,

1536s, 1475s, 1409s, 1334s, 1207w, 1151w, 1114w, 1066s, 1023s, 833vs, 753vs, 738vs, 690vs, 553w, 488w, 467w; δ_H(300 MHz; $CDCl_3$; 25 °C; Me_4Si) 7.38 (2 H, d, $^3J_{HH}$ 7.3 Hz, Acenapyl 4,7-H), 7.33-7.16 (12 H, m, Acenapyl 3,8-H, SPh 12-16-H), 6.87 (2 H, s, Acenapyl 9,10-H); δ_C(75.5 MHz; $CDCl_3$; 25 °C; Me_4Si) 148.2(q), 136.4(q), 132.6(s), 132.4(s), 131.1(q), 129.8(s), 129.6(q), 129.0(s, *C*H x 2), 127.9(s), 127.0(q), 125.0(s), 120.8(q); MS (ES^+): *m/z* 390.79 (100%, M + Na).

The other acenaphthylenes were similarly prepared and the physical and spectral data are as follows.

[Acenapyl(SePh)$_2$] (Ay2): From DDQ (0.74 g, 3.26 mmol) and [Acenap(SePh)$_2$] (1.01 g, 2.16 mmol) to yield an orange solid which was recrystallised by diffusion of hexane into a saturated solution of the compound in dichloromethane to give orange crystals (0.53 g, 53%); mp 82-84 °C; elemental analysis (Found: C, 62.3; H, 3.55. Calc. for $C_{24}H_{16}Se_2$: C, 62.4; H, 3.5%); IR (KBr disk) ν_{max} cm^{-1} 3053w, 1881w, 1573s, 1475s, 1460s, 1435s, 1408vs, 1360s, 1190w, 1080s, 1065s, 1019s, 997s, 889s, 838vs, 738vs, 690vs, 665s, 644s, 460s, 307w; δ_H(300 MHz; $CDCl_3$; 25 °C; Me_4Si) 7.73-7.69 (2 H, m, SePh 12,16-H), 7.67 (2 H, d, $^3J_{HH}$ 7.7 Hz, Acenapyl 3,8-H), 7.50 (2 H, d, $^3J_{HH}$ 7.7 Hz, Acenapyl 4,7-H) 7.46-7.44 (3 H, m, SePh 13-15-H), 7.05 (2 H, s, Acenapyl 9,10-H); δ_C(75.5 MHz; $CDCl_3$; 25 °C; Me_4Si) 140.3(q), 135.05(s), 134.7(s), 134.3(q), 133.6(q), 131.4(q), 131.2(q), 130.2(s), 129.2(s, *C*H x 2), 128.5(s), 125.3(s); δ_{Se}(51.5 MHz; $CDCl_3$; 25 °C; MeSeSeMe) 428.1(s, $^1J_{SeC}$ 136 Hz, $^1J_{SeC}$ 112 Hz); MS (ES^+): *m/z* 463.78 (100%, M + H).

[Acenapyl(TePh)$_2$] (Ay3): From DDQ (0.30 g, 1.32 mmol) and [Acenap(TePh)$_2$] (0.50 g, 0.89 mmol) to yield a red solid which was recrystallized by evaporation of dichloromethane to give red crystals (0.22 g, 45%); mp 123-125 °C; elemental analysis (Found: C, 51.2; H, 3.0 Calc. for $C_{24}H_{16}Te_2$: C, 51.5; H, 2.9%); IR (KBr disk) ν_{max} cm^{-1} 3047w, 2921w, 2363s, 1571s, 1472s, 1433s, 1405s, 1323w, 1262s, 1059s, 1015s, 997s, 837s, 803s, 730vs, 688vs, 637s, 454s; δ_H(300 MHz; $CDCl_3$; 25 °C; Me_4Si) 7.80 (2 H, d, $^3J_{HH}$ 7.2 Hz, Acenapyl 4,7-H), 7.69-7.62 (2 H, m, TePh 12,16-H), 7.23-7.13 (5 H, m, Acenapyl 3,8-H, TePh 13-15-H) 6.78 (2 H, s, Acenapyl 9,10-H); δ_C(75.5 MHz; $CDCl_3$; 25 °C; Me_4Si) 141.4(s), 138,6(s), 136.4(q), 131.0(q), 130.2(s), 129.2(s, *C*H x 2), 128.6(s), 125.3(s), 121.9(q), 121.6(q), 120.0(q); $\delta_{125_{Te}}$(81.2 MHz; $CDCl_3$; 25 °C; MeTeTeMe) 618.3(s); $\delta_{123_{Te}}$(70.7 MHz; $CDCl_3$; 25 °C; MeTeTeMe) 618.9 (s, $^4J_{TeTe}$ 1706 Hz); MS (ES^+): *m/z* 590.96 (100%, M + OMe), 484.93 (62%, M - Ph).

[Acenapyl(SePh)(SPh)] (Ay4): From DDQ (0.45 g, 1.98 mmol) and [Acenap(SePh)(SPh)] (0.52 g, 1.25 mmol) to yield an oily yellow solid which was recrystallized from evaporation of dichloromethane to give red crystals (0.16 g, 31%); mp 75-77 °C; elemental analysis (Found: C, 69.3; H, 3.9. Calc. for $C_{24}H_{16}SSe$: C, 69.4; H, 3.9%); IR (KBr disc) ν_{max} cm^{-1} 3070s, 2925w, 1884w, 1639w, 1576vs, 1476vs, 1438s, 1413vs, 1362s, 1333w, 1196w, 1109w, 1080vs, 1023vs, 1000w, 898s, 738vs, 691vs, 666s, 649vs; δ_H(300 MHz; $CDCl_3$; 25 °C; Me_4Si) 7.88 (1 H, d, $^3J_{HH}$ 7.2 Hz, Acenapyl 4-H), 7.87-7.82 (2 H, m, SePh 12,16-H), 7.68 (1 H, d, $^3J_{HH}$ 7.2 Hz, Acenapyl 3-H), 7.60-7.48 (3 H, m, SePh 13-15-H), 7.48-7.30 (7 H, m, Acenapyl 7,8-H, SPh 12-16-H), 7.12 (1 H, d, $^3J_{HH}$ 5.3 Hz, C*H*), 7.06 (1 H, d, $^3J_{HH}$ 5.3 Hz, C*H*); δ_C(75.5 MHz; $CDCl_3$; 25 °C; Me_4Si) 142.0(q), 139.0(q), 138.6(q), 137.6(s), 137.3(s), 133.1(q), 131.8(q), 131.3(q), 130.7(s), 130.4(s, *C*H), 130.2(q), 129.8(s), 129.6(s), 129.4(s), 129.0(s), 128.2(s, *C*H), 126.9 (s), 125.7(s), 124.9(s) 124.6(q); δ_{Se}(51.5 MHz; $CDCl_3$; 25 °C; MeSeSeMe) 456.3 (s); MS (ES^+): *m/z* 416.01 (100%, M + H).

[Acenapyl(TePh)(SPh)] (Ay5): From DDQ (0.78 g, 1.67 mmol) and [Acenap(TePh)(SPh)] (0.57 g, 2.53 mmol) to yield an oily yellow solid (0.09 g, 12%); mp 113-115 °C; IR (KBr disc) ν_{max} cm^{-1} 3450w, 3054w, 2925w, 2356w, 1576w, 1475s, 1457s, 1435s, 1416s, 1329w, 1187w, 1080w, 1051s, 1022w, 996s, 824s, 736vs, 685s, 643s, 455s; δ_H(300 MHz; $CDCl_3$; 25 °C; Me_4Si) 8.36-8.32 (2 H, m, TePh 12,16-H), 7.88 (1 H, d, $^3J_{HH}$ 7.1 Hz, Acenapyl 4-H), 7.83 (1 H, d, $^3J_{HH}$ 7.3 Hz, Acenapyl 7-H), 7.61 (1 H, d, $^3J_{HH}$ 7.0 Hz, Acenapyl 3-H) 7.58-7.42 (4 H, m, Acenapyl 8-H, TePh 13-15-H), 7.22-7.14 (5 H, m, SPh 12-16-H), 7.01 (1 H, d, $^3J_{HH}$ 5.3 Hz, C*H*), 6.96 (1 H, d, $^3J_{HH}$ 5.3 Hz, C*H*); δ_C(75.5 MHz; $CDCl_3$; 25 °C; Me_4Si) 140.4(s), 136.6(s), 136.4(q), 136.2(s), 136.1(s), 135.0(q), 132.6(q), 132.5(q), 132.3(s, *C*H), 132.0(s), 130.7 (s, *C*H), 130.6(q), 130.4(s), 129.8(s), 129.6(q), 129.3(s), 127.6(s), 126.2(q), 125.8(s), 125.6(q); $\delta_{125_{Te}}$(81.2 MHz; $CDCl_3$; 25 °C; MeTeTeMe) 951.4(s); MS (ES^+): *m/z* 495.02 (95%, M + OMe).

[Acenapyl(SPh)(Br)] (Ay7): From DDQ (1.05 g, 4.63 mmol) and [Acenap(SPh)(Br)] (1.00 g, 2.93 mmol) to yield a red solid (0.48 g, 48%); mp 80-82 °C; elemental analysis (Found: C, 63.7; H, 3.4. Calc. for $C_{18}H_{11}BrS$: C, 63.7; H, 3.3%); IR (KBr disk) ν_{max} cm^{-1} 3054w, 2921w, 1719w, 1574s, 1475vs, 1438s, 1411vs, 1322s, 1232w, 1199w, 1079s, 1024vs, 891s, 831vs, 735vs, 688vs, 663s, 640s, 474w; δ_H(300 MHz; $CDCl_3$; 25 °C; Me_4Si) 7.69 (1 H, d, $^3J_{HH}$ 7.4 Hz, Acenapyl 4-H), 7.36-7.23 (7 H, m, Acenapyl 3,8-H, SPh 12-16-H) 7.05 (1 H, d, $^3J_{HH}$ 7.4 Hz, Acenapyl 7-H), 6.79 (2 H, s, 2 x C*H*); δ_C(75.5 MHz; $CDCl_3$; 25 °C; Me_4Si) 140.3(q), 139.1(q), 138.6(q), 135.8(q), 134.7(s), 133.8(s), 13.3(q),

131.0(s), 129.3(s, *C*H x 2), 128.7(s), 128.65(s), 127.1(q), 125.3(s), 125.25(s), 120.7(q); MS (ES^+): *m/z* 701.09 (100%, 2M + Na), 260.12 (50, M - Br).

[Acenapyl(SePh)(Br)] (Ay8): From DDQ (0.86 g, 3.81 mmol) and [Acenap(SePh)(Br)] (1.00 g, 2.59 mmol) to yield an orange solid which was recrystallized from evaporation of dichloromethane to give yellow crystals (0.18 g, 18%); mp 100-102 °C; elemental analysis (Found: C, 55.9; H, 2.85. Calc. for $C_{18}H_{11}BrSe$: C, 56.0; H, 2.9%); IR (KBr disk) ν_{max} cm^{-1} 3044w, 1629w, 1597w, 1567s, 1485s, 1469s, 1435w, 1409vs, 1362w, 1079s, 1019s, 883s, 830vs, 745vs, 728s, 691s, 635s, 468w; δ_H(300 MHz; $CDCl_3$, 25 °C; Me_4Si) 7.86 (1 H, d, $^3J_{HH}$ 7.2 Hz, Acenapyl 4-H), 7.84-7.82 (2 H, m, SePh 12,16-H), 7.55-7.51 (3 H, m, SePh 13-15-H), 7.43 (1 H, d, $^3J_{HH}$ 7.3 Hz, Acenapyl 3-H), 7.32 (1 H, d, $^3J_{HH}$ 7.6 Hz, Acenapyl 7-H), 7.23 (1 H, d, $^3J_{HH}$ 7.6 Hz, Acenapyl 8-H), 6.97 (1 H, d, $^3J_{HH}$ 5.3 Hz, C*H*), 6.94 (1H, d, $^3J_{HH}$ 5.3 Hz, C*H*); δ_C(75.5 MHz; $CDCl_3$; 25 °C; Me_4Si) 140.6(q), 138.7(q), 137.6(s), 137.1(q), 133.9(s), 131.6(q), 130.6(s), 130.5(q), 130.4(s), 129.7(s), 129.5(s, *C*H), 128.2(q), 128.1(s, *C*H), 125.6(s), 125.2(s), 121.8(q); δ_{Se}(51.5 MHz; $CDCl_3$; 25 °C; MeSeSeMe) 447.7(s); MS (ES^+): *m/z* 386.95 (50%, M + H).

[Acenapyl(TePh)(Br)] (Ay9): From DDQ (0.57 g, 2.49 mmol) and [Acenap(TePh)(Br)] (0.73 g, 1.66 mmol) to yield an orange solid which was recrystallised by diffusion of hexane into a saturated solution of the compound in dichloromethane to give red crystals (0.17 g, 23%); mp 105-107 °C; elemental analysis (Found: C, 49.6; H, 2.6. Calc. for $C_{18}H_{11}BrTe$: C, 49.7; H, 2.6%); IR (KBr disk) ν_{max} cm^{-1} 3042w, 1872w, 1595w, 1564s, 1487s, 1470w, 1433w, 1406vs, 1364w, 135w, 1079s, 1015s, 998w, 880w, 833vs, 732vs, 692s, 633s, 456w; δ_H(300 MHz; $CDCl_3$; 25 °C; Me_4Si) 7.91-7.86 (2 H, m, TePh 12,16-H), 7.67 (1 H, d, $^3J_{HH}$ 7.3 Hz, Acenapyl 4-H), 7.42-7.36 (1 H, m, TePh 14-H), 7.33-7.25 (3 H, m, Acenapyl 3-H, TePh 13,15-H) 7.23 (1 H, d, $^3J_{HH}$ 7.4 Hz, Acenapyl 7-H), 7.08 (1 H, d, $^3J_{HH}$ 7.4 Hz, Acenapyl 8-H), 6.81 (1 H, d, $^3J_{HH}$ 5.3 Hz, C*H*), 6.74 (1 H, d, $^3J_{HH}$ 5.3 Hz, C*H*); δ_C(75.5 MHz; $CDCl_3$; 25 °C; Me_4Si) 141.9(s), 141.1(q), 139.3(q), 135.0(s), 133.1(s), 131.8(q), 130.6(s), 129.7(s), 129.5(s), 127.8(s, *C*H), 125.6(s, *C*H), 125.0(s), 123.4(q), 121.8(q), 118.8(q), 30.5(q); $\delta_{^{125}Te}$(81.2 MHz; $CDCl_3$; 25 °C; MeTeTeMe) 723.5(s); MS (ES^+): *m/z* 466.87 (100%, M + OMe), 435.90 (40, M + H).

[Acenapyl(SPh)(I)] (Ay10): From DDQ (0.41 g, 1.81 mmol) and [Acenap(SPh)(I)] (0.46 g, 1.19 mmol) to yield a brown oil (0.17 g, 37%); elemental analysis (Found: C, 55.9; H, 2.8. Calc. for $C_{18}H_{11}BrS$: C, 56.0; H, 2.9%); IR (NaCl plate) ν_{max} cm^{-1} 3071s, 2919w, 1881w, 1597s, 1570vs,

1491vs, 1476vs, 1457vs, 1409vs, 1360s, 1325s, 1200s, 1080vs, 1022vs, 889vs, 837vs, 735vs, 641vs, 372vs; δ_H(300 MHz; $CDCl_3$; 25 °C; Me_4Si) 8.38 (1 H, d, $^3J_{HH}$ 7.3 Hz, Acenapyl 4-H), 7.60-7.38 (7 H, m, Acenapyl 7,8-H, SPh 12-16-H) 7.30 (1 H, d, $^3J_{HH}$ 7.3 Hz, Acenapyl 3-H), 7.05 (1 H, d, $^3J_{HH}$ 5.3 Hz, C*H*), 6.99 (1 H, d, $^3J_{HH}$ 5.3 Hz, C*H*); δ_C(75.5 MHz; $CDCl_3$; 25 °C; Me_4Si) 143.9(s), 141.3(q), 140.8(q), 137.1(q), 136.8(q), 134.1(s), 132.2(s), 131.1(q), 130.2(s), 129.7(q), 129.5(s, *C*H), 129.4(s, *C*H), 128.0(s), 126.0(s), 125.42(s), 92.5(q); MS (ES^+): *m/z* 259.03 (100%, M - I).

[Acenapyl(SePh)(I)] (Ay11): From DDQ (0.18 g, 0.78 mmol) and [Acenap(SePh)(I)] (0.22 g, 0.51 mmol) to yield an orange solid which was recrystallised by diffusion of hexane into a saturated solution of the compound in dichloromethane to give yellow crystals (0.08 g, 34%); mp 83-85 °C; elemental analysis (Found: C, 49.8; H, 2.6. Calc. for $C_{18}H_{11}IS$: C, 49.9; H, 2.6%); IR (KBr disc) ν_{max} cm^{-1} 2922w, 2367w, 1865w, 1561s, 1485s, 1468w, 1435w, 1405vs, 1359w, 1077s, 1017vs, 878s, 829vs, 744vs, 692vs, 633s, 467s, 307w; δ_H(300 MHz; $CDCl_3$; 25 °C; Me_4Si) 8.10 (1 H, d, $^3J_{HH}$ 7.3 Hz, Acenapyl 4-H), 7.55-7.52 (2 H, m, SePh 12,16-H), 7.32-7.23 (3 H, m, SePh 13-15-H), 7.17-7.09 (3 H, m, Acenapyl 3,7,8-H), 6.75 (1 H, d, $^3J_{HH}$ 5.3 Hz, C*H*), 6.72 (1 H, d, $^3J_{HH}$ 5.3 Hz, C*H*); δ_C(75.5 MHz; $CDCl_3$; 25 °C; Me_4Si) 142.6(s), 141.3(q), 139.6(q), 136.8(s), 131.9(s), 131.7(q), 131.5(q), 131.2(q), 130.4(s), 129.3 (s, *C*H), 128.8(s), 128.3 (s, *C*H), 125.6(s), 125.4(s), 30.2(q); δ_{Se}(51.5 MHz; $CDCl_3$; 25 °C; MeSeSeMe) 426.6 (s); MS (ES^+): *m/z* 464.89 (100%, M + OMe).

[Acenapyl(TePh)(I)] (Ay12): From DDQ (0.88 g, 3.85 mmol) and [Acenap(TePh)(I)] (1.22 g, 2.52 mmol) to yield an orange solid which was recrystallised by diffusion of hexane into a saturated solution of the compound in dichloromethane to give orange crystals (0.87 g, 71%); mp 134-136 °C; elemental analysis (Found: C, 44.9; H, 2.3. Calc. for $C_{18}H_{11}ITe$: C, 44.9; H, 2.3%); IR (KBr disk) ν_{max} cm^{-1} 3425s, 3044w, 1562s, 1487s, 1467w, 1432s, 1404vs, 1361w, 1324w, 1078s, 1012s, 876w, 833vs, 731vs, 693s, 632s, 456s ; δ_H(300 MHz; $CDCl_3$; 25 °C; Me_4Si) 8.03 (1 H, d, $^3J_{HH}$ 7.3 Hz, Acenapyl 4-H), 7.85-7.83 (2 H, m, TePh 12, 16-H), 7.66 (1 H, d, $^3J_{HH}$ 7.3 Hz, Acenapyl 7-H), 7.41-7.21 (4 H, m, acenapyl 8-H, TePh 13-15H), 7.14 (1 H, d, $^3J_{HH}$ 7.3 Hz, Acenapyl 3-H), 6.74 (1 H, d, $^3J_{HH}$ 5.3 Hz, C*H*), 6.71 (1 H, d, $^3J_{HH}$ 5.3 Hz, C*H*); δ_C(75.5 MHz; $CDCl_3$; 25 °C; Me_4Si) 141.9(s), 141.5(s), 141.1(q), 140.0(q), 139.3(q), 136.0(s), 135.0(s), 133.8(q), 133.1(s), 130.6(s), 129.6(s, *C*H), 127.9(s, *C*H), 125.6(s), 120.7(q), 118.8(q), 97.7(q); $\delta_{125_{Te}}$(81.2 MHz; $CDCl_3$; 25 °C; MeTeTeMe) 686.8(s, $^1J_{TeC}$ 203 Hz); MS (ES^+): *m/z* 512.91 (95%, M + OMe).

[Acenapyl(Br_2)] ($AyBr_2$): From DDQ (10.92 g, 48.12 mmol) and [Acenap(Br_2)] (10.00g, 32.08 mmol) to yield a yellow solid which was recrystallised by diffusion of hexane into a saturated solution of the compound in dichloromethane to give yellow crystals (2.0 g, 20%); mp 80-82 °C; elemental analysis (Found: C, 46.4; H, 2.0. Calc. for $C_{12}H_6Br_2$: C, 46.5; H, 1.95%); IR (KBr disk) ν_{max} cm^{-1} 3421w, 3071w, 3035w, 2924w, 2377w, 2345w, 1876w, 1799w, 1719w, 1664w, 1609w, 1569s, 1492s, 1461s, 1434w, 1409vs, 1362s, 1328w, 1231w, 1205w, 1186w, 1163w, 1102w, 1078vs, 1045s, 1018vs, 940w, 879s, 830vs, 764s, 722s, 629s, 560w, 524w, 492w, 473w, 305w; δ_H(300 MHz; $CDCl_3$; 25 °C; Me_4Si) 7.86 (2 H, d, $^3J_{HH}$ 7.4 Hz, Acenapyl 4,7-H), 7.39 (2 H, d, $^3J_{HH}$ 7.4 Hz, Acenapyl 3,8-H), 6.91 (2 H, s, Acenapyl 9,10-H); δ_C(75.5 MHz; $CDCl_3$; 25 °C; Me_4Si) 140.4(q), 135.5(s), 129.6(q), 129.2(s), 126.5(q), 125.3(s), 121.1(q); MS (ES^+): *m/z* 310.89 (100%, M + H).

Alternative route to **($AyBr_2$)** *via* **(ABr_4):** A solution of **(ABr_4)** (0.32 g, 0.69 mmol), zinc powder (0.22 g, 3.43 mmol) and glacial acetic acid (50 mL) was heated to reflux for 4 h, cooled and filtered. The yellow filtrate was concentrated under reduced pressure then redissolved in ethyl acetate (25 mL). The solution was then washed with saturated aqueous sodium hydrogen carbonate (2 x 50 mL), dried ($MgSO_4$), filtered and concentrated under reduced pressure to give an orange solid. An analytically pure sample was obtained by recrystallization from hexane (0.18 g, 86%).

[Acenapyl(I_2)] (AyI_2): From DDQ (0.94 g, 4.12 mmol) and [Acenap(I_2)] (1.08 g, 2.67 mmol) to yield a yellow solid (0.16 g, 15%); mp 109-111 °C; elemental analysis (Found: C, 35.6; H, 1.6. Calc. for $C_{12}H_6I_2$: C, 35.7; H, 1.5%); IR (KBr disk) ν_{max} cm^{-1} 2923s, 2853w, 2372w, 1654w, 1559s, 1493s, 1459s, 1403vs, 1360s, 1205w, 1184w, 1075, vs, 1012vs, 871w, 828vs, 721s, 626s, 474w; δ_H(300 MHz; $CDCl_3$; 25 °C; Me_4Si) 8.29 (2 H, d, $^3J_{HH}$ 7.4 Hz, Acenapyl 4,7-H), 7.15 (2 H, d, $^3J_{HH}$ 7.4 Hz, Acenapyl 3,8-H), 6.80 (s, C*H* x 2); δ_C(75.5 MHz; $CDCl_3$; 25 °C; Me_4Si) 144.8(s), 144.7(q), 153.7(q), 129.6(q), 129.44(s, *C*H x 2), 125.9(s), 125.5(q); MS (ES^+): *m/z* 404.86 (100%, M + H).

1,2,5,6-tetrabromoacenaphthene (ABr_4): A solution of 5,6-dibromoacenaphthene (1.18 g, 3.77 mmol), *N*-bromosuccinimide (1.48 g, 8.29 mmol), benzoyl peroxide (0.20 g, 0.83 mmol) and chloroform (40 mL) was heated to reflux for 5 h under an atmosphere of nitrogen, cooled, washed with saturated aqueous sodium hydrogen carbonate (3 x 50 mL), dried ($MgSO_4$), filtered and concentrated under reduced pressure to give an orange solid. The crude solid was purified by column chromatography with a hexane eluent and an analytically pure sample was obtained by recrystallization from hexane (1.30 g, 74%); mp 148-150 °C; elemental analysis (Found: C, 31.1; H,

1.3. Calc. for $C_{12}H_6Br_4$: C, 30.9; H, 1.3%); IR (KBr disk) ν_{max} cm^{-1}: 3420w, 3072w, 3002w, 2954w, 2922w, 2852w, 1879w, 1718w, 1669w, 1607w, 1560s, 1482w, 1461w, 1440w, 1413s, 1320s, 1245w, 1231w, 1205vs, 1160w, 1140vs, 1112s, 1050w, 1028vs, 984s, 876s, 838vs, 827vs, 795s, 737w, 714vs, 665vs, 614s, 576w, 527s, 491w, 475w, 349s, 310w; δ_H(300 MHz; $CDCl_3$; 25 °C; Me_4Si) 8.00 (2 H, d, $^3J_{HH}$ 7.5 Hz, Acenap 4,7-H), 7.42 (2 H, d, $^3J_{HH}$ 7.5 Hz, Acenap 3,8-H), 5.86 (2 H, s, Acenap 9,10-H); δ_C(75.5 MHz; $CDCl_3$; 25 °C; Me_4Si) 141.5(q), 137.0(s), 136.7(q), 127.7(q), 124.2(s), 119.3(q), 53.2(s); MS (ES^+): *m/z* 309.76 (100%, M + H).

References

[1] C. A. Coulson, R. Daudel and J. M. Robertson, *Proc. R. Soc. London, Ser. A*, 1951, **207**, 306; D. W. Cruickshank, *Acta Crystallogr.,* 1957, **10**, 504; C. P. Brock and J. D. Dunitz, *Acta Crystallogr., Sect. B: Struct. Crystallogr. Cryst. Chem.,* 1982, **38**, 2218; J. Oddershede and S. Larsen, *J. Phys. Chem. A,* 2004, **108**, 1057.

[2] A. C. Hazell, R. G. Hazell, L. Norskov-Lauritsen, C. E. Briant and D. W. Jones, *Acta Crystallogr., Sect. C: Cryst. Struct. Commun.,* 1986, **42**, 690.

[3] A. D. Rae, R. A. Wood and T. R. Welberry, *J. Chem. Soc., Perkin Trans. 2,* 1985, **3**, 451.

[4] A. Bondi, *J. Phys. Chem.,* 1964, **68**, 441.

[5] V. Balasubramaniyan, *Chem. Rev.,* 1966, **66**, 567.

[6] R. W. Alder, P. S. Bowman, W. R. S. Steele and D. R. Winterman, *Chem. Commun.,* 1968, 723; R. W. Alder, M. R. Bryce, N. C. Goode, N. Miller and J. Owen, *J. Chem. Soc., Perkin Trans. 1,* 1981, 2840; J. D. Hoefelmeyer, M. Schulte, M. Tschinkl and F. P. Gabbai, *Coord. Chem. Rev.,* 2002, **235**, 93; P. Kilian, F. R. Knight and J. D. Woollins, *Chem. Eur. J.,* 2011, **17**, 2302; P. Kilian, F. R. Knight and J. D. Woollins, *Coord. Chem. Rev.,* 2011, **255**, 1387.

[7] P. Wawrzyniak, A. M. Z. Slawin, A. L. Fuller, J. D. Woollins and P. Kilian, *Dalton Trans.,* 2009, **38**, 7883; V. V. Mezheritskii, A. N. Antonov, A. A. Milov and K. A. Lysenko, *Russ. J. Org. Chem.,* 2010, **46(6)**, 844; F. R. Knight, K. S. Athukorala Arachchige, R. A. M. Randall, M. Bühl, A. M. Z. Slawin and J. D. Woollins, *Dalton Trans.,* 2012, **41(11)**, 3154; M-L. Lechner, F. R. Knight, K. S. Athukorala Arachchige, R. A. M. Randall, M. Bühl, A. M. Z. Slawin and J. D. Woollins, *Organometallics*, 2012, **31**, 2922.

[8] F. R. Knight, A. L. Fuller, M. Bühl, A. M. Z. Slawin and J. D. Woollins, *Chem. Eur. J.,* 2010, **16**, 7503.

[9] F. R. Knight, A. L. Fuller, M. Bühl, A. M. Z. Slawin and J. D. Woollins, *Chem. Eur. J.,* 2010, **16**, 7605.

[10] L. A. Aschenbach, F. R. Knight, R. A. M. Randall, D. B. Cordes, A. Baggott, M. Bühl, A. M. Z. Slawin and J. D. Woollins, *Dalton Trans.,* 2012, **41**, 3141.

[11] L. Chiang and J. Meinwald, *Tetrahedron Lett.,* 1980, **21**, 4565; H. Miyamoto, K. Yui, Y. Aso, T. Otsubo and F. Ogura, *Tetrahedron Lett.,* 1986, **27**, 2011; R. H. Mitchell, M. Chaudhary, R. V. Williams, R. Fyles, J. Gibson, M. J. Ashwood-Smith and A. J. Fry, *Can. J. Chem.,* 1992, **70**, 1015.

[12] W. Nakanishi, S. Hayashi and S. Toyota, *Chem. Commun.,* 1996, 371; W. Nakanishi, S. Hayashi, A. Sakaue, G. Ono and Y. Kawada, *J. Am. Chem. Soc.,* 1998, **120**, 3635; W. Nakanishi, S. Hayashi and S. Toyota, *J. Org. Chem.,* 1998, **63**, 8790; S. Hayashi and W. Nakanishi, *J. Org. Chem.,* 1999, **64**, 6688; W. Nakanishi, S. Hayashi and T. Uehara, *J. Phys. Chem.,* 1999, **103**, 9906; W. Nakanishi and S. Hayashi, *Phosphorus, Sulfur, Silicon Relat. Elem.,* 2002, **177**, 1833; S. Hayashi and W. Nakanishi, *J. Org. Chem.,* 2002, **67**, 38; S. Hayashi and W. Nakanishi, *Bull. Chem. Soc. Jpn.,* 2008, **81**, 1605.

[13] P. Nagy, D. Szabó, I. Kapovits, Á. Kucsman, G. Argay and A. Kálmán, *J. Mol. Struct.,* 2002, **606**, 61.

[14] All images of molecular structures were generated using OLEX2: O. V. Dolomanov, L. J. Bourhis, R. J. Gildea, J. A. K. Howard and H. Puschmann, *J. Appl. Cryst*., 2009, **42**, 339.

[15] G. P. Petrenko and E. N. Tel'nyuk, *Zh. Org. Khim.,* 1967, **3**, 180.

[16] R. C. Santos, C. E. S. Bernardes, H. P. Diogo, M. Fátima M. Piedade, J. N. Canongia Lopes and M. E. Minas da Piedade, *J. Phys. Chem. A,* 2006, **110**, 2299.

[17] The extent of covalent bonding is conveniently probed by the Wiberg bond index (WBI), which usually approaches a value of one for a true single bond: K. B. Wiberg, *Tetrahedron*, 1968, **24**, 1083.

Chapter 5

Exploring weak intramolecular Te···Te interactions using through-space spin-spin coupling

Introduction

Spin-spin coupling constants (SSCCs) are becoming an important tool in the analysis of structures, giving us an insight into the environment surrounding coupled nuclei within a molecule. The amount of contact between nuclear magnetic dipoles determines the degree of spin-spin coupling. In through-bond (scalar) coupling the two nuclei are in contact through the *s*-electrons of the bond(s) that connect them. The coupling constant thus depends on the extent of *s*-orbital participation in the bond and the polarisability of these electrons.[1] Through-bond coupling is transmitted through the bonds, therefore as the number of bonds between the two nuclei increases the magnitude of the coupling generally decreases with anything larger than ^{4}J being deemed rare.[2]

In *peri*-substituted naphthalenes and related systems the two *peri*-atoms are forced to occupy space that is within the sum of their van der Waals radii without them being formally bonded. If these *peri*-atoms are NMR active nuclei, their close contact allows for the transmission of coupling *via* the lone-pair orbitals (so called through-space coupling). We can assume through-space coupling is occurring because the *J* values observed in these systems are too large to simply be attributed to ^{4}J coupling. The degree of through-space coupling is dependent on the extent of orbital overlap which is directly related to the *peri*-distance and conformation of the molecule.

Several studies have been carried out by Mallory *et al*.[3] regarding through-space coupling in fluorine-fluorine systems. For a series of 1,8-difluoronaphthalenes they determined that J_{FF} increases as the fluorine-fluorine distance decreases. However, it was noted that the size of J_{FF} was not only dependent on distance, but also on the angular orientation of the lone-pairs and thus the extent of overlap of their orbitals. They also studied an analogous series of 1,8-difluoroacenaphthenes and 1,8-difluoroacenaphthylenes and found that a smooth trend was not observed and they were subsequently omitted from the study. The authors suggested that the anomalous J_{FF} values observed in the acenaphthylene derivatives were due to the difference in aromaticity of the acenaphthylene backbone. They postulated that an interaction between the lone-pair orbitals and the π-system was occurring, subsequently reducing the lone-pair lone-pair orbital overlap; this was later supported by DFT calculations.[3]

In 2013, M. Bühl and co-workers[4] used NMR and DFT methods to study weak Te···Te interactions in *peri*-substituted systems. The rigid 'naphthalene' backbone in these systems forces the *peri*-substituted tellurium atoms to experience sub van der Waals contact without them being formally bonded. This close contact can lead to a 3c-4e type interaction, which strengthens the Te, Te couplings causing remarkably large $J(^{125}Te, ^{125}Te)$ values.

Previously, the group studied the cationic methylated species **A** and **B** (Figure 1). **A** and **B** were found to have WBIs of ~0.18, Te-Te *peri*-distances of ~3.4 Å and surprisingly large $J(^{125}Te, ^{125}Te)$ SSCCs of 1093 Hz (**A**) and 946 Hz (**B**). At the ZORA-SO/BP//B3LYP level, the computed SSCCs for **A** and **B** were 2779 Hz and 1543 Hz, respectively. These values are overestimated; however the author deems them to be in the right order of magnitude for comparison with the experimental values.[4]

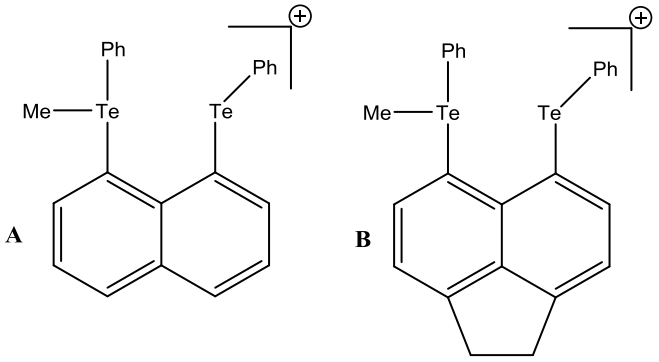

Figure 1 The cationic methylated species, **A** and **B**, studied by M. Bühl and co-workers.[4]

In the 2013 study,[4] the computed and experimental SSCCs for 1,8-*bis*(phenyltelluro)naphthalene (**C**) and 5,6-*bis*(phenyltelluro)acenaphthene (**D**) were compared. The computed values (ZORA-SO/BP//B3LYP level) for **C** and **D** were found to be 2779 Hz and 1543 Hz, respectively. Compounds **C** and **D** contain two magnetically equivalent tellurium atoms due to the molecule being symmetrical. Therefore, $J(^{125}Te, ^{125}Te)$ cannot be directly observed in the ^{125}Te spectrum. Fortunately, the coupling can be detected as satellites in the ^{123}Te spectrum. The $J(^{125}Te, ^{125}Te)$ value can be obtained by multiplying the $J(^{123}Te, ^{125}Te)$ values by 1.206 (NB. 1.206 is calculated by dividing the gyromagnetic ratios for ^{125}Te (-8.51×10^7 rad T^{-1} S^{-1})[1] and ^{123}Te (-7.06×10^7 rad T^{-1} S^{-}

[1]).[1] Using this technique $J(^{125}Te, ^{125}Te)$ values of 2505 Hz and 2110 Hz were calculated for **C** and **D**, respectively.

In order to gain a better understanding of what controls the magnitude of spin-spin coupling in these systems, additional computational studies were performed. The group computed, using 1,8-*bis*(methyltelluro)naphthalene, that there is an energy difference of 1 kcal mol^{-1} between the AB and CC*t* conformations (Figure 2 - top plot), with CC*t* being the global minimum. They also found that the CC*t* conformation would result in *J* values of ~2500 Hz whereas the AB conformation would result in significantly lower *J* values of ~1500 Hz (Figure 2 - bottom plot).[4]

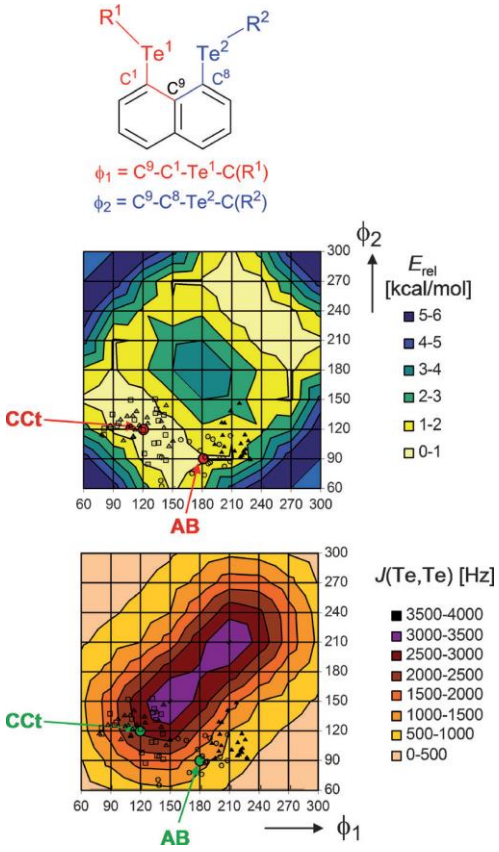

Figure 2 Relative energies (plot 1 - B3LYP level) and $J(^{125}Te, ^{125}Te)$ (plot 2 - ZORA-SO/BP level) as a function of the conformation, as defined by the two dihedral angles shown in the top image ($R^1 = R^2 = Me$).[4]

In the solid, **C** adopts an AB conformation and **D** the CC*t* conformation. However, in solution the compounds appear to fluctuate between conformers, indicating that the variations observed in *J*(^{125}Te, ^{125}Te) SSCCs are caused by a shift in conformer equilibrium. Due to large differences in *J* value being observed for different conformers, both experimentally and computationally, the values have potential as a tool for predicting a structures conformation.[4]

The *J*(^{125}Te, ^{125}Te) value of 3398 Hz for 5,6-*bis*(mesityltelluro)acenaphthene was measured experimentally. However, as no crystal structure was successfully obtained, the structure was predicted to have a CC*t* conformation based on the SSCCs.[4] This compound (**A18**) was prepared during the course of this study and the findings will be discussed later in this chapter.

A recent study has been conducted by the Woollins group into through space spin-spin coupling in a series of eight 5-(TeY)-6-(SePh)acenaphthenes (where Y = FP, Tol, An-*p*, An-*o*, TP, Mes, Tip and Nap).[5] *J*(Te, Se) SSCCs in the range -688 to -748 Hz were observed, indicating strong through-space *peri*-interactions were occurring between the Te and Se atoms. The group determined that changing the Y group had no apparent effect on the conformation of the molecule, the level of molecular distortion or the degree of 3c-4e interaction observed. The bulk of the Y group was calculated and named the steric parameter (θ). A good correlation was observed between θ and the ^{125}Te chemical shift, however no correlation was observed between θ and the ^{77}Se chemical shift or the *J*(Te, Se) SSCCs.[5]

The aim of the work in this chapter was to expand the study carried out by M. Bühl *et al.*[4] into weak Te, Te interactions in *peri*-substituted systems. A series of acenaphthene and acenaphthylene compounds containing ArTe moieties at the 5,6-positions in **A3**,[6] **A13**-**A19** (Acenap[TeAr]$_2$) (Acenap = acenaphthene-5,6-diyl; Ar = Ph, FP, Tol, An-*p*, An-*o*, TP, Mes, Tip) and **Ay3**,[7] **Ay13-Ay19** (Acenap[TeAr]$_2$) (Acenapyl = acenaphthylene-5,6-diyl; Ar = Ph, FP, Tol, An-*p*, An-*o*, TP, Mes, Tip) were prepared, and a spectroscopic and structural study was undertaken. The molecular structures and spectroscopic data were compared to an analogous series of naphthalene compounds; **N3**,[8] **N13**-**N19**[9] (Nap[TeAr]$_2$) (Nap = naphthalene-1,8-diyl; Ar = Ph, FP, Tol, An-*p*, An-*o*, TP, Mes, Tip).

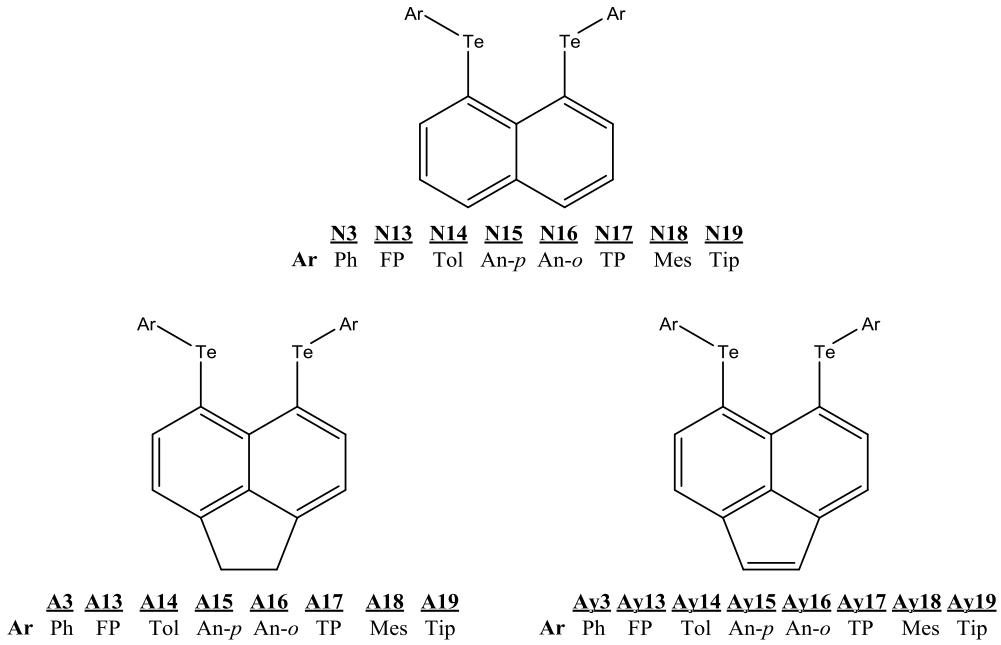

Figure 3 Naphthalenes **N3**,[8] **N13**-**N19**, acenaphthenes **A3**,[6] **A13**-**A19** and acenaphthylenes **Ay3**,[7] **Ay13**-**Ay19**.

Results and Discussion

Compounds (**A13**-**A19** and **Ay13**-**Ay19**) were synthesised and crystal structures were determined for **A13**-**A19** and **Ay13**-**Ay15** and **Ay17**-**Ay19**. **A3** and **Ay3**, were previously reported and the data has been taken from the literature.[6,7]

The diaryl ditellurides, *bis*(4-fluorophenyl) ditelluride (FPTeTeFP), *bis*(4-methylphenyl) ditelluride (TolTeTeTol), *bis*(4-methoxyphenyl) ditelluride (An-*p*TeTeAn-*p*), *bis*(2-methoxyphenyl) ditelluride (An-*o*TeTeAn-*o*), *bis*(4-tertbutylphenyl) ditelluride (TPTeTeTP), *bis*(2,4,6-trimethylphenyl) ditelluride (MesTeTeMes) and *bis*(2,4,6-triisopropylphenyl) ditelluride (TipTeTeTip), were prepared using a modification of the procedure followed by Ando *et al*.[10] Magnesium was added to a solution of the aryl bromide in THF and the mixture was refluxed for 1 h. After cooling to room temperature, tellurium powder was added and the mixture was refluxed for a further 1 h. After cooling to room temperature, the reaction mixture was diluted with toluene and exposed

to an air stream overnight for mild oxidation. Appropriate work up yielded the respective diaryl ditelluride in all cases as a red solid.

The acenaphthenes were prepared following the procedure for **A3** (Scheme 1);[6] 5,6-dibromoacenaphthene was reacted with TMEDA (2.7 eq.) and *n*BuLi (2.4 eq.) to create 5,6-dilithioacenaphthene.2TMEDA complex. This complex was then reacted with the respective diaryl ditelluride (2 eq.) to yield a series of 5,6-*bis*(aryltelluro)acenaphthenes **A3**,[6] **A13**-**A19**.

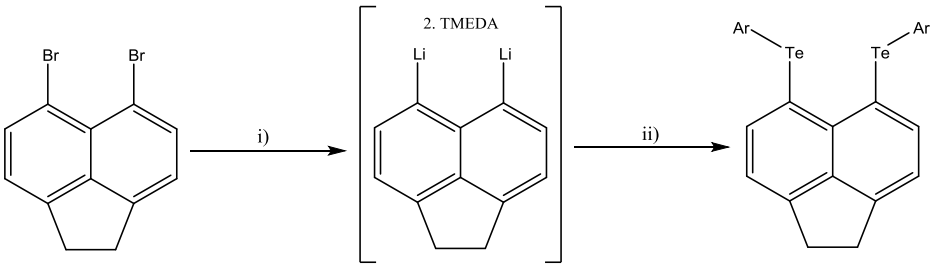

Scheme 1 The preparation of 5,6-*bis*(aryltelluro)acenaphthenes **A3**, **A13**-**A19** *via* 5,6-dilithioacenaphthene-TMEDA complex: i) TMEDA, *n*BuLi, diethyl ether, -10-0 °C, 1 h; ii)ArTeTeAr, diethyl ether, -78 °C, 2 h.[6]

Ay13-**Ay19** were prepared following the known procedure, discussed in Chapter 4, for **Ay3** (Scheme 2).[7] A solution of the desired acenaphthene in benzene and 2,3-dichloro-5,6-dicyano-1,4-benzoquinone (DDQ) (1.5 eq.) was heated to reflux, under a nitrogen atmosphere, for twenty four hours. Once the solution was cooled to room temperature, pentane was added resulting in precipitation of a brown solid. The solution was filtered and the filtrate passed through a short silica column with a pentane eluent. The collected solution was concentrated under reduced pressure to yield the anticipated acenaphthylene.

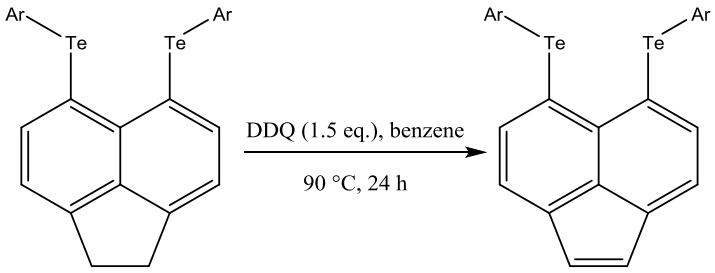

Scheme 2 The preparation of 5,6-*bis*(aryltelluro)acenaphthylenes **Ay3**, **Ay13**-**Ay19**.[7]

X-ray Investigations

Crystals of **A3**,[6] **A13**-**A18** and **Ay13** were obtained by diffusion of hexane into a saturated solution of the compound in dichloromethane. Crystals of **Ay3**,[7] **Ay14**, **Ay15**, **Ay18** and **Ay19** were obtained by evaporation of a saturated solution of the compound in dichloromethane. Crystals were also obtained for **Ay17** and **A18** by evaporation of a saturated solution of the compound in chloroform and hexane, respectively. All compounds crystallise with one molecule in the asymmetric unit. In addition **A16** crystallises with one dichloromethane molecule per unit. The molecular structures of **A3**,[6] **A13**-**A18** and **Ay13** and **Ay3**,[7] **Ay14**, **Ay15**, **Ay18** and **Ay19** are shown in Figures 7 and 8, respectively. Selected bond lengths, angles and torsion angles are recorded in Tables 1 to 4.

The molecular distortion observed in the structures of the acenaphthene compounds **A3**,[6] **A13**-**A19** and their acenaphthylene counterparts **Ay3**,[7] **Ay13**-**Ay19** is comparable, following the same trend as was discussed in Chapter 4. However, much greater distortion is observed in the corresponding set of naphthalene compounds **N3**,[8] **N13**-**N19**. This is best illustrated by comparing the extent to which each set of compounds deviates from the ideal configuration of the respective *peri*-substituted backbone.[11,12,13] The *peri*-distances observed in **N3**,[8] **N13**-**N19** range from 3.26-3.34 Å compared to 2.44 Å[11] in naphthalene. Consequently, the C(1)-C(10)-C(9) angle increases (118° in naphthalene)[11] to an average of 127° and the C(4)-C(5)-C(6) angle decreases (122° in naphthalene)[11] to an average of 119°. There is also a significant reduction in planarity of the naphthalene backbone in **N3**,[8] **N13**-**N19** with the torsion angles deviating from the ideal 0° by an average of 4°.

The introduction of the ethane bridge in the acenaphthene compounds (**A3**,[6] **A13**-**A19**) and the ethene bridge in the acenaphthylene compounds (**Ay3**,[7] **Ay13**-**Ay19**) causes compression of the C(4)-C(5)-C(6) angle (average 111° compared to the ideal 112° for acenaphthenes and average 108° compared to ideal 109° for acenaphthylenes)[12,13] and a subsequent increase in the C(1)-C(10)-C(9) angle (average 131° compared to the ideal 127° for acenaphthenes and average 131° compared to ideal 128° for acenaphthylenes).[12,13] This leads to a minor reduction in planarity of the carbon framework with torsion angles deviating from the ideal 0° by an average of 3°. The natural reduction in planarity within the acenaphthene/acenaphthylene backbones compared

with naphthalene causes the exocyclic *peri*-atom bonds to lie non-parallel within the plane increasing the *peri*-distance in ideal acenaphthene and acenaphthylene to ~2.7 Å (*cf*. naphthalene 2.44 Å).[11,12,13] This increase is reflected in the *peri*-distances of **A3**,[6] **A13**-**A19** and **Ay3**,[7] **Ay13**-**Ay19** which are notably larger than in equivalent naphthalene systems with distances in the range of 3.32-3.37 Å and 3.33-3.39 Å, respectively.

The naphthalene (**N3**,[8] **N13**-**N19**), acenaphthene (**A3**,[6] **A13**-**A19**) and acenaphthylene (**Ay3**,[7] **Ay13**-**Ay19**) compounds all exhibit similar out-of-plane distortion with distances varying from 0.05-0.6 Å in all cases. The increase in the C(1)-C(10)-C(9) angle experienced by the acenaphthene and acenaphthylene compounds naturally causes them to have greater bay region angles than the naphthalene compounds (average splay angle of 19° for **A3**,[6] **A13**-**A19** and **Ay3**,[7] **Ay13**-**Ay19** and 17° for **N3**,[8] **N13**-**N19**). The change observed in splay angle is reflected by the *peri*-distances with lengths of 3.32-3.37 Å and 3.33-3.39 Å observed for **A3**,[6] **A13**-**A19** and **Ay3**,[7] **Ay13**-**Ay19** compared to 3.26-3.34 Å for **N3**,[8] **N13**-**N19**. The *peri*-distances observed are still less than the sum of the van der Waals radii for two tellurium atoms (4.12 Å)[14] by 18-20%. The ethane and ethene bridges introduce rigidity into the carbon backbone thus reducing the system's ability to relieve distortion through deformation of the naphthalene rings with central C-C-C-C torsion angles averaging 3° in the acenaphthene/acenaphthylenes compared to 4° in the naphthalenes.

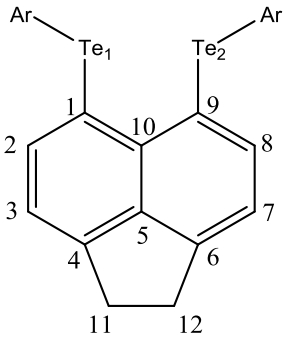

Figure 4 X-ray crystallography numbering scheme for [Acenap(TeAr)$_2$].

Table 1 Selected interatomic distances [Å] and angles [°] for compounds **A3**,[6] **A13-A15**.

Compound	**A3**[6]	**A13**	**A14**	**A15**
X-ray code	Ferg84-1OFF2	FK-479	Ferg195-1	Ferg197-1
R[a]	Ph	FP	Tol	An-*p*
Peri-region-distances				

Te(1)···Te(2)	**3.3674(19)**	**3.3612(11)**	**3.3285(7)**	**3.3204(15)**
Σr_{vdW} - Te···Te[b]	0.7526	0.7588	0.7915	0.916
% Σr_{vdW}[b]	82	82	81	81
Te(1)-C(1)	2.180(17)	2.149(11)	2.152(6)	2.150(11)
Te(2)-C(9)	2.155(17)	2.123(10)	2.140(7)	2.155(11)
Acenaphthene bond lengths				
C(1)-C(2)	1.367(19)	1.393(15)	1.369(10)	1.364(17)
C(2)-C(3)	1.43(3)	1.406(17)	1.405(10)	1.419(18)
C(3)-C(4)	1.36(2)	1.362(15)	1.351(9)	1.346(18)
C(4)-C(5)	1.410(17)	1.427(14)	1.426(9)	1.412(18)
C(5)-C(10)	1.43(2)	1.409(15)	1.424(9)	1.429(15)
C(5)-C(6)	1.443(20)	1.415(14)	1.414(9)	1.400(16)
C(6)-C(7)	1.318(19)	1.387(14)	1.359(10)	1.374(18)
C(7)-C(8)	1.42(3)	1.388(16)	1.393(10)	1.401(17)
C(8)-C(9)	1.38(2)	1.392(14)	1.377(9)	1.372(16)
C(9)-C(10)	1.430(18)	1.429(13)	1.441(9)	1.442(16)
C(10)-C(1)	1.43(2)	1.436(13)	1.439(9)	1.436(15)
C(4)-C(11)	1.50(2)	1.508(15)	1.515(9)	1.526(18)
C(11)-C(12)	1.545(18)	1.545(14)	1.556(10)	1.533(18)
C(12)-C(6)	1.55(2)	1.494(16)	1.518(10)	1.510(17)
Peri-region bond angles				
Te(1)-C(1)-C(10)	123.9(10)	123.8(7)	123.3(5)	123.2(8)
C(1)-C(10)-C(9)	131.7(16)	130.8(9)	131.3(6)	131.8(10)
Te(2)-C(9)-C(10)	122.8(12)	123.9(7)	124.1(5)	123.3(8)
Σ of bay angles	**378.4(24)**	**378.5(13)**	**378.7(9)**	**378.3(15)**
Splay angle[c]	18.4	18.5	18.7	18.3
C(4)-C(5)-C(6)	113.3(14)	110.0(9)	111.2(6)	110.8(10)
Te(2)-Te(1)-C_R	174.0(4)	173.33(1)	158.25(1)	158.30(1)
Te(1)-Te(2)-C_R	94.1(4)	95.30(1)	145.06(1)	149.92(1)
Out-of-plane displacement				
Te(1)	0.310(1)	0.343(1)	-0.070(1)	0.058(1)
Te(2)	-0.404(1)	0.381(1)	0.058(1)	-0.168(1)
Central naphthalene ring torsion angles				
C:(6)-(5)-(10)-(1)	176.19(1)	-176.6(6)	176.6(7)	-179.7(11)
C:(4)-(5)-(10)-(9)	179.03(1)	-176.9(6)	179.8(6)	-178.0(11)

[a] **Ph** = phenyl; **FP** = (4-fluorophenyl); **Tol** = toluene (4-methylphenyl); **An-*p*** = *para*-anisole (4-methoxyphenyl); [b] van der Waals radii used for calculations: r_{vdW}(Te) 2.06 Å;[14] [c] Splay angle: Σ of the three bay region angles – 360.

Table 2 Selected interatomic distances [Å] and angles [°] for compounds **A16-A19**.

Compound	**A16**	**A17**	**A18**	**A19**
X-ray code	FK404A	FK464	Ferg196-1off	FK-391-FS_OFF
R[a]	An-*o*	TP	Mes	Tip
Peri-region-distances				
Te(1)···Te(2)	**3.3456(8)**	**3.3933(13)**	**3.3380(11)**	**3.3638(6)**
Σr_{vdW} - Te···Te[b]	0.7744	0.7267	0.782	0.7562
%Σr_{vdW}[b]	81	82	81	82
Te(1)-C(1)	2.145(4)	2.140(13)	2.141(7)	2.135(5)
Te(2)-C(9)	2.132(5)	2.096(13)	2.136(7)	2.137(6)
Acenaphthene bond lengths				
C(1)-C(2)	1.378(8)	1.403(17)	1.390(10)	1.370(7)
C(2)-C(3)	1.394(7)	1.378(19)	1.401(11)	1.414(8)
C(3)-C(4)	1.360(7)	1.359(17)	1.357(12)	1.344(7)
C(4)-C(5)	1.407(8)	1.423(17)	1.405(11)	1.408(7)
C(5)-C(10)	1.418(7)	1.399(17)	1.429(10)	1.420(7)
C(5)-C(6)	1.416(7)	1.404(17)	1.414(11)	1.397(7)
C(6)-C(7)	1.379(9)	1.400(18)	1.355(11)	1.352(8)
C(7)-C(8)	1.397(7)	1.38(2)	1.416(11)	1.410(9)
C(8)-C(9)	1.381(7)	1.419(18)	1.406(12)	1.385(7)
C(9)-C(10)	1.427(8)	1.433(16)	1.412(11)	1.425(7)
C(10)-C(1)	1.432(7)	1.464(16)	1.429(11)	1.434(6)
C(4)-C(11)	1.510(7)	1.51(2)	1.519(11)	1.522(8)
C(11)-C(12)	1.543(8)	1.562(19)	1.536(12)	1.541(8)
C(12)-C(6)	1.508(7)	1.49(2)	1.511(10)	1.518(9)
Peri-region bond angles				
Te(1)-C(1)-C(10)	123.6(4)	124.7(9)	123.6(5)	123.8(4)
C(1)-C(10)-C(9)	130.9(5)	128.7(11)	129.9(7)	130.6(5)
Te(2)-C(9)-C(10)	123.5(4)	126.8(9)	126.5(6)	123.7(4)
Σ of bay angles	**378.0(8)**	**380.2(17)**	**380.0(10)**	**378.1(8)**
Splay angle[c]	18.0	20.2	20.0	18.1
C(4)-C(5)-C(6)	110.8(4)	110.5(11)	111.5(7)	111.9(5)
Te(2)-Te(1)-C_R	175.03(1)	176.49(1)	155.28(1)	126.58(1)
Te(1)-Te(2)-C_R	99.52(1)	84.47(1)	144.69(1)	173.52(1)
Out-of-plane displacement				
Te(1)	-0.333(1)	0.271(1)	-0.059(1)	-0.494(1)
Te(2)	0.389(1)	-0.263(1)	0.249(1)	0.339(1)
Central naphthalene ring torsion angles				
C:(6)-(5)-(10)-(1)	-177.9(4)	178.0(8)	-177.1(7)	-175.1(5)
C:(4)-(5)-(10)-(9)	-177.2(4)	177.2(8)	179.5(7)	-175.7(5)

[a] **An-*o*** = *ortho*-anisole (2-methoxyphenyl); **TP** = (4-*tert*butylphenyl); **Mes** = mesityl (2,4,6-trimethylphenyl); **Tip** = (2,4,6-triisopropylphenyl); [b] van der Waals radii used for calculations: r_{vdW}(Te) 2.06 Å;[14] [c] Splay angle: Σ of the three bay region angles – 360.

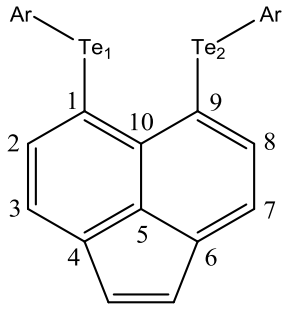

Figure 5 X-ray crystallography numbering scheme for [Acenapyl(TeAr)$_2$].

Table 3 Selected interatomic distances [Å] and angles [°] for compounds **Ay3**,[7] **Ay13-Ay15**, **Ay17-A19**.

Compound	**Ay3**[7]	**Ay13**	**Ay14**	**Ay15**	**Ay17**	**Ay18**	**Ay19**
X-ray code	LMD0-15	LMD122-FS	LMD0-60-1-FS	LMD075	LMD118-fs	LMD0-27	LMD0-85-FS
R[a]	Ph	FP	Tol	An-*p*	TP	Mes	Tip
Peri-region-distances							
Te(1)···Te(2)	**3.393(3)**	**3.3749(6)**	**3.3527(14)**	**3.3337(12)**	**3.437(3)**	**3.3415(11)**	**3.3786(8)**
Σr_{vdW} - Te···Te[b]	0.727	0.7451	0.7673	0.7863	0.683	0.7785	0.7414
% Σr_{vdW}[b]	82	82	81	81	83	81	82
Te(1)-C(1)	2.123(15)	2.149(4)	2.123(11)	2.147(8)	2.14(3)	2.129(9)	2.124(4)
Te(2)-C(9)	2.151(14)	2.128(4)	2.136(12)	2.143(9)	2.15(3)	2.141(10)	2.124(4)
Acenaphthylene bond lengths							
C(1)-C(2)	1.394(19)	1.376(7)	1.365(18)	1.359(12)	1.42(6)	1.383(13)	1.378(6)
C(2)-C(3)	1.40(3)	1.413(6)	1.394(19)	1.404(12)	1.38(5)	1.424(15)	1.423(6)
C(3)-C(4)	1.383(19)	1.368(5)	1.370(18)	1.354(14)	1.43(5)	1.384(13)	1.374(7)
C(4)-C(5)	1.422(19)	1.403(7)	1.399(18)	1.395(12)	1.44(6)	1.420(12)	1.416(6)
C(5)-C(10)	1.40(2)	1.415(6)	1.423(16)	1.416(11)	1.42(4)	1.391(13)	1.403(8)
C(5)-C(6)	1.43(2)	1.419(4)	1.419(16)	1.421(12)	1.44(4)	1.433(12)	1.416(6)
C(6)-C(7)	1.387(19)	1.367(7)	1.38(2)	1.348(12)	1.41(6)	1.370(13)	1.374(7)
C(7)-C(8)	1.40(3)	1.399(6)	1.398(18)	1.407(13)	1.45(5)	1.401(14)	1.423(6)
C(8)-C(9)	1.41(2)	1.383(4)	1.387(16)	1.358(13)	1.43(4)	1.391(12)	1.378(6)
C(9)-C(10)	1.434(17)	1.416(6)	1.453(16)	1.460(12)	1.42(5)	1.433(12)	1.439(5)
C(10)-C(1)	1.425(19)	1.452(4)	1.444(15)	1.457(12)	1.43(4)	1.451(12)	1.439(5)
C(4)-C(11)	1.46(3)	1.471(5)	1.433(17)	1.470(13)	1.39(4)	1.453(14)	1.456(6)
C(11)-C(12)	1.37(2)	1.356(6)	1.331(19)	1.341(13)	1.37(6)	1.346(13)	1.344(7)
C(12)-C(6)	1.48(2)	1.475(7)	1.445(19)	1.450(12)	1.42(5)	1.477(14)	1.456(6)

Peri-region bond angles							
Te(1)-C(1)-C(10)	124.5(10)	123.4(3)	124.7(9)	123.3(6)	124(3)	124.5(6)	123.2(3)
C(1)-C(10)-C(9)	131.2(13)	131.6(4)	130.6(10)	131.5(8)	132(3)	130.5(8)	130.4(5)
Te(2)-C(9)-C(10)	124.1(10)	124.5(2)	123.8(8)	123.0(7)	126(2)	124.2(6)	123.2(3)
Σ of bay angles	**379.8(13)**	**379.5(5)**	**379.1(16)**	**377.8(12)**	**382(5)**	**379.2(12)**	**376.8(7)**
Splay angle[c]	19.8	19.5	19.1	17.8	22.0	19.2	16.8
C(4)-C(5)-C(6)	108.7(13)	109.3(4)	108.6(11)	109.8(8)	106(3)	107.7(8)	108.9(5)
Te(2)-Te(1)-C_R	92.99(1)	173.47(1)	158.80(1)	148.68(1)	79.02(1)	149.02(1)	153.23(1)
Te(1)-Te(2)-C_R	174.06(4)	99.18(1)	147.75(1)	157.02(1)	174.33(1)	158.41(1)	153.23(1)
Out-of-plane displacement							
Te(1)	0.306(1)	0.315(1)	0.139(1)	-0.186(1)	0.086(1)	-0.073(1)	-0.525(1)
Te(2)	-0.387(1)	-0.143(1)	-0.084(1)	0.048(1)	-0.523(1)	-0.310(1)	0.525(1)
Central naphthalene ring torsion angles							
C:(6)-(5)-(10)-(1)	177.5(8)	179.4(4)	-175.0(11)	-178.6(8)	175.5(19)	179.8(8)	174.6(3)
C:(4)-(5)-(10)-(9)	175.2(8)	178.4(4)	178.7(11)	178.4(8)	180(2)	176.8(8)	174.6(3)

[a] **Ph** = phenyl; **FP** = (4-fluorophenyl); **Tol** = toluene (4-methylphenyl); **An-*p*** = *para*-anisole (4-methoxyphenyl); **TP** = (4-*tert*butylphenyl); **Mes** = mesityl (2,4,6-trimethylphenyl); **Tip** = (2,4,6-triisopropylphenyl); [b] van der Waals radii used for calculations: r_{vdW}(Te) 2.06 Å;[14] [c] Splay angle: Σ of the three bay region angles – 360.

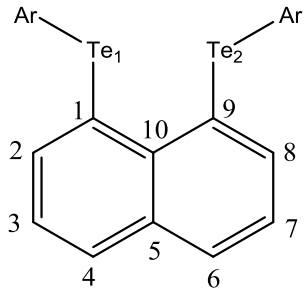

Figure 6 X-ray crystallography numbering scheme for [Nap(TeAr)$_2$].

Table 4 Selected interatomic distances [Å] and angles [°] for compounds **N3**,[8] **N13-N18**

Compound	**N3**[8]	**N13**	**N14**	**N15**	**N16**	**N17**	**N18**
X-ray code	FERG16	FK478	FK-376-FS	FK378-2	FK388	FK-469	FK-374-FS
R[a]	Ph	FP	Tol	An-*p*	An-*o*	TP	Mes
Peri-region-distances							
Te(1)···Te(2)	**3.287(1)**	**3.2703(7)**	**3.2706(8)**	**3.2657(15)**	**3.3172(8)**	**3.3436(6)**	**3.2623(7)**
Σr_{vdW} - Te···Te[b]	0.833	0.8497	0.8494	0.8543	0.7909	0.7764	0.8577
% Σr_{vdW}[b]	80	79	79	79	81	81	79
Te(1)-C(1)	2.14(1)	2.152(5)	2.153(7)	2.155(10)	2.162(9)	2.112(4)	2.148(6)

Te(2)-C(9)	2.14(2)	2.149(5)	2.153(6)	2.161(10)	2.139(9)	2.158(4)	2.138(5)
Naphthene bond lengths							
C(1)-C(2)	1.34(1)	1.369(8)	1.376(8)	1.374(14)	1.365(13)	1.385(5)	1.375(9)
C(2)-C(3)	1.38(1)	1.413(8)	1.397(10)	1.388(15)	1.392(14)	1.388(6)	1.379(9)
C(3)-C(4)	1.34(1)	1.343(8)	1.353(10)	1.372(17)	1.332(15)	1.352(4)	1.359(9)
C(4)-C(5)	1.46(1)	1.425(8)	1.421(9)	1.422(16)	1.450(14)	1.412(5)	1.416(9)
C(5)-C(10)	1.42(1)	1.445(7)	1.415(10)	1.418(13)	1.438(13)	1.438(5)	1.412(7)
C(5)-C(6)	1.39(1)	1.405(8)	1.416(9)	1.407(16)	1.379(16)	1.409(4)	1.425(9)
C(6)-C(7)	1.35(1)	1.361(8)	1.354(9)	1.373(17)	1.348(16)	1.354(5)	1.356(10)
C(7)-C(8)	1.38(1)	1.403(8)	1.399(10)	1.412(14)	1.370(16)	1.401(6)	1.388(8)
C(8)-C(9)	1.37(1)	1.372(7)	1.364(8)	1.406(14)	1.393(15)	1.374(4)	1.381(8)
C(9)-C(10)	1.41(2)	1.437(7)	1.425(8)	1.422(13)	1.419(13)	1.445(4)	1.426(8)
C(10)-C(1)	1.45(1)	1.437(7)	1.420(8)	1.424(14)	1.439(13)	1.440(3)	1.447(8)
Peri-region bond angles							
Te(1)-C(1)-C(10)	123(1)	124.3(4)	124.8(5)	124.7(7)	124.1(6)	126.8(3)	125.2(4)
C(1)-C(10)-C(9)	128(1)	127.5(5)	127.2(6)	126.6(9)	128.8(8)	127.0(3)	126.2(5)
Te(2)-C(9)-C(10)	124(1)	124.2(4)	123.9(4)	123.9(7)	126.0(7)	125.9(2)	125.2(4)
Σ of bay angles	**375.0(2)**	**376.0(8)**	**375.9(9)**	**375.5(13)**	**378.9(12)**	**379.7(5)**	**376.6(8)**
Splay angle[c]	15.0	16.0	15.9	15.5	18.9	19.7	16.6
C(4)-C(5)-C(6)	118.0(1)	119.8(5)	117.3(7)	117.7(10)	120.4(9)	119.4(4)	117.2(5)
Te(2)-Te(1)-C_R	145.70(1)	161.39(1)	166.43(1)	147.19(1)	171.98(1)	83.92(1)	153.80(1)
Te(1)-Te(2)-C_R	154.19(1)	161.55(1)	167.58(1)	153.56(1)	100.37(1)	175.17(1)	157.83(1)
Out-of-plane displacement							
Te(1)	-0.51(1)	+0.431(1)	-0.442(1)	-0.535(1)	+0.191(1)	-0.054(1)	+0.389(1)
Te(2)	+0.57(1)	-0.351(1)	+0.467(1)	+0.507(1)	-0.319(1)	+0.408(1)	-0.384(1)
Central naphthalene ring torsion angles							
C:(6)-(5)-(10)-(1)	174.2(1)	177.0(5)	-176.2(5)	-175.5(10)	177.6(8)	-176.2(3)	175.9(5)
C:(4)-(5)-(10)-(9)	175.1(1)	176.7(5)	-176.9(5)	-172.3(9)	177.9(7)	-178.4(3)	174.4(5)

[a] **Ph** = phenyl; **FP** = (4-fluorophenyl); **Tol** = toluene (4-methylphenyl); **An-*p*** = *para*-anisole (4-methoxyphenyl); **An-*o*** = *ortho*-anisole (2-methoxyphenyl); **TP** = (4-*tert*butylphenyl); **Mes** = mesityl (2,4,6-trimethylphenyl); [b] van der Waals radii used for calculations: r_{vdW}(Te) 2.06 Å;[14] [c] Splay angle: Σ of the three bay region angles – 360.

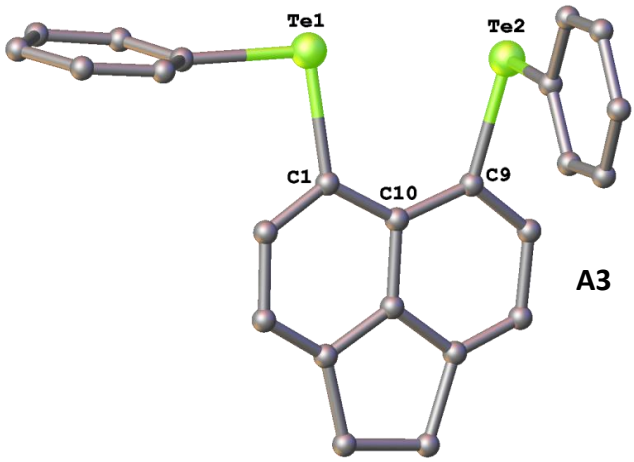

A3

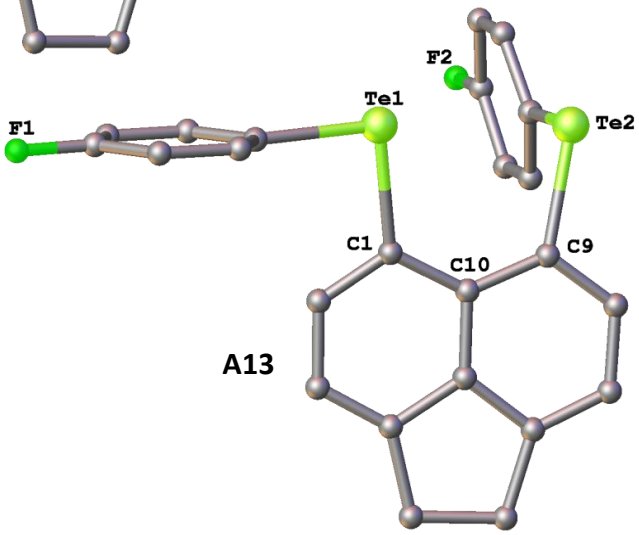

A13

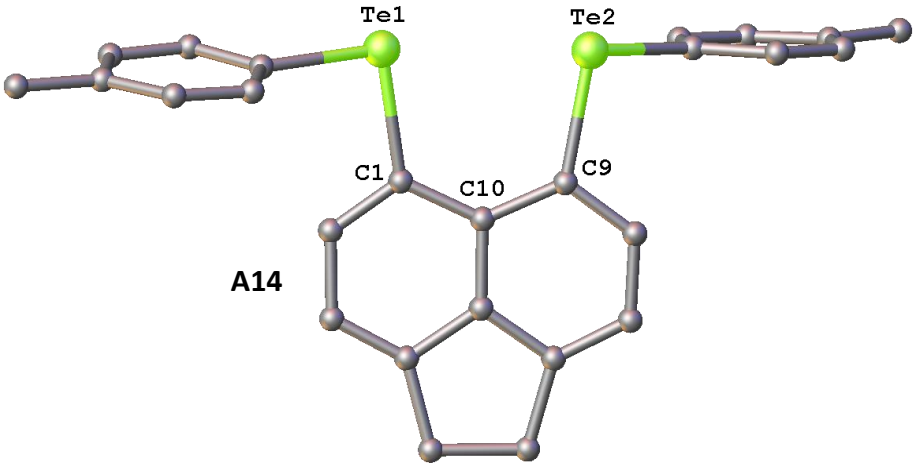

A14

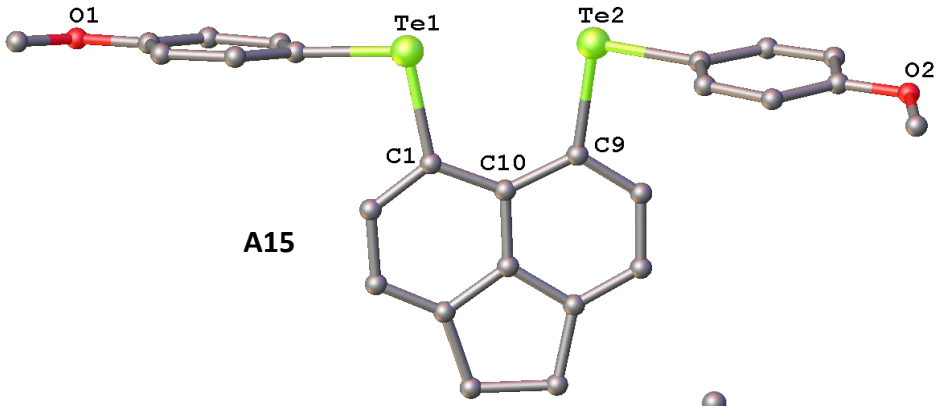

A15

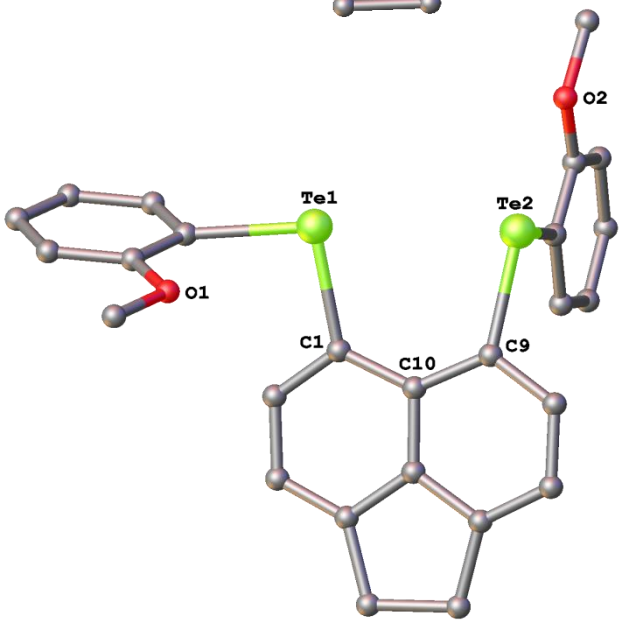

A16

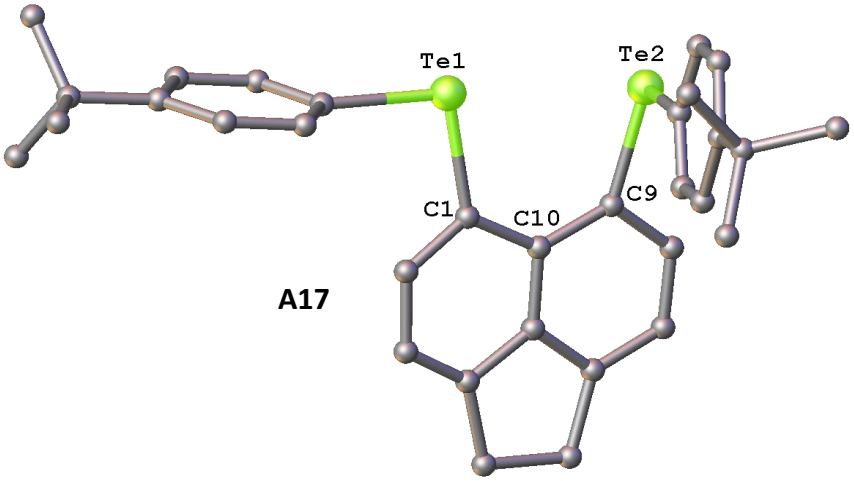

A17

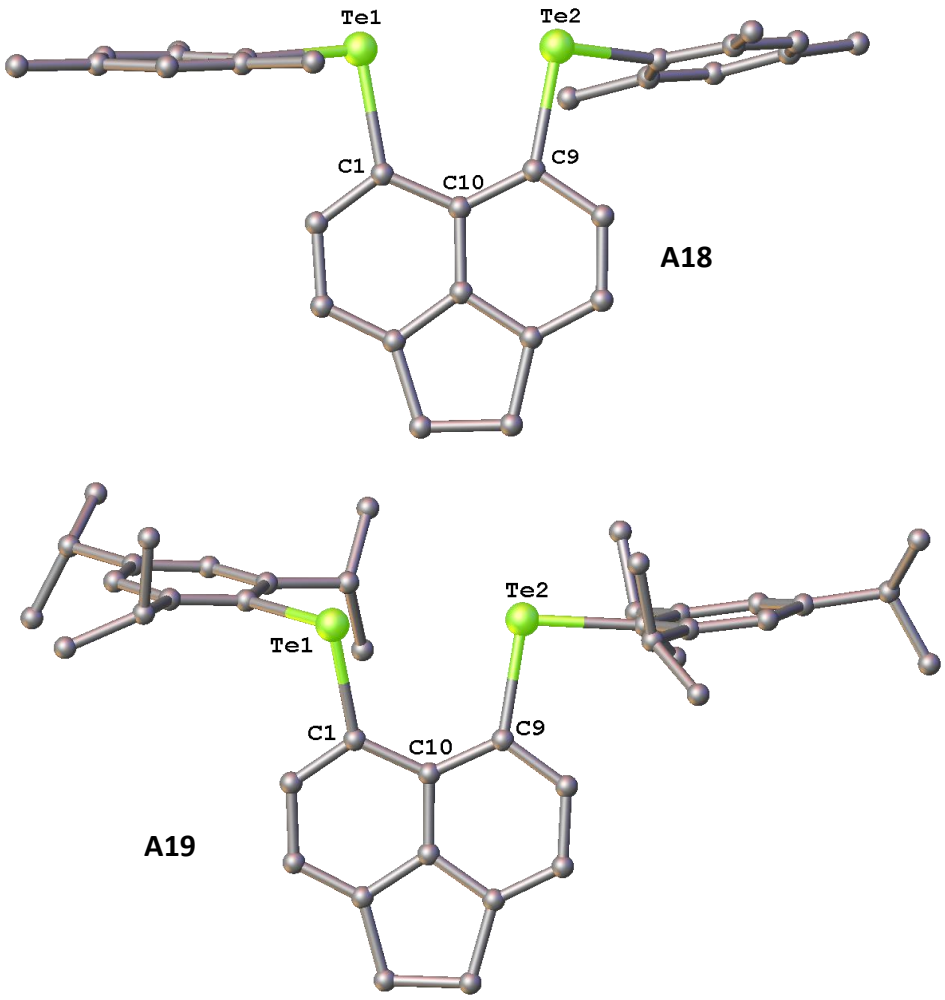

Figure 7 The molecular structures of **A3**,[6] **A13-A19** with H atoms and solvent molecules omitted for clarity.[15]

As previously discussed, the molecular structures of the acenaphthylene compounds **Ay3**,[7] **Ay13-Ay15** and **Ay17-Ay19** were found to have similar levels of distortion as their acenaphthene counterparts. This has been shown in Figure 8 by overlaying the molecular structures of the acenaphthene and acenaphthylene compounds. On the other hand, fluorophenyl derivatives **A13** and **Ay13** differ in the orientation of one phenyl ring whilst the triisopropyl compounds **A19** and **Ay19** display significant differences in the orientation of the aryl groups. Figure 8 also allows the difference in length of the C11-C12 ethane/ethene linkers to be clearly observed.

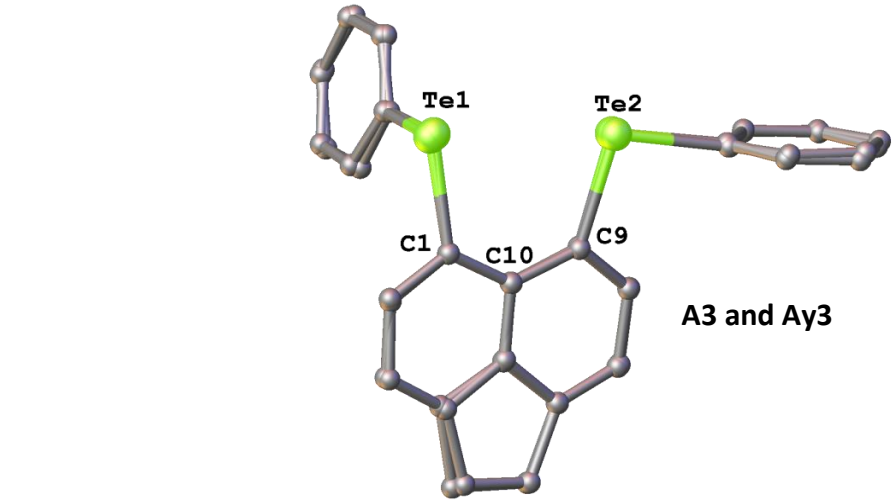

A3 and Ay3

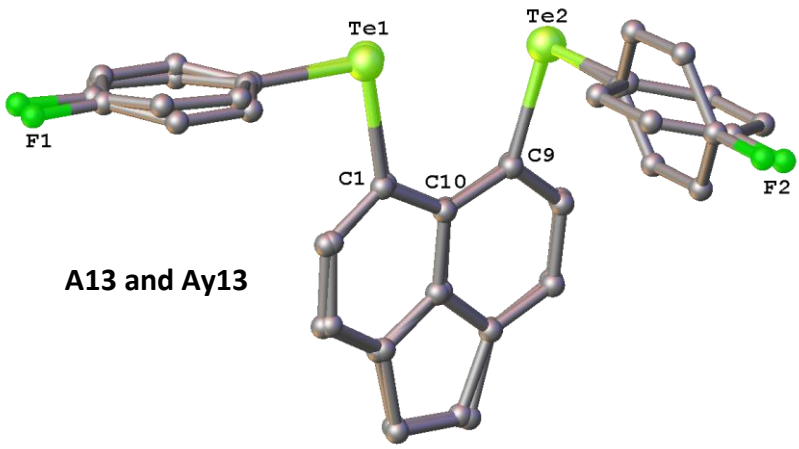

A13 and Ay13

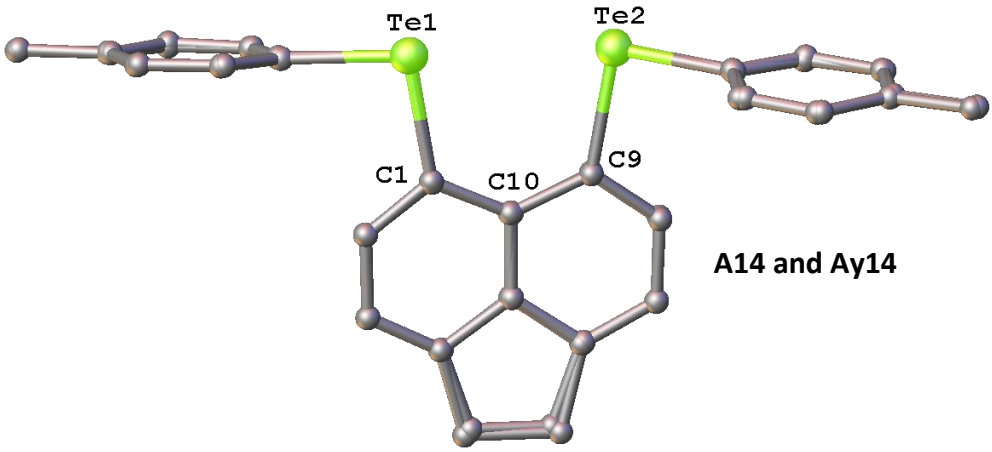

A14 and Ay14

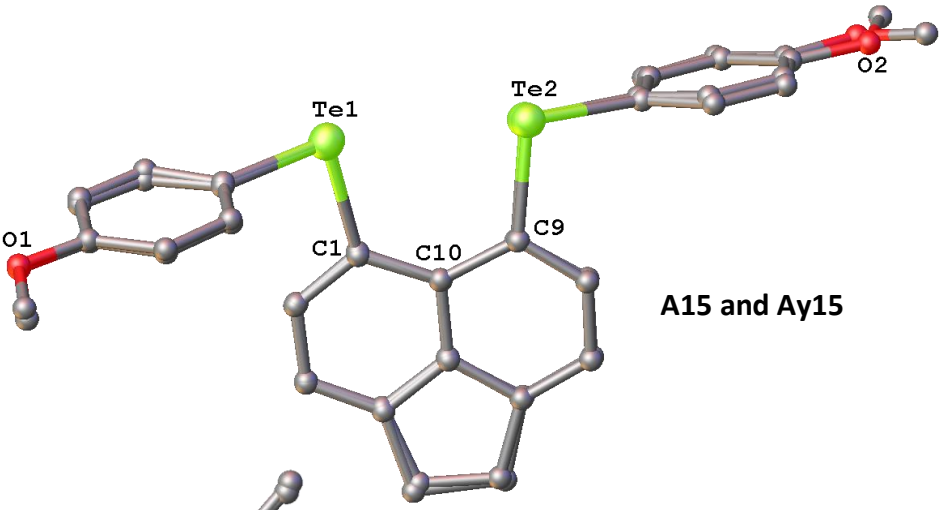

A15 and Ay15

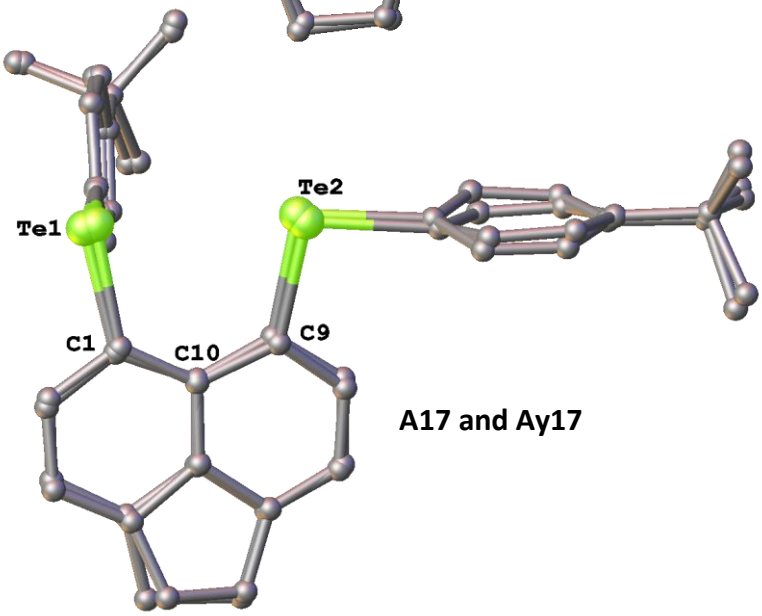

A17 and Ay17

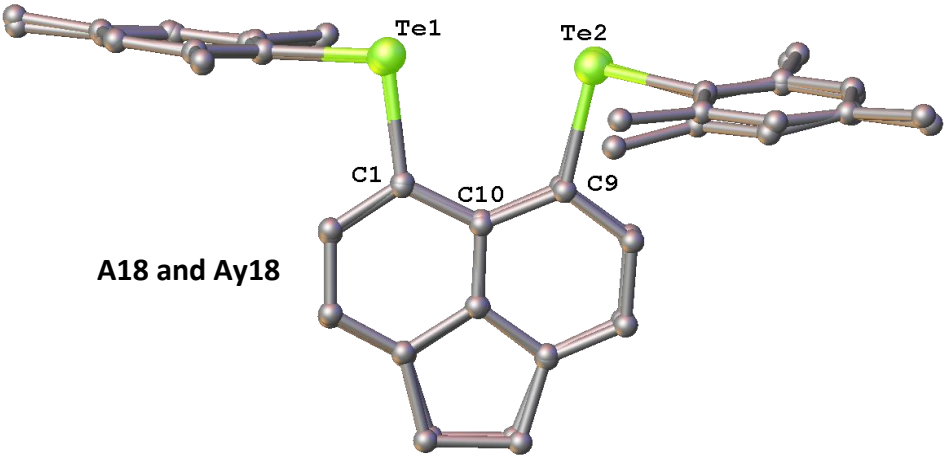

A18 and Ay18

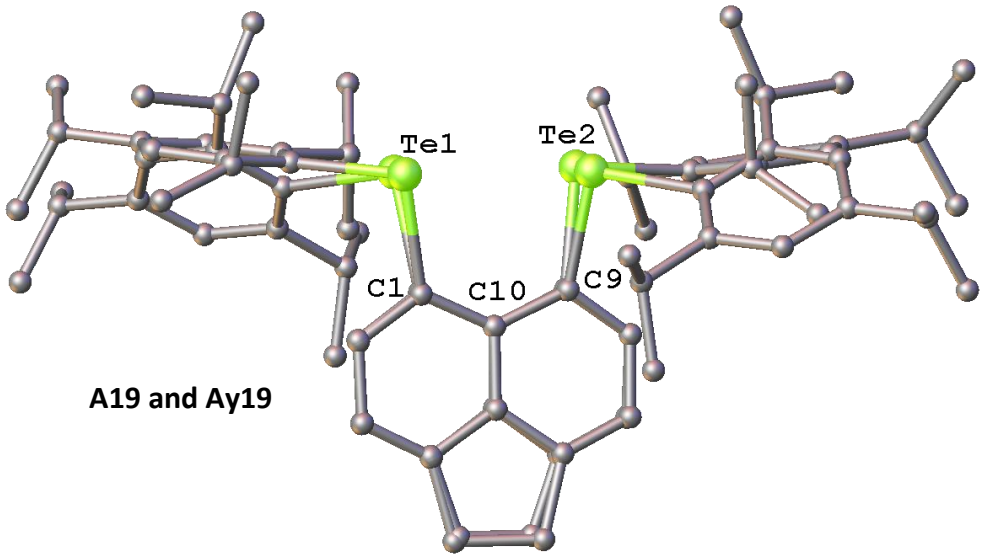

Figure 8 The molecular structures of **A3**,[6] **A13-A15**, **A17**-**A19** overlaid with those of **Ay3**,[7] **Ay13-A15**, **Ay17-A19** with H atoms and solvent molecules omitted for clarity.

Under certain circumstances weak intermolecular interactions are present between neighbouring molecules, which exist in order to stabilise these *bis*-tellurium systems. It was found previously, that **Ay3**[7] behaves like its acenaphthene and naphthalene analogues, **A3**[6] and **N3**,[8] by forming short intermolecular contacts between the Te atoms of neighbouring molecules to create Te_4 parallelograms.

The majority of compounds in this study were found to have similar weak intermolecular Te···Te interactions linking neighbouring molecules, however two different types of bimolecular conformation were observed (Table 5). The first conformation, previously observed in **Ay3**,[7] forms a Te_4 parallelogram with internal angles totalling 360° and two unequal Te···Te non-bonded distances. For e.g. in **A13** the intramolecular *peri*-distance of 3.3612(11) Å is shorter than the intermolecular Te···Te distance of 3.927(1) Å, however both distances are still shorter than the sum of the van der Waals radii for two tellurium atoms (4.12 Å)[14] (Figure 9).

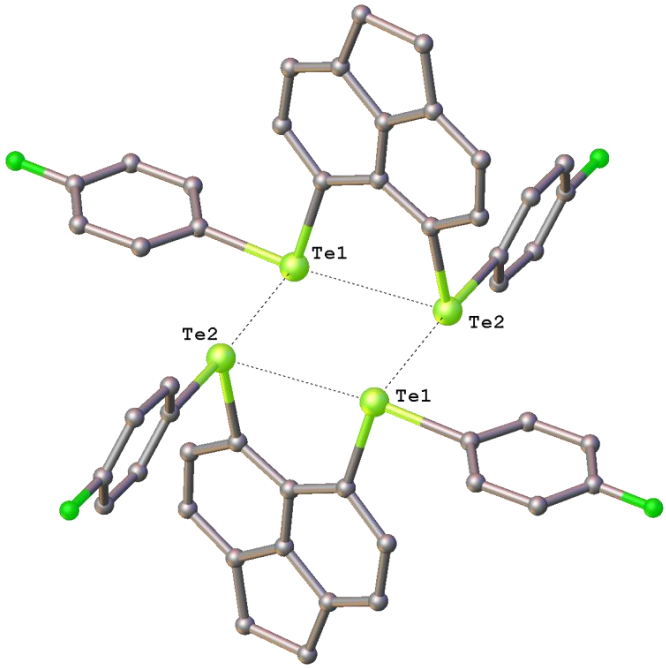

Figure 9 The Te_4 parallelogram conformation shown for **A13** with all H atoms omitted for clarity.

The second motif is best described as a zig-zag, where there is only one intermolecular Te···Te interaction and a Te···Te···Te···Te torsion angle close to 180°. For e.g. in **A18** there is an intermolecular Te···Te distance of 3.879(1) Å and a Te···Te···Te···Te torsion angle of 180° (Figure 10).

Table 5 Bimolecular conformation and corresponding intramolecular and intermolecular distances [Å] for **N3**,[8] **N13**-**N18**, **A3**,[6] **A13**-**A19**, **Ay3**,[7] **Ay13**-**Ay15** and **Ay17**-**Ay19**.

Naphthalene Compound	Intramolecular distance	Intermolecular distances	Bimolecular Conformation
N3[8]	3.287(1)	3.792(1)	parallelogram
N13	3.2703(7)	3.856(1)	zig-zag
N14	3.2706(8)	3.731(1)	zig-zag
N15	3.2657(1)	n/a	n/a
N16	3.3172(8)	n/a	n/a
N17	3.3436(6)	3.855(1)	zig-zag
N18	3.2623(7)	3.718(1)	zig-zag
Acenaphthene Compound	**Intramolecular distance**	**Intermolecular distance**	**Bimolecular conformation**
A3[6]	3.3674(19)	3.853(1)	parallelogram

A13	3.3612(11)	3.927(1)	parallelogram
A14	3.3285(7)	3.934(1)	zig-zag
A15	3.3204(15)	n/a	n/a
A16	3.3456(8)	4.088	zig-zag
A17	3.3933(13)	n/a	n/a
A18	3.3380(11)	3.879(1)	zig-zag
A19	3.3638(6)	n/a	n/a
Acenaphthylene Compound	**Intramolecular distance**	**Intermolecular distance**	**Bimolecular conformation**
Ay3[7]	3.393(3)	3.843(1)	parallelogram
Ay13	3.3749(6)	3.861(1)	zig-zag
Ay14	3.3527(14)	3.972(1)	zig-zag
Ay15	3.3337(12)	4.119(1)	zig-zag
Ay17	3.437(3)	3.886(1)	parallelogram
Ay18	3.3415(11)	3.649(1)	zig-zag
Ay19	3.3786(8)	n/a	n/a

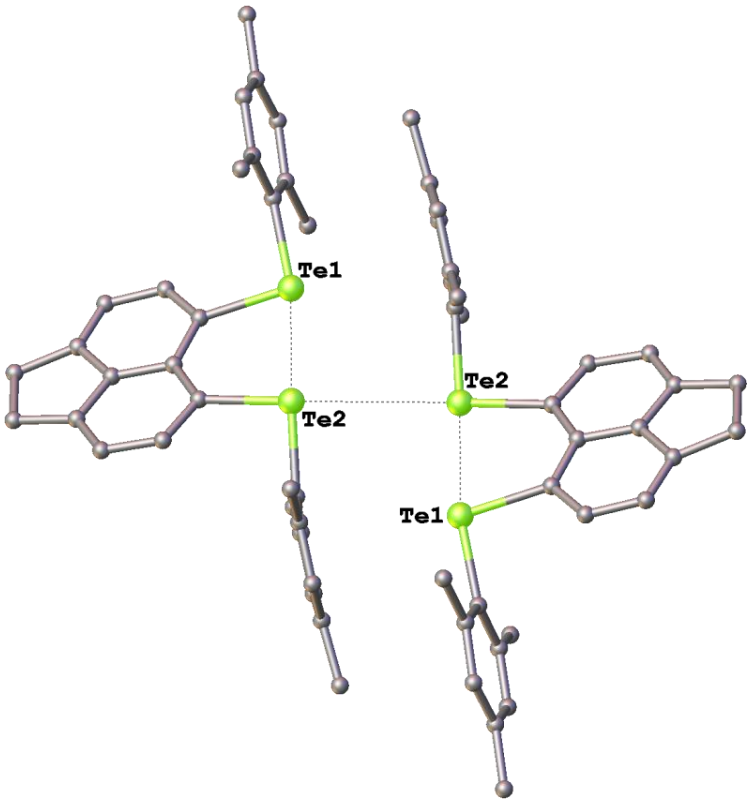

Figure 10 The zig-zag conformation shown for **A18** with all H atoms omitted for clarity.

Recently, the Woollins group introduced a steric parameter (θ) as a method of semi-quantifying the steric bulk of the aryl group bound to their Te atoms in a series of eight 5-(TeY)-6-(SePh)acenaphthenes (where Y = FP, Tol, An-*p*, An-*o*, TP, Mes, Tip and Nap).[5] The steric parameter involves measuring the angle of a triangle, with the Te atom at the tip of the triangle and the hydrogen atoms lying at the extreme edges (Figure 11).

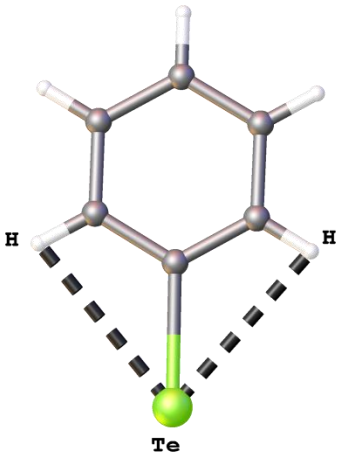

Figure 11 A crystallographic depiction of the steric parameter (θ) using **A3** as an example.

The steric parameters have been measured for the naphthalene, acenaphthene and acenaphthylene series (Table 6). The steric parameter measured for the Ph, FP, Tol, An-*p* and TP structures are all similar with values in the range 80.59-81.31(1)°. This is expected as the steric bulk around the tellurium atom is the same in these compounds with the bulk differing at the opposite end of the aryl ring. Significant differences are observed in the steric parameter for the An-*o*, Mes and Tip compounds with values increasing from ~105° for An-*o* to 122° for Mes and 134° for Tip. Again this is expected, as there is now additional bulk around the tellurium atom as well as the aryl ring.

Table 6 Steric parameter (θ) measured in [°] for the naphthalene, acenaphthene and acenaphthylene compounds.

Naphthalene Compound	Aryl Group	Steric Parameter (θ)
N3[8]	Ph	81.31(1)
N13	FP	81.16(1)
N14	Tol	81.16(1)
N15	An-*p*	81.23(1)
N16	An-*o*	105.26(1)
N17	TP	80.68(1)
N18	Mes	121.08(1)
Acenaphthene Compound	**Aryl Group**	**Steric Parameter (θ)**
A3[6]	Ph	81.18(1)
A13	FP	80.79(1)
A14	Tol	81.10(1)
A15	An-*p*	80.98(1)
A16	An-*o*	105.38(1)
A17	TP	80.79(1)
A18	Mes	120.93(1)
A19	Tip	129.76(1)
Acenaphthylene Compound	**Aryl Group**	**Steric Parameter (θ)**
Ay3[7]	Ph	80.79(1)
Ay13	FP	81.00(1)
Ay14	Tol	80.59(1)
Ay15	An-*p*	80.79(1)
Ay17	TP	81.01(1)
Ay18	Mes	125.34(1)
Ay19	Tip	138.67(1)

Ph = phenyl; **FP** = (4-fluorophenyl); **Tol** = toluene (4-methylphenyl); **An-*p*** = *para*-anisole (4-methoxyphenyl); **An-*o*** = *ortho*-anisole (2-methoxyphenyl); **TP** = (4-*tert*butylphenyl); **Mes** = mesityl (2,4,6-trimethylphenyl); **Tip** = (2,4,6-triisopropylphenyl).

Acenaphthenes **A3**,[6] **A13**-**A15**, **A17** and **A18** adopt the same configurations as analogous acenaphthylenes **Ay3**,[7] **Ay13**-**Ay15**, **Ay17** and **Ay18**, with the exception of **A19** and **Ay19**, according to the classification system developed by Nakanishi *et al.*[16] and Nagy *et al*.[17] The conformation of each compound is determined by observing how the the Te('naphthalene') and Te(aryl) rings align with respect to the C(ar)-Te-C(ar) planes.[17] This is calculated from the torsion angles θ and γ (Table 7); where the rotation around the Te-$C_{Naphthyl}$ bond is defined by θ and the rotation around the Te-C_{Ar} bond is defined by γ (See Chapter 4).

The AB conformation is adopted by **A3**,[6] **Ay3**,[7] **A13**, **Ay13**, **A17** and **Ay17** (Figure 13). In this conformation one Te-C_{Ar} bond lies on or close to the acenaphthene plane and the other Te-C_{Ar} bond lies perpendicular to the plane.[16,17] This conformation results in a *quasi*-linear three-body fragment with Te···Te-C_{Ar} angles (Ψ) in the range 173-176° and non-bonded *peri*-distances shorter than the sum of the van der Waals radii for tellurium by 18%. The CC*t* conformation is adopted by **A14**, **Ay14**, **A15**, **Ay15**, **A18** and **Ay18** (Figure 13). Type CC*t* occurs when the Te-C_{Ar} bonds are neither axial nor equatorial, with the *t* indicating that both bonds are in a *trans* orientation, with respect to the mean plane of the molecule.[16,17] The anomalies in this series are **A19** and **Ay19** (Figure 13) which do not assume the same configuration. **A19** adopts the BC*c* conformation, where one Te-C_{Ar} bonds lies on or close to the acenaphthene plane and the other Te-C_{Ar} bond lies neither axial nor equatorial. The *c* denotes that both bonds are in a *cis* orientation.[16,17] In comparison **Ay19** adopts the CC*t* conformation.

Naphthalene compounds **N14**, **N15**, **N17** and **N18** (Figure 13) adopt the same conformation as their acenaphthene and acenaphthylene counterparts; with the CC*t* conformation seen in **N14**, **N15** and **N18** and the AB conformation seen in **N17**. The Te···Te-C_{Ar} angle (Ψ) of 175.17(1)° in **N17** is similar to the angles of 176.49(1)° and 174.33(1)° observed in **A17** and **Ay17**, respectively. **N16** and **A16** also display an AB conformation (Figure 13), again with the Te···Te-C_{Ar} angle (Ψ) of 171.99(1)° in **N16** being similar in size to that observed in **A16** (175.03(1) Å). **N3**[8] and **N13** are the 'odd ones out' in this series, adopting a CC*t* conformation while their acenaphthene and acenaphthylene derivatives adopt an AB conformation (Figure 13).

For example, upon going from **A3** to **A19**, the size of the aryl group generally increases. This general increase in steric bulk around the tellurium seemingly has no effect on the conformation adopted or the level of molecular distortion. For e.g. **A14** and **A18** both adopt the CC*t* conformation despite **A14** having a significantly smaller steric parameter than **A18** with values of 81.10(1)° and 120.93(1)°, respectively. In addition the *peri*-distances observed in **A14** (3.3285(7) Å) and **A18** (3.3380(11) Å) are statistically the same. Similar trends are found within the naphthalene, acenaphthene and acenaphthylene series as depicted in Figure 12 which plots steric parameter against *peri*-distance.

Table 7 Torsion angles [°] categorising the 'naphthalene' and aryl ring conformations in **N3**,[8] **N13-N18**, **A3**,[6] **A13-A19** and **Ay3**,[7] **Ay13-15**, **Ay17-18**.

	Naphthalene ring conformations		***Configuration***	***Aryl ring conformations***	
	C(10)-C(1)-Te(1)-C(11)	**C(10)-C(9)-Te(2)-C(18)**	**Type**	**C(1)-Te(1)-C(11)-C(12)**	**C(9)-Te(2)-C(18)-C(19)**
N3[8]	θ_1 -124.79(1) twist	θ_2 -132.46(1) twist	CC*t*	γ_1 100.88(1) axial	γ_2 57.21(1) twist
N13	θ_1 -145.4(4) twist	θ_2 -146.2(4) twist	CC*t*	γ_1 96.0(4) axial	γ_2 -71.5(4) axial
N14	θ_1 -148.5(4) twist	θ_2 -149.4(4) twist	CC*t*	γ_1 -96.3(4) axial	γ_2 73.6(5) axial
N15	θ_1 -125.1(8) twist	θ_2 -134.8(8) twist	CC*t*	γ_1 80.7(7) axial	γ_2 -97.5(8) axial
N16	θ_1 177.2(6) equatorial	θ_2 -110.1(6) axial	AB	γ_1 -84.3(7) axial	γ_2 -169.8(5) equatorial
N17	θ_1 -77.0(3)axial	θ_2 -169.3(3) equatorial	AB	γ_1 -3.11(19) equatorial	γ_2 -92.0(3)axial
N18	θ_1 138.8(4) twist	θ_2 142.8(4) twist	CC*t*	γ_1 -87.0(4) axial	γ_2 94.5(4) axial
	Acenaphthene ring conformations			***Aryl ring conformations***	
	C(10)-C(1)-Te(1)-C(13)	**C(10)-C(9)-Te(2)-C(19)**		**C(1)-Te(1)-C(13)-C(14)**	**C(9)-Te(2)-C(19)-C(20)**
A3[6]	θ_1 166.60(1) equatorial	θ_2 79.56(1) axial	AB	γ_1 86.4(11) axial	γ_2 -167.34(1) equatorial
A13	θ_1 -167.3(6) equatorial	θ_2 -80.3(5) axial	AB	γ_1 100.9(8) axial	γ_2 155.7(7) twist
A14	θ_1 -153.3(5) twist	θ_2 -142.0(5) twist	CC*t*	γ_1 83.1(5) axial	γ_2 -97.3(5) axial
A15	θ_1 153.3(9) twist	θ_2 144.2(9) twist	CC*t*	γ_1 101.7(8) axial	γ_2 96.1(8) axial
A16	θ_1 -165.8(4) equatorial	θ_2 -84.4(4) axial	AB	γ_1 -108.2(3) axial	γ_2 175.6(4) equatorial
A17	θ_1 169.3(6) equatorial	θ_2 72.5(8) axial	AB	γ_1 86.5(8) axial	γ_2 7.1(8) equatorial

A18	θ_1 -152.1(6) twist	θ_2 -136.4(6) twist	CC*t*	γ_1 85.3(5) axial	γ_2 -107.2(5) axial
A19	θ_1 142.6(4) twist	θ_2 -169.4(4) equatorial	BC*c*	γ_1 -78.1(4) axial	γ_2 100.1(4) axial
	Acenaphthylene ring conformations			***Aryl ring conformations***	
	C(10)-C(1)-Te(1)-C(13)	**C(10)-C(9)-Te(2)-C(19)**		**C(1)-Te(1)-C(13)-C(14)**	**C(9)-Te(2)-C(19)-C(20)**
Ay3[7]	θ_1 78.8(7) axial	θ_2 166.2(7) equatorial	AB	γ_1 -159.2(8) equatorial	γ_2 86.1(10) axial
Ay13	θ_1 165.4(3) equatorial	θ_2 90.5(3) axial	AB	γ_1 -87.4(3) axial	γ_2 89.8(3) axial
Ay14	θ_1 152.2(9) twist	θ_2 145.7(9) twist	CC*t*	γ_1 -81.7(9) axial	γ_2 95.7(9) axial
Ay15	θ_1 -142.6(7) twist	θ_2 -152.0(7) twist	CC*t*	γ_1 79.2(6) axial	γ_2 85.4(7) axial
Ay17	θ_1 68.2(17) axial	θ_2 164.5(19) equatorial	AB	γ_1 11(2) equatorial	γ_2 -86.6(16) axial
Ay18	θ_1 145.3(7) twist	θ_2 152.9(7) twist	CC*t*	γ_1 -84.7(6) axial	γ_2 98.5(6) axial
Ay19	θ_1 133.1(3) twist	θ_2 133.1(3) twist	CC*t*	γ_1 124.0(3) twist	γ_2 124.0(3) twist

axial: perpendicular to C(ar)-Te-C(ar) plane; **equatorial**: coplanar with C(ar)-Te-C(ar) plane; **twist**: intermediate of axial and equatorial.

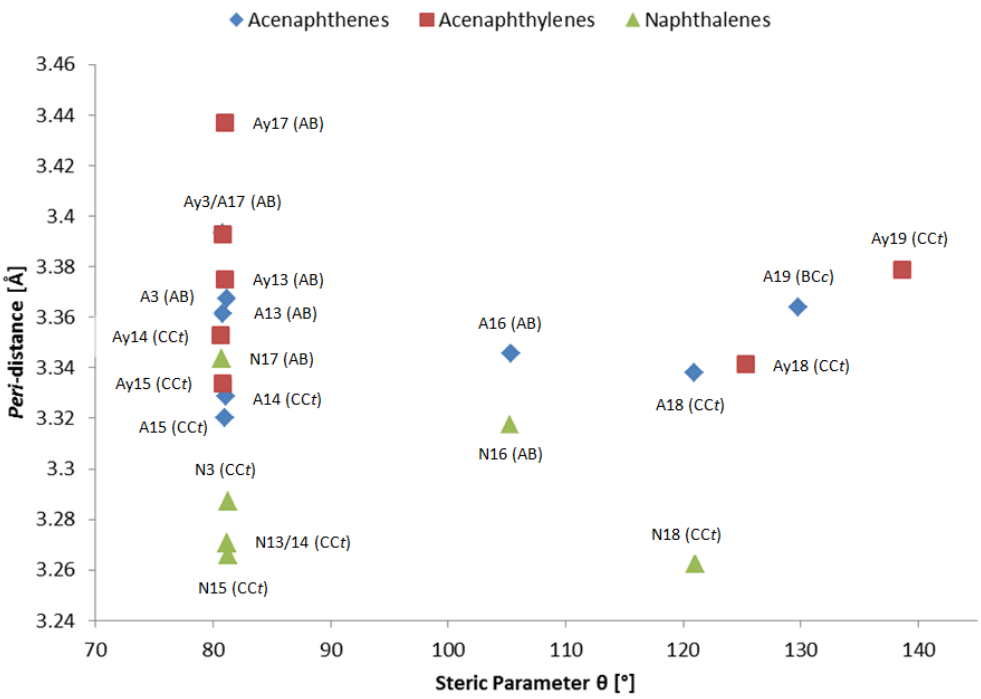

Figure 12 Plot of steric parameter versus *peri*-distance for the naphthalene, acenaphthene and acenaphthylene compounds with their respective conformations in brackets.

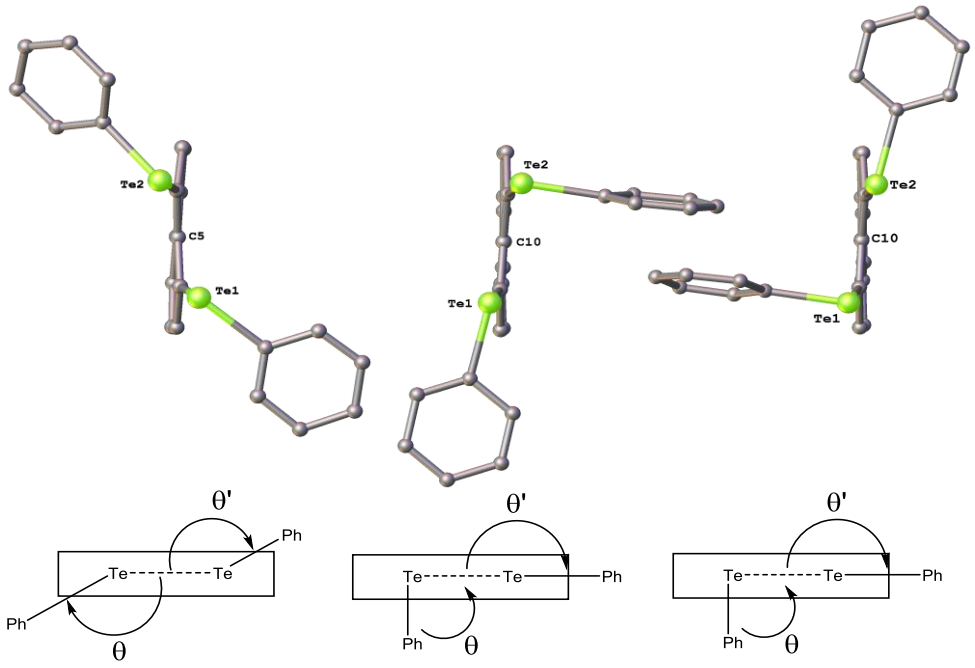

N3
CC*t*
θ = 125°
θ' = 132°

A3
AB
θ = 80°
θ' = 167°

Ay3
AB
θ = 79°
θ' = 166°

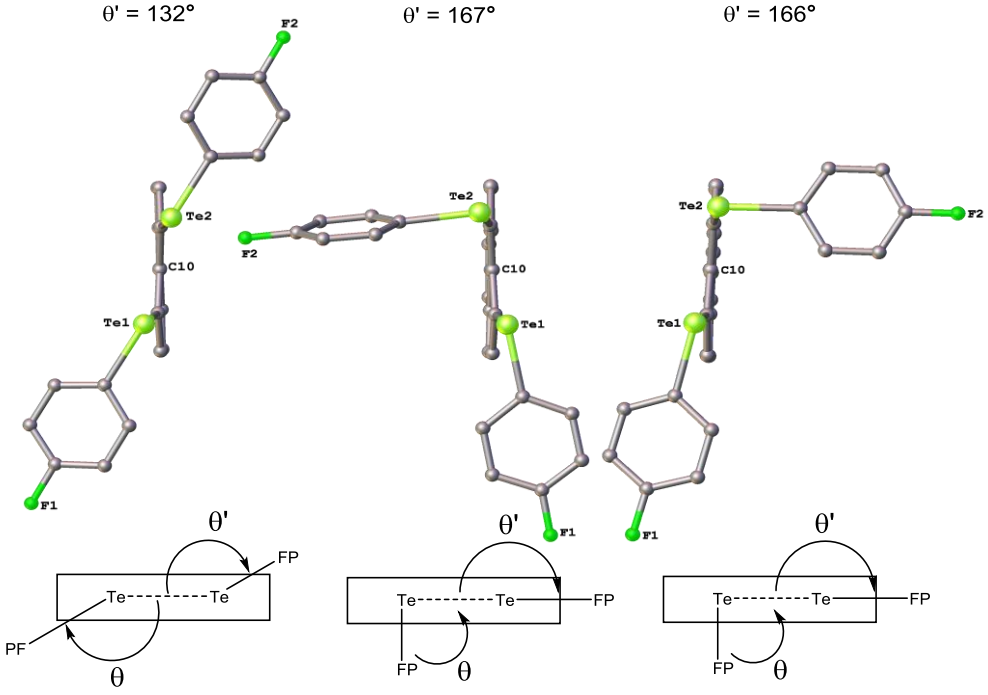

N13
CC*t*
θ = 145°
θ' = 146°

A13
AB
θ = 80°
θ' = 167°

Ay13
AB
θ = 91°
θ' = 165°

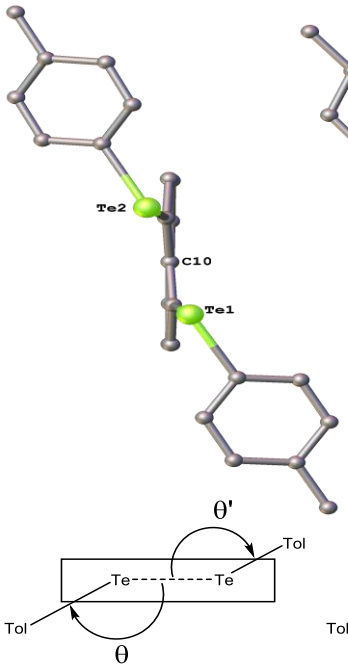

N14
CC*t*
θ = 149°
θ' = 149°

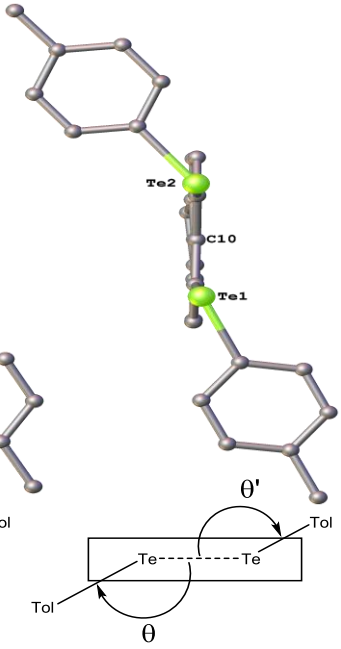

A14
CC*t*
θ = 153°
θ' = 142°

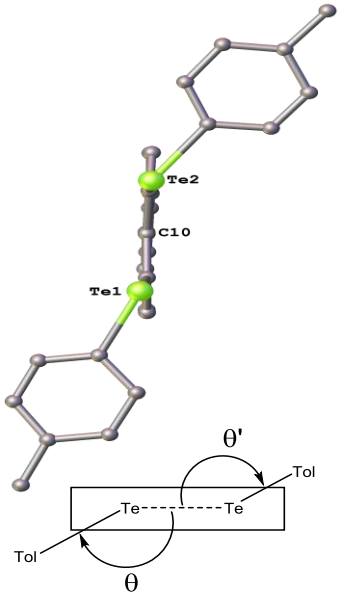

Ay14
CC*t*
θ = 152°
θ' = 146°

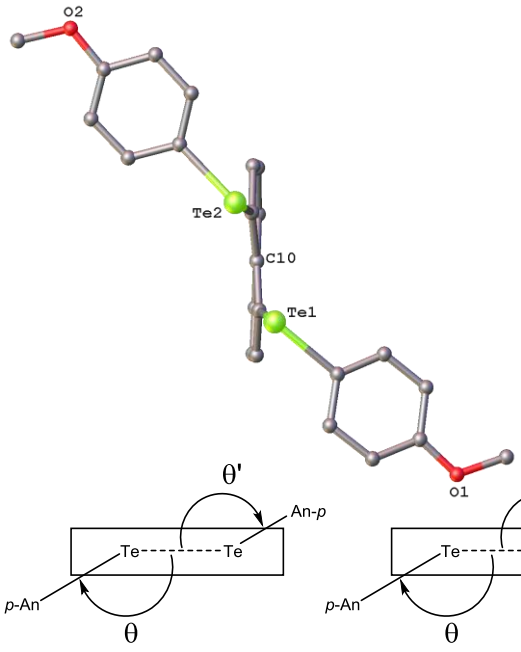

N15
CC*t*
θ = 125°
θ' = 135°

A15
CC*t*
θ = 153°
θ' = 144°

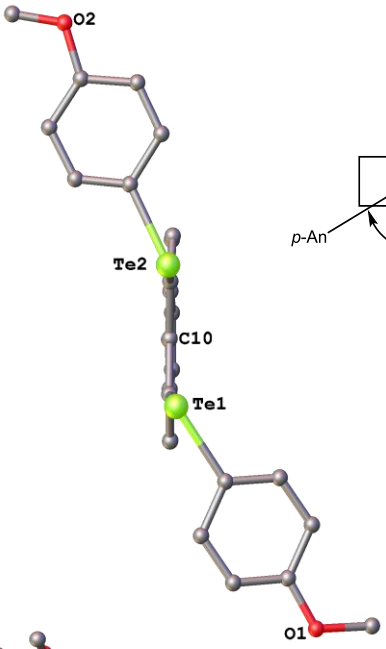

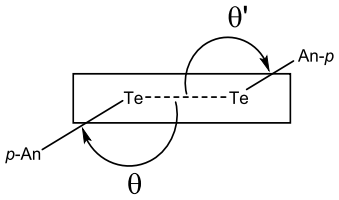

Ay15
CC*t*
θ = 143°
θ' = 152°

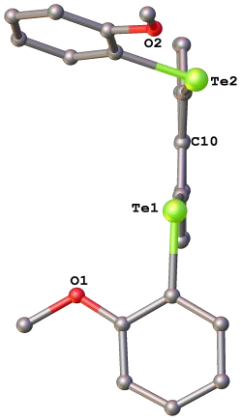

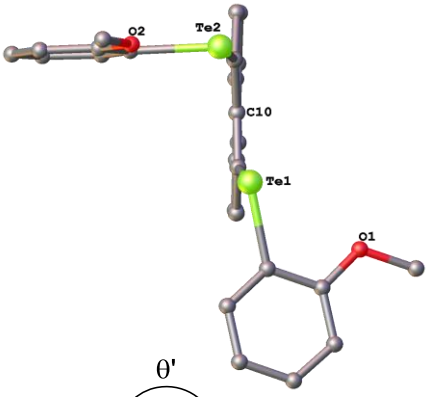

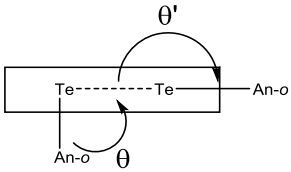

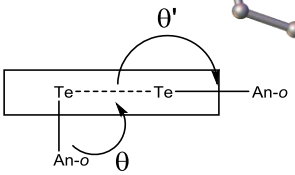

N16
AB
θ = 110°
θ' = 177°

A16
AB
θ = 84°
θ' = 166°

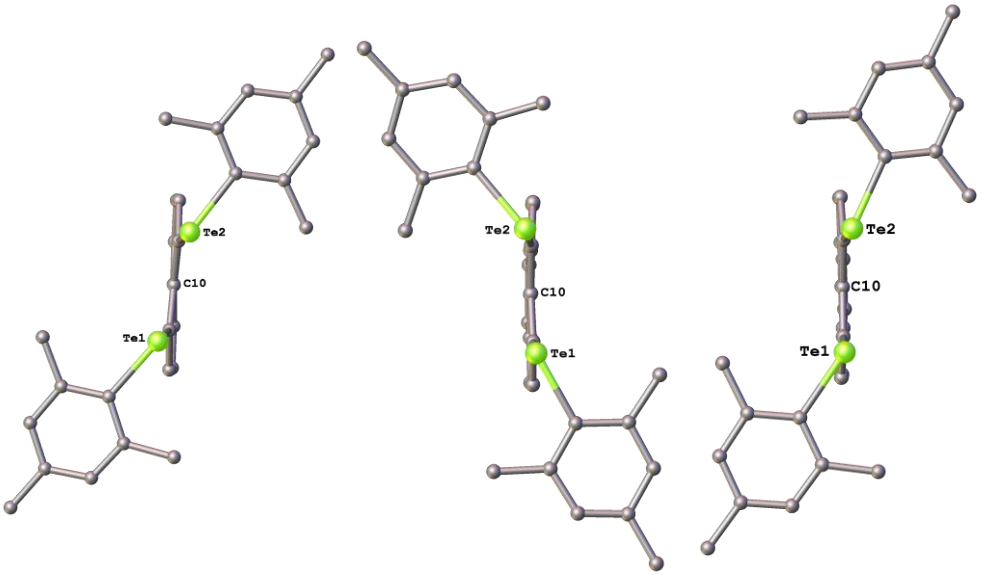

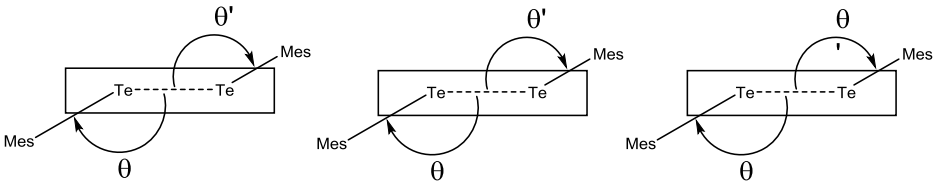

N18
type CC*t*
θ = 139°
θ' = 143°

A18
type CC*t*
θ = 152°
θ' = 136°

Ay18
type CC*t*
θ = 145°
θ' = 153°

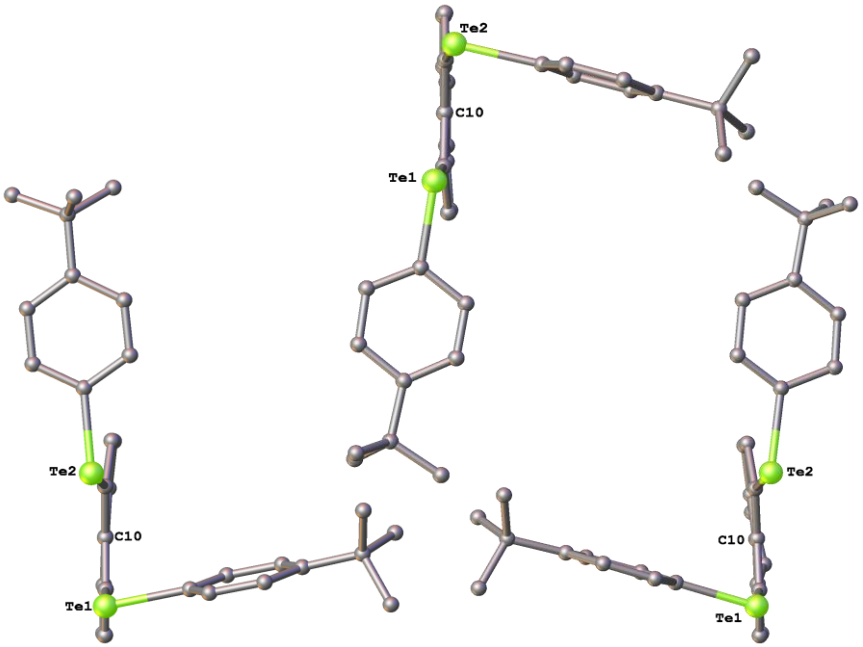

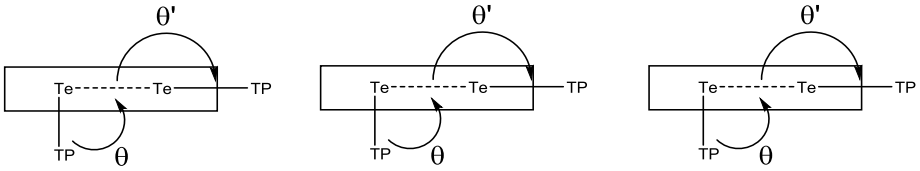

N17
AB
θ = 77°
θ' = 169°

A17
AB
θ = 73°
θ' = 169°

Ay17
AB
θ = 68°
θ' = 165°

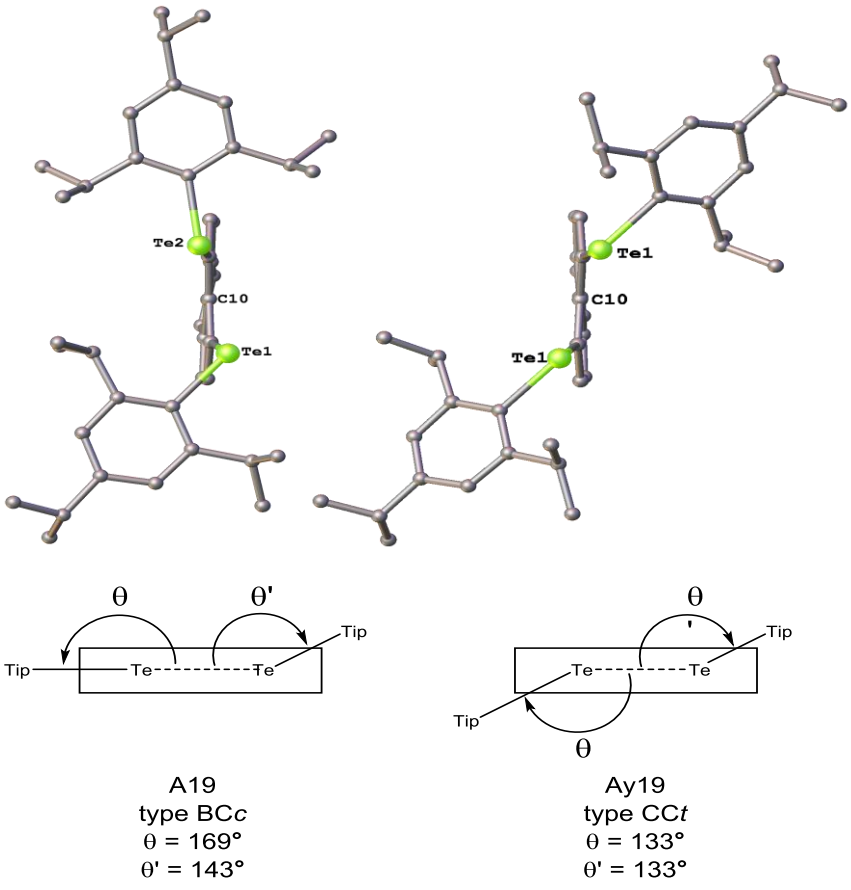

Figure 13 The orientation of the Te(Ar) groups, the three-linear fragment arrangements and structural conformations for **N3**,[8] **N13**-**N18**, **A3**,[6] **A13**-**A19** and **Ay3**,[7] **Ay13**-**Ay15** and **Ay17**-**Ay19**.

NMR Investigations

As expected, the ^{125}Te NMR spectra for the ditellurides, naphthalene, acenaphthene and acenaphthylene compounds exhibit single peaks, with coupling to ^{123}Te nuclei unobserved due to the exceptionally low natural abundance of this isotope (0.87%).[1] The corresponding ^{123}Te NMR spectra also exhibit single peaks; however, the increased natural abundance of the ^{125}Te nuclei (7.00%)[1] allows satellites for ^{123}Te-^{125}Te coupling to be observed. The J(^{125}Te, ^{125}Te) coupling was calculated and all values are shown in Tables 8 and 9.

Table 8 ^{125}Te and ^{123}Te NMR spectroscopy data for naphthalene, acenaphthene and acenaphthylene compounds.

Naphthalenes	**N3**[8]	**N13**	**N14**	**N15**	**N16**	**N17**	**N18**	**N19**
Aryl group	Ph	FP	Tol	An-*p*	An-*o*	TP	Mes	Tip
^{125}Te NMR (ppm)	619.7	615.8	607.6	601.9	514.6	603.8	397.4	346.4
^{123}Te NMR (ppm)	620.3	616.1	607.4	601.8	514.0	604.9	396.7	346.1
***J*(^{123}Te,^{125}Te) (Hz)**	2077	2082	2145	2189	2219	2097	3191	3095
***J*(^{125}Te,^{125}Te) (Hz)**[a]	2505	2511	2587	2640	2676	2529	3848	3733
Acenaphthenes	**A3**[6]	**A13**	**A14**	**A15**	**A16**	**A17**	**A18**	**A19**
Aryl group	Ph	FP	Tol	An-*p*	An-*o*	TP	Mes	Tip
^{125}Te NMR (ppm)	585.9	581.7	574.4	567.8	482.4	571.4	363.3	316.0
^{123}Te NMR (ppm)	586.6	579.9	574.1	567.8	481.9	571.6	362.9	315.8
***J*(^{123}Te,^{125}Te) (Hz)**	1750	1746	1780	1835	1796	1766	2818	2727
***J*(^{125}Te,^{125}Te) (Hz)** [a]	2110	2106	2147	2213	2166	2130	3398	3289
Acenaphthylenes	**Ay3**[7]	**Ay13**	**Ay14**	**Ay15**	**Ay16**	**Ay17**	**Ay18**	**Ay19**
Aryl group	Ph	FP	Tol	An-*p*	An-*o*	TP	Mes	Tip
^{125}Te NMR (ppm)	618.9	610.3	605.7	540.9	n/a	600.5	406.6	353.7
^{123}Te NMR (ppm)	618.9	610.1	605.2	541.0	n/a	600.1	406.3	353.3
***J*(^{123}Te,^{125}Te) (Hz)**	1706	1700	1796	n/a	n/a	1772	2956	2958
***J*(^{125}Te,^{125}Te) (Hz)** [a]	2057	2050	2166	n/a	n/a	2137	3565	3567

[a] The *J*(^{125}Te, ^{125}Te) value was obtained by multiplying the *J*(^{123}Te, ^{125}Te) values by 1.206.

Table 9 ^{125}Te and ^{123}Te NMR spectroscopy data for ditellurides.

Ditelluride	$(TePh)_2$	$(TeFP)_2$	$(TeTol)_2$	$(TeAn\text{-}p)_2$	$(TeAn\text{-}o)_2$	$(TeTP)_2$	$(TeMes)_2$	$(TeTip)_2$
^{125}Te NMR (ppm)	427.6	463.1	432.8	461.3	175.9	408.9	201.6	183.2
^{125}Te NMR (ppm)	431.1	463.9	432.3	461.0	175.9	409.9	201.6	182.6
$J(^{123}Te,^{125}Te)$ (Hz)	268	129	787	216	279	198	532	650
$J(^{125}Te,^{125}Te)$ (Hz) [a]	323	156	949	260	336	239	642	784

[a] The $J(^{125}Te, ^{125}Te)$ value was obtained by multiplying the $J(^{123}Te, ^{125}Te)$ values by 1.206.

As the number of bonds between two NMR active nuclei increases, transmission of through-bond coupling generally decreases.[2] Thus if through-bond coupling is the only mechanism at work one would expect $^4J(^{125}Te, ^{125}Te)$ values calculated for the naphthalene, acenaphthene and acenaphthylene compounds to be lower than the $^1J(^{125}Te, ^{125}Te)$ values of the ditelluride starting materials. However, the values we observe for $^4J(^{125}Te, ^{125}Te)$ are much larger than the $^1J(^{125}Te, ^{125}Te)$ values for the ditellurides which confirms that, in addition to through-bond coupling, additional coupling is being transmitted through-space.

The degree of molecular distortion occurring in acenaphthene compounds **A3**,[6] **A13**-**A19** was found to be comparable with that observed in their acenaphthylene counterparts **Ay3**,[7] **Ay13**-**Ay19**, with much greater *peri*-distances observed compared to the corresponding set of naphthalene compounds **N3**,[8] **N13**-**N19**. The differences observed between the backbones are reflected in $J(^{125}Te, ^{125}Te)$ values, with the naphthalene compounds having notably larger $J(^{125}Te, ^{125}Te)$ SSCCs than both the acenaphthene and acenaphthylene series, whose $J(^{125}Te, ^{125}Te)$ were found to be comparable (Figure 14).

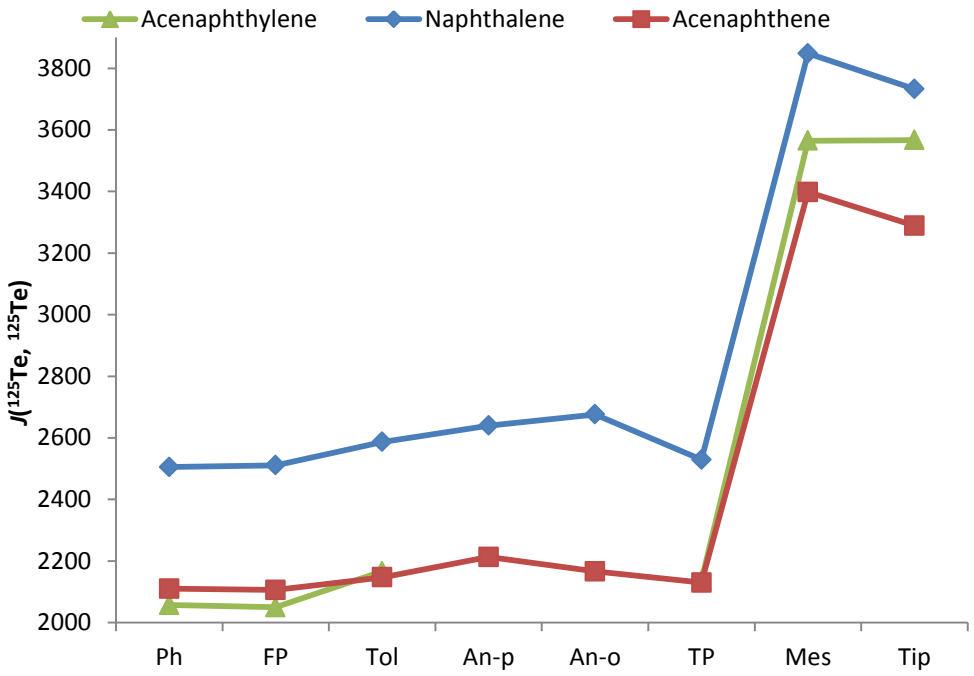

Figure 14 Plot showing the differences in $J(^{125}Te, ^{125}Te)$ for each series.

The ^{125}Te NMR chemical shift values for **N3**,[8] **N13**-**N19** were plotted against those for **A3**,[6] **A13**-**A19** (Figure 15). Addition of a trendline shows an excellent linear relationship with a correlation coefficient of 0.9999 being observed. This shows that the conformation around the Te atoms is similar in solution for respective naphthalene and acenaphthene compounds. The same relationship is observed when plotting the respective $J(^{125}Te, ^{125}Te)$ values (Figure 16). Nakanishi and Hayashi observed a similar result when they plotted the ^{77}Se NMR chemical shifts of two series of 1-(arylselanyl)naphthalenes against one another.[16]

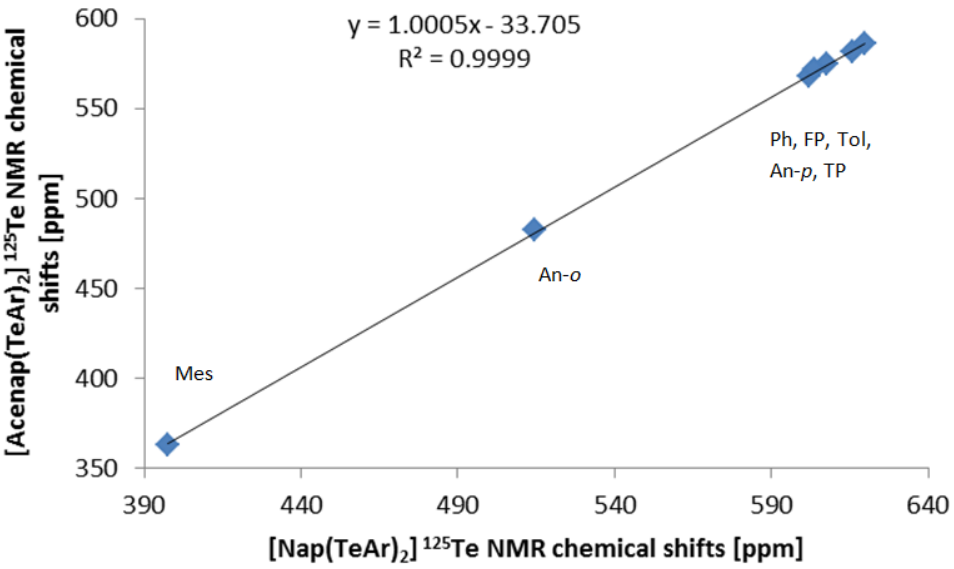

Figure 15 A plot of ^{125}Te NMR chemical shifts for naphthalenes vs. ^{125}Te NMR chemical shifts for acenaphthenes.

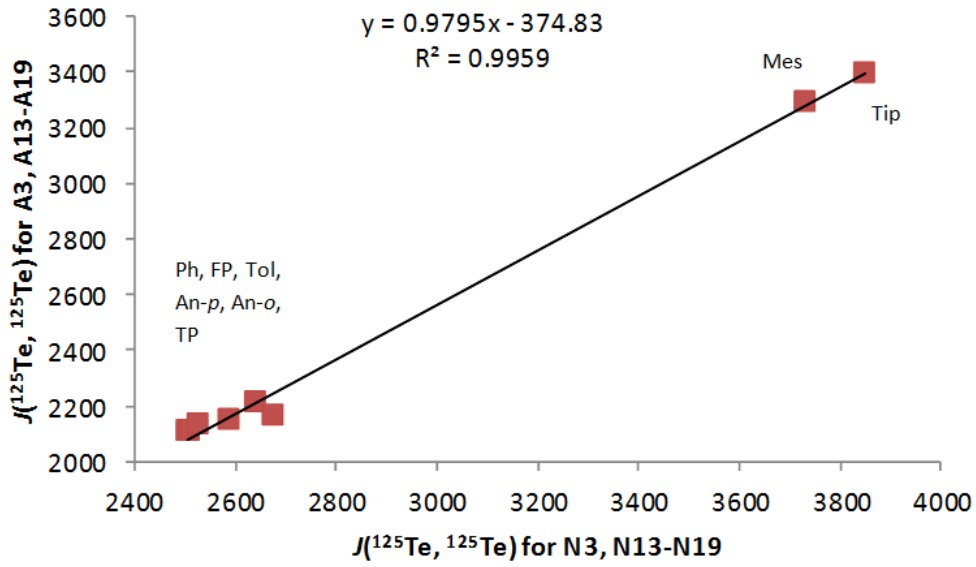

Figure 16 A plot of $J(^{125}Te, ^{125}Te)$ for naphthalenes vs. $J(^{125}Te, ^{125}Te)$ for acenaphthenes.

Linear relationships with correlation coefficients in the range 0.9161-0.9959 were also observed when plotting $J(^{125}Te, ^{125}Te)$ and ^{125}Te NMR chemical shifts for acenaphthene against acenaphthylene and naphthalene against acenaphthylene (see Appendix).

^{125}Te NMR chemical shift data plotted against the steric parameter (Figure 17) shows that when the aryl groups are of a similar size there is not a large difference observed in the chemical shift. However, as the aryl group increases in size from An-*o*, to Mes to Tip a steady decrease is observed in the chemical shift. A similar correlation between ^{125}Te chemical shift and steric parameter was observed in a recent study of 5-(aryltelluro)-6-(phenylselenyl)acenaphthenes.[5]

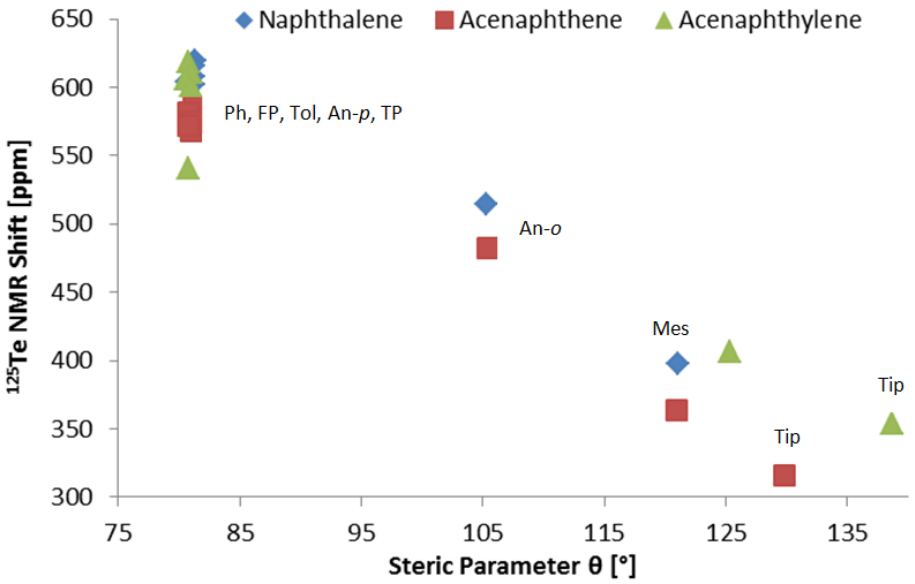

Figure 17 Plot of ^{125}Te chemical shifts against the steric parameter θ.

$J(^{125}Te, ^{125}Te)$ data were also plotted against the steric parameter (Figure 18). As seen previously, the naphthalene compounds have the larger $J(^{125}Te, ^{125}Te)$ SSCCs with acenaphthene and acenaphthylene having similar values. Within each series the compounds containing the aryl groups, Ph, FP, Tol, An-*p* and TP, do not show a large variation in the value of $J(^{125}Te, ^{125}Te)$ couplings. Overall, as the steric parameter increases there is a general increase observed in $J(^{125}Te, ^{125}Te)$.

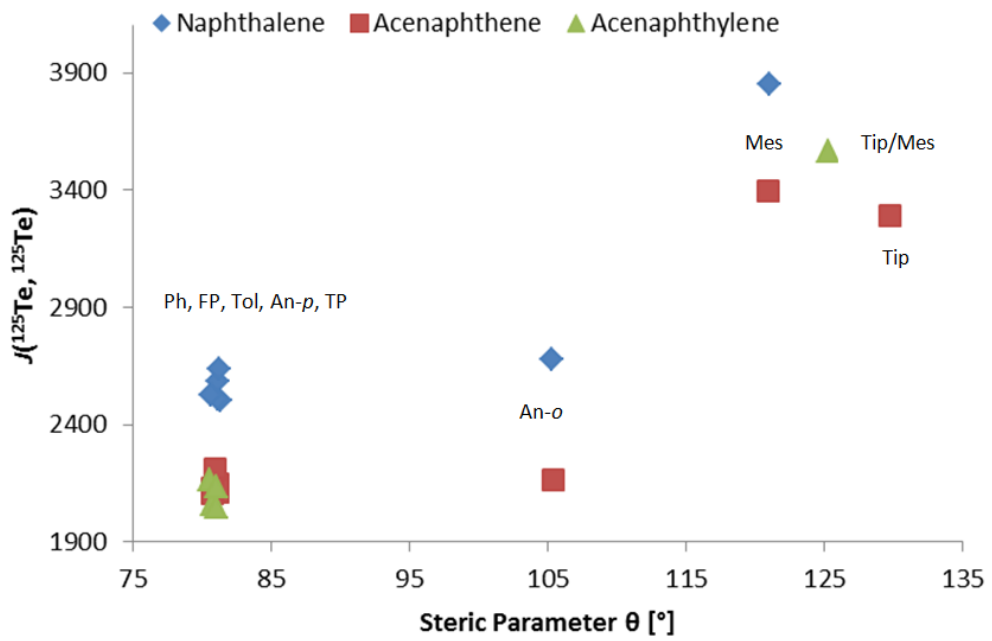

Figure 18 Plot of $J(^{125}Te, ^{125}Te)$ against the steric parameter θ.

Experimentally obtained dihedral angles, ϕ_1 and ϕ_2 (Figure 19), for **A3**,[6] **A13**-**A19** and **Ay3**,[7] **Ay13**-**Ay15**, **Ay17**-**Ay19** were plotted against each other following the method used by M. Bühl *et al.*[4] in order to observe the $J(^{125}Te, ^{125}Te)$ coupling constants as a function of conformation (Figure 20). In general, compounds that exhibit the AB conformation were found to have the smallest $J(^{125}Te, ^{125}Te)$ SSCCs with values in the range 2050-2166 Hz and compounds that adopt the CC*t* conformation have the largest $J(^{125}Te, ^{125}Te)$ with values in the range 3398-3567 Hz. Out of the 15 structures studied, 4 did not confer to this pattern. **A14** (2147 Hz), **A15** (2213 Hz) and **Ay14** (2166 Hz) have much smaller $J(^{125}Te, ^{125}Te)$ than expected from a CC*t* conformation, suggesting in solution there is some fluctuation between conformations. **A19** which adopts a BC*c* conformation in the solid exhibits a large $J(^{125}Te, ^{125}Te)$ value of 3289 Hz, in line with what one might expect from a CC*t* conformation.

It was concluded by Nakanishi and Hayashi using similar *peri*-substituted selenium compounds that in solution the AB conformation is in equilibrium with the CC*t* conformation.[18] M. Bühl *et al.*[4] calculated that an energy difference of 1 kcal mol^{-1} exists between these conformations therefore

it is not unreasonable to suggest that an equilibrium exists in solution. Our findings regarding **A14**, **A15**, **A19** and **Ay14** also imply that an equilibrium exists in solution and we are hoping this can be confirmed by ^{125}Te solid state NMR spectroscopy in the future.

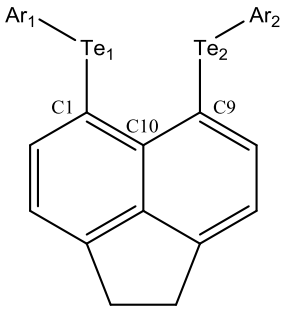

ϕ_1 = C10-C1-Te1-C(Ar1)

ϕ_2 = C10-C9-Te2-C(Ar2)

Figure 19 The two dihedral angles, ϕ_1 and ϕ_2, used to define the rotation around the Te-C_{Acenap} bond and hence the conformation of the molecule. (NB. The same angles are used for the acenaphthylene structures).

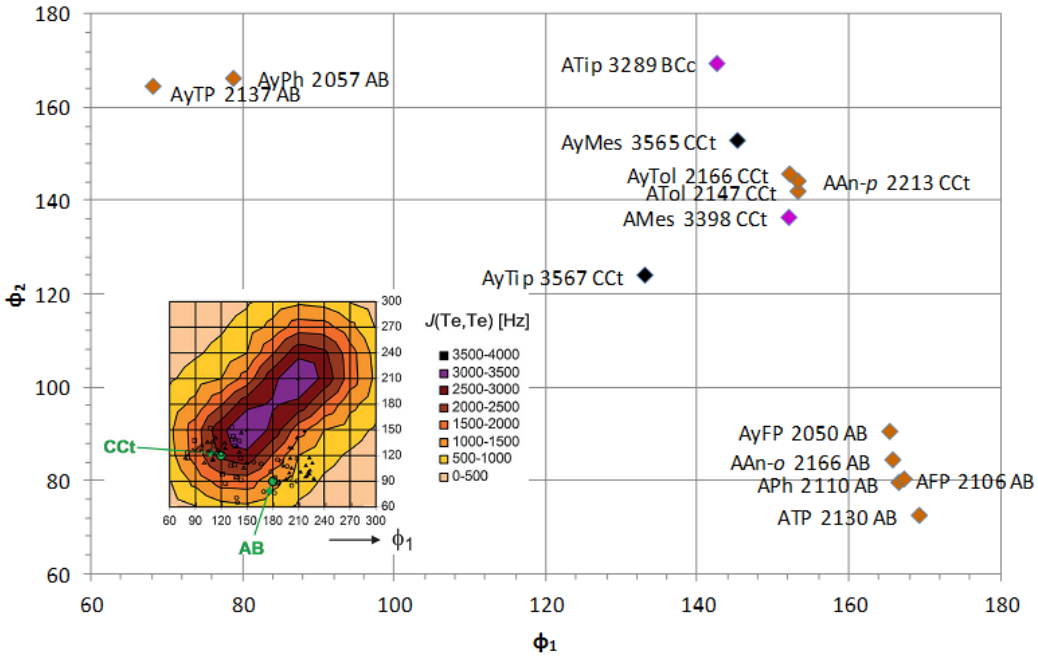

Figure 20 *J*(^{125}Te, ^{125}Te) as a function of the conformation, defined by the two dihedral angles ϕ_1 and ϕ_2, with the inlay plot taken from M. Buhl *et al.*[4] for comparison.

The experimental figures for ϕ_1 were plotted against those of ϕ_2 for **N3**,[8] **N13**-**N18** (see Appendix). Like their acenaphthene and acenaphthylene counterparts, the naphthalene compounds adopting an AB conformation have the smallest *J*(^{125}Te, ^{125}Te) values and compounds with a CC*t* conformation have the largest *J*(^{125}Te, ^{125}Te) values. **N16**, **N17** and **N18** have *J*(^{125}Te, ^{125}Te) values that are in agreement with their adopted conformations. The remaining four compounds **N3**,[8] **N13**-**N15** all adopt the CC*t* conformation, however their *J*(^{125}Te, ^{125}Te) values are much lower than expected, more in line with that of an AB conformation. Again, it seems that an equilibrium is occurring in solution between the AB and CC*t* conformers and ^{125}Te solid state NMR spectroscopy could help determine this.

J(^{125}Te, ^{125}Te) SSCCs for the CC*t* and AB conformations were computed (ZORA-SO/BP level) for the three acenaphthene compounds shown in Table 10. These compounds have been characterised and we can compare the predicted data with the experimental data.

Table 10 Experimental vs. computed *J*(^{125}Te, ^{125}Te) values [Hz] for the CC*t* and AB conformations of **A3**,[6] **A15**, and **A18**.

Compound	*J*(^{125}Te, ^{125}Te) exp.	*J*(^{125}Te, ^{125}Te) CC*t*	*J*(^{125}Te, ^{125}Te) AB	ΔE (kcal mol^{-1})
A3	*2110*	2604	1543	0.1
A15	*2213*	2842	1375	0.1
A18	*3398*	2738	-	-

From structural analysis it is found that **A3**[6] adopts an AB conformation in the solid. Interestingly, the experimentally determined *J*(^{125}Te, ^{125}Te) was found to be 2110 Hz, intermediate between the computed values for an AB (1543 Hz) and a CC*t* (2604 Hz) conformation. Nevertheless, as the calculated energy difference between the two conformations is only 0.1 kcal mol^{-1}, the intermediate *J*(^{125}Te, ^{125}Te) value suggests that an equilibrium exists in solution with the conformation fluctuating between AB and CC*t*. The same differences are observed in **A15**, again with the experimentally obtained value for the coupling (2213 Hz) lying midway between that calculated for the AB (1375 Hz) and the CC*t* (2842 Hz); however it is the CC*t* conformation that is adopted by **A15** in the solid.

For the mesityl derivative **A18**, no minimum is computed for the AB conformation. The experimentally obtained $J(^{125}Te, ^{125}Te)$ value of 3398 Hz is much larger than the predicted value for the CC*t* conformation (2738 Hz), consistent with that found in the solid.

Conclusion

A series of acenaphthenes (**A3**,[6] **A13**-**A19**) and acenaphthylenes (**Ay3**,[7] **Ay13**-**Ay19**), bearing ArTe moieties (where Ar = Ph, FP, Tol, An-*p*, An-*o*, TP, Mes and Tip) at the *peri*-positions, have been prepared and compared to their naphthalene analogues (**N3**,[8] **N13**-**N19**).

Similar degrees of molecular distortion were observed in the acenaphthene and acenaphthylene compounds, with the naphthalene compounds displaying greater molecular distortion and shorter *peri*-distances. The steric parameters for the Ph, FP, Tol, An-*p* and TP compounds were found to be similar, however An-*o*, Mes and Tip had increasingly larger values. This increase in steric parameter was found to have no effect on the molecular distortion or conformation in any of the compounds studied. With the exception of **A19**, **A3**,[6] **A13**-**A15**, **A17** and **A18** had the same conformation as their acenaphthylene analogues. The naphthalene compounds displayed less correlation, with only **N14**, **N15**, **N17** and **N18** having the same conformation as their acenaphthene/acenaphthylene counterparts.

The naphthalene compounds had larger $J(^{125}Te, ^{125}Te)$ SSCCs than the acenaphthene and acenaphthylene compounds (which were comparable) as expected from the shorter *peri*-distances in the former. A linear correlation in ^{125}Te chemical shift and $J(^{125}Te, ^{125}Te)$ SSCCs was found between all three series, which shows that the conformation around the Te atoms is similar in solution for all backbones. No difference was observed in the ^{125}Te chemical shift or $J(^{125}Te, ^{125}Te)$ values for the compounds containing Ar groups of similar size. However, for the larger aryl groups (An-*o*, Mes and Tip) as the size of the group increased a steady decrease in ^{125}Te chemical shift and a general increase in $J(^{125}Te, ^{125}Te)$ value occurred.

In general, compounds that exhibit the AB conformation were found to have the smallest $J(^{125}Te, ^{125}Te)$ SSCCs and compounds that adopt the CC*t* conformation have the largest. Out of the 15 acenaphthene and acenaphthylene compounds, 4 did not confer to this trend. **A14**, **A15** and

Ay14 had smaller *J*(^{125}Te, ^{125}Te) values, which were more in line with an AB conformation than the CC*t* conformation found in the solid. **A19** adopts the BC*c* conformation in the solid, but its *J*(^{125}Te, ^{125}Te) value is more in line with what would be expected for the CC*t* conformation. Similar discrepancies were seen in the *J*(^{125}Te, ^{125}Te) SSCCs of the naphthalene compounds. It has been previously concluded, that in solution an energy difference of only 1 kcal mol^{-1} exists between the AB and CC*t* conformations, allowing the molecular structure to easily fluctuate between the two conformers.[4,18] Our findings are in agreement with an equilibrium occurring in solution and we are hoping this can be confirmed by ^{125}Te solid state NMR spectroscopy in the future. Overall the ability of SSCCs to aid prediction of structural conformation in these systems has a promising future.

Experimental

All experiments were carried out under an oxygen- and moisture-free nitrogen atmosphere using standard Schlenk techniques and glassware. Reagents were obtained from commercial sources and used as received. Dry solvents were collected from a MBraun solvent system. Elemental analyses were performed by Stephen Boyer at the London Metropolitan University. Infra-red spectra were recorded for solids as KBr discs in the range 4000-350 cm^{-1} on a Perkin-Elmer System 2000 Fourier transform spectrometer. ^{1}H, ^{13}C and ^{19}F NMR spectra were recorded on a Bruker Avance 300 MHz spectrometer with δ(H) and δ(C) referenced to external tetramethylsilane and δ(F) referenced to external trichlorofluoromethane. ^{123}Te and ^{125}Te NMR spectra were recorded on a Jeol GSX 270 MHz spectrometer with δ(Te) referenced to Me_2Te, with a secondary reference for δ(Te) to diphenyl ditelluride [δ(Te) = 428 ppm]. NB. All J_{TeTe} values listed in the experimental represent experimentally obtained $^{1}J(^{123}Te,^{125}Te)$ SSCCs. Assignments of ^{13}C and ^{1}H NMR spectra were made with the help of H-H COSY and HSQC experiments. All measurements were performed at 25 °C. All values reported for NMR spectroscopy are in parts per million (ppm). Coupling constants (*J*) are given in Hertz (Hz). All measurements were performed at 25 °C. Mass spectrometry was performed by the University of St. Andrews Mass Spectrometry Service. Electrospray Mass Spectrometry (ESMS) was carried out on a Micromass LCT orthogonal accelerator time of flight mass spectrometer. DFT calculations were carried out by Michael Bühl at the University of St Andrews. 5,6-dibromoacenaphthene[19] was prepared following standard literature procedure.

Diaryl ditellurides (ArTeTeAr)

Diphenyl ditelluride was obtained from commercial sources and used as received.

PhTeTePh: $\delta_{^{125}Te}$(85.2 MHz, $CDCl_3$, 25 °C, PhTeTePh) 427.6 (s); $\delta_{^{123}Te}$(70.7 MHz, $CDCl_3$, 25 °C, PhTeTePh) 434.1 (s, $^{1}J_{TeTe}$ 268 Hz).

Bis(4-fluorophenyl) ditelluride (FPTeTeFP), *Bis*(4-methylphenyl) ditelluride (TolTeTeTol), *bis*(4-methoxyphenyl) ditelluride (An-*p*TeTeAn-*p*), *bis*(2-methoxyphenyl) ditelluride (An-*o*TeTeAn-*o*), *bis*(4-*tert*butylphenyl) ditelluride (TPTeTeTP), *bis*(2,4,6-trimethylphenyl) ditelluride

(MesTeTeMes) and *bis*(2,4,6-triisopropylphenyl) ditelluride (TipTeTeTip) were synthesised from the respective aryl bromides following a modification of the original procedure used by Ando and collegues.[10]

For example, **FPTeTeFP:** Magnesium (2.33 g, 95.85 mmol) was added to a solution of FPBr (15.30 g, 87.43 mmol) in THF (80 mL) and the mixture was refluxed for 1 h. The mixture was then cooled to room temperature and tellurium powder (11.29 g, 88.47 mmol) was added. The mixture was refluxed for a further 1 h. After cooling to room temperature, the reaction mixture was diluted with toluene (40 mL) and exposed to an air stream overnight for mild oxidation. The mixture was then passed through a shallow layer of silica to remove tellurium by-products. The filtrate was dried over anhydrous magnesium sulfate and then concentrated under reduced pressure to afford a crude red solid. An analytically pure sample was obtained by recrystallisation from ethanol (12.40 g, 64%). $\delta_{^{125}Te}$(85.2 MHz, $CDCl_3$, 25 °C, PhTeTePh) 463.1 (s); $\delta_{^{123}Te}$(70.7 MHz, $CDCl_3$, 25 °C, PhTeTePh) 463.9 (s, $^1J_{(TeTe)}$ 129 Hz). ^{1}H NMR was in agreement with literature value.[10]

The other diaryl ditellurides were similarly prepared. ^{1}H NMR were in agreement with literature values.[10] The ^{125}Te NMR and ^{123}Te NMR data are as follows.

TolTeTeTol: $\delta_{^{125}Te}$(85.2 MHz, $CDCl_3$, 25 °C, PhTeTePh) 432.8 (s); $\delta_{^{123}Te}$(70.7 MHz, $CDCl_3$, 25 °C, PhTeTePh) 432.3 (s, $^1J_{TeTe}$787 Hz).

An-*p*TeTeAn-*p*: $\delta_{^{125}Te}$(85.2 MHz, $CDCl_3$, 25 °C, PhTeTePh) 461.3 (s); $\delta_{^{123}Te}$(70.7 MHz, $CDCl_3$, 25 °C, PhTeTePh) 461.0 (s, $^1J_{TeTe}$ 216 Hz).

An-*o*TeTeAn-*o*: $\delta_{^{125}Te}$(85.2 MHz, $CDCl_3$, 25 °C, PhTeTePh) 175.9 (s); $\delta_{^{123}Te}$(70.7 MHz, $CDCl_3$, 25 °C, PhTeTePh) 175.9 (s, $^1J_{TeTe}$ 279 Hz).

TPTeTeTP: $\delta_{^{125}Te}$(85.2 MHz, $CDCl_3$, 25 °C, PhTeTePh) 408.9 (s); $\delta_{^{123}Te}$(70.7 MHz, $CDCl_3$, 25 °C, PhTeTePh) 409.9 (s, $^1J_{TeTe}$ 198 Hz).

MesTeTeMes: $\delta_{^{125}Te}$(85.2 MHz, $CDCl_3$, 25 °C, PhTeTePh): 201.6 (s); $\delta_{^{123}Te}$(70.7 MHz, $CDCl_3$, 25 °C, PhTeTePh) 201.6 (s, $^1J_{TeTe}$ 532 Hz).

TipTeTeTip: $\delta_{^{125}Te}$(85.2 MHz, $CDCl_3$, 25 °C, PhTeTePh) 183.2 (s); $\delta_{^{123}Te}$(70.7 MHz, $CDCl_3$, 25 °C, PhTeTePh) 182.6 (s, $^1J_{TeTe}$ 650 Hz).

Acenaphthenes [Acenap(TeAr)$_2$]

5,6-*Bis*(aryltelluro)acenaphthenes **A3-A19** were prepared from 5,6-dibromoacenaphthene following a similar procedure used for the preparation of the parent phenyl derivative **A3**.[6]

For example, **5,6-*Bis*(phenyltelluro)acenaphthene [Acenap(TePh)$_2$] (A3)[6]:** A solution of 5,6-dibromoacenaphthene (1.01 g, 3.24 mmol) in diethyl ether (40 mL) was cooled to -10 – 0 °C on an ice-ethanol bath and to this a solution of TMEDA (1.4 mL, 9.34 mmol) was added. The mixture was allowed to stir for 15 min before a solution of *n*-butyllithium (2.5 M) in hexane (3.4 mL, 8.50 mmol) was added dropwise. The mixture was then stirred at -10 – 0 °C for 1 h, before being cooled to -78 °C. A solution of diphenyl ditelluride (2.84 g, 6.95 mmol) in diethyl ether (150 mL) was then added dropwise and the resulting solution was stirred at -78 °C for a further 2 h. The mixture was allowed to warm to room temperature and was then washed with 0.1 N sodium hydroxide (2 x 60 mL). The organic layer was dried over magnesium sulfate and concentrated under reduced pressure to afford a red solid. The crude product was washed with hexane affording a cream solid which was collected by filtration. An analytically pure sample was obtained from recrystallisation by diffusion of hexane into a saturated solution of the compound in dichloromethane (0.59 g, 32%). ^{1}H NMR was in agreement with literature values.[6]

5,6-*Bis*(4-fluorophenyltelluro)acenaphthene [Acenap(TeFP)$_2$] (A13): From 5,6-dibromoacenaphthene (1.17 g, 3.74 mmol), TMEDA (1.7 mL, 9.92 mmol), *n*-butyllithium (2.5 M) in hexane (3.6 mL, 8.97 mmol) and (FPTeTeFP) (3.33 g, 7.47 mmol) to yield a cream solid. An analytically pure sample was obtained from recrystallisation by diffusion of hexane into a saturated solution of the compound in dichloromethane (1.21 g, 54%); mp 140-142 °C; elemental analysis (Found: C, 48.3; H, 2.6 Calc. for $C_{24}H_{16}F_2Te_2$: C, 48.2; H, 2.7%); IR (KBr disk) ν_{max} cm^{-1} 3450w, 3056w, 2904w, 2831w, 1871w, 1621w, 1600w, 1573s, 1479vs, 1430s, 1404w, 1385w, 1321s, 1290w, 1219vs, 1156vs, 1096w, 1082w, 1047w, 1009s, 928w, 839s, 812vs, 747s, 698w,

599w, 567s, 507w, 494s, 411w, 322w; δ_H(300 MHz, $CDCl_3$, 25 °C, Me_4Si) 7.73 (2 H, d, $^3J_{HH}$ 7.2 Hz, Acenap 4,7-H), 7.60-7.50 (4 H, m, Te*Fp* 12,16,18,22-H), 6.94 (2 H, d, $^3J_{HH}$ 7.2 Hz, Acenap 3,8-H), 6.85-6.74 (4 H, m, Te*Fp* 13,15,19,21-H), 3.22 (4 H, s, 2 x CH_2); δ_C(75.5 MHz; $CDCl_3$; 25 °C; Me_4Si) 163.4 (q, $^1J_{CF}$ 247.9 Hz), 148.7(q), 142.3(s), 141.2(q), 140.4(d, $^3J_{CF}$ 7.6 Hz), 138.7(q), 121.6(s), 117.3(d, $^2J_{CF}$ 20.7 Hz), 116.7 (q, $^4J_{CF}$ 3.6 Hz), 113.5(q), 30.3 (s, 2 x *C*H_2); δ_F(282.3 MHz, $CDCl_3$, 25 °C, CCl_3F) -113.6 (s); $\delta_{125_{Te}}$(85.2 MHz, $CDCl_3$, 25 °C, PhTeTePh) 581.7 (s); $\delta_{123_{Te}}$(70.7 MHz, $CDCl_3$, 25 °C, PhTeTePh) 579.9 (s, $^4J_{TeTe}$ 1746 Hz); MS (ES^+): *m/z* 628.95 (100; M+OMe^+).

5,6-*Bis*(4-methylphenyltelluro)acenaphthene [Acenap(TeTol)$_2$] (A14): From 5,6-dibromoacenaphthene (0.36 g, 1.14 mmol), TMEDA (0.5 mL, 3.03 mmol), *n*-butyllithium (2.5 M) in hexane (1.1 mL, 2.74 mmol) and (TolTeTeTol) (1.01 g, 2.28 mmol) to yield a yellow solid. An analytically pure sample was obtained from recrystallisation by diffusion of hexane into a saturated solution of the compound in dichloromethane (0.26 g, 38%); mp 155-157 °C; elemental analysis (Found: C, 52.7; H, 3.8 Calc. for $C_{26}H_{22}Te_2$: C, 53.0; H, 3.8%); IR (KBr disk) ν_{max} cm^{-1} 3386w, 3009w, 2946w, 2911w, 2374w, 2345w, 2291w, 1905w, 1864w, 1800w, 1739w, 1640w, 1601w, 1586w, 1550w, 1525w, 1480s, 1443w, 1405w, 1385s, 1321s, 1299w, 1245w, 1231w, 1204w, 1179w, 1109w, 1093w, 1056w, 1037w, 1008s, 941w, 835s, 797vs, 695w, 673w, 630w, 600s, 571w, 489s, 475vs, 311w; δ_H(300 MHz, $CDCl_3$, 25 °C, Me_4Si) 7.78 (2 H, d, $^3J_{HH}$ 7.2 Hz, Acenap 4,7-H), 7.55-7.46 (4 H, m, Te*Tol* 12,16,18,22-H), 6.98-6.89 (6 H, m, Acenap 3,8-H, Te*Tol* 13,15,19,21-H), 3.23 (4 H, s, 2 x CH_2), 2.23 (6 H, s, 2 x CH_3); δ_C(75.5 MHz; $CDCl_3$; 25 °C; Me_4Si) 148.3(q), 142.2(s), 141.1(q), 138.5(s), 138.3(q), 130.9(s), 130.8(q), 121.5(s), 118.8(q), 113.7(q), 30.3(s, 2 x *C*H_2), 21.7 (s, 2 x *C*H_3); $\delta_{125_{Te}}$ (85.2 MHz, $CDCl_3$, 25 °C, PhTeTePh) 574.4 (s); $\delta_{123_{Te}}$ (70.7 MHz, $CDCl_3$, 25 °C, PhTeTePh) 574.1 (s, $^4J_{TeTe}$ 1781 Hz); MS (ES^+): *m/z* 606.98 (100%, M+OH^+).

5,6-*Bis*(4-methoxyphenyltelluro)acenaphthene [Acenap(TeAn-*p*)$_2$] (A15): From 5,6-dibromoacenaphthene (0.36 g, 1.16 mmol), TMEDA (0.5 mL, 3.09 mmol), *n*-butyllithium (2.5 M) in hexane (1.1 mL, 2.74 mmol) and (An-*p*TeTeAn-*p*) (1.10 g, 2.33 mmol) to yield a brown solid. An analytically pure sample was obtained from recrystallisation by diffusion of hexane into a saturated solution of the compound in dichloromethane (0.39 g, 53%); mp 140-142 °C (decomp.); elemental analysis (Found: C, 50.0; H, 3.6 Calc. for $C_{26}H_{22}O_2Te_2$: C, 50.2; H, 3.6%); IR (KBr disk) ν_{max} cm^{-1} 3407w, 3052w, 3009w, 2930w, 2832w, 2533w, 2370w, 2273w, 2035w, 1960w, 1884w, 1786w, 1760w, 1650w, 1581vs, 1562vs, 1484vs, 1454s, 1435s, 1397w, 1321s, 1285vs, 1246vs,

1172vs, 1097s, 1060s, 1027vs, 1000w, 929w, 840s, 820vs, 787s, 702w, 624w, 585s, 514s, 474w, 353w, 322w; δ_H(300 MHz, $CDCl_3$, 25 °C, Me_4Si)7.88 (2 H, d, $^3J_{HH}$ 7.3 Hz, Acenap 4,7-H), 7.75-7.66 (4 H, m, TeAn-*p* 12,16,18,22-H), 7.06 (2 H, d, $^3J_{HH}$ 7.3 Hz, Acenap 3,8-H), 6.84-6.77 (4 H, m, TeAn-*p* 13,15,19,21-H), 3.82 (6 H, s, 2 x TeAn-*p* O*C*H_3), 3.35 (4 H, s, 2 x *C*H_2); δ_C(75.5 MHz; $CDCl_3$; 25 °C; Me_4Si) 160.2(q), 148.2(q), 141.8(s), 141.2(q), 140.4(s), 138.7(q), 121.4(s), 115.9(s), 113.9(q), 112.1(q), 55.6 (s, 2 x O*C*H_3), 30.3 (s, 2 x *C*H_2); $\delta_{^{125}Te}$(85.2 MHz, $CDCl_3$, 25 °C, PhTeTePh) 567.8 (s); $\delta_{^{123}Te}$(70.7 MHz, $CDCl_3$, 25 °C, PhTeTePh) 567.8 (s, $^4J_{TeTe}$ 1835 Hz); MS (ES^+): *m/z* 652.99 (72%, M+OMe^+), 638.97 (100%, M+OH^+).

5,6-*Bis*(2-methoxyphenyltelluro)acenaphthene [Acenap(TeAn-*o*)$_2$] (A16): From 5,6-dibromoacenaphthene (1.32 g, 4.24 mmol), TMEDA (1.8 mL, 11.27 mmol), *n*-butyllithium (2.5 M) in hexane (4.1 mL, 10.19 mmol) and (An-*o*TeTeAn-*o*) (4.02 g, 8.48 mmol) to yield a cream solid. An analytically pure sample was obtained from recrystallisation by diffusion of hexane into a saturated solution of the compound in dichloromethane (1.03 g, 39%); mp 75-77 °C; elemental analysis (Found: C, 50.0; H, 3.6 Calc. for $C_{26}H_{22}O_2Te_2$: C, 50.2; H, 3.6%); IR (KBr disk) ν_{max} cm^{-1} 3055s, 3001s, 2926s, 2867w, 2831s, 2026w, 1880w, 1597w, 1571vs, 1466vs, 1429vs, 1324s, 1303s, 1271vs, 1238vs, 1177s, 1162s, 1118s, 1096s, 1051vs, 1019vs, 933w, 837s, 811s, 787s, 747vs, 645s, 614w, 599s, 568s, 534w, 482w, 442w, 428w; δ_H(300 MHz, $CDCl_3$, 25 °C, Me_4Si) 7.94 (2 H, d, $^3J_{HH}$ 7.2 Hz, Acenap 4,7-H), 7.31-7.20 (2 H, m, TeAn-*o* 15,22-H), 7.16-7.06 (4 H, m, TeAn-*o* 13,20-H, Acenap 3,8-H), 6.87 (2 H, dd, $^3J_{HH}$ 8.2 Hz, $^4J_{HH}$ 0.8 Hz, TeAn-*o* 16,23-H), 6.79-6.69 (2 H, m, TeAn-*o* 14,21-H), 3.86 (6 H, s, 2 x TeAn-*o* O*C*H_3), 3.42 (4 H, s, 2 x *C*H_2); δ_C(75.5 MHz; $CDCl_3$; 25 °C; Me_4Si) 159.7(q), 148.6(q), 143.2(s), 141.2(q), 140.2(q), 137.3(s), 129.4(s), 122.8(s), 121.6(s), 114.3(q), 112.2(q), 110.3(s), 56.4 (s, 2 x O*C*H_3), 30.4 (s, 2 x *C*H_2); $\delta_{^{125}Te}$(85.2 MHz, $CDCl_3$, 25 °C, PhTeTePh) 482.4 (s); $\delta_{^{123}Te}$(70.7 MHz, $CDCl_3$, 25 °C, PhTeTePh) 481.9 (s, $^4J_{TeTe}$ 1796 Hz); MS (ES^+): *m/z* 652.98 (100%, M+OMe^+).

5,6-*Bis*(4-tertbutylphenyltelluro)acenaphthene [Acenap(TeTP)$_2$] (A17): From 5,6-dibromoacenaphthene (1.10 g, 3.53 mmol), TMEDA (1.6 mL, 9.37 mmol), *n*-butyllithium (2.5 M) in hexane (3.4 mL, 8.48 mmol) and (TPTeTeTP) (3.68 g, 7.06 mmol) to yield a brown solid. An analytically pure sample was recrystallised by diffusion of hexane into a saturated solution of the compound in dichloromethane (1.56 g, 61%); mp 55-57 °C; elemental analysis (Found: C, 56.8; H,

5.0 Calc. for $C_{32}H_{34}Te_2$: C, 57.0; H, 5.1%); IR (KBr disk) ν_{max} cm^{-1} 3129w, 3049w, 2958vs, 2902vs, 2865s, 2588w, 2377w, 1901w, 1864w, 1784w, 1653w, 1587s, 1552w, 1483vs, 1460s, 1419s, 1391s, 1360s, 1325s, 1264s, 1230s, 1198s, 1109s, 1058s, 1006s, 939w, 905w, 884w, 838vs, 817vs, 771w, 720w, 677w, 644w, 598w, 545s, 482w, 460w, 404w, 346w; δ_H(300 MHz, $CDCl_3$, 25 °C, Me_4Si) 7.83 (2 H, d, $^3J_{HH}$ 7.3 Hz, Acenap 4,7-H), 7.54 (4 H, d, $^3J_{HH}$ 8.4 Hz, Te*Tp* 13,15,23,25-H), 7.34 (4 H, d, $^3J_{HH}$ 8.4 Hz, Te*Tp* 12,16,22,26-H), 6.96 (2 H, d, $^3J_{HH}$ 7.3 Hz, Acenap 3,8-H), 3.24 (4 H, s, 2 x CH_2), 1.21 (18 H, s, 2 x *p*-*t*Bu); δ_C(75.5 MHz; $CDCl_3$; 25 °C; Me_4Si) 151.4(q), 148.3(q), 142.4(s), 138.0(s), 136.8(q), 127.1(s), 127.0(q), 121.5(s), 119.0(q), 113.6(q), 31.7 (s, 2 x *p*-*tBu*), 30.3 (s, 2 x *C*H_2); $\delta_{125_{Te}}$(85.2 MHz, $CDCl_3$, 25 °C, PhTeTePh) 571.4 (s); $\delta_{123_{Te}}$(70.7 MHz, $CDCl_3$, 25 °C, PhTeTePh) 571.6 (s, $^4J_{TeTe}$ 1766 Hz); MS (ES^+): *m/z* 705.09 (100%, M+OMe^+).

5,6-*Bis*(2,4,6-trimethylphenyltelluro)acenaphthene [Acenap(TeMes)$_2$] (A18): From 5,6-dibromoacenaphthene (0.23 g, 0.96 mmol), TMEDA (0.4 mL, 2.55 mmol), *n*-butyllithium (2.5 M) in hexane (0.9 mL, 2.31 mmol) and (MesTeTeMes) (0.96 g, 1.92 mmol) to yield a yellow crystalline solid. An analytically pure sample was obtained from recrystallisation by diffusion of hexane into a saturated solution of the compound in dichloromethane (0.14 g, 22%); mp 125-127 °C (decomp.); elemental analysis (Found: C, 55.6; H, 4.6 Calc. for $C_{30}H_{30}Te_2$: C, 55.8; H, 4.7%); IR (KBr disk) ν_{max} cm^{-1} 3385w, 3018w, 2918s, 2855w, 2373w, 1889w, 1718s, 1699s, 1636w, 1594vs, 1565s, 1444vs, 1417s, 1377s, 1320s, 1292s, 1260w, 1209w, 1107w, 1029s, 949w, 922w, 843vs, 696vs, 612vs, 540w, 467s, 408w, 329w; δ_H(300 MHz, $CDCl_3$, 25 °C, Me_4Si) 7.33 (2 H, d, $^3J_{HH}$ 7.3 Hz, Acenap 4,7-H), 6.80 (4 H, s, Te*Mes* 13,15,18,22-H), 6.75 (2 H, d, $^3J_{HH}$ 7.3 Hz, Acenap 3,8-H), 3.12 (4 H, s, 2 x CH_2), 2.30 (12 H, s, 4 x CH_3), 2.15 (6 H, s, 2 x CH_3); δ_C(75.5 MHz; $CDCl_3$; 25 °C; Me_4Si) 147.2(q), 144.9(q), 144.6(q), 141.0(q), 139.2(q), 138.8(s), 128.2(s), 126.9(q), 121.5(s), 114.5(q), 30.2(s, 2 x *C*H_2), 29.2(s, 4 x *C*H_3), 21.5(s, 2 x *C*H_3); $\delta_{125_{Te}}$(85.2 MHz, $CDCl_3$, 25 °C, PhTeTePh) 363.3 (s); $\delta_{123_{Te}}$(70.7 MHz, $CDCl_3$, 25 °C, PhTeTePh) 362.9 (s, $^4J_{TeTe}$ 2819 Hz); MS (ES^+): *m/z* 677.06 (100%, M+OMe^+).

5,6-*Bis*(2,4,6-triisopropylphenyltelluro)acenaphthene [Acenap(TeTip)$_2$] (A19): From 5,6-dibromoacenaphthene (1.13 g, 3.63 mmol), TMEDA (1.5 mL, 9.55 mmol), *n*-butyllithium (2.5 M) in hexane (3.5 mL, 8.63 mmol) and (TipTeTeTip) (4.78 g, 7.23 mmol) to yield a brown solid. An analytically pure sample was recrystallised from hexane (1.60 g, 54%); mp 164-166 °C (decomp.);

elemental analysis (Found: C, 62.0; H, 6.4 Calc. for $C_{42}H_{52}Te_2$: C, 62.0; H, 6.7%); IR (KBr disk) ν_{max} cm^{-1} 3200w, 3040w, 2957vs, 2925vs, 2865s, 1853w, 1757w, 1589s, 1554s, 1458s, 1416s, 1380w, 1359s, 1322w, 1245w, 1231w, 1165w, 1153w, 1098s, 1066w, 1054s, 1006s, 933w, 873s, 834s, 811s, 742w, 646w, 599w, 511w, 460w, 398w; δ_H(300 MHz, $CDCl_3$, 25 °C, Me_4Si) 7.69 (2 H, d, $^3J_{HH}$ 7.3 Hz, Acenap 4,7-H), 7.27 (4 H, s, Te*Tip* 13,15,28,30-H), 7.07 (2 H, d, $^3J_{HH}$ 7.3 Hz, Acenap 3,8-H), 4.02 (4 H, septet, $^3J_{HH}$ 6.8 Hz, Te*Tip o*-$CHMe_2$), 3.39 (4 H, s, Acenap 2 x CH_2), 3.12 (2 H, septet, $^3J_{HH}$ 6.9 Hz, Te*Tip p*-$CHMe_2$), 1.49 (12 H, d, $^3J_{HH}$ 6.9 Hz, Te*Tip p*-$CHMe_2$), 1.31 (24 H, d, $^3J_{HH}$ 6.8 Hz, Te*Tip o*-$CHMe_2$); $\delta_{^{125}Te}$(85.2 MHz, $CDCl_3$, 25 °C, PhTeTePh) 316.0 (s); $\delta_{^{123}Te}$(70.7 MHz, $CDCl_3$, 25 °C, PhTeTePh) 315.8 (s, $^4J_{TeTe}$ 2727 Hz); MS (ES^+): *m/z* 847.23 (100%, $M+H_2OMe^+$), 831.23 (85%, $M+OH^+$), 814.23 (20%, M^+).

Acenaphthylenes [Acenapyl(TeAr)$_2$]

Compounds **Ay3**, and **Ay13-19** were prepared using a modification of the procedure described for the formation of 5,6-dibromoacenaphthylene by Mitchell and co-workers.[7,20]

For example **5,6-*Bis*(phenyltelluro)acenaphthylene [Acenapyl(TePh)$_2$] (Ay3)**: DDQ (0.30 g, 1.32 mmol) was added to a stirred solution of [Acenap(TePh)$_2$] (**A3**) (0.50 g, 0.89 mmol) in benzene (200 mL) and the mixture was heated under reflux for 24 h. After cooling to room temperature, pentane (200 mL) was added and the mixture was filtered. The filtrate was passed through a short column of silica with a pentane eluent. The resulting solution was then evaporated under reduced pressure to yield a crude red solid, which was recrystallized by evaporation of dichloromethane to give red crystals (0.22 g, 45%). ^{1}H NMR was in agreement with the literature value.[7]

The other acenaphthylenes were similarly prepared and the physical and spectral data are as follows.

5,6-*Bis*(4-fluorophenyltelluro)acenaphthylene [Acenapyl(TeFP)$_2$] (Ay13): From DDQ (1.5 g, 6.65 mmol) and [Acenap(TeFP)$_2$] (**A13**) (2.65 g, 4.43 mmol) to yield the title compound as an orange solid. An analytically pure sample was obtained from recrystallisation by diffusion of hexane into a saturated solution of the compound in dichloromethane (0.48 g, 18%); mp 150-152 °C; elemental analysis (Found: C, 48.2; H, 2.3 Calc. for $C_{24}H_{14}F_2Te_2$: C, 48.4; H, 2.4%); IR (KBr disk) ν_{max}

cm^{-1} 3054w, 2923w, 1573s, 1481vs, 1406s, 1385s, 1325w, 1294w, 1226vs, 1157vs, 1078s, 1050s, 1013s, 877w, 831vs, 820vs, 728w, 637s, 572w, 506s, 413w, 328w; δ_H(300 MHz, $CDCl_3$, 25 °C, Me_4Si) 7.71 (2 H, d, $^3J_{HH}$ 7.2 Hz, Acenapyl 4,7-H), 7.62-7.57 (4 H, m, Te*Fp* 12,16-H), 7.17 (2 H, d, $^3J_{HH}$ 7.2 Hz, Acenapyl 3,8-H), 6.86-6.79 (6 H, m, Te*Fp* 13-15-H), 6.75 (2 H, s, Acenapyl 9, 10-H); δ_C(75.5 MHz; $CDCl_3$; 25 °C; Me_4Si) 162.1 (q, $^1J_{CF}$ 248.7 Hz), 147.2(q), 140.1(q), 139.8(s), 139.3(d, $^3J_{CF}$ 7.6 Hz), 134.7(q), 129.6(q), 127.8(s), 123.8(s), 120.0(q), 116.1 (d, $^2J_{CF}$ 21.0 Hz), 114.3 (q, $^4J_{CF}$ 3.6 Hz); δ_F(282.3 MHz, $CDCl_3$, 25 °C, CCl_3F) -112.9 ppm (s); $\delta_{^{125}Te}$(85.2 MHz, $CDCl_3$, 25 °C, PhTeTePh) 610.3 ppm (s); $\delta_{^{123}Te}$(70.7 MHz, $CDCl_3$, 25°C, PhTeTePh) 610.1 ppm (s, $^4J_{TeTe}$ 1700 Hz); MS (ES^+): *m/z* 628.93 (100%, M+OMe^+), 614.92 (93%, M+OH^+).

5,6-*Bis*(4-methylphenyltelluro)acenaphthylene [Acenapyl(TeTol)$_2$] (Ay14): From DDQ (0.32 g, 1.41 mmol) and [Acenap(TeTol)$_2$] (**A14**) (0.56 g, 0.94 mmol) to yield a red solid, which was recrystallized by evaporation of a dichloromethane solution of the product to afford red crystals (0.13 g, 23%); mp 180-182 °C; elemental analysis (Found: C, 52.9; H, 3.4 Calc. for $C_{26}H_{20}Te_2$: C, 53.1; H, 3.4%); IR (KBr disk) ν_{max} cm^{-1} 3633vs, 3519vs, 3498vs, 2916w, 1263w, 2343w, 2106vs, 1561w, 1485s, 1405vs, 1325w, 1300w, 1206s, 1180s, 1077s, 1010vs, 876w, 836s, 800vs, 728w, 637w, 475vs; δ_H(300 MHz, $CDCl_3$, 25 °C, Me_4Si) 7.79 (2 H, d, $^3J_{HH}$ 7.2 Hz, Acenapyl 4,7-H), 7.59 (2 H, d, $^3J_{HH}$ 8.0, Te*Tol* 12,16-H), 7.22 (2 H, d, $^3J_{HH}$ 7.2, Acenapyl 3,8-H), 7.00 (2 H, d, $^3J_{HH}$ 7.6, Te*Tol* 13,15-H), 6.78 (2 H, s, Acenapyl 9, 10-H), 2.28 (6 H, s, Te*Tol* 2 x CH_3); δ_C(75.5 MHz; $CDCl_3$; 25 °C; Me_4Si) 141.3(q), 141.0(s), 139.3(q), 138.9(s), 138.7(q), 131.1(s), 129.2(q), 129.0(s), 125.2(s), 121.9(q), 117.8(q), 21.8 (s, *C*H_3); $\delta_{^{125}Te}$(85.2 MHz, $CDCl_3$, 25 °C, PhTeTePh) 605.7 (s); $\delta_{^{123}Te}$(70.7 MHz, $CDCl_3$, 25 °C, PhTeTePh) 605.9 (s, $^4J_{TeTe}$ 1785 Hz); MS (ES^+): *m/z* 618.98 (100%, M+OMe^+).

5,6-*Bis*(4-methylphenyltelluro)acenaphthylene [Acenapyl(TeAn-*p*)$_2$] (Ay15): From DDQ (0.72 g, 3.17 mmol) and [Acenap(TeAn-*p*)$_2$] (**A15**) (1.31 g, 2.10 mmol) to yield a red solid, which was recrystallized by evaporation of a dichloromethane solution of the product to afford red crystals (0.05 g, 4%); δ_H(300 MHz, $CDCl_3$, 25 °C, Me_4Si) 7.74 (2 H, d, $^3J_{HH}$ 7.0 Hz, Acenapyl 4,7-H), 7.64-7.58 (4 H, m, TeAn-*p*), 7.33 (2 H, d, $^3J_{HH}$ 7.0 Hz, Acenapyl 3, 8-H), 7.17 (2 H, s, Acenapyl 9, 10-H), 6.72-6.66 (4 H, m, TeAn-*p*), 3.69 (6 H, s, TeAn-*p* OCH_3); δ_C(75.5 MHz; $CDCl_3$; 25 °C; Me_4Si) 147.0(q), 141.0(s), 140.5(q), 138.8(s), 132.4(q), 129.6(s), 129.2(q), 125.2(s), 119.6(q), 116.0(s), 103.7(q), 55.6(s) (s, 2 x O*C*H_3); $\delta_{^{125}Te}$(85.2 MHz, $CDCl_3$, 25 °C, PhTeTePh) 540.9 (s).

5,6-*Bis*(4-tertbutylphenyltelluro)acenaphthylene [Acenapyl(TeTP)$_2$] (Ay17): From DDQ (1.06 g, 4.66 mmol) and [Acenap(TeTP)$_2$] (**A17**) (2.00 g, 2.97 mmol) to yield a red solid, which was recrystallized by evaporation of a chloroform solution of the product to afford red crystals (0.23 g, 12%); mp 187-189 °C; elemental analysis (Found: C, 57.1; H, 4.9 Calc. for $C_{32}H_{32}Te_2$: C, 57.2; H, 4.7%); IR (KBr disk) ν_{max} cm^{-1} 3050w, 2959vs, 2902s, 2866s, 1584w, 1483vs, 1459s, 1404vs, 1361s, 1325s, 1264s, 1200w, 1111s, 1076s, 1058s, 1007vs, 877w, 837vs, 818vs, 730s, 638s, 544s, 405w; δ_H(300 MHz, $CDCl_3$, 25 °C, Me_4Si) 7.83 (2 H, d, $^3J_{HH}$ 7.2 Hz, Acenapyl 4,7-H), 7.61 (2 H, d, $^3J_{HH}$ 8.3 Hz, Te*Tp* 12,16-H), 7.24-7.18 (4 H, m, Acenapyl 3,8-H, Te*Tp* 13,15-H), 6.77 (2 H, s, Acenapyl 9, 10-H), 1.22 (18 H, s, Te*Tp* 2 x *p*-*t*Bu); δ_C(75.5 MHz; $CDCl_3$; 25 °C; Me_4Si) 151.8(q), 141.2(q), 141.1(s), 138.5(s), 136.3(q), 130.9(q), 129.0(s), 127.3(s), 125.1(s), 121.7(q), 117.9(q), 35.0(q), 31.2 (s, 2 x *p*-^{t}*Bu*); $\delta_{125_{Te}}$(85.2 MHz, $CDCl_3$, 25 °C, PhTeTePh) 600.5 (s); $\delta_{123_{Te}}$(70.7 MHz, $CDCl_3$, 25 °C, PhTeTePh) 600.7 (s, $^4J_{TeTe}$ 1772 Hz); MS (ES$^+$): *m/z* 703.08 (100%, M+OMe$^+$).

5,6-*Bis*(2,4,6-trimethylphenyltelluro)acenaphthylene [Acenapyl(TeMes)$_2$] (Ay18): From DDQ (0.19 g, 0.83 mmol) and [Acenap(TeMes)$_2$] (**A18**) (0.36 g, 0.55 mmol) to yield a red solid which was recrystallized by evaporation of a dichloromethane solution of the product affording red crystals (0.03 g, 9%); mp 171-173 °C (decomp.); elemental analysis (Found: C, 55.9; H, 4.5 Calc. for $C_{30}H_{28}Te_2$: C, 56.0; H, 4.4%); IR (KBr disk) ν_{max} cm^{-1} 3493w, 3463w, 3397w, 3377w, 2964s, 2912w, 2367w, 2129vs, 1561w, 1485w, 1439w, 1405s, 1374w, 1291w, 1261vs, 1096vs, 1073vs, 1017vs, 873w, 836s, 801vs, 729w, 698w, 637w, 539w; δ_H(300 MHz, $CDCl_3$, 25 °C, Me_4Si) 7.31 (2 H, d, $^3J_{HH}$ 7.3 Hz, Acenapyl 4,7-H), 7.06 (2 H, d, $^3J_{HH}$ 7.2 Hz, Acenapyl 3,8-H), 6.90 (2 H, s, Te*Mes* 13,15-H), 6.70 (2 H, s, Acenapyl 9, 10-H), 2.42 (6 H, s, = Te*Mes* 2 x C*H*$_3$), 2.22 (3 H, s, Te*Mes* 1 x C*H*$_3$); δ_C(75.5 MHz; $CDCl_3$; 25 °C; Me_4Si) 143.9(q), 138.8(q), 138.(q), 135.0(s), 134.9(q), 129.7(q), 126.9(s), 126.8(s), 124.0(q), 123.8(s), 121.4(q), 27.8 (s, 2 x *C*H$_3$), 20.0 (s, *C*H$_3$); $\delta_{125_{Te}}$ (85.2 MHz, $CDCl_3$, 25 °C, PhTeTePh) 406.9 ppm (s); $\delta_{123_{Te}}$(70.7 MHz, $CDCl_3$, 25 °C, PhTeTePh) 406.3 (s, $^4J_{TeTe}$ 2956 Hz); MS (ES$^+$): *m/z* 690.94 (100%, M+Na$_2^+$), 674.96 (55%, M+OMe$^+$).

5,6-*Bis*(2,4,6-triisopropanylphenyltelluro)acenaphthylene [Acenapyl(TeTip)$_2$] (Ay19): From DDQ (0.66 g, 2.91 mmol) and [Acenap(TeTip)$_2$] (**A19**) (1.56 g, 1.92 mmol) to yield an orange solid which was recrystallized by evaporation of a dichloromethane solution of the product affording orange crystals (0.21 g, 14%); mp 75-77 °C; elemental analysis (Found: C, 62.25; H, 6.4 Calc. for

$C_{42}H_{52}Te_2$: C, 62.1; H, 6.45%); IR (KBr disk) ν_{max} cm^{-1} 3432s, 2958vs, 2866s, 1561w, 1460s, 1405vs, 1360w, 1312w, 1074w, 1007w, 876w, 838s, 638w; δ_H(300 MHz, $CDCl_3$, 25 °C, Me_4Si) 7.58 (2 H, d, $^3J_{HH}$ 7.3 Hz, Acenapyl 4,7-H), 7.32 (2 H, d, $^3J_{HH}$ 7.3 Hz, Acenapyl 3,8-H), 7.27 (4 H, s, Te*Tip* 13,15,28,30-H), 6.92 (2 H, s, Acenapyl 9,10-H), 3.09 (4 H, septet, $^3J_{HH}$ 6.7 Hz, Te*Tip o*-C*H*Me_2), 3.92 (4 H, septet, $^3J_{HH}$ 6.9 Hz, Te*Tip p*-C*H*Me_2), 1.45 (12 H, d, $^3J_{HH}$ 6.9 Hz, Te*Tip p*-C*H*Me_2), 1.30 (24 H, d, $^3J_{HH}$ 6.8 Hz, Te*Tip o*-C*H*Me_2); δ_C(75.5 MHz; $CDCl_3$; 25 °C; Me_4Si) 155.3(q), 151.4(q), 140.3(s), 137.4(q), 135.7(q), 131.5(q), 128.2(s), 126.6(q), 125.0(s), 124.0(q), 122.6(s), 40.3 (s, *o*-*C*HMe_2), 34.7(s, *p*-*C*HMe_2), 25.4(s, *p*-CH*Me*$_2$), 24.6 (s, *o*-CH*Me*$_2$); $\delta_{^{125}Te}$(85.2 MHz, $CDCl_3$, 25 °C, PhTeTePh) 353.7 (s); $\delta_{^{123}Te}$(70.7 MHz, $CDCl_3$, 25 °C, PhTeTePh) 353.3 (s, $^4J_{TeTe}$ 2958 Hz); MS (ES^+): *m/z* 833.19 (100%, $M+Na^+$).

References

[1] R. V. Parish, *NMR, NQR, EPR, and Mössbauer Spectroscopy in Inorganic Chemistry*, Ellis Horwood Limited, Chichester England, 1990.

[2] J. A. Iggo (Ed.), *NMR Spectroscopy in Inorganic Chemistry*, Oxford University Press Inc., New York, 1999.

[3] F. B. Mallory, *J. Am. Chem. Soc*., 1973, **95 (23)**, 7747; F. B Mallory, C. W. Mallory and M. C. Fedarko, *J. Am. Chem. Soc*., 1974, **96 (11)**, 3536; F. B Mallory, C. W. Mallory and R. M. Wendella, *J. Am. Chem. Soc*., 1975, **97 (16)**, 4770; F. B. Mallory, C. W. Mallory, K. E. Butler, M. B. Lewis, A. Q. Xia, E. D. Luzik Jr., L. E. Fredenburgh, M. M. Ramanjulu, Q. N. Van, M. M. Francl, D. A. Freed, C. C. Wray, C. Hann, M. Nerz-Stormes, P. J. Carroll and L. E. Chirlian, *J. Am. Chem. Soc*., 2000, **122**, 4108.

[4] M. Bühl, F. R. Knight, A. Křístková, I. M. Ondík, O. L. Malkina. R. A. M. Randall. A. M. Z. Slawin and J. D. Woollins, *Angew. Chem. Int. Ed*., 2013, **52**, 2495.

[5] M. W. Stanford, F. R. Knight, K. S. Athukorala Arachchige, P. Sanz Camacho, S. E. Ashbrook, M. Bühl, A. M. Z. Slawin and J. D. Woollins, *Dalton Trans*., 2014, **43(17)**, 6548.

[6] L. A. Aschenbach, F. R. Knight, R. A. M. Randall, D. B. Cordes, A. Baggott, M. Bühl, A. M. Z. Slawin and J. D. Woollins, *Dalton Trans.,* 2012, **41**, 3141.

[7] L. M. Diamond, F. R. Knight, K. S. Athukorala Arachchige, R. A. M. Randall, M. Bühl. A. M. Z. Slawin and J. D. Woollins, *Eur. J. Inorg. Chem*., 2014, **9**, 1512.

[8] S. Hayashi and W. Nakanishi, *Bull. Chem. Soc. Jpn*. 2008, **81**, 1605; H. Fujihara, H. Ishitani, Y. Takaguchi, N. Furukawa, *Chem. Lett.*, 1995, 571; F. R. Knight, A. L. Fuller, M. Bühl, A. M. Z. Slawin and J. D. Woollins, *Chem. Eur. J*., 2010, **16**, 7503.

[9] This series of naphthalene compounds (unpublished) were prepared by another member of the Woollins group as part of this study.

[10] M. Oba, Y. Okada, M. Endo, K. Tanaka, K. Nishiyama, S. Shimada and W. Ando, *Inorg. Chem*., 2010, **49**, 10680.

[11] C. A. Coulson, R. Daudel and J. M. Robertson, *Proc. R. Soc. London, Ser. A*, 1951, **207**, 306; D. W. Cruickshank, *Acta Crystallogr.,* 1957, **10**, 504; C. P. Brock and J. D. Dunitz, *Acta Crystallogr., Sect. B: Struct. Crystallogr. Cryst. Chem.,* 1982, **38**, 2218; J. Oddershede and S. Larsen, *J. Phys. Chem. A,* 2004, **108**, 1057.

[12] A. C. Hazell, R. G. Hazell, L. Norskov-Lauritsen, C. E. Briant and D. W. Jones, *Acta Crystallogr., Sect. C: Cryst. Struct. Commun.,* 1986, **42**, 690.

[13] A. D. Rae, R. A. Wood and T. R. Welberry, *J. Chem. Soc., Perkin Trans. 2,* 1985, **3**, 451.

[14] A. Bondi, *J. Phys. Chem.,* 1964, **68**, 441.

[15] All images of molecular structures were generated using OLEX2: O. V. Dolomanov, L. J. Bourhis, R. J. Gildea, J. A. K. Howard and H. Puschmann, *J. Appl. Cryst*., 2009, **42**, 339.

[16] W. Nakanishi, S. Hayashi and S. Toyota, *Chem. Commun.,* 1996, 371; W. Nakanishi, S. Hayashi, A. Sakaue, G. Ono and Y. Kawada, *J. Am. Chem. Soc.,* 1998, **120**, 3635; W. Nakanishi, S. Hayashi and S. Toyota, *J. Org. Chem.,* 1998, **63**, 8790; S. Hayashi and W. Nakanishi, *J. Org. Chem.,* 1999, **64**, 6688; W. Nakanishi, S. Hayashi and T. Uehara, *J. Phys. Chem.,* 1999, **103**, 9906; W. Nakanishi and S. Hayashi, *Phosphorus, Sulfur, Silicon Relat. Elem.,* 2002, **177**, 1833; S. Hayashi and W. Nakanishi, *J. Org. Chem.,* 2002, **67**, 38; S. Hayashi and W. Nakanishi, *Bull. Chem. Soc. Jpn.,* 2008, **81**, 1605.

[17] P. Nagy, D. Szabó, I. Kapovits, Á. Kucsman, G. Argay and A. Kálmán, *J. Mol. Struct.,* 2002, **606**, 61.

[18] W. Nakanishi and S. Hayashi, *Chem. Eur. J.*, 2008, **14**, 5645.

[19] W. D. Neudorff, D. Lentz, M. Anibarro and A. Dieter Schlüter, *Chem. Eur. J.*, 2003, **9**, 2745.

[20] R. H. Mitchell, M. Chaudhary, R. V. Williams, R. Fyles, J. Gibson, M. J. Ashwood-Smith and A. J. Fry, *Can. J. Chem.,* 1992, **70**, 1015.

Chapter 6

Platinum complexes of acenaphtho[5,6-*cd*][1,2]dichalcogenoles

Introduction

In 2004 the Woollins group reported the synthesis of a series of platinum *bis*(phosphine) complexes constructed from dichalcogen-derivatised naphthalene, acenaphthene and phenanthrene ligands.[1] These complexes were prepared through two routes; a metathetical reaction where the parent ligand was reduced with lithium triethylborohydride to form the dilithio-species, which was then reacted with *cis*-$[Pt(PR_3)_2Cl_2]$ (where R = Ph or Me) and an oxidative addition reaction of the corresponding ligand with the zero-valent platinum species $[Pt(PPh_3)_4]$ or $[Pt(C_2H_4)(PMe_3)_2]$.[1]

The group furthered this study in 2013 by preparing and fully characterising six platinum *bis*(phosphine) complexes constructed from 5,6-dihydroacenaphtho[5,6-*cd*]-1,2-dithiole (**AS_2**) and 5,6-dihydroacenaphtho[5,6-*cd*]-1,2-diselenole (**ASe_2**).[2] These complexes were prepared through metathetical reaction of the dilithio salt of the parent acenaphthene, with a suspension of *cis*-$[Pt(PR_3)_2Cl_2]$ (where R = Ph_3, Ph_2Me, $PhMe_2$).

The aim of the work reported in this chapter was to build on the aforementioned studies by first synthesising and fully characterising acenaphtho[5,6-*cd*][1,2]dithiole (**AyS_2**) and acenaphtho[5,6-*cd*][1,2]diselenole (**$AySe_2$**) and then reacting them with platinum *bis*(phosphines) to form a series of complexes.

Acenaphtho[5,6-*cd*][1,2]dithiole (**AyS_2**) and acenaphtho[5,6-*cd*][1,2]diselenole (**$AySe_2$**) were previously prepared by Chiang and Meinwald in 1980 however, they had not been fully characterised. They used 5,6-dibromoacenaphthylene to prepare the intermediate 5,6-dilithioacenaphthylene, which they then used to synthesise the dichalcogen-bridged acenaphthylenes (Scheme 1); acenaphtho[5,6-*cd*]-1,2-dithiole, acenaphtho[5,6-*cd*]-1,2-diselenole and acenaphtho[5,6-*cd*]-1,2-ditellurole.[3]

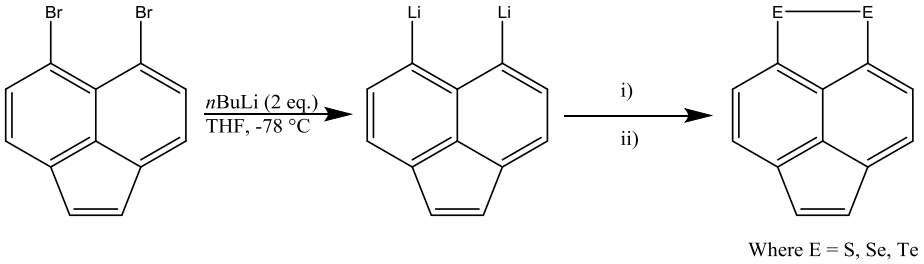

Scheme 1 Synthetic route to dichalcogen-bridged acenaphthylenes:
i) E, -78 °C (-30 °C for Te); 25% $C_2H_4O_2$ in THF; ii) r.t., [O], 1 h.[3]

Results and Discussion

Compounds **AyS_2, $AySe_2$** and **Ay20-Ay27** (Figures 1 and 2) were synthesised and crystal structures were determined for **AyS_2**, **Ay20**,[4] **Ay22** and **Ay25**.

Initial attempts to prepare the ligands acenaphtho[5,6-*cd*]-1,2-dithiole (**AyS_2**) and acenaphtho[5,6-*cd*]-1,2-diselenole (**$AySe_2$**) using Chiang and Meinwald's[3] original method resulted in complex mixtures which could not be purified. Therefore, **AyS_2** and **$AySe_2$** were prepared following a modification of the original synthesis (Scheme 2).[3]

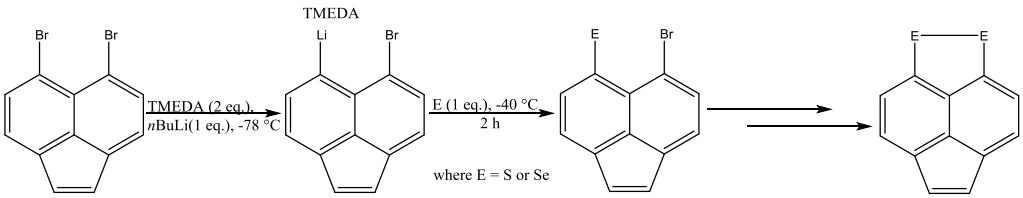

Scheme 2 Synthetic route to acenaphtho[5,6-*cd*]-1,2-dithiole (**AyS_2**)
and acenaphtho[5,6-*cd*]-1,2-diselenole (**$AySe_2$**).

Two equivalents of TMEDA was added to a solution of 5,6-dibromoacenaphthylene in diethyl ether at -78 °C. One equivalent of *n*BuLi was added dropwise and the solution was left to stir for fifteen minutes. One equivalent of the appropriate chalcogen was added, the temperature was raised to -40 °C and the reaction left to stir for two hours. A further one equivalent of *n*BuLi and chalcogen were added to replace the remaining bromine and then a further equivalent of chalcogen was added. After mild oxidation in air and purification the dichalcogen bridged ligands

acenaphtho[5,6-*cd*]-1,2-dithiole (**AyS_2**) and acenaphtho[5,6-*cd*]-1,2-diselenole (**$AySe_2$**) were collected in yields of 5% and 26%, respectively.

The chalcogen-chalcogen bonds in **AyS_2** and **$AySe_2$** were reduced with two equivalents of lithium triethylborohydride to form the dilithio-species, which was then added to a suspension of the appropriate *cis*-dichloro*bis*(phosphine)platinum in THF resulting in the formation of the platinum complexes [Pt(5,6-AcenapylE_2)(PR_3)$_2$] (Scheme 3).

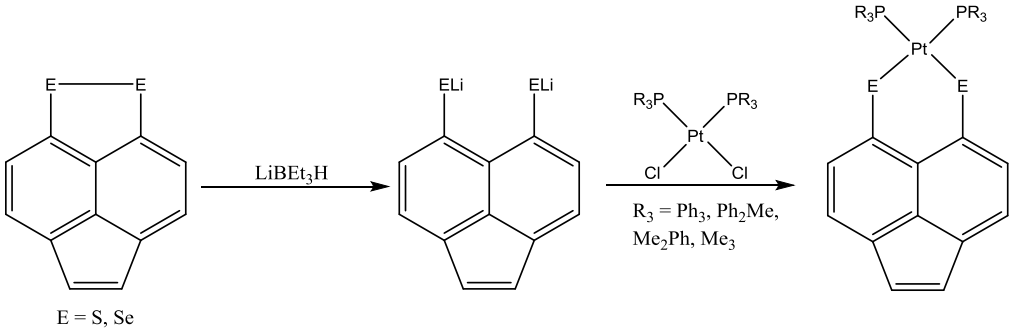

Scheme 3 Reaction route for synthesis of the platinum complexes [Pt(5,6-AcenapylE_2)(PR_3)$_2$].

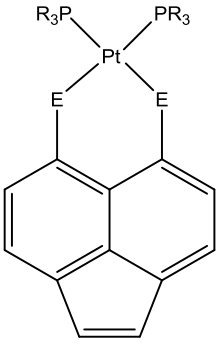

	Ay20	Ay21	Ay22	Ay23	Ay25	Ay26	Ay27
E	S	S	S	S	Se	Se	Se
R_3	Ph_3	Ph_2Me	$PhMe_2$	Me_3	Ph_3	Ph_2Me	$PhMe_2$

Figure 1 The acenaphthylene platinum complexes **Ay20-Ay23** and **Ay25-Ay27**.

The dilithio-species of **AyS_2** and **$AySe_2$** were also reacted with (1,5-cyclooctadiene)platinum(II) dichloride. This reaction was successful with **AyS_2** resulting in the platinum complex [Pt(5,6-AcenapylS_2)(COD)] (**Ay24**).

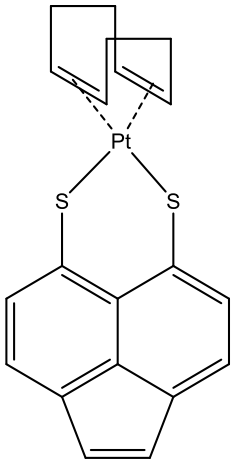

Figure 2 The acenaphthylene platinum complex **Ay24**.

The $^{31}P\{^{1}H\}$ NMR ($CDCl_3$) spectra for the sulfur complexes **Ay20**-**Ay23** (Table 1) all display a singlet with appropriate platinum satellites.

Table 1 $^{31}P\{^{1}H\}$ NMR data for complexes **Ay20-Ay23**.

	Chemical Shifts [ppm]	**Coupling Constants [Hz]**
Product	**$\delta(^{31}P)$**	**^{1}J(P-Pt)**
Ay20	23.9	2953
Ay21	3.5	2880
Ay22	-14.5	2819
Ay23	-24.7	2768

The $^{31}P\{^{1}H\}$ NMR ($CDCl_3$) spectra for the selenium complexes **Ay25**-**Ay27** (Table 2) all displaya singlet with ^{77}Se satellites. The low abundance of the NMR active isotope ^{77}Se (7.6%)[5] means that when two selenium atoms are present in a molecule the probability of both being NMR active is very low. Therefore in **Ay25**-**Ay27** only one selenium atom is effectively NMR active, the molecule is no longer symmetrical, creating two magnetically inequivalent ^{31}P environments.[2] The two ^{31}P atoms (AA') can therefore align in either a *cis* or *trans* configuration to the NMR active ^{77}Se isotope (X), giving AA'X spin system for satellite part of the spectrum. The effects of this are clearly observed in the $^{31}P\{^{1}H\}$ NMR ($CDCl_3$) spectrum for the acenaphthene platinum complex $[Pt(AcenapSe_2)(PPhMe_2)_2]$[2] (Figure 3).

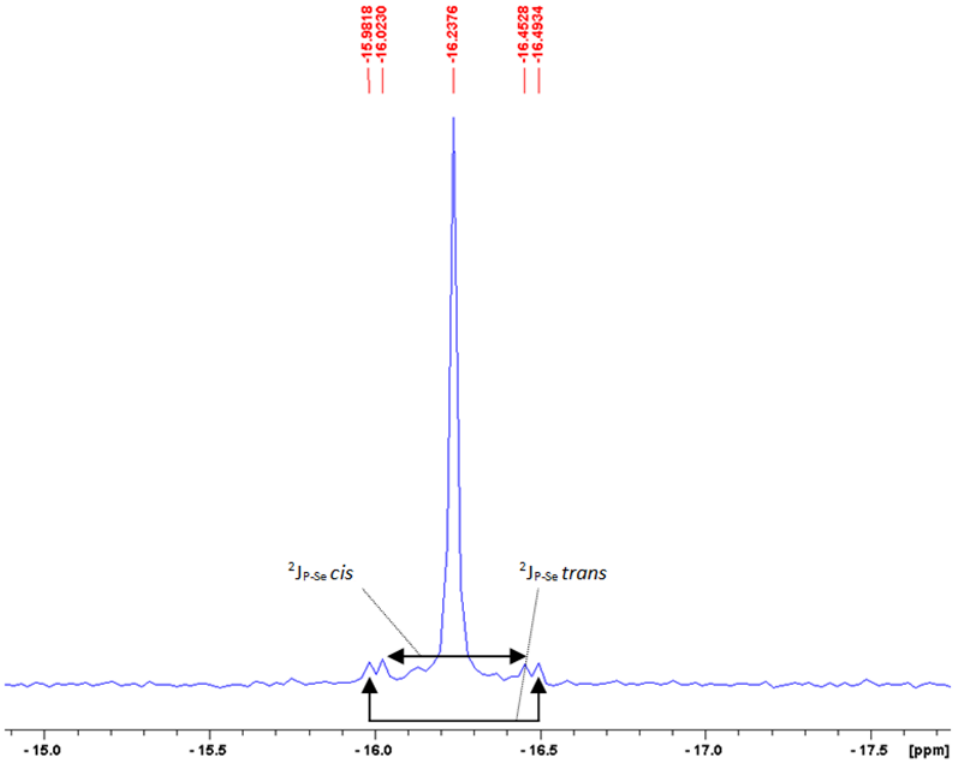

Figure 3 $^{31}P\{^1H\}$ NMR ($CDCl_3$) spectrum for [Pt(AcenapSe$_2$)(PPhMe$_2$)$_2$] showing the *cis* and *trans* satellites with $^2J_{PSe}$ coupling.[2]

In the previously reported spectrum for [Pt(AcenapSe$_2$)(PPhMe$_2$)$_2$] $^2J_{PSe}$ coupling is observed for the *cis* and the *trans* configurations with values of 47 Hz and 56 Hz, respectively.[2] This is not observed in the $^{31}P\{^1H\}$ NMR ($CDCl_3$) spectra for **Ay25**-**Ay27** (Figure 4). In these spectra one set of satellites is observed for the $^2J_{PSe}$ coupling, this is due to the *cis* and *trans* satellites having coupling of similar magnitude which leads to overlap of the signals and therefore they cannot be fully assigned. The *cis* and *trans* satellites overlapping to give one ^{31}P environment is confirmed by measuring the integral peak intensity of ^{31}P:^{77}Se.

Table 2 $^{31}P\{^{1}H\}$ NMR data for complexes **Ay25-Ay27**.

	Chemical Shifts [ppm]	Coupling Constants [Hz]	
Product	**$\delta(^{31}P)$**	**^{1}J(P-Pt)**	**^{2}J(P-Se)**
Ay25	20.2	3014	54
Ay26	0.6	2932	54
Ay27	-17.6	2873	52

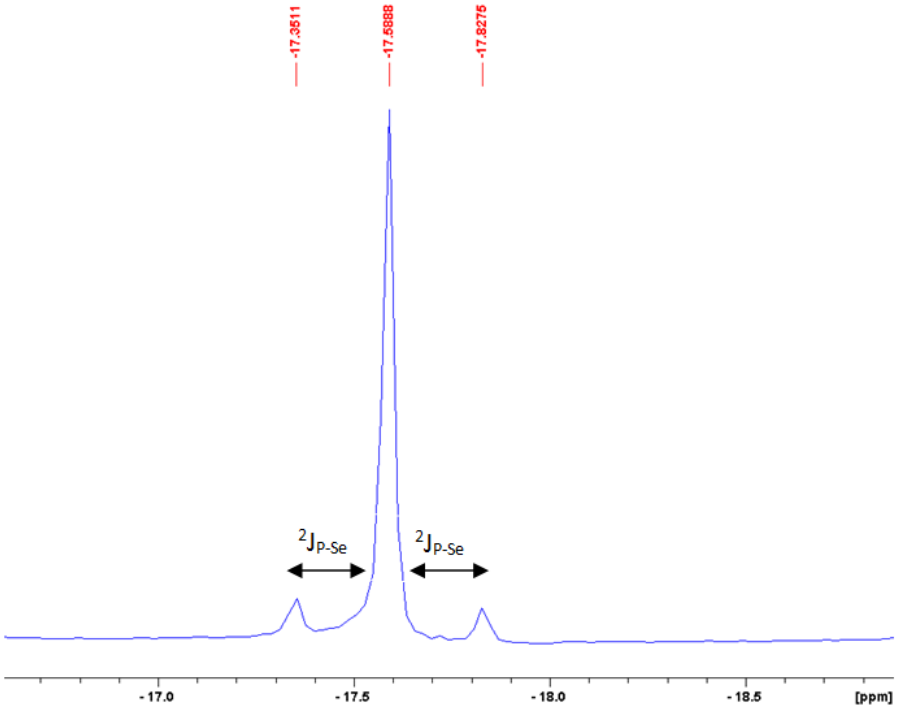

Figure 4 $^{31}P\{^{1}H\}$ NMR ($CDCl_3$) spectrum for **Ay27** showing the overlapping *cis* and *trans* satellites with $^{2}J_{PSe}$ coupling.

Previously it has been observed that higher $^{1}J(^{31}P\text{-}^{195}Pt)$ coupling constants exist for more electron withdrawing R groups, with $^{1}J(^{31}P\text{-}^{195}Pt)$ decreasing as phenyl groups are replaced with electron donating methyl groups.[1,2,6] It can be seen for **Ay20**-**Ay23** (Table 1) and **Ay25**-**Ay27** (Table 2) that there is a steady decrease in value for $^{1}J(^{31}P\text{-}^{195}Pt)$ coupling constant as the phenyl groups are replaced by methyl groups, as expected.

With regards to the ^{77}Se NMR spectra of **Ay25**-**Ay27** we would expect to observe a doublet of doublets due to the ^{77}Se atom being coupled to two inequivalent ^{31}P nuclei. However, from the ^{31}P NMR spectra we know that the $^{2}J_{SeP}$ *cis* and *trans* satellites are of similar magnitude and indistinguishable. Therefore, in the ^{77}Se NMR spectra (Figure 5) the two central peaks of the expected doublet of doublets overlap and a pseudo triplet is observed. The peak intensity of the pseudo triplet is again consistent with coupling to two ^{31}P atoms. In addition supplementary $^{1}J_{SePt}$ satellites are observed, also displaying a similar pseudo triplet pattern. The values seen for the $^{1}J_{SePt}$ satellites are similar to those observed by other groups.[7]

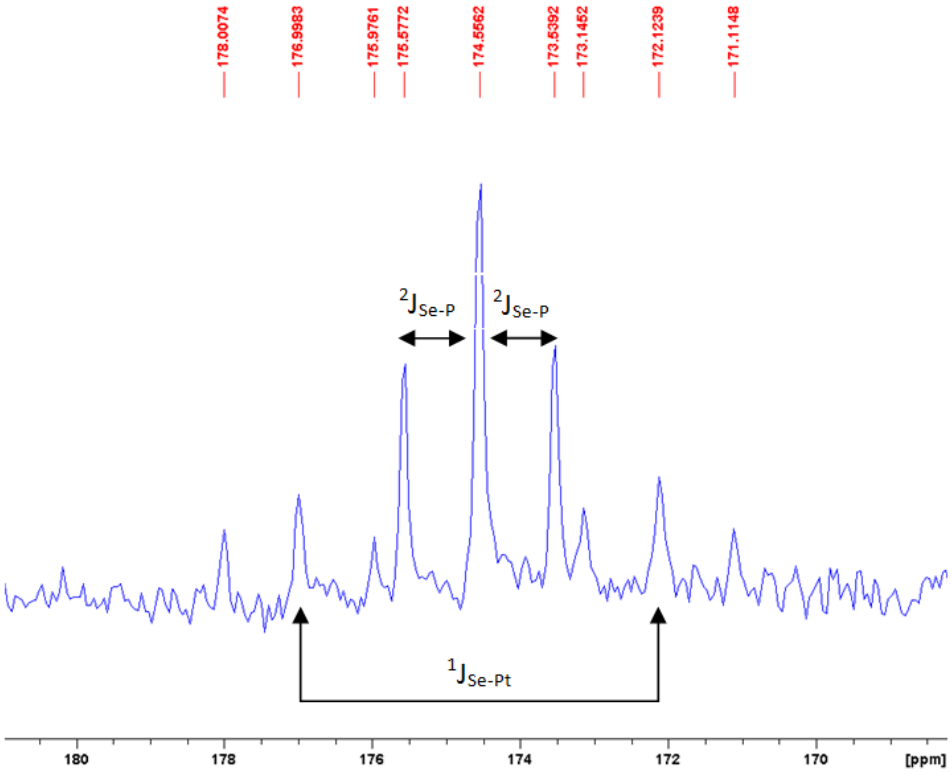

Figure 5 ^{77}Se NMR ($CDCl_3$) spectrum for **Ay27** displaying the pseudo triplet pattern.

Table 3 ^{77}Se NMR data for complexes **Ay25-Ay27**.

	Chemical Shifts [ppm]	**Coupling Constants [Hz]**	
Product	***δ*(^{77}Se)**	**^{2}*J*(Se-P)**	**^{1}*J*(Se-Pt)**
Ay25	227.6	55	178
Ay26	204.5	55	210
Ay27	174.6	53	251

As previously discussed, a steady decrease in magnitude is observed in the $^{1}J(^{31}P\text{-}^{195}Pt)$ coupling constant as the phenyl groups are replaced by methyl groups. In contrast, a steady increase in magnitude is observed in the $^{1}J(^{77}Se\text{-}^{195}Pt)$ coupling constant (Table 4). These opposing trends are due to a combination of factors. A decrease in electronegativity of the alkyl groups occurs each time a phenyl is replaced by a methyl. The platinum centre becomes more electron rich as a consequence of the alkyl groups becoming more electropositive, this causes a decrease in the *s*-character of the P-Pt bond. This implies the lone pair on the phosphorus is less tightly bound and subsequently strengthens the P-Pt bond. The *s*-character of the P-Pt bond decreases because as the platinum becomes more electron rich as methyl groups are added the P-C_R bond adopts more *s*-character to stabilise the local negative charge.[8]

In addition, the increase in $^{1}J(^{77}Se\text{-}^{195}Pt)$ coupling constants can be partially attributed to phenyl groups being greater π-acceptors than methyl groups. When π-acceptors are in the *trans* position they reduce the magnitude of the coupling constant between the metal and the ligand i.e. platinum and selenium. As phenyl is replaced with the poorer π-acceptor methyl the coupling constant increases. However, the *trans* influence is not fully responsible for the increase we observe in coupling constant, the *s*-character in the Pt-Se bond and the subsequent *s*-electron density at the platinum centre is also responsible.[8]

Table 4 A comparison of the coupling constants observed in complexes **Ay25-Ay27**.

	Coupling Constants [Hz]	
Product	**^{1}J(P-Pt)**	**^{1}J(Se-Pt)**
Ay25	3014	178
Ay26	2932	210
Ay27	2873	251

The reaction of **$AySe_2$** with *cis*-dichloro*bis*(trimethylphosphine)platinum yielded unusual results. The ^{31}P NMR spectra of the collected solid displayed no peaks. However, ^{31}P NMR spectra of the filtrate displayed the expected pattern that was observed in **Ay25**-**Ay27**; with a single phosphorus peak at δ -11.5 ppm and appropriate platinum and selenium satellites. The $^{2}J(^{31}P, ^{77}Se)$ of 56 Hz was consistent with that seen in **Ay25**-**Ay27**, but the $^{1}J(^{31}P\text{-}^{195}Pt)$ of 4359 Hz was significantly higher than expected. In the analogous sulfur compounds **Ay20**-**Ay23**, there is a steady decrease in magnitude of the $^{1}J(^{31}P\text{-}^{195}Pt)$ coupling constant as the phenyl groups are replaced by methyl groups with **Ay23** having the lowest value of 2768 Hz. The same trend is observed in **Ay25**-**Ay27**, therefore we would expect the coupling constant of the trimethylphosphine derivative to be less than that of **Ay27** (2873 Hz). Further insight using ^{77}Se NMR could not be obtained due to poor yield and solubility.

X-ray Investigations

Single crystals were obtained for **AyS_2** by cooling a hot hexane solution to -35 °C overnight. The molecular structure of **AyS_2** is shown in Figure 7. Although **AyS_2** is a known compound with published characterisation data,[3] no crystal data have been published and therefore I have included a brief discussion below.

The crystal structure of **AyS_2** has a *peri* sulfur-sulfur bond distance of 2.084(2) Å. This is much shorter than the *peri*-distance in unsubstituted acenaphthylene of *ca.* 2.73 Å[9]; this is expected as a bond has formed between the *peri*-substituents. However, the S-S bond does fall within the 'normal' length for a compound of this type with typical values of *ca.* 2.05 Å being reported.[10] The *peri*-angles in acenaphthylene are 120.3(8)°, 127.8(6)° and 120.3(8)° with the sum being 368.4°.[9] In **AyS_2** the sum of the bay angles is 348.32(28)° with a resulting negative splay angle of -11.68°; this is less than the sum in ideal acenaphthylene confirming a favourable interaction is occurring

between the *peri*-atoms resulting in the formation of a *peri*-bond. Minor out-of-plane distortion is observed with both sulfur atoms sitting 0.02(1) Å and 0.09(1) Å away from the naphthyl plane. This is accompanied by a minor distortion to the geometry of the 'naphthalene' framework with torsion angles deviating by 1.88° and 2.20° from the 'ideal' 180°.

It is not surprising that **AyS_2** displays similar characteristics to naphtha[1,8-*cd*][1,2]dithiole (**$NapS_2$**)[11] and 5,6-dihydroacenaphtho[5,6-*cd*]-1,2-dithiole (**$AcenapS_2$**).[2] The *peri*-distances observed in all three compounds are statistically equivalent with values of 2.0879(8) Å,[11] 2.1025(19) Å[2] and 2.084(2) Å for **$NapS_2$**, **$AcenapS_2$** and **AyS_2**, respectively. The C(4)-C(5)-C(6) angle in **$NapS_2$** is 125°,[11] the addition of the ethane/ethene bridge in **$AcenapS_2$**/**AyS_2** causes compression of this angle, with values of 114.9(5)°[2] and 116.30(16)°, respectively. One would expect compression of the C(4)-C(5)-C(6) angle to cause an expansion in the C(1)-C(10)-C(9) angle however, this is not strictly the case. An increase in the C(1)-C(10)-C(9) angle is seen between **$NapS_2$** and **$AcenapS_2$** (118.65(16)° to 120.2(5)°)[2,11], but a decrease then occurs with **AyS_2** having a C(1)-C(10)-C(9) angle of 118.78(16)°. This is reflected in the splay angles with values of -11.21°, -11.8° and -11.68° for **$NapS_2$**, **$AcenapS_2$** and **AyS_2**, respectively. All three ligands have similar out-of-plane displacement with the sulfur atoms sitting *ca.* 0.02 Å from the naphthyl plane. **AyS_2** has the largest, although still minor, naphthalene framework distortion with torsion angles deviating from 180° by 1.88° and 2.20° (*cf*. **$NapS_2$** and **$AcenapS_2$** *ca*. 0.40°).[2,11]

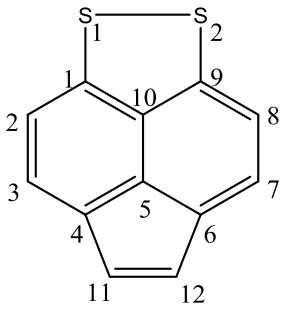

Figure 6 X-ray crystallography numbering scheme for **AyS_2**.

Table 5 Selected Bond Lengths [Å] and Angles [°] of **AyS_2.**

Compound	**AyS_2**
X-ray code	LMD133n
E, E'	S, S
Peri-region distance	
E(1)-E(2)	**2.084(2)**
Bond lengths	
C(1)-E(1)	1.671(2)
C(9)-E(2)	1.684(2)
C(1)-C(2)	1.392(3)
C(2)-C(3)	1.406(3)
C(3)-C(4)	1.376(3)
C(4)-C(5)	1.409(3)
C(5)-C(10)	1.369(2)
C(5)-C(6)	1.408(3)
C(6)-C(7)	1.389(3)
C(7)-C(8)	1.409(3)
C(8)-C(9)	1.383(3)
C(9)-C(10)	1.410(3)
C(1)-C(10)	1.407(3)
C(11)-C(12)	1.386(15)
Peri-region bond angles	
E(1)-C(1)-C(10)	113.88(16)
C(1)-C(10)-C(9)	118.78(16)
E(2)-C(9)-C(10)	115.66(16)
∑ of bay angles	**348.32(28)**
Splay angle[a]	-11.68
Bond angles	
C(4)-C(5)-C(6)	116.30(16)
E(2)-E(1)-C(1)	97.26(12)
E(1)-E(2)-C(9)	94.41(10)
Out of plane displacement	
E(1)	+0.090(1)
E(2)	+0.020(1)
Central naphthalene ring torsion angles	
C(6)-C(5)-C(10)-C(1)	178.12(15)
C(4)-C(5)-C(10)-C(9)	-177.80(16)

[a]Splay angle: ∑ of the three bay region angles - 360.

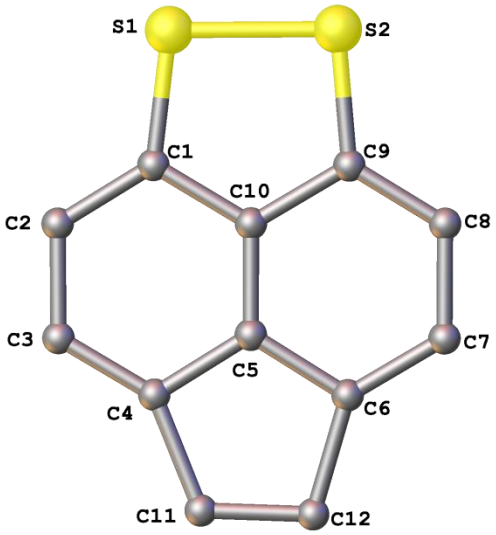

Figure 7 The molecular structure of **AyS_2** with H atoms omitted for clarity.[12]

Single crystals were obtained for **Ay20** by evaporation of a saturated solution of the compound in chloroform. **Ay20** crystallises with two dichloromethane molecules per platinum molecule. Single crystals of **Ay22** and **Ay25** were obtained by diffusion of hexane into a saturated solution of the compound in diethylether. The molecular structures of **Ay20**, **Ay22** and **Ay25** are shown in Figures 11, 12 and 16, respectively. In the three complexes, the dichalcogenole acenaphthylene acts as a bidentate ligand, coordinating to the platinum *via* the two chalcogen atoms to form a six-membered PtC_3E_2 chelate ring. A distorted square planar geometry is adopted by the platinum centre in each case, with angles deviating from the ideal (90°).

As expected the *peri*-distances in **Ay20** and **Ay22** have been elongated due to the breaking of the sulfur-sulfur bond and insertion of the platinum. The non-bonded sulfur-sulfur distance being 3.343(3) Å for **Ay20** and 3.431(11) Å for **Ay22** compared to the bonded distance of 2.084(2) Å in the free ligand **AyS_2**. However, the *peri*-distance in the two complexes is still shorter than the sum of the van der Waals radii for two sulfur atoms by 5-7%. The angles of the bay region increase as a consequence of the increase in *peri*-distance, with positive splay angles of 20.5° and 26° being seen for **Ay20** and **Ay22** respectively. This is significantly greater than the negative splay angle of -11.68° that is observed in **AyS_2** due to the presence of the sulfur-sulfur bridge.

Ay20 displays much greater distortion of the naphthalene skeleton than **Ay22**. The non-bonded *peri*-distance and the splay angle in **Ay22** are larger than those in **Ay20** creating a more relaxed geometry around the platinum centre which can accommodate the dimethylphenylphosphine groups without causing great distortion to the naphthalene backbone. In **AyS_2** the sulfur atoms lie 0.09(1) Å and 0.02(1) Å above the naphthyl plane. **Ay20** displays significant out-of-plane distortion in comparison to the ligand; one sulfur atom sits 0.525(1) Å below the naphthyl plane and the other sits 0.449(1) Å above the plane. **Ay22** shows less out-of-plane distortion than **Ay20**, with one sulfur atom lying 0.105(1) Å above the naphthyl plane and the other lying on the plane. The torsion angles also deviate from the free ligand by *ca.* 1-7.3° with **Ay20** showing the greatest buckling of the naphathalene carbon framework. Greater distortion is observed in **Ay20** due to the bulky triphenylphosphine groups making it more difficult for the complex to maintain a square planar environment around the platinum centre when compared to the smaller dimethylphenylphosphine groups.

Changing the alkyl groups from triphenylphosphines to dimethylphenylphosphines has a minor effect on the geometry of the corresponding acenaphthene complexes, [Pt(AcenapS_2)(PPh_3)$_2$] and [Pt(AcenapS_2)($PPhMe_2$)$_2$].[2] Unfortunately a comparison with the equivalent naphthalene complexes is not possible, as [Pt(NapS_2)(PPh_3)$_2$] could not be crystallised and [Pt(NapS_2)($PPhMe_2$)$_2$] has not been prepared.[1]

In **Ay20** a weak π···π interaction is observed with two phenyl rings, one from each PPh_3 group, adopting a face-to-face alignment (Figure 10) with a Cg(C13-C18)····Cg(C31-C36) distance of 3.620(1) Å. This value is comparable with that found in the acenaphthene complex [Pt(AcenapS_2)(Pt(PPh_3)$_2$] which has a Cg(C25-C30)····Cg(C31-C36) distance of 3.765(1) Å.[2] However, in **Ay22** the intramolecular interaction observed is a C-H····π interaction, it is now a phenyl ring, from one PPh_2Me group, that is interacting with a methyl group, from the other PPh_2Me group (Figure 11) giving a C28-H28B····Cg(C13-C18) distance of 2.847(1) Å. Again, this value is comparable with [Pt(AcenapS_2)($PPhMe_2$)$_2$] which has a C14-H14····Cg(C23-C28) distance of 2.61(1) Å.[2]

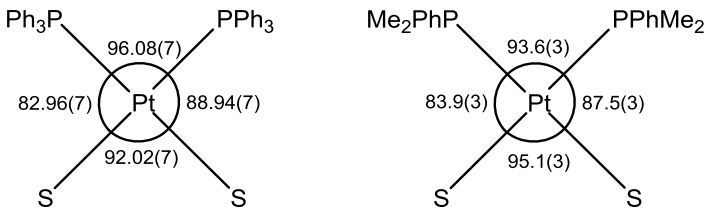

Figure 8 Comparison of the angles (°) associated with the square planar geometry of the platinum metal in complexes **Ay20** (left) and **Ay22** (right).

The platinum metal centre in **Ay20** and **Ay22** maintains a distorted square planar geometry (Figure 8). The P(1)-Pt(1)-P(2) angle of 96.08(7)° for **Ay20** is larger than the P(1)-Pt(1)-P(2) angle of 93.6(3)° in **Ay22**. This angle is larger in **Ay20** in order to accommodate the bulky triphenylphosphine groups; replacement of two phenyl groups with the less sterically demanding methyl groups allows reduction of this angle to occur in **Ay22**. One would expect the S(1)-Pt(1)-P(2) and S(2)-Pt(1)-P(1) angles to be equal, however this is not the case. This is a consequence of the distortion in the naphthalene framework. The P(1)-Pt(1)-P(2) angle in **Ay20** is smaller than that in **Ay22** (92.02(7)° and 95.1(3)°) this is expected as the *peri*-distance and splay angle observed in **Ay22** is more relaxed than those in **Ay20**. No significant differences in the Pt bond lengths are observed between the complexes.

The platinum metal also adopts a distorted square planar geometry in the acenaphthene complexes [Pt(AcenapS_2)(PPh_3)$_2$] and [Pt(AcenapS_2)($PPhMe_2$)$_2$], with values differing from those of **Ay20** and **Ay22**. Despite replacing the bulky triphenylphosphine groups with dimethylphenylphosphine groups, the P(1)-Pt(1)-P(2) angle of 97.51(8)° in [AcenapS_2(Pt(PPh_3)$_2$] is smaller than that in [Pt(AcenapS_2)($PPhMe_2$)$_2$], which is 100.84(15)°. The S(1)-Pt(1)-S(2) angles are compressed as a consequence of the widening of the P(1)-Pt(1)-P(2) angle. Surprisingly, the S(1)-Pt(1)-S(2) angles are the same in both complexes with values of 89.07(8)° and 89.61(15)° for [Pt(AcenapS_2)(PPh_3)$_2$] and [Pt(AcenapS_2)$PPhMe_2$)$_2$], respectively. These angles are larger and closer to the ídeal' 90° than those found in the acenaphthylene equivalents. Unlike in the acenaphthylene complexes the S-Pt(1)-P angles are equal in the acenaphthene equivalents, this is due to the distortion in the naphthalene framework being minimal in the acenaphthene complexes. No differences are observed in the Pt bond lengths in **Ay20** and **Ay22**. The Pt(1)-S bond lengths are comparable for [Pt(AcenapS_2)(PPh_3)$_2$] and [Pt(AcenapS_2)($PPhMe_2$)$_2$]. However

the Pt(1)-P bond lengths are longer in [Pt(AcenapS_2)(PPh_3)$_2$] (2.301(2) Å and 2.295(2) Å) than in [Pt(AcenapS_2)($PPhMe_2$)$_2$] (2.258(5) Å and 2.267(4) Å).[2]

As previously discussed, the **AyS_2** ligand in **Ay20** and **Ay22**, acts as a bidentate ligand, coordinating to the platinum *via* the chalcogen atoms to form a six-membered chelate ring. This six-membered PtS_2C_3 ring can be described as having a twisted envelope type conformation with the S···S vector as the hinge (Figure 9). In **Ay20** C(1), C(10) and C(9) all lie in a plane with S(1) lying 0.525(1) Å below the plane and S(2) lying 0.449(1) Å above the plane. This results in a non-planar, twisted PtS_2C_3 ring. In **Ay22** the PtS_2C_3 ring is closer to planar with the sulfur atoms deviating from the plane by 0.009(1) Å and 0.105(1) Å. The mean plane of S(1), S(2), C(1), C(10) and C(9) and the displacement of Pt(1), which sits in the *peri*-gap above the plane, is measured. In **Ay20** the Pt(1) sits 0.937(1) Å above the mean plane and the angle of the S(1)···S(2) hinge is 35.87(1)°. Whereas in **Ay22** the Pt(1) sits 0.576(1) Å above the mean plane and the S(1)···S(2) hinge angle is 25.21(1)°. The smaller angle and in turn shorter Pt(1) displacement observed for **Ay22** is expected due to this complex displaying less distortion than **Ay20**.

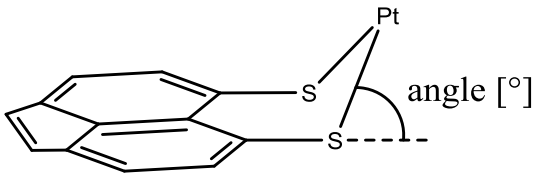

Figure 9 Diagram illustrating the twisted envelope type confirmation adopted by **Ay20** and **Ay22**.

The twisted envelope conformation parameters for **Ay20** and **Ay22** are different due to their differing levels of molecular distortion. These parameters are similar for [Pt(AcenapS_2)(PPh_3)$_2$] and [Pt(AcenapS_2)($PPhMe_2$)$_2$], which is expected as the complexes show similar levels of distortion. The Pt(1) is displaced from the essentially coplanar C(1)-C(10)-C(9)-S(1)-S(2) by *ca*. 1.16 Å and the S(1)···S(2) hinge angles are similar with values of 44.08(1)° and 45.56(1)° for [Pt(AcenapS_2)(PPh_3)$_2$] and [Pt(AcenapS_2)($PPhMe_2$)$_2$], respectively.[2]

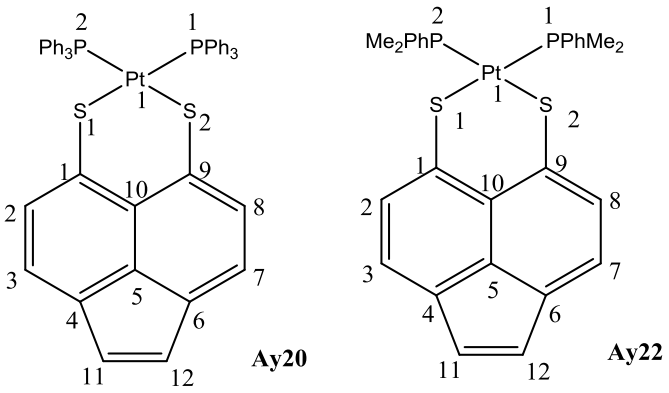

Figure 10 X-ray crystallography numbering scheme for **Ay20** and **Ay22**.

Table 6 Selected Bond Lengths [Å] and Angles [°] of **Ay20** and **Ay22.**

Compound	**Ay20**	**Ay22**
X-ray Code	2	139
E, E'	S, S	S, S
Peri-region distance and sub-van der Waals contacts		
E(1)···E(2)	**3.343(3)**	**3.431(11)**
Σr_{vdW} - E(1)···E(2); % Σr_{vdW}[a]	0.257; 93%	0.169; 95%
Naphthalene bond lengths		
C(1)-C(2)	1.400(11)	1.38(5)
C(2)-C(3)	1.401(11)	1.42(5)
C(3)-C(4)	1.360(12)	1.38(5)
C(4)-C(5)	1.427(11)	1.41(5)
C(5)-C(10)	1.399(11)	1.41(4)
C(5)-C(6)	1.430(11)	1.40(5)
C(6)-C(7)	1.375(12)	1.37(5)
C(7)-C(8)	1.422(13)	1.37(5)
C(8)-C(9)	1.391(11)	1.39(4)
C(9)-C(10)	1.435(11)	1.44(5)
C(1)-C(10)	1.434(11)	1.46(5)
C(11)-C(12)	1.358(12)	1.37(6)
Peri-region bond angles		
E(1)-C(1)-C(10)	124.6(6)	127(3)
C(1)-C(10)-C(9)	128.8(7)	131(3)
E(2)-C(9)-C(10)	127.1(6)	128(2)
∑ of bay angles	**380.5(11)**	**386(5)**
Splay angle[b]	20.5	26
Bond angles		

C(4)-C(5)-C(6)	109.1(7)	109(3)
E(2)-E(1)-C(1)	77.41(1)	77.02(1)
E(1)-E(2)-C(9)	75.29(1)	76.98(1)
Out of plane displacement		
E(1)	-0.525(1)	-0.009(1)
E(2)	+0.449(1)	+0.105(1)
Central naphthalene ring torsion angles		
C(6)-C(5)-C(10)-C(1)	-172.7(7)	179(3)
C(4)-C(5)-C(10)-C(9)	-177.7(7)	-174(3)
Platinum geometry - bond lengths		
Pt(1)-P(1)	2.289(2)	2.293(9)
Pt(1)-P(2)	2.2991(19)	2.293(9)
Pt(1)-E(1)	2.326(2)	2.334(9)
Pt(1)-E(2)	2.3212(19)	2.315(8)
Platinum geometry - bond angles		
E(1)-Pt(1)-E(2)	92.02(7)	95.1(3)
E(1)-Pt(1)-P(2)	82.96(7)	83.9(3)
E(2)-Pt(1)-P(1)	88.94(7)	87.5(3)
P(1)-Pt(1)-P(2)	96.08(7)	93.6(3)
Intramolecular Interactions		
Cg(C13-C18)···Cg(C31-C36)	3.620(1)	-
C28-H28B···Cg(C13-C18)	-	2.847(1)

[a] van der Waals radii used for calculations: r_{vdW}(S) 1.80 Å, r_{vdW}(Se) 1.90 Å.[13]

[b] Splay angle: ∑ of the three bay region angles - 360.

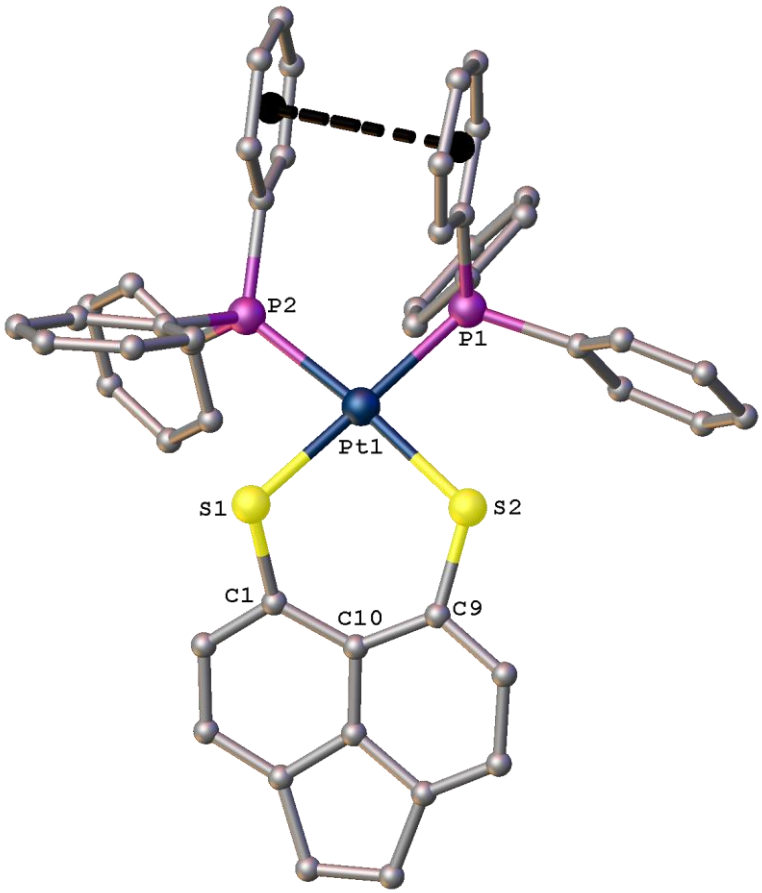

Figure 11 The molecular structure of **Ay20** showing the weak π···π interaction with H atoms and solvent molecules omitted for clarity.

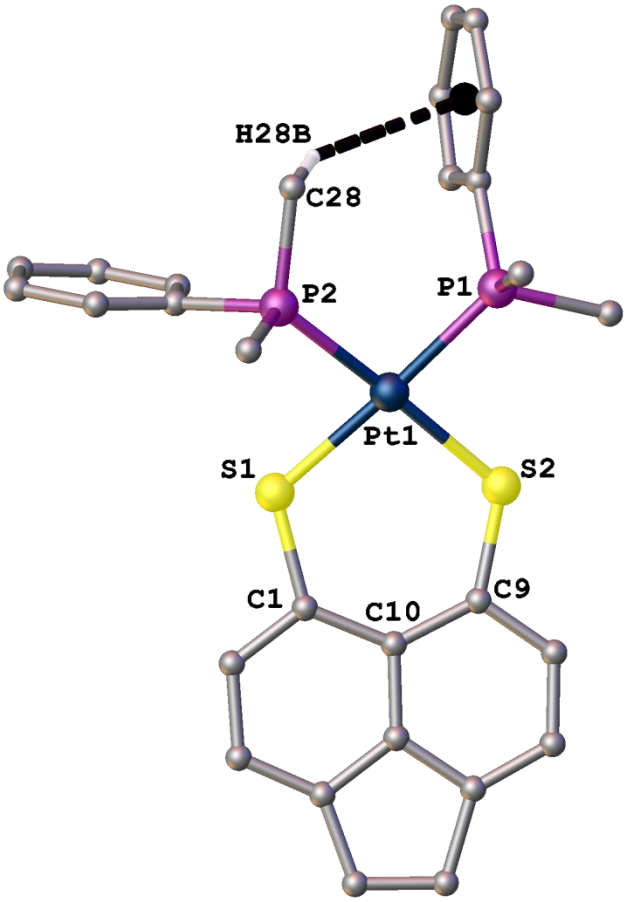

Figure 12 The molecular structure of **Ay22** showing the weak C-H···π interaction with H atoms and solvent molecules omitted for clarity.

The non-bonded *peri*-distance in **Ay20** of 3.343(3) Å is shorter than that of 3.452(4) Å in **Ay25**. This is expected due to the van der Waals radius of sulfur being smaller than that of selenium (1.80 Å vs. 1.90 Å).[13] The *peri*-distance observed in both complexes is shorter than the sum of their respective van der Waals radii by 7-9%. As expected, breaking of the chalcogen-chalcogen *peri*-bond and insertion of the platinum results in a positive splay angle being observed in both complexes with **Ay25** having a larger splay angle than **Ay20** (26.2° and 20.5°). Significant out-of-plane distortion is observed in **Ay20** with one sulfur atom lying 0.525(1) Å below the acenaphthylene plane and the other lying 0.449(1) Å above the plane. This is accompanied by distortion of the acenaphthylene ring with torison angles deviating from the ideal 180° by 2.3-

7.2°. In comparison, **Ay25** shows much less distortion with the selenium atoms lying 0.012(1) Å and 0.019(1) Å above and below the acenaphthylene plane. The acenaphthylene ring shows little buckling with torsion angles varying from 180° by 0.8-1.3°.

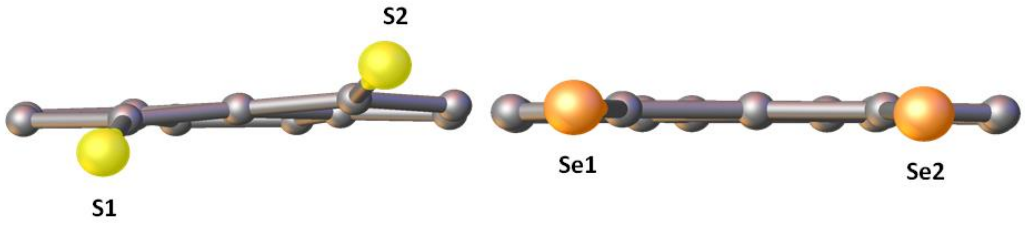

Figure 13 Comparison of the out-of-plane distortion and naphthalene ring deformation seen in **Ay20** and **Ay25**, other atoms have been omitted for clarity.

Similar trends in *peri*-distance and splay angle are seen between [Pt(AcenapS_2)(PPh_3)$_2$] and [Pt(AcenapSe_2)(PPh_3)$_2$]. However, differences are observed in out-of-plane distortion and torsion angles with both acenaphthene complexes having similar values and therefore similar levels of distortion.[2]

In **Ay20** two phenyl rings, one from each of the two PPh_3 groups, adopt a face-to-face alignment leading to a weak π···π interaction (Figure 10) with a Cg(C13-C18)····Cg(C31-C36) distance of 3.620(1) Å. **Ay25** also shows a weak π···π interaction (Figure 15) with a Cg(C13-C18)····Cg(C37-C42) distance of 3.801(1) Å. These values are comparable with those seen in [Pt(AcenapS_2)(PPh_3)$_2$] (3.765(1) Å and [Pt(AcenapSe_2)(PPh_3)$_2$] (3.764(1) Å).[2]

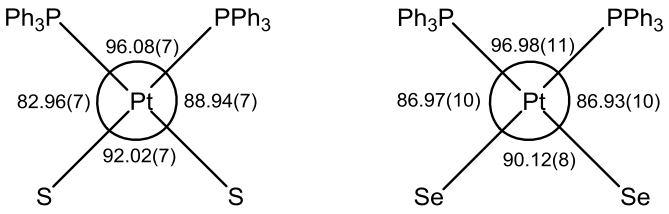

Figure 14 Comparison of the angles (°) associated with the square planar geometry of the platinum metal in complexes **Ay20** (left) and **Ay25** (right).

In **Ay20** and **Ay25** the platinum metal centre adopts a distorted square planar geometry (Figure 14). The P(1)-Pt(1)-P(2) angle of 96.08(7)° and 96.98(11)° for **Ay20** and **Ay25**, respectively is larger than the ideal 90° in order to accommodate the bulky triphenylphosphine groups. The E-Pt-P angles observed in both complexes are smaller than 90°, the expansion of the P(1)-Pt(1)-P(2) angle causes compression of these angles due to the restriction imposed by the *peri*-geometry which fixes the sulfur and selenium atoms. The Se(1)-Pt(1)-P(2) and Se(2)-Pt(1)-P(1) angles of 86.97(10)° and 86.93(10)° are equal. In comparison the S(1)-Pt(1)-P(2) angle of 82.96(7)° is much smaller than the S(2)-Pt(1)-P(1) angle of 88.94(7)°, this is due to the large out-of-plane distortion of the sulfur atoms causing twisting in the PtS_2C_3 ring. The S(1)-Pt(1)-S(2) angle of 92.02(7)° is larger than the Se(1)-Pt(1)-Se(2) of 90.12(8)°. One would expect the S(1)-Pt(1)-S(2) to be the smaller angle as the non-bonded *peri*-distance observed in **Ay20** is smaller than that of **Ay25** (3.343(3) Å and 3.452(4) Å, respectively). However, the out-of-plane distortion in **Ay20** is much greater than that in **Ay25**, as a consequence of this the most comfortable position for the sulfur atoms to sit results in a larger angle than that of the selenium atoms. No significant differences in the Pt-P bond lengths are observed between the complexes; however there are differences in the Pt-E bond lengths. The Pt-Se bond lengths of 2.432(2) Å and 2.4449(19) Å are longer than the Pt-S bond lengths of 2.326(2) Å and 2.3212(19) Å.

The platinum centre also adopts a distorted square planar geometry in the acenaphthene complexes $[Pt(AcenapS_2)(PPh_3)_2]$ and $[Pt(AcenapSe_2)(PPh_3)_2]$. The P(1)-Pt(1)-P(2) angles are comparable with those in the acenaphthylene complexes **Ay20** and **Ay25**. Due to the out-of-plane distortion and torsion angles in $[Pt(AcenapS_2)(PPh_3)_2]$ and $[Pt(AcenapSe_2)(PPh_3)_2]$ being similar, the E-Pt-P angles are also similar. These angles have values close to those of **Ay25** with **Ay20** being the 'odd one out' as a consequence of its large out-of-plane distortion and buckled naphthalene framework. The same is true for the E(1)-Pt(1)-E(2) angles with values of 89.07(8)°, 89.27(6)° and 90.12(8)° for $[Pt(AcenapS_2)(PPh_3)_2]$, $[Pt(AcenapSe_2)(PPh_3)_2]$ and **Ay25**; and a larger value of 92.02(7)° for **Ay20**. The observed bond lengths around the platinum centre are similar for the acenaphthylene and acenaphthene complexes.[2]

As previously discussed for **Ay20** and **Ay22** the six-membered PtE_2C_3 chelate ring, that forms when the dichalcogenole ligand binds to the platinum centre, can be described as having a twisted envelope type conformation with the E···E vector as the hinge. In **Ay20** C(1), C(10) and C(9) all lie in a plane with S(1) lying 0.525(1) Å below the plane and S(2) lying 0.449(1) Å above

the plane. This results in a non-planar, twisted PtS_2C_3 ring. In **Ay25** the $PtSe_2C_3$ ring is close to planar with the selenium atoms deviating from the plane by 0.012-0.019(1) Å. The mean plane of E(1), E(2), C(1), C(10) and C(9) and the displacement of Pt(1), which sits in the *peri*-gap above the plane, is measured. In **Ay20** the Pt(1) sits 0.937(1) Å above the mean plane and the angle of the S(1)···S(2) hinge is 35.87(1)°. Whereas in **Ay25** the Pt(1) sits 1.037(1) Å above the mean plane and the Se(1)···Se(2) hinge angle is 37.02(1)°.

Differences are observed in the twisted envelope parameters for $[Pt(AcenapS_2)(PPh_3)_2]$ and $[Pt(AcenapSe_2)(PPh_3)_2]$, compared to **Ay20** and **Ay25**. For the acenaphthene complexes the displacement of Pt(1) is similar with values of 1.150(1) Å and 1.137(1) Å for $[Pt(AcenapS_2)(PPh_3)_2]$ and $[Pt(AcenapSe_2)(PPh_3)_2]$, respectively. In the acenaphthylene complexes, the selenium structure has the smallest E(1)···E(2) hinge angle whereas in the acenaphthene complexes it is the sulfur structure that has the smallest hinge angle with a value of 44.08(1)°.[2]

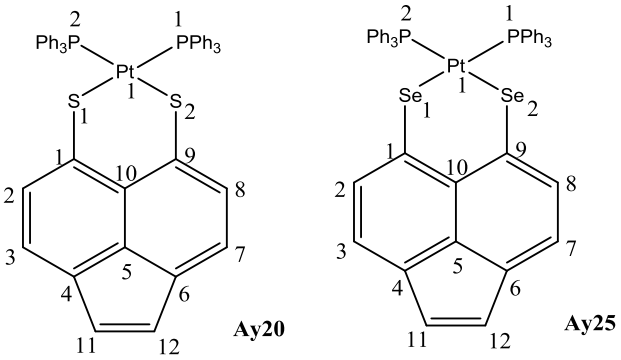

Figure 15 X-ray crystallography numbering scheme for **Ay20** and **Ay25**.

Table 7 Selected Bond Lengths [Å] and Angles [°] of **Ay20** and **Ay25.**

Compound	**Ay20**	**Ay25**
X-ray Code	2	44
E, E'	S, S	Se, Se
Peri-region distance and sub-van der Waals contacts		
E(1)···E(2)	**3.343(3)**	**3.452(4)**
Σr_{vdW} - E(1)···E(2); % Σr_{vdW}[a]	0.257; 93%	0.348; 91%
Naphthalene bond lengths		
C(1)-C(2)	1.400(11)	1.380(13)
C(2)-C(3)	1.401(11)	1.396(14)
C(3)-C(4)	1.360(12)	1.372(15)

C(4)-C(5)	1.427(11)	1.389(15)
C(5)-C(10)	1.399(11)	1.433(13)
C(5)-C(6)	1.430(11)	1.429(15)
C(6)-C(7)	1.375(12)	1.345(16)
C(7)-C(8)	1.422(13)	1.423(14)
C(8)-C(9)	1.391(11)	1.418(13)
C(9)-C(10)	1.435(11)	1.418(13)
C(1)-C(10)	1.434(11)	1.426(13)
C(11)-C(12)	1.358(12)	1.334(16)
Peri-region bond angles		
E(1)-C(1)-C(10)	124.6(6)	127.8(7)
C(1)-C(10)-C(9)	128.8(7)	131.0(8)
E(2)-C(9)-C(10)	127.1(6)	127.4(7)
∑ of bay angles	**380.5(11)**	**386.2**
Splay angle[b]	20.5	26.2
Bond angles		
C(4)-C(5)-C(6)	109.1(7)	109.7(9)
E(2)-E(1)-C(1)	77.41(1)	76.66(1)
E(1)-E(2)-C(9)	75.29(1)	77.12(1)
Out of plane displacement		
E(1)	-0.525(1)	+0.012(1)
E(2)	+0.449(1)	-0.019(1)
Central naphthalene ring torsion angles		
C(6)-C(5)-C(10)-C(1)	-172.7(7)	-179.2(9)
C(4)-C(5)-C(10)-C(9)	-177.7(7)	178.7(9)
Platinum geometry - bond lengths		
Pt(1)-P(1)	2.289(2)	2.305(3)
Pt(1)-P(2)	2.2991(19)	2.290(3)
Pt(1)-E(1)	2.326(2)	2.432(2)
Pt(1)-E(2)	2.3212(19)	2.4449(19)
Platinum geometry - bond angles		
E(1)-Pt(1)-E(2)	92.02(7)	90.12(8)
E(1)-Pt(1)-P(2)	82.96(7)	86.97(10)
E(2)-Pt(1)-P(1)	88.94(7)	86.93(10)
P(1)-Pt(1)-P(2)	96.08(7)	96.98(11)
Intramolecular Interactions		
Cg(C13-C18)···Cg(C31-C36)	3.620(1)	-
Cg(C13-C18)··· Cg(C37-C42)	-	3.801(1)

[a] van der Waals radii used for calculations: r_{vdW}(S) 1.80 Å, r_{vdW}(Se) 1.90 Å.[13]

[b] Splay angle: ∑ of the three bay region angles - 360.

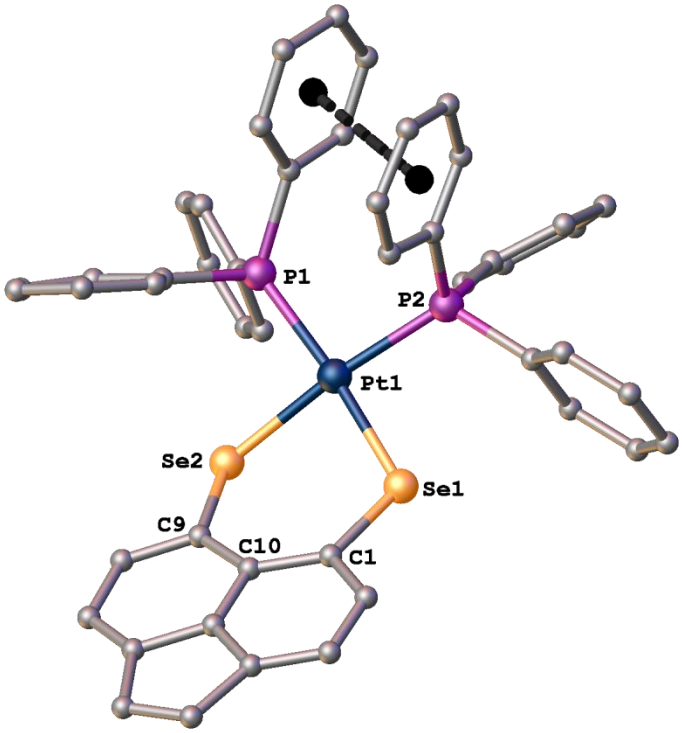

Figure 16 The molecular structure of **Ay25** showing the weak π···π interaction with H atoms omitted for clarity.

Unfortunately Woollins *et al.* could not obtain a molecular structure of $[Pt(NapS_2)(PPh_3)_2]$[1] and therefore a comparison of the different *peri*-dithiole backbones and their effect on the platinum metal geometry cannot be discussed. However, molecular structures were obtained for the selenium complexes; $[Pt(NapSe_2)(PPh_3)_2]$,[1] $[Pt(AcenapSe_2)(PPh_3)_2]$[2] and **Ay25** (Figure 17), allowing a direct comparison between backbones to me made. $[Pt(NapSe_2)(PPh_3)_2]$[1] crystallises with two molecules in the asymmetric unit and one molecule of dichloromethane; $[Pt(AcenapSe_2)(PPh_3)_2]$[2] and **Ay25** crystallise as single molecules.

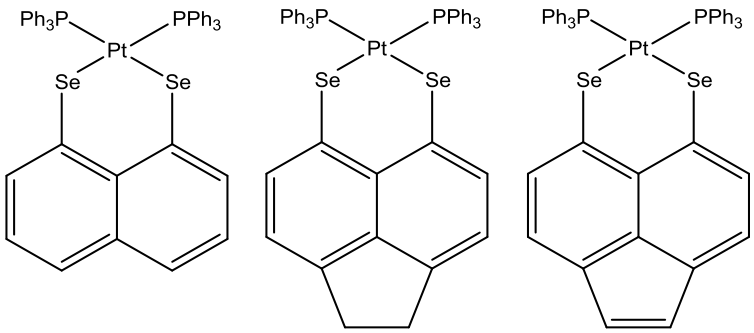

Figure 17 The platinum triphenylphosphine selenium complexes bearing different *peri*-backbones; [Pt(NapSe$_2$)(PPh$_3$)$_2$], [Pt(AcenapSe$_2$)(PPh$_3$)$_2$] and **Ay25**.[1,2]

An increase in the non-bonded *peri*-distance is observed as the diselenole ligand changes from naphthalene to acenaphthylene with values of 3.3721(9) Å, 3.437(3) Å and 3.452(4) Å for [Pt(NapSe$_2$)(PPh$_3$)$_2$], [Pt(AcenapSe$_2$)(PPh$_3$)$_2$] and **Ay25**, respectively. This is accompanied by a steady increase in splay angle with values of 23.8°, 25.7° and 26.2°, respectively. This pattern is expected due to the addition of the ethane/ethene linker in acenaphthene/acenaphthylene causing the C(4)-C(5)-C(6) angle to decrease from 118.64(1)° in [Pt(NapSe$_2$)(PPh$_3$)$_2$] to *ca*. 109° in [Pt(AcenapSe$_2$)(PPh$_3$)$_2$] and **Ay25**. A decrease in this angle at the bottom of the ring causes an increase in the angles of the splay region which consequently leads to an increase in *peri*-distance. A decrease in out-of-plane distortion occurs with [Pt(NapSe$_2$)(PPh$_3$)$_2$] displaying the greatest out-of-plane displacement with one selenium atom lying 0.234(1) Å above the naphthyl plane and one 0.165(1) Å below. [Pt(NapSe$_2$)(PPh$_3$)$_2$] also has the largest deformation of the naphthalene scaffold with torsion angles varying form the 'ideal' 180° by 1.1-2.4°. The naphthalene complex has the largest out-of-plane distortion and deformation of the backbone due to the absence of the ethane/ethene linker in the backbone which allows the system more flexibility.

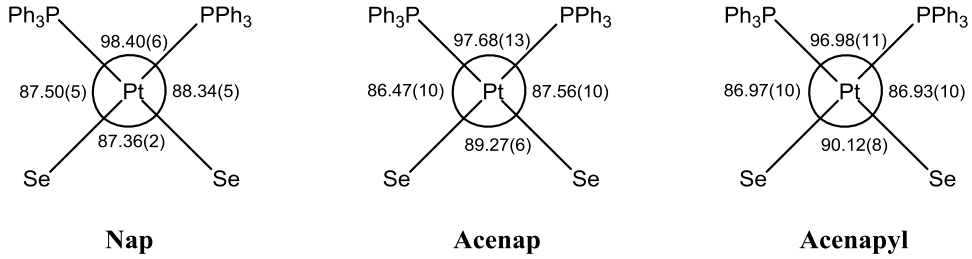

Figure 18 Comparison of the angles (°) associated with the square planar geometry of the platinum metal in complexes [Pt(NapSe$_2$)(PPh$_3$)$_2$], [Pt(AcenapSe$_2$)(PPh$_3$)$_2$] and **Ay25**.[1,2]

The platinum metal adopts a distorted square planar geometry in all three complexes, with **Ay25** displaying the most regular geometry (Figure 18). A steady increase in the Se(1)-Pt(1)-Se(2) angle is observed with values of 87.36(2)°, 89.27(6)° and 90.12(8)° for [Pt(NapSe$_2$)(PPh$_3$)$_2$], [Pt(AcenapSe$_2$)(PPh$_3$)$_2$] and **Ay25**, respectively. This increase is a direct consequence of the increasing splay angle which is caused by the compression of the C(4)-C(5)-C(6) angle. As the Se(1)-Pt(1)-Se(2) angle increases, and therefore becomes closer to the ideal '90°', the P(1)-Pt(1)-P(2) angle decreases with values of 98.40(6)°, 97.68(13)° and 96.98(11)° for [Pt(NapSe$_2$)(PPh$_3$)$_2$], [Pt(AcenapSe$_2$)(PPh$_3$)$_2$] and **Ay25**, respectively. No significant differences occur between the P-Pt-Se angles with values in the range of 86.5-88.3°. There are no differences observed in the Pt bond lengths between complexes. However, within the complexes the Pt(1)-Se bonds are longer (*ca.* 2.43-2.45 Å) than the Pt(1)-P bonds (*ca.* 2.28-2.30 Å).

Table 8 Selected Bond Lengths [Å] and Angles [°] of [Pt(NapSe$_2$)(PPh$_{3)2}$],[1] [Pt(AcenapSe$_2$)(PPh$_3$)$_3$][2] and **Ay25** [values in parentheses are for independent molecules].

Compound	**[Pt(NapSe$_2$)(PPh$_3$)$_2$)]**	**[Pt(AcenapSe$_2$)(PPh$_3$)$_2$)]**	**Ay25**
E, E'	Se, Se	Se, Se	Se, Se
Peri-region distance and			
sub-van der Waals contacts			
E(1)···E(2)	**3.3721(9) [3.551(10)]**	**3.437(3)**	**3.452(4)**
Σr_{vdW} - E(1)···E(2); % Σr_{vdW}[a]	0.4279; 89% [0.249; 93%]	0.363; 90%	0.348; 91%
Peri-region bond angles			
E(1)-C(1)-C(10)	126.4(5) [129.0(5)]	127.2(12)	127.8(7)
C(1)-C(10)-C(9)	126.4(6) [126.1(6)]	128.0(13)	131.0(8)
E(2)-C(9)-C(10)	131.0(5) [124.9(5)]	130.5(10)	127.4(7)
∑ of bay angles	**383.8(9) [380.0(9)]**	**385.7(20)**	**386.2**

Splay angle[b]	23.8 [20.0]	25.7	26.2
Bond angles			
C(4)-C(5)-C(6)	118.64(1) [119.45(1)]	109.4(13)	109.7(9)
E(2)-E(1)-C(1)	79.06(1) [74.84(1)]	77.99(1)	76.66(1)
E(1)-E(2)-C(9)	74.84(1) [78.51(1)]	76.21(1)	77.12(1)
Out of plane displacement			
E(1)	+0.234(1) [-0.165(1)]	+0.155(1)	+0.012(1)
E(2)	-0.165(1) [+0.499(1)]	+0.015(1)	-0.019(1)
Central naphthalene ring torsion angles			
C(6)-C(5)-C(10)-C(1)	177.6(6) [173.9(7)]	178.51(1)	-179.2(9)
C(4)-C(5)-C(10)-C(9)	178.9(6) [177.7(6)]	178.25(1)	178.7(9)
Platinum geometry - bond lengths			
Pt(1)-P(1)	2.289(2) [2.292(2)]	2.304(4)	2.305(3)
Pt(1)-P(2)	2.283(2) [2.287(2)]	2.294(4)	2.290(3)
Pt(1)-E(1)	2.447(1) [2.4301(7)]	2.4558(16)	2.432(2)
Pt(1)-E(2)	2.436(1) [2.4595(7)]	2.4356(16)	2.4449(19)
Platinum geometry - bond angles			
E(1)-Pt(1)-E(2)	87.36(2) [86.65(2)]	89.27(6)	90.12(8)
E(1)-Pt(1)-P(2)	87.50(5) [90.04(4)]	86.47(10)	86.97(10)
E(2)-Pt(1)-P(1)	88.34(5) [85.11(5)]	87.56(10)	86.93(10)
P(1)-Pt(1)-P(2)	98.40(6) [98.84(6)]	97.68(13)	96.98(11)
Intramolecular Interactions			
Cg(C25-C30)···Cg(C31-C36)	-	3.764(1)	-
Cg(C13-C18)··· Cg(C37-C42)	-	-	3.801(1)

[a] van der Waals radii used for calculations: r_{vdW}(Se) 1.90 Å.[13]

[b] Splay angle: ∑ of the three bay region angles - 360.

Experimental

All experiments were carried out under an oxygen- and moisture-free nitrogen atmosphere using standard Schlenk techniques and glassware. Reagents were obtained from commercial sources and used as received. Dry solvents were collected from a MBraun solvent system. Elemental analyses were performed by Stephen Boyer at the London Metropolitan University. Infra-red spectra were recorded for solids as KBr discs in the range 4000-350 cm^{-1} on a Perkin-Elmer System 2000 Fourier transform spectrometer. ^{1}H and ^{13}C NMR spectra were recorded on a Bruker Avance 300 MHz spectrometer with δ(H) and δ(C) referenced to external tetramethylsilane. Assignments of ^{13}C and ^{1}H NMR spectra were made with the help of H-H COSY and HSQC experiments. ^{31}P were recorded on a Jeol GSX 110 MHz spectrometer with δ(P) referenced to external phosphoric acid. ^{77}Se NMR spectra were recorded on a Jeol GSX 270 MHz spectrometer with δ(Se) referenced to external Me_2Se. All measurements were performed at 25 °C. All values reported for NMR spectroscopy are in parts per million (ppm). Coupling constants (*J*) are given in Hertz (Hz). All measurements were performed at 25 °C. Mass spectrometry was performed by the University of St. Andrews Mass Spectrometry Service. Electrospray Mass Spectrometry (ESMS) was carried out on a Micromass LCT orthogonal accelerator time of flight mass spectrometer. All *cis*-dichloro*bis*(phosphine)platinum reagents were prepared following standard literature procedures.[14,15,16] 5,6-Dibromoacenaphthylene was also prepared following literature procedure.[17]

Acenaphtho[5,6-*c,d*][1,2]dithiole (AyS_2): TMEDA (5.8 mL, 38.4 mmol) was added in one portion to a solution of 5,6-dibromoacenaphthylene (5.95 g, 19.2 mmol) in diethyl ether (250 mL). The reaction was cooled to -78 °C and stirred for 15 min. A 2.5 M hexane solution of *n*-butyllithium (7.7 mL, 19.2 mmol) was added dropwise and the mixture was stirred for 15 min. Sulfur powder (0.62 g, 19.3 mmol) was added and the mixture was stirred at -40 °C for 2 h. The mixture was cooled again to -78 °C and a 2.5 M hexane solution of *n*-butyllithium (7.7 mL, 19.2 mmol) was added dropwise and the mixture was stirred for 15 min. Sulfur powder (0.62 g, 19.3 mmol) was added and the mixture was stirred at -40 °C for a further 2 h. The mixture was then warmed to room temperature, quenched with acetic acid (2 mL) and exposed to an air stream overnight for mild oxidation. The resulting solution was evaporated under reduced pressure and after water (200 mL) was added, the mixture was extracted with dichloromethane (4 x 200 mL). The extract was dried with anhydrous magnesium sulfate and concentrated under reduced pressure to give a

deep red oil. The oil was dissolved in hexane (100 mL) and refluxed for an hour. The hot solution was placed in the freezer at - 30 °C overnight to yield an orange solid (0.22 g, 5%); mp 166-168 °C; elemental analysis (Found: C, 67.1; H, 2.7. Calc. for $C_{12}H_6S_2$: C, 67.25; H, 2.8%); IR (KBr disc) ν_{max} cm^{-1} 3423w, 3035w, 2953s, 2924s, 2856s, 1596s, 1487w, 1462s, 1413vs, 1396vs, 1371vs, 1195w, 1108w, 1077s, 1025s, 823vs, 732w, 645w, 529w, 388w; δ_H(300 MHz; $CDCl_3$; 25 °C; Me_4Si) 7.88 (2 H, d, $^3J_{HH}$ 7.5 Hz, Acenapyl 4,7-H), 7.54 (2 H, d, $^3J_{HH}$ 7.7 Hz, Acenapyl 3,8-H), 7.25 (2 H, s, Acenapyl 9,10-H); δ_C(75.5 MHz; $CDCl_3$; 25 °C; Me_4Si) 126.2(s), 126.0(s), 116.5(s); MS (ES^+): *m/z* 215.00 (30%, M^+).

Acenaphtho[5,6-*c,d*][1,2]diselenole (**$AySe_2$**) was prepared following the same procedure as above, the physical and spectral data are as follows.

Acenaphtho[5,6-*c,d*][1,2]diselenole ($AySe_2$): From 5,6-dibromoacenaphthylene (2.27 g, 7.34 mmol), TMEDA (2.2 mL, 14.7 mmol), a 2.5 M hexane solution of *n*-butyllithium (5.9 mL, 14.7 mmol) and selenium powder (1.16 g, 14.7 mmol) to yield a dark orange-brown solid (0.58 g, 26%; mp 147-149 °C (decomp.); elemental analysis (Found: C, 46.7; H, 2.0. Calc. for $C_{12}H_6Se_2$: C, 46.8; H, 2.0%); IR (KBr disc) ν_{max} cm^{-1} 2921w, 2366w, 2344w, 1596w, 1463w, 1400vs, 1213w, 1079s, 1020s, 822vs, 793s, 726w, 639s, 496w; δ_H(300 MHz; $CDCl_3$; 25 °C; Me_4Si) 7.76 (2 H, d, $^3J_{HH}$ 7.5 Hz, Acenapyl 4,7-H), 7.66 (2 H, d, $^3J_{HH}$ 7.7 Hz, Acenapyl 3,8-H), 7.17 (2 H, s, Acenapyl 9,10-H); δ_C(75.5 MHz; $CDCl_3$; 25 °C; Me_4Si) 126.3(s), 125.8(s), 121.4(s); δ_{Se} (51.5 MHz; $CDCl_3$; 25 °C; MeSeSeMe) 542.7 (s); MS (ES^+): *m/z* 310.89 (100%, M^+).

[Pt(5,6-AcenapylS_2)(PPh_3)$_2$] (Ay20): Lithium triethylborohydride (0.95 mL of a 1.0 M solution in THF, 0.95 mmol) was added to a solution of acenaphtho[5,6-*c,d*][1,2]dithiole (0.10 g, 0.47 mmol) in THF (20 mL). An immediate colour change occurred from orange to deep red, along with the evolution of gas. After stirring for 30 min, the resulting solution was transferred *via* a stainless steel cannula to a suspension of *cis*-dichloro*bis*(triphenylphosphine)platinum (0.38 g, 0.47 mmol) in THF (10 mL). The mixture was stirred for 24 h resulting in a red solution. The solution was poured through a shallow pad of silica and eluted with dichloromethane (100 mL). The filtrate was evaporated to dryness under reduced pressure and redissolved in dichloromethane (10 mL). Slow addition of a mixture of diethyl ether (25 mL) and hexane (75 mL) resulted in precipitation of a dark red solid, which was collected and dried *in vacuo*; (0.10 g, 23%); mp 227-229 °C (decomp.); elemental analysis (Found: C, 57.9; H, 3.7. Calc. for $C_{48}H_{36}P_2PtS_2$.1.5 x CH_2Cl_2: C, 57.8;

H, 3.8%); IR (KBr disc) ν_{max} cm^{-1} 3051w, 2361w, 1579s, 1479s, 1433vs, 1400vs, 1333s, 1309s, 1184w, 1115s, 1097vs, 1073vs, 1032vs, 998s, 828s, 737s, 691vs, 653s, 540vs, 521vs, 509vs, 495vs, 457w, 420w; δ_H(300 MHz; $CDCl_3$; 25 °C; Me_4Si) 7.62-7.44 (14 H, m, Acenapyl 4, 7-H, P-Phenyl), 7.42-7.30 (6 H, m, P-Phenyl), 7.28 (2 H, d, $^3J_{HH}$ 5.3 Hz, Acenapyl 3, 8-H), 7.26-7.13 (12 H, m, P-Phenyl), 6.85 (2 H, s, Acenapyl 9, 10-H); δ_C(75.5 MHz; $CDCl_3$; 25 °C; Me_4Si) 135.9-135.2(m), 130.8(s), 128.5-127.9(m), 126.9-126.7(m), 125.3(s), 124.4(s); δ_P(110 MHz; $CDCl_3$; 25 °C; H_3PO_4) 23.9 (s, $^1J_{PPt}$ 2953 Hz); MS (ES^+): *m/z* 934.14 (28%, M^+).

The other platinum complexes were similarly prepared and the physical and spectral data are as follows.

[Pt(5,6-AcenapylS$_2$)(PPh$_2$Me)$_2$] (Ay21): From acenaphtho[5,6-*c,d*][1,2]dithiole (0.11 g, 0.49 mmol), lithium triethylborohydride (0.95 mL of a 1.0 M solution in THF, 0.95 mmol), and *cis*-dichloro*bis*(diphenylmethylphosphine)platinum (0.32 g, 0.49 mmol) to yield an orange solid (0.17 g, 42%); mp 117-119 °C (decomp.); elemental analysis (Found: C, 54.4; H, 3.8. Calc. for $C_{38}H_{32}PtP_2S_2.1/2CH_2Cl_2$: C, 54.3; H, 3.9%); IR (KBr disc) ν_{max} cm^{-1} 3424w, 3053w, 2922w, 2363s, 2342w, 1576w, 1463w, 1436s, 1402vs, 1332s, 1310w, 1180w, 1102s, 1072s, 1035s, 890vs, 830w, 736s, 693s, 510s, 452w; δ_H(300 MHz; $CDCl_3$; 25 °C; Me_4Si) 7.52 (2 H, d, $^3J_{HH}$ 7.4 Hz, Acenapyl 4, 7-H), 7.49-7.42 (8 H, m, P-Phenyl), 7.38-7.28 (4 H, m, P-Phenyl), 7.28-7.18 (8 H, m, P-Phenyl), 7.11-7.04 (2 H, m, Acenapyl 3, 8-H), 6.80 (2 H, s, Acenapyl 9, 10-H), 1.83 (6 H, d, $^1J_{PH}$ 9.4 Hz); δ_C(75.5 MHz; $CDCl_3$; 25 °C; Me_4Si) 133.6-133.5(m), 131.1(s), 128.8-128.6(m), 126.7(s), 125.0(s), 124.4(s), 14.6 (d, $^1J_{CP}$ 41 Hz); δ_P(110 MHz; $CDCl_3$; 25 °C; H_3PO_4) 3.5 (s, $^1J_{PPt}$ 2880 Hz); MS (ES^+): *m/z* 796.20 (100%, M^+ - Me).

[Pt(5,6-AcenapylS$_2$)(PPhMe$_2$)$_2$] (Ay22): From acenaphtho[5,6-*c,d*][1,2]dithiole (0.11 g, 0.51 mmol), lithium triethylborohydride (0.95 mL of a 1.0 M solution in THF, 0.95 mmol), and *cis*-dichloro*bis*(dimethylphenylphosphine)platinum (0.26 g, 0.48 mmol) to yield an orange solid (0.09 g, 27%); mp 68-70 °C (decomp.); elemental analysis (Found: C, 48.95; H, 4.0. Calc. for $C_{28}H_{28}PtP_2S_2$: C, 49.05; H, 4.1%); IR (KBr disc) ν_{max} cm^{-1} 3425w, 2913w, 1577s, 1462w, 1435s, 1402vs, 1332w, 1308w, 1176w, 1107s, 1072s, 948s, 911vs, 836vs, 744s, 716w, 694s, 654w, 533w, 488w, 444w; δ_H(300 MHz; $CDCl_3$; 25 °C; Me_4Si) 7.82 (2 H, d, $^3J_{HH}$ 7.5 Hz, Acenapyl 4, 7-H), 7.45-7.36 (4 H, m, P-Phenyl), 7.39 (2 H, d, $^3J_{HH}$ 7.5 Hz, Acenapyl 3, 8-H), 7.35-7.27 (2 H, m, P-Phenyl), 7.26-7.17 (4 H, m, P-Phenyl), 6.87 (2 H, s, Acenapyl 9, 10-H), 1.62 (12 H, d, $^1J_{PH}$ 10.0 Hz); δ_C(75.5

MHz; $CDCl_3$; 25 °C; Me_4Si) 131.8-131.4(m), 129.4(br s), 129.1-129.0(m), 126.7(s), 124.8(s), 124.4(s), 13.7 (d, $^1J_{CP}$ 40 Hz) ; δ_P(110 MHz; $CDCl_3$; 25 °C; H_3PO_4) -14.5 (s, $^1J_{PPt}$ 2819 Hz); MS (ES^+): *m/z* 578.08 (100%, M^+ - $PhMe_2$).

[Pt(5,6-AcenapylS$_2$)(PMe$_3$)$_2$] (Ay23): From acenaphtho[5,6-*c,d*][1,2]dithiole (0.10 g, 0.48 mmol), lithium triethylborohydride (0.95 mL of a 1.0 M solution in THF, 0.95 mmol), and *cis*-dichloro*bis*(trimethylphosphine)platinum (0.20 g, 0.48 mmol) to yield an impure brown solid; δ_P(110 MHz; $CDCl_3$; 25 °C; H_3PO_4) -24.7 (s, $^1J_{PPt}$ 2768 Hz).

[Pt(5,6-AcenapylS$_2$)(COD)] (Ay24): From acenaphtho[5,6-*c,d*][1,2]dithiole (0.10 g, 0.47 mmol), lithium triethylborohydride (0.95 mL of a 1.0 M solution in THF, 0.95 mmol), and (1,5-cyclooctadiene)platinum(II) dichloride (0.18 g, 0.47 mmol) to yield an orange solid (0.04 g, 14%); mp >300 °C; elemental analysis (Found: C, 46.3; H, 3.6. Calc. for $C_{20}H_{18}PtS_2$: C, 46.4; H, 3.5%); IR (KBr disc) ν_{max} cm^{-1} 2923s, 2872s, 2363s, 2343w, 1580w, 1462w, 1408vs, 1335w, 1261s, 1179w, 1073vs, 1034vs, 831s, 800s, 729w, 651w, 535w; δ_H(300 MHz; $CDCl_3$; 25 °C; Me_4Si) 7.73 (2 H, d, $^3J_{HH}$ 7.5 Hz, Acenapyl 4, 7-H), 7.48 (2 H, d, $^3J_{HH}$ 7.5 Hz, Acenapyl 3, 8-H), 6.97 (2 H, s, Acenapyl 9, 10-H), 5.18 (4 H, s, COD-C*H*$_2$), 2.71-2.59 (4 H, m, COD-C*H*$_2$), 2.55-2.34 (4 H, m, COD-C*H*$_2$); δ_C(75.5 MHz; $CDCl_3$; 25 °C; Me_4Si) 125.6(s), 125.3(s), 124.6(s), 100.6(s), 30.7(s); MS (ES^+): *m/z* 518.06 (100%, M^+ + H).

[Pt(5,6-AcenapylSe$_2$)(PPh$_3$)$_2$] (Ay25): From acenaphtho[5,6-*c,d*][1,2]diselenole (0.10 g, 0.34 mmol), lithium triethylborohydride (0.65 mL of a 1.0 M solution in THF, 0.65 mmol), and *cis*-dichloro*bis*(triphenylphosphine)platinum (0.26 g, 0.33 mmol) to yield a red solid (0.16 g, 48%); mp 159-161 °C; elemental analysis (Found: C, 55.9; H, 3.6. Calc. for $C_{48}H_{36}PtP_2Se_2$: C, 56.1; H, 3.5%); IR (KBr disc) ν_{max} cm^{-1} 3408w, 3052w, 2925w, 1581w, 1479s, 1435vs, 1400vs, 1331s, 1185w, 1159w, 1094vs, 1073s, 1026s, 1000w, 831w, 743s, 693vs, 646w, 539vs, 522vs, 496s, 459w, 422w; δ_H(300 MHz; $CDCl_3$; 25 °C; Me_4Si) 7.70 (2 H, d, $^3J_{HH}$ 7.3 Hz, Acenapyl 4, 7-H), 7.60-7.48 (12 H, m, P-Phenyl), 7.39-7.27 (8 H, m, Acenapyl 3, 8-H, P-Phenyl), 7.25-7.12 (12 H, m, P-Phenyl), 6.85 (2 H, s, Acenapyl 9, 10-H); δ_C(75.5 MHz; $CDCl_3$; 25 °C; Me_4Si) 135.8-135.0(m), 130.8(s), 129.7(br s), 128.3-127.8(m), 125.9(s), 124.2(s); δ_P(110 MHz; $CDCl_3$; 25 °C; H_3PO_4) 20.2 (s, $^1J_{PPt}$ 3014 Hz); δ_{Se}(51.5 MHz; $CDCl_3$; 25 °C; MeSeSeMe) 227.6 (pseudo-triplet,[18] $^2J_{SeP}$ 55 Hz, $^1J_{SePt}$ 178 Hz); MS (ES^+): *m/z* 1028.03 (100%, M^+ + H).

[Pt(5,6-AcenapylSe$_2$)(PPh$_2$Me)$_2$] (Ay26): From acenaphtho[5,6-*c,d*][1,2]diselenole (0.10 g, 0.33 mmol), lithium triethylborohydride (0.66 mL of a 1.0 M solution in THF, 0.66 mmol), and *cis*-dichloro*bis*(diphenylmethylphosphine)platinum (0.21 g, 0.32 mmol) to yield a red solid (0.07 g, 25%); mp 116-118 °C; elemental analysis (Found: C, 50.4; H, 3.7. Calc. for $C_{38}H_{32}PtP_2Se_2$: C, 50.5; H, 3.6%); IR (KBr disc) ν_{max} cm^{-1} 3422w, 3051w, 2922w, 2361s, 2343w, 1579s, 1561w, 1475s, 1435vs, 1399vs, 1330s, 1182w, 1101s, 1072s, 1026s, 999w, 889vs, 831s, 734s, 693vs, 647w, 509s, 490s, 451s; δ_H(300 MHz; $CDCl_3$; 25 °C; Me_4Si) 7.87 (2 H, d, $^3J_{HH}$ 7.3 Hz, Acenapyl 4, 7-H), 7.49-7.38 (8 H, m, P-Phenyl), 7.49-7.38 (4 H, m, P-Phenyl), 7.38-7.29 (8 H, m, P-Phenyl), 7.25 (2 H, d, $^3J_{HH}$ 7.4 Hz, Acenapyl 3, 8-H), 6.85 (2 H, s, Acenapyl 9, 10-H), 1.91 (6 H, d, $^1J_{PH}$ 8.9 Hz); δ_C(75.5 MHz; $CDCl_3$; 25 °C; Me_4Si) 133.5 (d, $^2J_{CP}$ 6.8 Hz), 131.8(s), 129.7 (d, $^4J_{CP}$ 4.3 Hz), 128.7 (d, $^3J_{CP}$ 4.9 Hz), 125.9(s), 124.2(s), 15.5 (br s); δ_P(110 MHz; $CDCl_3$; 25 °C; H_3PO_4) 0.6 (s, $^1J_{PPt}$ 2932 Hz); δ_{Se}(51.5 MHz; $CDCl_3$; 25 °C; MeSeSeMe) 204.5 (pseudo-triplet,[18] $^2J_{SeP}$ 55 Hz, $^1J_{SePt}$ 210 Hz); MS (ES$^+$): *m/z* 750.06 (45%, M^+ - Ph_2).

[Pt(5,6-AcenapylSe$_2$)(PPhMe$_2$)$_2$] (Ay27): From acenaphtho[5,6-*c,d*][1,2]diselenole (0.10 g, 0.34 mmol), lithium triethylborohydride (0.65 mL of a 1.0 M solution in THF, 0.65 mmol), and *cis*-dichloro*bis*(dimethylphenylphosphine)platinum (0.18 g, 0.33 mmol) to yield a red solid (0.06 g, 22%); mp 66-68 °C (decomp.); elemental analysis (Found: C, 39.1; H, 3.6. Calc. for $C_{28}H_{28}PtP_2Se_2$: C, 43.1; H, 3.6%); IR (KBr disc) ν_{max} cm^{-1} 3423vs, 3050w, 2908w, 2361w, 2344w, 1638w, 1579s, 1561w, 1467w, 1435s, 1398vs, 1329s, 1312w, 1283w, 1181w, 1105s, 1072s, 1027s, 1000w, 1105s, 1072s, 1027s, 946vs, 908vs, 834s, 743s, 714s, 694s, 647s, 489s, 443s, 371w; δ_H(300 MHz; $CDCl_3$; 25 °C; Me_4Si) 8.14 (2 H, d, $^3J_{HH}$ 7.2 Hz, Acenapyl 4, 7-H), 7.62-7.49 (4 H, m, P-Phenyl), 7.50-7.30 (8 H, m, P-Phenyl, Acenapyl 3, 8-H), 6.92 (2 H, s, Acenapyl 9, 10-H), 1.72 (12 H, d, $^1J_{PH}$ 9.7 Hz); δ_C(75.5 MHz; $CDCl_3$; 25 °C; Me_4Si) 131.5-131.1(m), 129.8(s), 129.5(br s), 129.1-128.9(m), 125.8(s), 124.3(s), 14.5 (d, $^1J_{CP}$ 40 Hz); δ_P(110 MHz; $CDCl_3$; 25 °C; H_3PO_4) -17.6 (s, $^1J_{PPt}$ 2873 Hz, $^2J_{PSe}$ 52 Hz); δ_{Se} (51.5 MHz; $CDCl_3$; 25 °C; MeSeSeMe) 174.6 (pseudo triplet,[18] $^2J_{SeP}$ 53 Hz, $^1J_{SePt}$ 251 Hz); MS (ES$^+$): *m/z* 786.04 (60%, M^+ + Li). NB. Elemental analysis was submitted multiple times with no success.

References

[1] S. M. Aucott, H. L. Milton, S. D. Robertson, A. M. Z. Slawin, G. D. Walker and J. D. Woollins, *Chem. Eur. J.,* 2004, **10**, 1666.

[2] C. G. M. Benson, C. M. Schofield, R. A. M. Randall, L. Wakefield, F. R. Knight, A. M. Z. Slawin and J. D. Woollins, *Eur. J. Inorg. Chem*., 2013, 427.

[3] L-Y. Chiang and J. Meinwald, *Tetrahedron Lett*., 1980, **21**, 4565.

[4] Preliminary work on this structure and the corresponding ligand was carried out as part of an undergraduate MChem project by Andy Ward.

[5] R. V. Parish, *NMR, NQR, EPR, and Mössbauer Spectroscopy in Inorganic Chemistry*, Ellis Horwood Limited, Chichester England, 1990.

[6] P. G. Waddell, PhD Thesis, University of St Andrews (UK), 2010. and the references therein.

[7] G. Matsubayahi and A. Yokozawa, *Inorg. Chim. Acta*., 1993, **208**, 95; V. C. Ginn, P. F. Kelly and J. D. Woollins, *Polyhedron*, 1994, **13 (10)**, 1501; M. Risto, E. M. Jahr, M. S. Hannu-Kuure, R. Oilunkaniemi and R. S. Laitinen, *J. Organomet. Chem*., 2007, **692**, 2193.

[8] J. A. Iggo (Ed.), *NMR Spectroscopy in Inorganic Chemistry*, Oxford University Press Inc., New York, 1999.

[9] A. D. Rae, R. A. Wood and T. R. Welberry, *J. Chem. Soc., Perkin Trans. 2,* 1985, **3**, 451.

[10] R. Steudel, Angew. *Chem. Int. Ed. Engl*., 1975, **14 (10)**, 655 and the references therein.

[11] S. M. Aucott, H. L. Milton, S. D. Robertson, A. M. Z. Slawin and J. D. Woollins, *Heteroat. Chem*., 2004, **15**, 530.

[12] All images of molecular structures were generated using OLEX2: O. V. Dolomanov, L. J. Bourhis, R. J. Gildea, J. A. K. Howard and H. Puschmann, *J. Appl. Cryst*., 2009, **42**, 339.

[13] A. Bondi, *J. Phys. Chem.,* 1964, **68**, 441.

[14] D. Drew and J. R. Doyle, *Inorg. Synth.,* 1972, **13**, 47.

[15] F. J. Ramos-Lima, A. G. Quiroga, J. M. Pérez, M. Font-Bardía, X. Solans and C. Navarro-Ranninger, *Eur. J. Inorg. Chem.,* 2003, **8**, 1591.

[16] J. Bailar, H. Itatani, *Inorg. Chem.,* 1965, **4**, 1618.

[17] L. M. Diamond, F. R. Knight, K. S. Athukorala Arachchige, R. A. M. Randall, M. Bühl. A. M. Z. Slawin and J. D. Woollins, *Eur. J. Inorg. Chem*., 2014, **9**, 1512.

[18] Pseudo triplet, actually overlapped doublet of doublets from ^{77}Se being coupled to two inequivalent ^{31}P environments, see discussion.

Concluding remarks

In Chapter 2, a series of platinum complexes **1a**-**1c** that incorporate 1,8-naphthosultone and *cis*-$[Pt(PR_3)_2Cl_2]$ (R_3 = Ph_3, Ph_2Me, $PhMe_2$) were prepared through a metathetical reaction. The sulfur-oxygen bond in 1,8-naphthosultone was reduced with two equivalents of lithium triethylborohydride to form the dilithio-species, which was then added to a suspension of the appropriate *cis*-dichloro*bis*(phosphine)platinum in THF resulting in the formation of [Pt(1-(SO_2),8-(O)-nap)(PPh_3)$_2$] (**1a**), [Pt(1-(SO_2),8-(O)-nap)(PPh_2Me)$_2$] (**1b**) and [Pt(1-(SO_2),8-(O)-nap)(PMe_2Ph)$_2$] (**1c**).

The $^{31}P\{^1H\}$ NMR spectra of the three complexes display the expected AX pattern with appropriate platinum satellites. A steady decrease in $^1J(^{31}P_X$-$^{195}Pt)$ value was observed for **1a** to **1c**, as the phenyl groups are replaced with electron donating methyl groups.

In **1a** to **1c**, 1,8-naphthosultone acts as a bidentate ligand, coordinating to the platinum *via* the sulfur and the oxygen atom to form a six-membered chelate ring which can be described as having a twisted envelope type conformation. The central platinum metal adopts a distorted square planar geometry in each case, with angles deviating significantly from the ideal (90°).
One would expect that the degree of molecular distortion would decrease upon going from **1a** to **1c**, as the bulkier phenyl groups are replaced with methyl groups, however this is not the case. In these complexes there is a competition between steric effects and intramolecular interactions which controls the level of molecular distortion.

The *peri*-distance has been elongated in the complexes due to the breaking of the sulfur-oxygen bond and insertion of the platinum. The non-bonded sulfur-oxygen distance being 2.842(3) Å for **1a** and 2.928(7) Å for **1b** compared to the bonded distance of 1.6407(14) Å in the free ligand **1**. This increase in *peri*-distance causes an increase in the angles of the bay region, with positive splay angles of 9° and 13° being seen for **1a** and **1b**, respectively. This is significantly greater than in 1,8-naphthosultone where there is a negative splay angle of 27° due to the presence of the sulfur-oxygen bond. **1b** shows little distortion when compared to the free ligand, however **1a** is greatly distorted with large out-of-plane displacement observed and torsion angles deviating from those in the free ligand by *ca.* 5.5-7°.

The differences observed between **1a** and **1b** are due to a combination of steric effects and weak intramolecular interactions. In **1a** there is a weak π···π interaction with a Cg(C23-C28)····Cg(C29-C34) distance of 3.605(1) Å and in **1b** there is a C-H····π interaction giving a C11-H11····Cg(C25-C30) distance of 3.697(1) Å. In going from **1a** to **1b** not only are we reducing the strain on the naphthalene system by replacing a bulky phenyl group with a methyl group, we are also changing and further weakening the intramolecular interaction from a π-π interaction to a C-H····π interaction.

In **1c** it would appear that the intramolecular interaction may dominate over steric effects, which in turn causes the complex to become more distorted than that of **1b**, but less than that of **1a**. The *peri*-distance, splay angle and naphthalene backbone distortion are all intermediate of those found in **1a** and **1b**. Like **1b**, **1c** also has a weak C-H····π interaction with a C18-H18····Cg(C19-C24) distance of 3.602(1) Å. This distance is shorter than that in **1b**, resulting in a stronger interaction which in turn will have more effect on the molecular structure of the overall complex.

The Tolman cone angles for PPh_3, PPh_2Me and $PPhMe_2$ are 145°, 136° and 122°, respectively. Therefore, one would anticipate a steady contraction in the P-Pt-P angle on going from **1a** to **1c** and this is observed. However, the S(1)-Pt(1)-O(9) angles reflect the levels of distortion seen in the backbone with **1b** having an angle that is intermediate of **1a** and **1c**.

When the analogous 1,8-naphthosultam was treated with two equivalents of lithium triethylborohydride, the sulfur-nitrogen bond was not reduced, instead the nitrogen atom was deprotonated. Methathetical addition of the appropriate *cis*-dichloro*bis*(phosphine)platinum to the deprotonated species resulted in the formation of a series of mono-substituted complexes: [Pt(1-(SO_2),8-(N)-nap)(PPh_3)$_2$(Cl)] (**mono-2a**), [Pt(1-(SO_2),8-(N)-nap)(PPh_2Me)$_2$(Cl)] (**mono-2b**), [Pt(1-(SO_2),8-(N)-nap)($PPhMe_2$)$_2$(Cl)] (**mono-2c**) and [Pt(1-(SO_2),8-(N)-nap)(PMe_3)$_2$(Cl)] (**mono-2d**). The reaction was also successful with (1,5-cyclooctadiene)platinum(II) dichloride to give [Pt(1-(SO_2),8-(N)-nap)(COD)(Cl)] (**mono-2e**).

The $^{31}P\{^1H\}$ NMR spectra of the mono-complexes display the expected AX pattern with appropriate platinum satellites. A steady decrease in $^1J(^{31}P_X\text{-}^{195}Pt)$ value was observed for **mono-2a** to **mono-2d**, as the phenyl groups are replaced with electron donating methyl groups.

Unfortunately, ^{31}P NMR revealed that the reactions were not going to completion with peaks seen for the corresponding *cis*-dichloro*bis*(phosphine)platinum reagent.

The reactions were repeated using a non-nucleophilic base 1,8-diazabicyclo[5.4.0]undec-7-ene (DBU) to purposefully deprotonate the nitrogen. The ^{31}P NMR data from the DBU reactions was in agreement with the data from the lithium triethylborohydride reactions indicating formation of the mono-platinum complexes, **mono-2a** to **mono-2d**, could be achieved through this route. Despite no peaks being observed for the corresponding *cis*-dichloro*bis*(phosphine)platinum reagent, peaks for a secondary product were observed. It was determined that the DBU was involved in a competitive side reaction with the *cis*-dichloro*bis*(triphenylphosphine)platinum reagent to form a Pt-DBU complex. Separation of the desired mono-complex and the Pt-DBU complex proved unsuccessful.

Due to the unwanted side reaction with DBU, the reactions were repeated using the stronger non-nucleophilic base sodium *tert*-butoxide. 1,8-Naphthosultam was reacted with sodium *tert*-butoxide and the corresponding *cis*-dichloro*bis*(phosphine)platinum in a 1:1:1 ratio. The ^{31}P NMR data from the sodium *tert*-butoxide reactions was in agreement with the data from previous reactions. However, apart from the reaction of 1,8-naphthosultam and *cis*-dichloro*bis*(triphenylphosphine)platinum to yield **mono-2a**, the reactions did not go to completion with peaks for the corresponding *cis*-dichloro*bis*(phosphine)platinum complexes dominating the ^{31}P NMR.

Crystal structures were obtained for **mono-2a** and **mono-2e**. Both structures possess the 1,8-naphthosultam system as a monodentate ligand, bonding through the nitrogen atom to a platinum centre, with the SNC_3 *peri*-region remaining intact. No differences were observed in the *peri*-distances of these complexes when compared to the free ligand. However, increased negative splay angles indicate a more favourable interaction is occurring in the complexes. The torsion angles measured in the complexes were similar to those in the free ligand. Significant changes in the out-of-plane displacement occurred, and these can be accredited to the atoms moving to the optimum position for minimal distortion to the naphthalene geometry.

A series of *bis*-complexes were obtained by reacting two equivalents of 1,8-naphthosultam with two equivalents of sodium *tert*-butoxide to yield two equivalents of the deprotonated 1,8-

naphthosultam species. The deprotonated species was then reacted with one equivalent of the appropriate *cis*-dichloro*bis*(phosphine)platinum to yield [Pt(1-(SO_2),8-(N)-nap)$_2$($PPh_2Me)_2$] (**bis-2b**), [Pt(1-(SO_2),8-(N)-nap)$_2$($PPhMe_2)_2$] (**bis-2c**) and [Pt(1-(SO_2),8-(N)-nap)$_2$($PMe_3)_2$] (**bis-2d**). The reaction was also successful with (1,5-cyclooctadiene)platinum(II) dichloride to give [Pt(1-(SO_2),8-(N)-nap)$_2$(COD)] (**bis-2e**). The **bis-2a** complex could not be prepared. It was concluded from DFT calculations that there was no steric or thermodynamic reason for **bis-2a** not forming.

The $^{31}P\{^1H\}$ NMR spectra for the complexes have an AX pattern with appropriate platinum satellites. Similar to the 1,8-naphthosultam mono-complexes and the 1,8-naphthosultone complexes, a steady decrease in value for $^1J(^{31}P\text{-}^{195}Pt)$ coupling constant is seen as the phenyl groups are replaced by methyl groups.

A crystal structure was obtained for **bis-2e** and the levels of molecular distortion observed were compared to those in **mono-2e**. The *peri*-distances were the same in both complexes and the splay angles were similar with values of ~27°, this is understandable as both complexes still have the sulfur-nitrogen bond intact. The sulfur and nitrogen atoms show little out-of-plane distortion in **bis-2e**, with greater displacement observed in **mono-2e**. As a consequence the naphthalene backbone in **bis-2e** shows greater distortion to relieve any geometrical constraints whereas the naphthalene backbone in **mono-2e** shows less distortion as the nitrogen atom has been displaced to relieve the majority of the strain. Both **bis-2e** and **mono-2e** show minor distortion from the 'ideal' square planar geometry with no significant differences seen in the bond angles or bond lengths between the two complexes. It can be concluded that replacing a chlorine atom with another 1,8-naphthosultam ligand has a minimal effect on the geometry around the platinum centre and the overall complex.

In Chapter 4, a series of *bis*-chalcogen (**Ay1**-**Ay3**), mixed chalcogen-chalcogen (**Ay4**-**Ay5**) and mixed halogen-chalcogen (**Ay7**-**Ay12**) acenaphthylenes were prepared by dehydrogenation of the respective acenaphthene with 1.5 equivalents of DDQ. **AyBr$_2$**, **AyI$_2$** and **ABr$_4$** were also prepared. Molecular structures of **Ay2**-**Ay4, Ay8, Ay9, Ay11** and **Ay12** were obtained and compared with their naphthalene and acenaphthene analogues. The acenaphthene and acenaphthylene structures display less molecular distortion than their naphthalene counterparts. This can be attributed to the natural lengthening of the *peri*-distance and the addition of the ethane/ethene bridge which lessens the system's ability to relieve strain *via* buckling. The acenaphthene and

acenaphthylene structures varied in behaviour, with some having similar *peri*-distances and others showing a small increase in *peri*-distance when going from the acenaphthene to the acenaphthylene derivative.

Along with their naphthalene and acenaphthene analogues, **Ay8, Ay9, Ay11** and **Ay12** adopt the B type configuration and **Ay2**-**Ay4** adopt the AB*t* type configuration. Both show an increase in *peri*-distance as the *peri*-atoms become larger. In comparison the acenaphthene compounds, **A2**-**A4**, and naphthalene compounds, **N2**-**N4**, do not all adopt the same configuration, with the *bis*-telluride derivative being the 'odd one out' in both cases. **A2** and **A4** adopt the AB*c* configuration whereas **A3** adopts the AB*t* configuration. **N2** and **N4** also adopt the AB*c* configuration; however **N3** adopts a CC*c* configuration.

Overall the series of acenaphthylenes is unremarkable showing similar trends to the acenaphthene derivatives.

In Chapter 5, a group of 5,6-*bis*(aryltelluro)acenaphthenes (**A3**, **A13**-**A19**) (where Aryl = Ph, FP, Tol, An-*p*, An-*o*, TP, Mes and Tip) were prepared by reacting 5,6-dibromoacenaphthene with TMEDA (2.7 eq.) and *n*BuLi (2.4 eq.) to create a 5,6-dilithioacenaphthene.2TMEDA complex. This complex was then reacted with the respective diaryl ditelluride (2eq.) to yield the desired 5,6-*bis*(aryltelluro)acenaphthene. The analogous group of 5,6-*bis*(aryltelluro)acenaphthylenes (**Ay3**, **Ay13**-**Ay19**) were prepared from dehydrogenation of the parent acenaphthene with DDQ (1.5 eq.). The acenaphthenes and acenaphthylenes were compared to their naphthalene counterparts (**N3**, **N13**-**N19**) and how repulsive and attractive interactions affect molecular conformation and Te···Te spin-spin coupling constants was explored.

Similar degrees of molecular distortion were observed in the acenaphthene and acenaphthylene compounds, with the naphthalene compounds displaying greater molecular distortion and shorter *peri*-distances. The Ph, FP, Tol, An-*p* and TP compounds were found to contain similar bulk around the Te centre; however An-*o*, Mes and Tip had increasingly larger values. This increase in bulk was found to have no effect on the molecular distortion or conformation in any of the compounds studied. With the exception of **A19**; **A3**, **A13**-**A15**, **A17** and **A18** had the same conformation as their acenaphthylene analogues. The naphthalene compounds displayed less

correlation, with only **N14** **N15**, **N17** and **N18** having the same conformation as their acenaphthene/acenaphthylene counterparts.

Acenaphthene and acenaphthylene compounds were found to have similar $J(^{125}Te, ^{125}Te)$ SSCCs. The naphthalene compounds had larger $J(^{125}Te, ^{125}Te)$ SSCCs, but this was expected due to their having shorter *peri*-distances. All three series displayed a linear correlation in ^{125}Te chemical shift and $J(^{125}Te, ^{125}Te)$ SSCCs, which shows that the conformation around the Te atoms is similar in solution for all backbones. Compounds containing aryl groups of similar size showed no difference in the $J(^{125}Te, ^{125}Te)$ values or ^{125}Te chemical shift. However, for the larger aryl groups (An-*o*, Mes and Tip) as the size of the group increased a steady decrease in ^{125}Te chemical shift and a general increase in $J(^{125}Te, ^{125}Te)$ value occurred.

In general, compounds that have the smallest $J(^{125}Te, ^{125}Te)$ SSCCs exhibit the AB conformation and compounds that have the largest adopt the CC*t* conformation. Out of the 15 acenaphthene and acenaphthylene compounds, 4 did not confer to this trend. **A14**, **A15** and **Ay14** were found to adopt a CC*t* conformation in the solid state, but they had smaller $J(^{125}Te, ^{125}Te)$ values which were more in line with an AB conformation. **A19** adopts the BC*c* conformation in the solid, but its $J(^{125}Te, ^{125}Te)$ value is more in line with what would be anticipated for the CC*t* conformation. Similar discrepancies were seen in the $J(^{125}Te, ^{125}Te)$ SSCCs of the naphthalene compounds. It has been previously concluded, that in solution an energy difference of only 1 kcal mol^{-1} exists between the AB and CC*t* conformations, allowing the molecular structure to easily fluctuate between the two conformers. Our findings are in agreement with an equilibrium occurring in solution and we are hoping this can be confirmed by ^{125}Te solid state NMR spectroscopy in the future. Future use of SSCCs as a tool to aid the prediction of structural conformation in these systems looks hopeful.

In Chapter 6, a related series of *bis*(phosphine) platinum complexes **Ay20**-**Ay23** and **Ay25**-**Ay27** that bear acenaphtho[5,6-*cd*]-1,2-dichalcogenole ligands were synthesised. The chalcogen-chalcogen bonds in acenaphtho[5,6-*cd*]-1,2-dithiole (**AyS_2**) and acenaphtho[5,6-*cd*]-1,2-diselenole (**$AySe_2$**) were reduced with lithium triethylborohydride (2 eq.) to form the dilithio-species, which was then added to a suspension of the appropriate *cis*-dichloro*bis*(phosphine)platinum in THF resulting in the formation of the platinum (II) complexes $[Pt(5,6\text{-}AcenapylE_2)(PR_3)_2]$ (**Ay20** E = S, $R_3 = Ph_3$; **Ay21** E = S, $R_3 = Ph_2Me$; **Ay22** E = S, $R_3 = PhMe_2$; **Ay23** E = S, $R_3 = Me_3$; **Ay25** E = Se, $R_3 = Ph_3$;

Ay26 E = Se, R_3 = Ph_2Me; **Ay27** E = Se, R_3 = $PhMe_2$). The dilithio-species of **AyS_2** and **$AySe_2$** were also reacted with (1,5-cyclooctadiene)platinum(II) dichloride. This reaction was successful with **AyS_2** resulting in the platinum complex [Pt(5,6-AcenapylS_2)(COD)] (**Ay24**).

The $^{31}P\{^1H\}$ NMR spectra of the sulfur complexes, **Ay20**-**Ay23**, display the expected single resonance with appropriate platinum satellites. The addition of the low abundance ^{77}Se NMR active isotope in **Ay25**-**Ay27** results in these compounds having more complex $^{31}P\{^1H\}$ NMR spectra with AA'X spin systems. Similar spectra were seen for the previously reported acenaphthene analogues. In [Pt(AcenapSe_2)($PPhMe_2$)$_2$] $^2J_{PSe}$ coupling is observed for the *cis* and the *trans* configurations. This was not observed for **Ay25**-**Ay27**, in their spectra one set of satellites is observed for the $^2J_{PSe}$ coupling. This is due to the *cis* and *trans* satellites having couplings of similar magnitude which leads to overlap of the signals and therefore they could not be fully assigned. As seen in similar systems, **Ay20**-**Ay23** and **Ay25**-**Ay27** display a steady decrease in value for $^1J(^{31}P\text{-}^{195}Pt)$ coupling constant as the phenyl groups are replaced by methyl groups.

It was expected that a doublet of doublets would be observed in the ^{77}Se NMR spectra of **Ay25**-**Ay27** due to the ^{77}Se atom being coupled to two inequivalent ^{31}P nuclei. However, from the ^{31}P NMR spectra we know that the $^2J_{SeP}$ *cis* and *trans* satellites are of similar magnitude and indistinguishable. Therefore, in the ^{77}Se NMR spectra the two central peaks of the expected doublet of doublets overlap and a pseudo triplet is observed. The peak intensity of the pseudo triplet is again consistent with coupling to two ^{31}P atoms. In addition supplementary $^1J_{SePt}$ satellites are observed, also displaying a similar pseudo triplet pattern.

Crystal structures were determined for the ligand **AyS_2** and the complexes **Ay20**, **Ay22** and **Ay25**. In each complex the acenaphtho[5,6-*cd*]-1,2-dichalcogenole ligand coordinates in a bidentate fashion to the platinum metal to form a six-membered PtE_2C_3 ring that can be described as having a twisted envelope type conformation. The platinum metal adopts a distorted square planar environment with angles deviating from the ideal 90°. Naturally, there is a significant increase in molecular distortion of the acenaphthylene ring system due to breaking of the chalcogen-chalcogen bond and insertion of the platinum.

Ay20 and **Ay22** both show an increase in *peri*-distance of *ca.* 1.3 Å when compared to the free ligand, this is accompanied with large positive splay angles of 20.5° and 26°. **Ay22** shows less distortion of the acenaphthylene backbone than **Ay20** due to the larger *peri*-distance and splay angle allowing a more relaxed geometry that can accommodate the dimethylphenyl groups comfortably. The platinum metal adopts a distorted square planar environment in both complexes. The P(1)-Pt(1)-P(2) angle is larger in **Ay20** in order to accommodate the bulky triphenylphosphine groups; replacement of two phenyl groups with the less sterically demanding methyl groups allows reduction of this angle to occur in **Ay22**.

Ay20 has a shorter *peri*-distance and thus smaller splay angle than **Ay25**, which was expected as the van der Waals radius of sulfur is smaller than selenium. The acenaphthylene backbone showed little distortion in **Ay25**, however **Ay20** showed significant buckling and out-of-plane displacement. Again, the platinum centre maintains a distorted square planar environment in both complexes with comparable P(1)-Pt(1)-P(2) angles.

Ay25 was compared to its previously reported naphthalene and acenaphthene counterparts. An increase in the non-bonded *peri*-distance is observed as the diselenole ligand changes from naphthalene to acenaphthylene with values increasing from *ca.* 3.37 to 3.45 Å. This is accompanied by a steady increase in splay angle with values increasing from 23.8° to 26.2°. This trend is expected due to the addition of the ethane/ethene linker in acenaphthene/acenaphthylene causing the C(4)-C(5)-C(6) angle to decrease from 118.64(1)° in [Pt(NapSe$_2$)(PPh$_3$)$_2$] to *ca.* 109° in [Pt(AcenapSe$_2$)(PPh$_3$)$_2$] and **Ay25**. A decrease in this angle at the bottom of the ring causes an increase in the angles of the splay region which consequently leads to an increase in *peri*-distance. A decrease in distortion occurs throughout the series with [Pt(NapSe$_2$)(PPh$_3$)$_2$] displaying the greatest out-of-plane displacement and the largest deformation of the naphthalene scaffold. The naphthalene complex has the largest levels of distortion due to the absence of the ethane/ethene linker in the backbone which allows the system more flexibility.

The platinum metal adopts a distorted square planar geometry in all three complexes, with **Ay25** displaying the most 'relaxed' geometry, A steady increase in the Se(1)-Pt(1)-Se(2) angle is observed which is a direct consequence of the increasing splay angle which is caused by the

compression of the C(4)-C(5)-C(6) angle. As the Se(1)-Pt(1)-Se(2) angle increases, and therefore becomes closer to the ideal ‘90°’, a steady decrease occurs in the P(1)-Pt(1)-P(2) angle.